ДОКЛАДЫ
АКАДЕМИИ НАУК СССР

SOVIET PHYSICS

"Doklady"

VOLUME 1 NUMBER 3

A Translation

of the

"Physics Section"

of the

Proceedings of the Academy of Sciences of the USSR

(RUSSIAN ORIGINAL VOL. 108, NOS. 1-6)

Published by the
AMERICAN INSTITUTE OF PHYSICS
INCORPORATED

SOVIET PHYSICS
"Doklady"

A translation of the "Physics Section" of the Proceedings of the Academy of Sciences of the USSR.

A publication of the

AMERICAN INSTITUTE OF PHYSICS

Governing Board

ALLEN V. ASTIN
ROBERT F. BACHER
W. S. BAIRD
H. A. BETHE
R. T. BIRGE
FRANK D. DEXTER
I. C. GARDNER
S. A. GOUDSMIT
CHARLES KITTEL
HUGH S. KNOWLES
R. B. LINDSAY
WILLIAM F. MEGGERS
HARRY F. OLSON
R. R. PALMER
R. F. PATON
ERIC RODGERS
RALPH A. SAWYER
FREDERICK SEITZ
H. D. SMYTH
MARK W. ZEMANSKY

Officers and Staff

FREDERICK SEITZ
Chairman, Governing Board
HENRY A. BARTON
Director
WALLACE WATERFALL
Executive Secretary
MARK W. ZEMANSKY
Treasurer
THEODORE VORBURGER
Advertising Manager
RUTH F. BRYANS
Publication Manager
KATHRYN SETZE
Assistant Treasurer
ALICE MASTROPIETRO
Circulation Manager
EUGENE H. KONE
Director of Public Relations

American Institute of Physics Advisory Board on Russian Translations

ELMER HUTCHISSON, *Chairman*

DWIGHT GRAY, MORTON HAMERMESH, VLADIMIR ROJANSKY,
VICTOR WEISSKOPF

SOVIET PHYSICS—"Doklady" is a bi-monthly journal published by the American Institute of Physics for the purpose of making available in English reports of current Soviet research in physics as contained in the "Physics Section" of the Proceedings of the Academy of Sciences of the USSR. The Proceedings appears thirty-six times per year and the "Physics Sections" are accumulated and English translations of them are published in six issues per year.

Transliteration of the names of Russian authors follows the system employed by the Library of Congress.

This translating and publishing project was undertaken by the Institute in the conviction that dissemination of the results of research everywhere in the world is invaluable to the advancement of science. The National Science Foundation of the United States encouraged the project initially and is supporting it in large part by a grant. Translation and printing are being handled by Consultants Bureau, Inc.

The American Institute of Physics and its translators propose to translate faithfully all of the scientific material in the "Physics Section" of the Proceedings of the Academy of Sciences of the USSR appearing after January 1, 1956. The views expressed in the translated material, therefore, are intended to be those expressed by the original authors, and not those of the translators nor of the American Institute of Physics.

One volume is published annually. Volume 1 will consist of six issues and will contain all scientific material published in the "Physics Section" of the original Russian journal during the 1956 calendar year.

Subscription Prices:

Per year (6 issues)	
United States and Canada	$25.00
Elsewhere	27.50
Back Numbers	
Single copies	$ 6.00

Subscriptions should be addressed to the American Institute of Physics, 57 East 55th Street, New York 22, N. Y.

Copyright by American Institute of Physics 1957

SOVIET PHYSICS
"Doklady"

A translation of the "Physics Section" of the Proceedings of the Academy of Sciences of the USSR.

VOLUME 1, NUMBER 3 MAY-JUNE, 1956

RELAXATION OF PHOTOCONDUCTIVITY IN STANNIC OXIDE

A. I. Andrievskii and V. A. Zhuravlev

(Presented by Academician A. F. Ioffe November 10, 1955)

The kinetics of photoconduction in semiconductors has been studied principally for semiconductors showing comparatively small time lag, so that in the majority of cases their photoconductivity relaxation times range from 10^{-2} to 10^{-5} sec. Much less attention has been paid to the investigation of the kinetics of photoconduction in semiconductors whose relaxation times are measured in tens of seconds [1,2]. There are no studies of semiconductors with relaxation times of the order of hundreds and thousands of seconds.

It is of interest to determine whether such large differences in relaxation time by several orders of magnitude are only quantitative differences or whether they are due to certain essential differences in the mechanism of photoconduction.

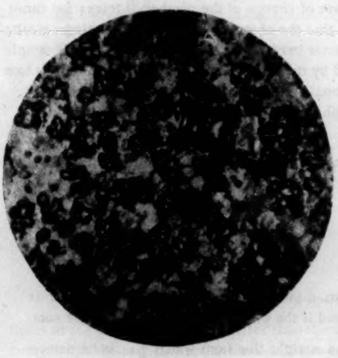

Fig. 1.

We have chosen stannic oxide whose photoconductivity relaxation time, according to our measurements, for different samples ranges from tens to thousands of seconds. The samples were prepared by oxidation, in an electric furnace, of thin films of tin produced by vacuum evaporation. The samples were kept in the furnace at 170° from two to several tens of hours. Under these conditions, not only is the tin oxide formed but there is a partial transformation from the amorphous to the crystalline phase. We observed the growth of stannic oxide crystals as a function of thermal treatment of the samples. The microphotograph in Fig. 1 (800 ×) shows the distribution of crystals in one portion of a sample after four hours in the furnace.

After radiation with ultraviolet light, the samples show marked photoconductivity. The ratio of the steady photoconduction to the dark conduction is approximately 2-2.5. The spectral sensitivity lies in the far ultraviolet with approximate long wave boundary at 2894 A. The stable photoconduction is proportional to the square root of the light intensity. The dark current of the sample as measured by the sign of the thermoelectromotive force is due to hole conduction.

The samples are characterized by a comparatively large inertia of the photoconduction. In order to attain steady photoconduction it was necessary to irradiate various samples from 10 minutes to 2 hours. The decay of photoconduction after illumination lasts 16 to 20 hours. Because of the large photoconduction inertia it is possible to measure the relaxation process with a suitable galvanometer and using a stop watch for time measurements [1,2].

The measurements of the rise of photoconduction during illumination and suitable treatment of the results show that this rise follows an exponential law. It may be described as the sum of several exponentials, each of which is characterized by a different relaxation time. Therefore the samples are characterized by a set of relaxation times. Fig. 2 is a semilogarithmic plot of the rise of photoconduction under different intensities of illumination for one sample. The light intensity (in arbitrary units) is shown above the respective broken lines. The relaxation times change from sample to sample within wide limits. We observed relaxation times ranging from 20 to 3000 seconds.

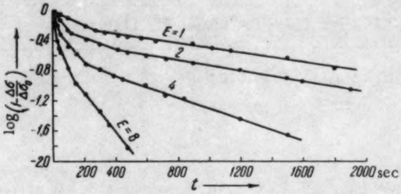

Fig. 2.

From Fig. 2 it can be seen that as the illumination intensity increases, the relaxation time decreases. This decrease may be due to the expulsion of electrons from trapping levels by the action of the light, which shortens the lifetime of electrons on these levels.

The set of relaxation times of each sample increases with increased intensity of illumination. But the number of relaxation times is not a monotonically increasing function of illumination intensity. For example, for one of the samples (Fig. 2) at $E = 1$ (in arbitrary units) two relaxation times are observed; at $E = 2$ there are three relaxation times; at $E = 4$ there are likewise three times, and at $E = 8$ we observed four relaxation times (on the scale of Fig. 2 for $E = 8$ it was possible to represent only three sections of the broken line, corresponding to three relaxation times). This rate of change of the number of relaxation times with the increase in illumination intensity refutes the assumption that the observed set of relaxation times results from absorption of light in the interior of the sample with consequent irradiation of different layers of the sample by light of different intensity. This dependence can be explained by the difference in the probability of electron trapping at different levels. At small intensities the levels with small trapping probability cannot be observed experimentally. To observe the effect of trapping on the rise of photoconduction it is necessary to increase the intensity of illumination.

If for any sample we designate the relaxation times as $\tau_1, \tau_2, \ldots \tau_n, \ldots$, then between the inverse relaxation times and the ordinal numbers $n = 1, 2, 3, \ldots$ there is the relationship

$$\frac{1}{\tau_n} = ke^{n/p},$$

where $\underline{k}$ is a coefficient which increases with increased illumination intensity, $\underline{p}$ is close to unity and $\underline{n}$ is the number of relaxation times. This relationship is easily observed if the graph is constructed using the coordinates $\log \frac{1}{\tau_n}$ and $\underline{n}$. In this case (Fig. 3) the graph will be a straight line from which $\underline{p}$ can be determined by the slope.

This relationship is very interesting. It is therefore useful to treat the data of other writers in the same way in order to study the kinetics of photoconduction of other semiconductors. We used the measurements of a set of relaxation times of silver bromide obtained by P. V. Meikliar [1] and obtained similar results. It is of interest to note that $\underline{p}$ is close to unity just as in our samples.

The following explanation of the relationship can be given*. It was shown by S. I. Pekar [3] that if electrons interact more strongly with one branch of the proper vibrations of the ions and atoms which surround them, then close to the line of a pure electronic transition a number of bands will appear whose intensity is represented by $I = GA_1\frac{c^{q_1\alpha}}{q_1!}$, where q_1 is the serial number of the band. On the other hand, there is a certain relationship between the band intensity and the relaxation time. This relationship of the band intensity to the relaxation time and the dependence of the band intensity on its serial number may explain the observed relationship between the relaxation times and their serial numbers.

---

*Pointed out by V. S. Milianchuk.

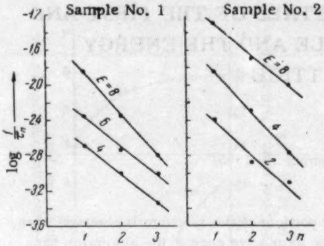

Fig. 3.

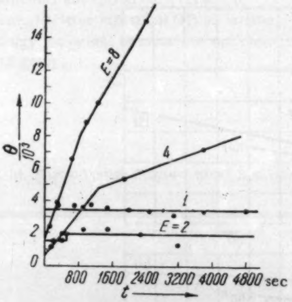

Fig. 4.

We treated results of measurements of photoconduction decay in darkness after illumination by a method suggested by N. A. Tolstoi and P. P. Feofilov [4]. "The specific slowness of relaxation". $\theta = \frac{\Delta\sigma}{d\Delta\sigma/dt}$ was determined by graphical differentiation of the corresponding quantities. The dependence of θ on time for different illumination intensities (E = 8, 4, 2, 1 in arbitrary units) preceding decay is given in Fig. 4.

From Fig. 4 it can be seen that after comparatively high intensities of illumination (E = 8, 4) the decay of photoconduction follows a hyperbolic law $\Delta\sigma = \frac{\Delta\sigma_0}{(1+at)^\alpha}$ (lines forming acute angles with the time axis), which consists of two successive hyperbolas differing in their parameters. The parameter a of the first hyperbola (the initial stages of decay) is larger than the second. As the illumination becomes more intense, a increases although in the initial stages of decay this increase is slight. In the initial stages of decay α is smaller than in the later stages. With greater intensity of the illumination before darkness α increases. However, samples are found in which α decreases, but for all samples $\alpha < 1$.

The final stages of decay of the photoconduction (not shown in Fig. 4) follow an exponential law.

After illumination with light of comparatively small intensity (E = 2, 1) the photoconduction decay processes in darkness follow an exponential law (straight lines parallel to the time axis). An analysis of these processes shows that they can be described by the sum of several exponentials and are thus characterized by a set of relaxation times. As the intensity of illumination before darkness increases, the set of relaxation times is enlarged. For the same intensity the rise and decay of photoconduction are characterized by an identical number of relaxation times. However, the magnitudes of the relaxation times under illumination are smaller than the corresponding relaxation times in darkness. This is evidently connected with the fact that under the conditions of darkness, the lifetimes of electrons on "sticking" levels is determined by the liberation of electrons from these levels through thermal motion, whereas under illumination there is an additional factor – the freeing of electrons from these levels by light. In the second case the lifetime of electrons on "sticking" levels will clearly be shorter.

The relationship between the inverse relaxation times and the serial numbers of the relaxation times during the rise of conduction $1/\tau_n = ke^{n/p}$ holds true also for decay. But during decay $\underline{p}$ is close to 0.5, while $\underline{k}$ is larger than for the rise of photoconduction under illumination.

LITERATURE CITED

[1] P. V. Meikliar, J. Exptl.-Theoret. Phys. (USSR) 21, 42 (1951).

[2] V. E. Lashkarev and G. A. Fedorus, Bull. Acad. Sci. USSR, Phys. Ser. 16, 81 (1952).

[3] S. I. Pekar, Progr. Phys. Sci. (USSR) 50, 197 (1953).

[4] N. A. Tolstoi and P. P. Feofilov, J. Exptl.-Theoret. Phys. (USSR) 19, 421 (1949).

L'vov Polytechnical Institute

Received October 17, 1955

OPTICAL ABSORPTION IN COMPOUNDS OF METALS OF THE FIRST AND SECOND GROUPS OF THE PERIODIC TABLE AND THE ENERGY OF THE CRYSTALLINE LATTICE

A. A. Vorob'ev

(Presented by Academician A. F. Ioffe November 10, 1955)

Optical absorption in ionic crystals in the visible and ultraviolet portions of the spectrum is observed when electrons are excited and make transitions to higher energy levels. The short wave edge of the absorption band in the infrared region is associated with the excitation of the normal modes of vibration of the lattice ions. In ionic crystals optical absorption is accompanied by electron transitions into the conduction zone, thus inducing photoconduction.

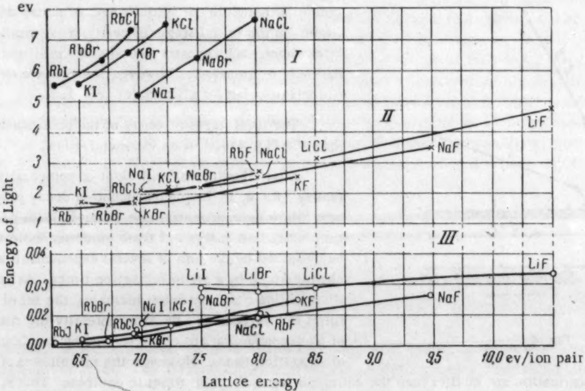

Fig. 1. Dependence of energy of light on lattice energy for alkali halides. I) fundamental absorption edge; II) absorption maximum in F band; III) fundamental absorption in infrared region.

Thus the position of a band in the absorption spectrum determines the energy which binds the electrons and ions in the lattice, and must be related to the magnitude of the energy of the crystalline lattice.

L. M. Shamovskii [1] has established a relationship between the long wave edge of the fundamental absorption edge of alkali halide crystals and the lattice energy. For alkali halide crystals E. K. Zavadovskaia [2] has established the relationship between the absorption maximum of the F band and the lattice energy.

A comparison of the experimental data shows that for compounds of metals of the first and second groups of the periodic table (see Fig. 1) which crystallize in a lattice of the rock salt type, the absorption in the infrared, visible and ultraviolet portions of the spectrum has a regular connection with the energy of the crystalline lattice. As the lattice energy increases, the beginning, edge and maximum of the absorption shifts in the short wave direction.

These regular relationships result from the periodic change of the properties of the elements in the periodic table and from the change of the properties of compounds formed from these elements. As a result of the relationship between light absorption in crystals and the lattice energy, there will be a dependence between the absorption and other properties of the crystals.

For alkali halide crystals it was shown previously [3] that there is a relationship between the absorption of light and the dielectric constant.

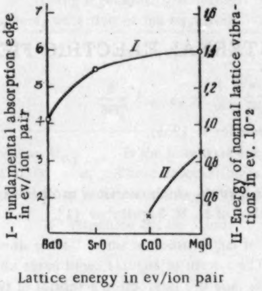

Fig. 2. Dependence of energy of fundamental absorption edge (I) and of normal lattice vibrations (II) on lattice energy for oxides of metals of the second group.

LITERATURE CITED

[1] L. M. Shamovskii, Absorption Spectra of Heteropolar Crystals and the Energy of the Crystalline Lattice (Moscow, 1938).

[2] E. K. Zavadovskaia, Doklady Akad. Nauk SSSR 98, 573 (1954).

[3] A. A. Vorob'ev, Doklady Akad. Nauk SSSR 90, 157 (1953).

S. M. Kirov Tomsk Polytechnical Institute

Received November 16, 1955

THE THEORY OF DIPOLAR CRYSTALS IN AN EXTERNAL ELECTRIC FIELD

A. E. Glauberman

(Presented by Academician M. A. Leontovich November 1, 1955)

A statistical theory describing the dielectric properties of molecular crystals which consist of molecules with definite electric moments can be constructed on the basis of the method of N. N. Bogoliubov [1].

Let us consider the simplest variant of the theory of dipolar crystals of cubic structure whose lattice sites contain molecules with constant dipole moments $\mathbf{P}_i$ ($i = 1, 2, \ldots, N$). The system of angular coordinates which determines the orientation of each dipole (ϑ_i, φ_i) will be designated by Θ_i and the interaction potential of two dipoles $\Phi_{a_i a_k}$ will be written in the usual form:

$$\Phi_{a_i a_k} = \frac{\mathbf{P}_{a_i} \cdot \mathbf{P}_{a_k}}{r^3_{a_i a_k}} - \frac{3(\mathbf{P}_{a_i} \cdot \mathbf{r}_{a_i a_k})(\mathbf{P}_{a_k} \cdot \mathbf{r}_{a_i a_k})}{r^5_{a_i a_k}}, \tag{1}$$

where the indices a_i designate the "type" of molecule. If it is assumed that the dipole moments of all molecules are of equal magnitude, the "type" characteristics are introduced as follows. A crystal, in which the centers of mass of the dipolar molecules are rigidly fixed at the lattice sites, will be considered to be a system consisting of particles of different types. The type of molecule will be determined by the lattice vector of the site in which the center of mass is located. In (1) the type characteristics enter in the form of numerical factors in connection with the equality

$$r_{a_i a_k} = |\mathbf{r}_{a_i} - \mathbf{r}_{a_k}| = d l^{1/2}_{a_i a_k}, \tag{2}$$

where d is half of the latice constant and the $l_{a_i a_k}$ are whole numbers, and through the cosines of the angles defining the direction of the line of centers of two dipoles.

On this model the dipolar crystal is represented at a temperature above the temperature of orientational melting as an "orientational" gas or liquid.

We introduce the distribution functions

$$F_{a_1 \ldots a_s}(\Theta_1, \ldots, \Theta_s),$$

normalized in such a way that the expression

$$\left(\frac{1}{4\pi}\right)^s F_{a_1 \ldots a_s}(\Theta_1, \ldots, \Theta_s)\, d\Omega_1 \ldots d\Omega_s, \tag{3}$$

where $d\Omega_i = \sin\vartheta_i\, d\vartheta_i\, d\varphi_i$ is the probability that the directions of the dipole moments of a fixed group of s dipoles of the sorts $a_1, \ldots, a_s$ lie inside the elements of solid angle $d\Omega_1, \ldots, d\Omega_s$, respectively, with arbitrary orientation of the remaining dipoles.

Using a generating functional, defined in the given case by a class of functions on the surface of a unit sphere, we arrive at the equations

$$\frac{\partial}{\partial\Theta_1^\alpha}F_{a_1\ldots a_s}+\frac{1}{\mu}\frac{\partial U_{a_1\ldots a_s}}{\partial\Theta_1^\alpha}F_{a_1\ldots a_s}+\frac{1}{4\pi\mu}\int\sum_{1<a_{s+1}<N}\frac{\partial\Phi_{a_1,a_{s+1}}}{\partial\Theta_1^\alpha}F_{a_1\ldots a_{s+1}}\,d\Omega_{s+1}=0, \tag{4}$$

where $U_{a_1\ldots a_s}$ is the potential energy of the system of $\underline{s}$ fixed molecules, $\mu = kT$, $\alpha = 1, 2$, with $\Theta_i^1 = \vartheta_i$ and $\Theta_i^2 = \varphi_i$. These calculations are similar to those of N. N. Bogoliubov for distribution functions of the positions of molecules in a gas or liquid [1].

We introduce the notation

$$\frac{1}{\mu}\Phi_{a_1a_2}=\frac{P^2}{d^3\mu}\Psi_{a_1a_2}=\alpha\Psi_{a_1a_2};\quad \frac{PE}{\mu}=\beta,$$

where P is the magnitude of the dipole moment of the molecules; E is the strength of the external electric field. Separating the term representing the external field we rewrite (4) as follows:

$$\begin{aligned}\frac{\partial}{\partial\Theta_1^\alpha}F_{a_1\ldots a_s}+\alpha\frac{\partial U^*_{a_1\ldots a_s}}{\partial\Theta_1^\alpha}F_{a_1\ldots a_s}+\frac{\alpha}{4\pi}\int\sum_{1<a_{s+1}<N}\frac{\partial\Psi_{a_1,a_{s+1}}}{\partial\Theta_1^\alpha}F_{a_1\ldots a_{s+1}}\,d\Omega_{s+1}-\\-\frac{1}{\mu}\sum_{a_1\leqslant a_i<a_s}(\mathbf{P}_{a_i}\cdot\mathbf{E})\,F_{a_1\ldots a_s}=0,\end{aligned} \tag{5}$$

where $U^*_{a_1\ldots a_s}=\sum_{a_i>a_k}\Psi_{a_ia_k}$.

We assume that the parameter α which characterizes our system is small ($\alpha \ll 1$) and represents the distribution functions by series

$$F_{a_1\ldots a_s}=F^0_{a_1\ldots a_s}+\alpha F^1_{a_1\ldots a_s}+\ldots \tag{6}$$

normalized by

$$\begin{gathered}\left(\frac{1}{4\pi}\right)^s\int F^0_{a_1\ldots a_s}\,d\Omega_1\ldots d\Omega_s=1,\\ \left(\frac{1}{4\pi}\right)^s\int F^k_{a_1\ldots a_s}\,d\Omega_1\ldots d\Omega_s=0,\quad k>0.\end{gathered} \tag{7}$$

This normalization insures satisfaction of the boundary condition according to which, when interactions are eliminated (in the limit $d \to \infty$) the distribution functions, which reduce in this case to $F^0_{a_1\ldots a_s}$ coincide with the familiar distribution function for an ideal system of dipoles in an external electric field.

Solving the equations for the zeroth and first approximation, we obtain:

$$F^0_{a_1\ldots a_s}=\left(\frac{\beta}{\operatorname{sh}\beta}\right)^s\exp\left\{\sum_{a_1\leqslant a_i\leqslant a_s}(\mathbf{P}_{a_i}\cdot\mathbf{E})\,/\,\mu\right\}, \tag{8}$$

$$F^{1}_{a_1\ldots a_s} = F^{0}_{a_1\ldots a_s}\Big[\Big(\frac{1}{4\pi}\Big)^{s}\int F^{0}_{a_1\ldots a_s} U^{*}_{a_1\ldots a_s}\, d\Omega_1\ldots d\Omega_s + \\ + \Big(\frac{1}{4\pi}\Big)^{s+1}\sum_{\substack{1<a_{s+1}<N\\ a_1\leqslant a_i<a_s}}\int \Psi_{a_i,\,a_{s+1}} F^{0}_{a_1\ldots a_{s+1}}\, d\Omega_1\ldots d\Omega_{s+1} - \\ - \frac{1}{2\pi}\sum_{\substack{1<a_{s+1}<N\\ a_1\leqslant a_i<a_s}}\int \Psi_{a_i,\,a_{s+1}} F^{0}_{a_{s+1}}\, d\Omega_{s+1} - U^{*}_{a_i\ldots a_s}\Big]. \tag{9}$$

Higher approximations are calculated comparatively easily; the calculations only gradually become more complicated. With the aid of the first approximation for the distribution functions the average "orientational" energy of the crystal is determined up to terms which are proportional to the second degree of α:

$$U_N = \frac{1}{2(4\pi)^2}\sum_{a_i,\,a_j}\int \Phi_{a_i a_j}[F^{0}_{a_i a_j} + \alpha F^{1}_{a_i a_j}]\, d\Omega_i\, d\Omega_j - \\ - \frac{1}{4\pi}\sum_{a_i}\int (\mathbf{P}_{a_i}\cdot\mathbf{E})[F^{0}_{a_i} + \alpha F^{1}_{a_i}]\, d\Omega_i \tag{10}$$

or

$$\overline{U}_N = -\frac{kT}{4\pi}\sum_{a_i}\Big[\beta\int \cos\vartheta_{a_i} F^{0}_{a_i} F^{0}_{a_i}\, d\Omega_{a_i} + \beta\alpha\int \cos\vartheta_{a_i} F^{1}_{a_i}\, d\Omega_i\Big] + \\ + \frac{kT}{32\pi^2}\sum_{a_i,\,a_j}\Big[\alpha\int \Psi_{a_i a_j} F^{0}_{a_i a_j}\, d\Omega_i d\Omega_j + \alpha^2\int \Psi_{a_i a_j} F'_{a_i a_j}\, d\Omega_i\, d\Omega_j\Big]. \tag{10a}$$

After the final calculations the equation, for the mean energy $\overline{U}_N$ is

$$\overline{U}_N = N\bar{u},$$

$$\bar{u} = -kT\beta L(\beta)\Big[1 + \alpha\Big(L^2(\beta) + \frac{2L(\beta)}{\beta} - 1\Big)\sigma_1\Big] + \\ + \alpha\frac{kT}{2}L^2(\beta)\sigma_1 + \alpha^2\frac{kT}{2}\Big\{\Big[L^4(\beta) - \Big(1 - \frac{2L(\beta)}{\beta}\Big)^2\Big]\sigma_2 + \\ + L^2(\beta)\Big(L^2(\beta) + \frac{2L(\beta)}{\beta} - 1\Big)\sigma_4 - \frac{L^3(\beta)}{\beta}\sigma_3 - \frac{L(\beta)}{\beta}\Big(1 - \frac{2L(\beta)}{\beta}\Big)\sigma_6 - \frac{L^2(\beta)}{\beta^2}\sigma_5\Big\}, \tag{11}$$

where $\bar{u}$ is the mean energy per molecule; $L(\beta)$ is Langevin's function; the σ_i are the structural coefficients of the crystalline lattice, defined by

$$\sigma_1 = \sum_{a_i}\gamma_{a_i}/N, \quad \sigma_2 = \sum_{a_i,a_j}\gamma^2_{a_i a_j}/N, \\ \sigma_3 = \sum_{a_i,a_j} 2(\delta_{a_i a_j}\delta_{a_i} + \delta^{+}_{a_i a_j}\delta^{+}_{a_i})/N, \quad \sigma_4 = \sum_{a_i,a_j} 2\gamma_{a_i a_j}/N, \tag{12} \\ \sigma_5 = \sum_{a_i,a_j}(\gamma^{+}_{a_i a_j} + 1/l^3_{a_i a_j})/N, \quad \sigma_6 = \sum_{a_i,a_j} 2(\delta^2_{a_i a_j} + \delta^{+2}_{a_i a_j})/N,$$

where

$$\begin{gathered}\gamma_{a_i a_j} = (1 - 3\cos^2\vartheta_{a_i a_j})/l_{a_i a_j}^{3/2}, \quad \gamma_{a_i} = \sum_{a_j} \gamma_{a_i a_j}, \\ \delta_{a_i a_j} = 3\sin\vartheta_{a_i a_j}\cos\vartheta_{a_i a_j}\cos\varphi_{a_i a_j}/l_{a_i a_j}^{3/2}, \\ \delta_{a_i a_j}^{+} = 3\sin\vartheta_{a_i a_j}\cos\vartheta_{a_i a_j}\sin\varphi_{a_i a_j}/l_{a_i a_j}^{3/2}, \\ \gamma_{a_i a_j}^{+} = (1 - 3\sin^2\vartheta_{a_i a_j})/l_{a_i a_j}^{3/2},\end{gathered} \tag{13}$$

and the angles $\vartheta_{a_i a_j}$ and $\varphi_{a_i a_j}$ in these equations determine the direction of the line of centers of two dipoles a_i and a_j.

The condition of smallness of the principal parameter α is satisfied for a number of dipolar crystals above the temperature of orientational melting, and the expression obtained for the mean energy can be used to calculate the orientational portion of the free energy of a system in connection with the familiar relationship

$$F_N = -T\int \frac{\bar{U}_N}{T^2}\,dT + cT, \tag{14}$$

where c is a constant which is independent of the temperature and which can be determined in a given instance from the requirement that when the interaction is "switched off", F_N coincides with the orientational portion of free energy of the corresponding ideal system. The above equations thus enable us to determine the electrical properties of the system under investigation.

The above theory can be utilized for a semiclassical investigation of the ferromagnetic and antiferromagnetic properties of crystals. For this purpose the energy of a system must be written as

$$H = -\sum_{jk} B_{jk}\mathbf{S}_j\cdot\mathbf{S}_k - g\beta_0 H\sum_i \mathbf{S}_i,$$

where S_i is the spin vector regarded as a classical vector subject to the condition $S_i^2 = \hbar^2 S(S+1)$; β_0 is the Bohr magneton; B_{jk} is twice the exchange integral; g is the Lande factor; and H is the external magnetic field. The parameter α in this case will be

$$\alpha = \frac{BS(S+1)}{kT},$$

where B is the value of the exchange integral for nearest neighbors; it is necessary to set $\Psi_{ij} = l_{ij}\cos\vartheta_{ij}$, where $l_{ij} = 1$ for nearest neighbors and $l_{ij} \ll 1$ for more distant neighbors. This procedure enables us to avoid the "sphericalization" approximation [2,3], which is not amenable to evaluation.

When the inequality

$$\alpha \ll 4\pi \tag{16}$$

is not satisfied it can be seen that a rigorous investigation of the above problems is generally impossible. The results obtained from the superposition approximation and an estimate of its value require separate discussion.

LITERATURE CITED

[1] N. N. Bogoliubov, Problems of Dynamic Theory and Statistical Physics (1946).

[2] B. S. Gourary and R. W. Hart, Phys. Rev. 95, 676 (1954).

[3] M. Lax, Phys. Rev. 97, 629 (1955).

I. Franko L'vovState University

Received October 30, 1955

ANOMALOUS DISPERSION OF LIGHT IN THE SIMPLEST SOLUTIONS OF INORGANIC COMPOUNDS

I. S. Gorban' and A. A. Shishlovskii

(Presented by Academician G. S. Landsberg November 11, 1955)

1. The overwhelming majority of papers on the anomalous dispersion of light are concerned with atomic vapors in which the interaction between individual atoms is small. The observed relationships then have a very simple form and are in comparatively good agreement with theory. The problem of the quantitative correspondence between the theory of dispersion in atomic vapors and experimental observations was solved, as is well known [1], by the classical work of D. S. Rozhdestvenskii and his pupils.

In the condensed state of matter there are broad absorption bands in which the intensity distribution is associated with intermolecular interactions.

In a number of earlier papers [2,3] it was shown that the dispersion curves within isolated absorption bands, such as those of solid films and concentrated solutions of cyanine, fuchsin and certain other dyes, cannot be described by the oscillator functions which are given by the theory for rarefied gases. We also undertook to obtain a mathematical approximation of experimental dispersion curves using a set of oscillator functions, which enabled us to introduce any number of new empirical constants with no limit on arbitrariness. This method was not widely used.

A theory of the dispersion of light in dilute solutions was recently developed by A. S. Davydov [4]. He assumes that the solvent is composed of a set of harmonic oscillators which vibrate normally with respect to fixed equilibrium positions. Under the stimulation of light, the optical transitions of molecules of the solute are accompanied by a change of the vibrational states of the atoms of the solvent.

It was shown that for weak interaction of the intramolecular excitations with the atomic vibrations of the solvent, the dispersion and absorption curves will be described by ordinary oscillator functions – the effect of the solvent reduces to only a shift of the resonance frequency. In the limiting case of strong interaction with the atomic vibrations of the solvent, the shape of the dispersion and absorption curves for small concentrations must be described by functions of the following form:

$$\mu = 1 + \alpha(\nu_0 - \nu)\exp\{-\beta(\nu_0 - \nu)^2\}, \tag{1}$$

$$\varkappa = \alpha \exp\{-\beta(\nu_0 - \nu)^2\}, \tag{2}$$

where μ is the index of refraction; κ is the absorption coefficient; α is a constant which is proportional to the oscillator strength, the concentration and the quantity β; and β is a function of the atomic vibrations of the solvent.

The present paper is an experimental study of the shape of dispersion curves in an absorption band of solid "solutions" for the case of the simplest types (in the sense of molecular structure) of absorption "centers", which are F-centers in alkali halide crystals and the Pb^{++} ions in KBr activated by $PbCl_2$.

2. The measurements were performed by the method described previously [5], which is similar to the method of D. S. Rozhdestvenskii, using a Rayleigh mirror interferometer of our own construction coupled with an ISP-22 quartz spectrograph.

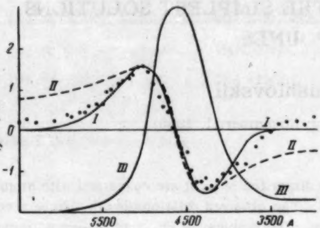

Fig. 1. Dispersion curve in the F-band of an x-irradiated NaCl crystal.

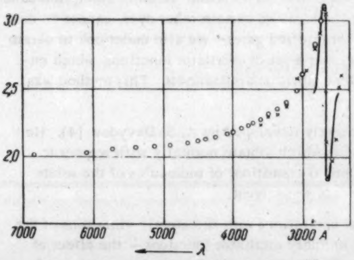

Fig. 2. Dispersion curve in the first ultraviolet band of a "solid solution" of KBr + $PbCl_2$.

A plane parallel slab of rock salt was colored on half of its area by x-rays while the other half (which was shielded by a lead plate) remained transparent. The colored crystal was placed in the interferometer in such a way that one light beam passed through the colored portion while another beam passed through the transparent part. It is clear that the resulting shift of the interference pattern resulted from the presence of F-centers in the path of one of the beams.

The interference pattern in the spectrum was photographed. The zero reference spectral interference pattern of the same specimen was taken before coloring. Interference pattern measurements were performed with a small microscope in the usual manner.

The measurements show that, because of the reduced contrast of the interference pattern in the absorption band, the shape of the dispersion curve can be measured with accuracy not higher than 5-8% of the maximum amplitude of the curve. The position of the interference band is determined with the standard 2-3% accuracy with respect to the separation of neighboring bands. The magnitude of this error agrees approximately with the accuracy which can be claimed for the quantitative results of the above-mentioned theory.

3. Fig. 1 shows the experimental points of the dispersion curve in the F-band of NaCl. The horizontal axis gives the wavelengths and the vertical axis gives the differences between the refractive index and A, which takes into consideration the effect of other absorption bands formed through coloration of the crystal. It is assumed that within the given absorption band A is a constant which is chosen so that for $\nu = \nu_0$, $\mu - A = 0$. The Solid Line I in this figure represents the dispersion curve as calculated from (1). The value of ν_0 corresponds to the absorption band maximum, which is represented by a bell-shaped curve, and the parameters α and β were calculated from the position of the maximum of the experimental dispersion curve. The same figure contains for comparison the dispersion Curve II, which was calculated using the usual oscillator function and with the parameters chosen exactly as for the first case.

It is easily seen from the figure that the experimental results are approximated better by Davydov's equation than by the usual oscillator function. It must be pointed out, however, that there are small discrepancies between experiment and theory, especially in the wings of the dispersion curve. The magnitude of these discrepancies is, to be sure, very close to the errors of measurement, but they are systematic in character. Our measurements for 6 different concentrations of F-centers in NaCl reproduce the nature of these discrepancies. The small asymmetry of the points near the maximum and minimum of the dispersion curve is evidently related to the asymmetry of absorption Curve III in the same figure.

If we use the value of the oscillator strength given in the literature [6] for the NaCl F-band (f = 0.7) we can then calculate the concentration of F-centers from the values obtained for the parameters α and β. The calculation gives by Equation (1) $N = 6.2 \cdot 10^{17}$ centers/cm^3, and with the oscillator function $N = 7.3 \cdot 10^{17}$ centers/cm^3. The discrepancy is of the order of 15%.

A second confirmation of Davydov's theory is provided by the solid solution of $PbCl_2$ in KBr, for which the measurement of the anomalous dispersion of light was performed by Hecht [7]. This author does not attempt to develop his results in any way but advances them as an illustration of the value of his method of measurement, which consists of a Young interferometer and spectral apparatus.

The approximation of Hecht's results which we obtained from (1) is shown in Fig. 2 where the circles and crosses are the measurements of the two experimenters and the theoretical curve is solid. The arrangement of the points on the long wave side of the absorption band is due to the very strong band on the short wave side. However, the discrepancy between experiment and theory cannot be considered large.

Thus, on the basis of the above evidence we may conclude that the final results of Davydov's theory, based on the assumption of strong interaction between the intramolecular excitations of the solute with the vibrations of solvent atoms for the simplest forms of molecular structure of the absorption "centers" within isolated absorption bands, can claim qualitative agreement with experiment.

LITERATURE CITED

[1] D. S. Rozhdestvenskii, Anomalous Dispersion in Metal Vapors (1951).

[2] G. de Metz, Outline of the History of the Anomalous Dispersion of Light to the Present Time (1885).

[3] Van der Plaats, Ann. Physik. 47, 12, 429 (1915).

[4] A. S. Davydov, J. Exptl.-Theoret. Phys. (USSR) 24, 2, 197 (1953); Bull. Acad. Sci. USSR, Phys. Ser. 17, 5 (1953).

[5] I. S. Gorban' and A. A. Shishlovskii, J. Tech. Phys. (USSR) 25, 7 (1955).

[6] S. I. Pekar, Study in the Electron Theory of Crystals (1951).

[7] K. Hecht, Z. Physik. 66, 3, 330 (1930).

T. G. Shevchenko, Kiev State University

Received October 13, 1955

A NEW TYPE OF RELATIVISTICALLY INVARIANT LINEAR EQUATION OF A LOCALIZABLE FIELD

R. S. Ingarden

(Presented by Academician I. E. Tamm November 15, 1955)

We shall examine equations which are not of the type investigated by I. Gel'fand and A. Iaglom [1] but which nevertheless do not violate the three principles which are the basis of the existing theory of elementary particles: 1) the principle of relativistic invariance*, 2) the principle of superposition and 3) the principle of localizability. The idea of our generalization is the consideration of linear differential equations with variable coefficients while rejecting the notion of a free field, i.e., of a field which exists independently of its sources.

Since the only intrinsic relativistic invariant, consisting of the coordinates, is the 4-dimensional distance between two points (interval)

$$s_{12}^2 = -(x_1^\mu - x_2^\mu)(x_1^\mu - x_2^\mu) = -r_{12}^2 + c^2t_{12}^2 \tag{1}$$

($\mu = 1, 2, 3, 4$, $x^4 = ct$) the coefficients of the differential equation can only be functions of quantities of the type of (1). If the localizability of the field is to be conserved, only one of the points x_1, x_2 may be a variable point of the field, while the second point must be interpreted as a given position of a point source of the field.

Thus, for example, the second order equation

$$\left[A(s_{12})\frac{\partial^2}{\partial x_1^\mu \partial x_1^\mu} + B(s_{12})(x_1^\mu - x_2^\mu)\frac{\partial}{\partial x_1^\mu} + C(s_{12})\right]\chi(x_1) = -4\pi a\delta(x_1 - x_2), \tag{2}$$

[A, B, C are arbitrary functions of s_{12}; a is a constant of the same tensor dimensions as χ** – the "charge" of the χ-field; $\delta(x) = \delta(x^1)\,\delta(x^2)\,\delta(x^3)\,\delta(x^4)$] satisfies all the above requirements. If the χ-field is not produced by instantaneously appearing and disappearing point sources but by sources which are distributed in a definite manner in time and space, it is necessary to take a suitable superposition of solutions of equations like Equation (2)***

In order to separate out of (2) the class of the simplest equations, we set up the following additional requirements: 1) the equations must result from the variation principle; 2) they must permit the separation of variables at $a = 0$ and with uniform boundary conditions at infinity; 3) they must have a solution at $a \neq 0$. It is easily seen that the only equation of the type of (2) which satisfies these conditions is

---

*For brevity by "relativistic invariance" we shall understand simultaneous invariance with respect to transformations of the 4-dimensional groups: 1) of rotation, 2) of translation, 3) of inversion of a rectilinear and orthogonal system of coordinates.

**χ and a may have, in general, an arbitrary finite or infinite number of components which are subject to a Lorentz transformation.

***It is important to note that, unlike the case of equations with constant coefficients, different positions of a point source correspond to different right and left ("homogeneous") sides of (2). Therefore the set of equations corresponding to a non-point-source (in the 4-dimensional sense) distribution can be replaced by one integro-differential equation (and not by a differential equation as in the usual theory).

$$\left(\frac{\partial^2}{\partial x_1^\mu \partial x_1^\mu} + \frac{s_{12}^2}{\lambda^4} - \varkappa^2\right)\chi(x_1) = -4\pi a \delta(x_1 - x_2), \tag{3}$$

where λ and $\varkappa$ are constants, λ being positive and

$$\frac{\varkappa^2\lambda^2}{2} \neq \pm 1, \pm 2, \ldots \tag{4}$$

Introducing the dimensionless variables

$$\xi_1 = \frac{x_1^1 - x_2^1}{\lambda}, \quad \xi_2 = \frac{x_1^2 - x_2^2}{\lambda}, \quad \xi_3 = \frac{x_1^3 - x_2^3}{\lambda}, \quad \tau = \frac{x_1^4 - x_2^4}{\lambda} = \frac{c(t_1 - t_2)}{\lambda} \tag{5}$$

and designating $\alpha = \varkappa\lambda$ we obtain from (3)

$$L\chi \equiv \left(\frac{\partial^2}{\partial \xi_1^2} + \frac{\partial^2}{\partial \xi_2^2} + \frac{\partial^2}{\partial \xi_3^2} - \frac{\partial^2}{\partial \tau^2} - \xi_1^2 - \xi_2^2 - \xi_3^2 + \tau^2 - \alpha^2\right)\chi =$$

$$= -\frac{4\pi a}{\lambda^2}\delta(\xi_1)\delta(\xi_2)\delta(\xi_3)\delta(\tau). \tag{6}$$

The eigenfunctions of the operator L which disappear at infinity of space and time, and the corresponding eigenvalues are [2-4]:

$$\chi_{n_1 n_2 n_3 n} = H_{n_1}(\xi_1) H_{n_2}(\xi_2) H_{n_3}(\xi_3) H_n(\tau) e^{-1/2(\xi_1^2 + \xi_2^2 + \xi_3^2 + \tau^2)},$$

$$L\chi_{n_1 n_2 n_3 n} = -2\left(n_1 + n_2 + n_3 - n + 1 + \frac{\alpha^2}{2}\right)\chi_{n_1 n_2 n_3 n}, \tag{7}$$

$$n_1, n_2, n_3, n = 0, 1, 2, \ldots$$

Developing the right hand side of (6) in terms of the functions of (7) we obtain solutions of (6) (see [5]):

$$\chi = \frac{a}{\pi\lambda^2} e^{-1/2(\xi_1^2 + \xi_2^2 + \xi_3^2 + \tau^2)} \times$$

$$\times \sum_{n_1, n_2, n_3, n=0}^{\infty} \frac{(-1)^{n_1+n_2+n_3+n} H_{2n_1}(\xi_1) H_{2n_2}(\xi_2) H_{2n_3}(\xi_3) H_{2n}(\tau)}{\left(n_1 + n_2 + n_3 - n + \frac{1}{2} + \frac{\alpha^2}{4}\right) 2^{2(n_1+n_2+n_3+n)} n_1!\, n_2!\, n_3!\, n!}. \tag{8}$$

Using the relationship of Hermite polynomials and Laguerre polynomials [6] and denoting $n_1 + n_2 + n_3 = m$, we rewrite (8) in the form

$$\chi = \frac{a}{\pi\lambda^2} e^{-1/2(\xi_1^2 + \xi_2^2 + \xi_3^2 + \tau^2)} \times$$

$$\times \sum_{n, m=0}^{\infty} \frac{L_n^{(-1/2)}(\tau^2)}{m - n + \frac{1}{2} + \frac{\alpha^2}{4}} \sum_{n_1+n_2+n_3=m} L_{n_1}^{(-1/2)}(\xi_1^2) L_{n_2}^{(-1/2)}(\xi_2^2) L_{n_3}^{(-1/2)}(\xi_3^2). \tag{9}$$

Using the addition theorem for Laguerre polynomials [7] and denoting $\rho^2 = \xi_1^2 + \xi_2^2 + \xi_3^2$, we obtain from (9):

$$\chi(\rho, \tau) = \frac{a}{\pi\lambda^2} e^{-{}^1/_2 (\rho^2+\tau^2)} \sum_{n,\, m=0}^{\infty} \frac{L_m^{({}^1/_2)}(\rho^2)\, L_n^{(-{}^1/_2)}(\tau^2)}{m - n + \frac{1}{2} + \frac{\alpha^2}{4}}. \tag{10}$$

If a point source of the χ-field existed up to the time of observation t_1 and was in motion in an inertial system, we have from (5) in the system of coordinates in which the source is at rest [6]:

$$\mathrm{X}(\rho) = \lambda \int_0^{\infty} \chi(\rho, \tau)\, d\tau =$$

$$= \sqrt{\frac{\pi}{2}}\, \frac{a}{\lambda}\, e^{-{}^1/_2\rho^2} \sum_{m=0}^{\infty} L_m^{({}^1/_2)}(\rho^2) \sum_{n=0}^{\infty} \frac{(-1)^n (2n-1)!!}{2^n n! \left(m - n + \frac{1}{2} + \frac{\alpha^2}{4}\right)}. \tag{11}$$

If $\alpha \ll 1$, i.e., if $\kappa \ll 1/\lambda$ (and, in particular, if $\kappa = 0$) the right-hand side of (11) may be summed approximately.

We note on the right-hand side that by Stirling's formula for large $\underline{n}$

$$a_n = \frac{(2n-1)!!}{2^n n!} = \frac{(2n)!}{2^{2n}(n!)^2} \approx \frac{1}{e\sqrt{2\pi}} \approx 0{,}142. \tag{12}$$

For the 16 initial n, a_n is equal to [8]: 1; 0.5; 0.375; 0.312; 0.273; 0.246; 0.225; 0.209; 0.196; 0.185; 0.176; 0.168; 0.161; 0.154; 0.149; 0.144.

Assuming that $(e\sqrt{2\pi})^{-1}$ is a sufficiently good approximation of a_n beginning with $n = 1$, we obtain for the sum over $\underline{n}$ in (11) (see [6]):

$$\frac{1}{m + {}^1/_2} + \frac{1}{e\sqrt{2\pi}} \sum_{n=1}^{\infty} \frac{(-1)^{n+1}}{n - m - {}^1/_2} = \frac{1}{m + {}^1/_2} - \frac{G(m + {}^1/_2)}{2e\sqrt{2\pi}} + \frac{1}{e}\sqrt{\frac{\pi}{2}}\,(-1)^m, \tag{13}$$

where $G(x) = \psi\left(\frac{x+1}{2}\right) - \psi\left(\frac{x}{2}\right)$ and $\psi(x) = \frac{d}{dx} \log \Gamma(x)$.

The ratio of the second term of the right-hand side of (13) to the first term tends rapidly towards zero for $m \to \infty$, but for the initial $\underline{m}$ it is −0.111; −0.091; −0.084; .... Therefore, neglecting the second term in (13) we obtain a small increase in the summation over $\underline{n}$ which, to a certain extent, compensates for its previous reduction in magnitude. Finally, for X we obtain (see [6])

$$\mathrm{X}(\rho) = \frac{\pi a}{\sqrt{2}\lambda} \left(\frac{e^{-{}^1/_2\rho^2}}{\rho} + \frac{1}{4e} \right). \tag{14}$$

The second term in (14) is obtained by a passage to the limit [6]*

---

*It must be noted that the series (15) is not convergent but only summable (for example, according to Abel' [9], since for large $\underline{m}$ this series can be represented as

$$(e\rho\sqrt{2\pi})^{-1} \exp\left(\frac{\rho^2}{2}\right) \Sigma (-1)^m \sqrt{m} \sin(2\rho\sqrt{m}).$$

$$\sum_{m=0}^{\infty} (-1)^m L_m^{(1/2)}(\rho^2) = \lim_{z \to -1} \sum_{m=0}^{\infty} z^m L_m^{(1/2)}(\rho^2) = \lim_{z \to -1} (1 - z^{-3/2})\, e^{\frac{\rho^2 z}{1-z}} = \frac{e^{1/2\,\rho^2}}{2^{3/2}}. \qquad (15)$$

If X is interpreted as the potential of some force field produced by a point source, the constant term in (14) will have no meaning and may be dropped.

Thus, assuming $r = \lambda\rho$, we obtain the following form for the "elementary law" of this potential:

$$X(r) = \text{const} \cdot \frac{e^{-r^2/2\lambda^2}}{r}. \qquad (16)$$

Although (16) is approximate, the character of the singularity for $r = 0$ was obtained correctly, as follows from an examination of (3) for $s_{12} \ll \lambda$.

If $\alpha \gg 1$, i.e., if $\kappa \gg 1/\lambda$, at distances s_{12} of the order of λ (where χ is considerably different from zero) we can neglect the second term in (13) by comparison with the third term and instead of (16) we obtain the Yukawa potential

$$X(r) = \text{const} \cdot \frac{e^{-\varkappa r}}{r}.$$

The author is deeply grateful to I. M. Lifshits, L. M. Piatigorskii and A. Ia. Povzner and to members of the staff of the Physico-Technical Institute of the USSR Academy of Sciences in Kharkov, where the present work was done, for helpful discussions and valuable advice and comments.

LITERATURE CITED

[1] I. Gel'fand and A. Iaglom, J. Exptl.-Theoret. Phys. (USSR) 18, 703 (1948).

[2] V. L. Ginzburg and I. E. Tamm, J. Exptl.-Theoret. Phys. (USSR) 17, 227 (1947).

[3] H. Yukawa, Phys. Rev. 91, 415, 416 (1953).

[4] M. Markov, Doklady Akad. Nauk SSSR 101, 51 (1955).

[5] D. Ivanenko and A. Sokolov, Classical Field Theory (Moscow, 1951).

[6] A. Erdelyi, Higher Transcendental Functions (N. Y., 1953), Vols. 1 and 2.

[7] W. Magnus and F. Oberhettinger, Formeln und Sätze für die speziellen Funktionen der mathematischen Physik (Berlin, 1948).

[8] I. M. Ryzhik and I. S. Gradshtein, Tables of Integrals, Sums, Series and Products (Moscow, 1951).

[9] G. Hardy, Divergent Series (Moscow, 1951).

B. Berut Vrotslav University and Physics Institute,
Academy of Sciences, Polish People's Republic

Received November 10, 1955

A GRAPHICAL METHOD OF CALCULATION FOR MULTILAYER FILMS

P. G. Kard

(Presented by Academician G. S. Landsberg November 11, 1955)

The analytic method of calculating for multilayer films at present lacks the desired generality. The most important results are the equation of Sukhanovskii [1] and its generalization by the author of the present article. However, these equations are restricted firstly to dielectric films and secondly to two-component films. However, multicomponent films which may possibly contain thin metal layers are of decided interest. But since an analytic calculation is evidently extremely complicated in the most general case, it is appropriate to propose a very simple graphical method of maximum generality.

Let us consider any multilayer film T_k (see Fig. 1), bounded by media with refractive indices n_k (above) and n_0 (below). We assume at first that the upper medium is a dielectric but impose no restrictions on the lower medium and the composition of the film T_k (except isotropy). Let r_k be the reflection coefficient of the amplitude of a plane wave impinging on the film T_k from above at angle ϑ_k.

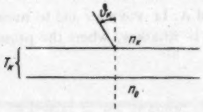

Fig. 1.

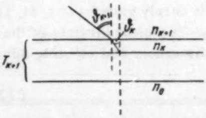

Fig. 2

We also bound the upper medium by a plane surface parallel to the film (Fig. 2) so that to the film there is added from above a new layer of thickness d_k, and above this surface we now place a dielectric medium with refractive index n_{k+1}. The new film thus produced is designated as T_{k+1}.

Now from the (k + 1)th medium, let a plane light wave impinge on T_{k+1} at angle ϑ_{k+1} in such a way that in the kth medium the angular direction of the light remains ϑ_k. The amplitude reflection coefficient from T_{k+1} under these conditions will be given as r_{k+1}.

In order to express r_{k+1} in terms of r_k, we shall consider T_{k+1} to be an ordinary plane parallel plate bounded above by the interface between the kth and (k + 1)th media and below by the film T_k. Since in the calculation of r_{k+1} neither the thickness of T_k nor its structure will play a part, but only the amplitude reflection coefficient from T_k will be important, it is actually correct to regard T_{k+1} as a plane parallel plate. If a_k is the amplitude reflection coefficient on the boundary between the (k+1)th and kth media, and b_k is the amplitude transmission coefficient (so that $a_k^2 + b_k^2 = 1$) when a plane wave of unit amplitude impinges on T_{k+1} we can (considering multiple reflection on the upper plane and on T_k) represent the reflected wave as a superposition of waves with amplitudes

$$a_k, \quad b_k^2 r_k e^{2i\delta_k}, \quad -a_k b_k^2 r_k^2 e^{4i\delta_k}, \quad a_k^2 b_k^2 r_k^3 e^{6i\delta_k}, \ \ldots,$$

where

$$\delta_k = k_0 n_k d_k \cos\vartheta_k \tag{1}$$

and k_0 is the wave number in a vacuum. Consequently,

$$r_{k+1} = a_k + b_k^2 r_k e^{2i\delta_k} - a_k b_k^2 r_k^2 e^{4i\delta_k} + \ldots$$

or

$$r_{k+1} = \frac{a_k + r_k e^{2i\delta_k}}{1 + a_k r_k e^{2i\delta_k}}. \tag{2}$$

This is the basic formula. In deducing it we assumed that the kth (and also the (k + 1)th) medium is a dielectric. But it is correct even without this limitation. Equation (2) could have been derived differently – on the basis of the boundary conditions for the field vectors on all interfaces. This procedure would have been very much more complicated, but the result would certainly have been the same. The initial assumptions now clearly drop out. In fact, the boundary conditions for complex ϑ_k $\left(\text{a metal layer or total reflection: } \frac{n_{k+1}\sin\vartheta_{k+1}}{n_k} > 1\right)$ and complex $\underline{n}$ (metal layer) and also for complex ϑ_{k+1} and n_{k+1} keep the same form as when they are real; consequently Equation (2) which is derived from them (although we obtained it differently) should preserve the same form. The only difference will lie in the fact that in this equation δ_k and a_k will be complex quantities like r_k.

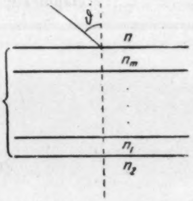

Fig. 3

Thus (2) is of universal applicability, as can be shown by its direct derivation from the boundary conditions. Although the method which we use to obtain (2) cannot be applied generally, the result is correct, as we have proved, without any limitations at all.

Equation (2) is a recursion formula. If we have a film T of $\underline{m}$ layers (Fig. 3) with refractive indices n_1, n_2, ..., n_m, with a medium of refractive index n_0 below and one of index $\underline{n}$ above, for the amplitude reflection coefficient of light which is incident on T at angle ϑ we have:

$$r = \frac{a_m + r_m e^{2i\delta_m}}{1 + a_m r_m e^{2i\delta_m}},$$

with

$$r_m = \frac{a_{m-1} + r_{m-1} e^{2i\delta_{m-1}}}{1 + a_{m-1} r_{m-1} e^{2i\delta_{m-1}}}$$

etc.; finally,

$$r_2 = \frac{a_1 + r_1 e^{2i\delta_1}}{1 + a_1 r_1 e^{2i\delta_1}}$$

and

$$r_1 \equiv a_0.$$

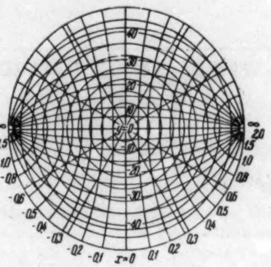

Fig. 4.

It is easy in principle to eliminate from these recursion formulas the indices $r_2, r_3, \ldots, r_m$ and to express $\underline{r}$ only in terms of $a_0, a_1, \ldots, a_m$ and $\delta_1, \delta_2, \ldots, \delta_m$ (or, alternatively, in terms of $n_0, n_1, \ldots, n_m, \underline{n}$ and $d_1, d_2, \ldots, d_m$). Thus, the amplitude reflection coefficient of the given film depends only on $a_0, a_1, \ldots, a_m$ and $\delta_1, \delta_2, \ldots, \delta_m$.

However, this elimination procedure is not advantageous in general since it would lead to a complicated expression. The successive calculation of $r_2, r_3, \ldots, r_m, \underline{r}$ from the recursion formulas is also laborious. On the other hand, we can point to the following very simple graphical method of successive derivation of these quantities.

The conformal representation of the complex plane

$$w = \text{th}\, z, \quad z = x + yi, \quad w = u + vi \tag{3}$$

transforms the Cartesian coordinate system in the z-plane into a system of bipolar coordinates in the w-plane:

$$(u - \text{cth}\, 2x)^2 + v^2 = \frac{1}{\text{sh}^2\, 2x}, \quad u^2 + (v + \text{ctg}\, 2y)^2 = \frac{1}{\sin^2 2y}. \tag{4}$$

Figure 4 shows this coordinate system inside the unit circle, together with the system of ordinary polar coordinates.

This kind of double coordinate system serves to give the magnitudes of $r_2, r_3, \ldots, r_m, \underline{r}$ graphically. Setting

$$a_k = \text{th}\, \alpha_k, \quad r_k e^{2i\delta_k} = \text{th}\, \rho_k, \tag{5}$$

we will have

$$r_{k+1} = \text{th}\, (\alpha_k + \rho_k). \tag{6}$$

From these equations it can be seen that a_k $(k = 0, 1, \ldots, m)$, r_k and $r_k e^{2i\delta_k}$ $(k = 1, 2, \ldots, m)$ may be represented by points in the complex plane $\underline{w}$, using polar coordinates. But the bipolar coordinates serve to obtain r_{k+1} from (6). r_{k+1} is the point in the graph whose bipolar coordinates are the sums of the bipolar coordinates of the points a_k and $r_k e^{2i\delta_k}$. From r_{k+1} one then finds $r_{k+1} e^{2i\delta_{k+1}}$. If δ_{k+1} is real (an ordinary dielectric layer), multiplication by $e^{2i\delta_{k+1}}$ is accomplished simply by rotation through an angle $2\delta_{k+1}$. If δ_{k+1} is complex, multiplication by $e^{2i\delta_{k+1}}$ is somewhat more complicated but still remains an easily accomplished operation.

Thus, in order to carry out a graphical calculation of the given multilayer film, i.e., to obtain the reflection coefficient at a given angle of incidence ϑ, one must:

1) calculate the angles of refraction $\vartheta_0, \vartheta_1, \ldots, \vartheta_m$;

2) calculate (by Fresnel's equation) the amplitude reflection coefficients $a_0, a_1, \ldots, a_m$ between adjoining media;

3) calculate $\delta_1, \delta_2, \ldots, \delta_m$ from (1);

4) plot on the graph the points $a_0 \equiv r_1, a_2, a_3, \ldots, a_m$;

5) obtain successively, as explained above, r_2, $r_2e^{2i\delta_2}$, r_3, $r_3e^{2i\delta_3}$, r_m, $r_me^{2i\delta_m}$, $\underline{r}$. Obviously, all these points will be inside the unit circle since $|r_k| \leq 1$ and $|r_ke^{2i\delta_k}| \leq 1$. The square of the distance of the last point from the origin is then equal to the desired reflection coefficient: $R = |r^2|$.

LITERATURE CITED

[1] V. V. Sukhanovskii, Doklady Akad. Nauk SSSR 95, 2 (1954).

Received July 19, 1955

A LOW PRESSURE DIFFUSION CHAMBER

Academician A. P. Komar, M. V. Stabnikov and D. A. Iashin

In recent times diffusion chambers have been rendering Wilson cloud chambers obsolete in nuclear laboratories, especially in work with beams of photons or charged particles from accelerators.

The products of nuclear reactions from the irradiation of nuclei with photons or charged particles up to 100 Mev are usually observed with energies not higher than 10-15 Mev and with a small range in the chamber at atmospheric pressure. When the usual magnetic field strength up to 20,000 oersted is used the radii of curvature of the tracks are very large and difficult to determine both because of the smallness of the deflection and because of Coulomb scattering of the reaction products (protons, deuterons or alpha particles). This makes it difficult to identify the particles which are the reaction products. The literature contains many different designs of diffusion chambers [1,2], but all of these chambers are unsuitable for the analysis of low energy nuclear reaction products. In work with gamma beams in chambers at atmospheric pressure and higher, there is an additional complicating circumstance: the strong background due to pair electrons and positrons. It is very important to eliminate this background.

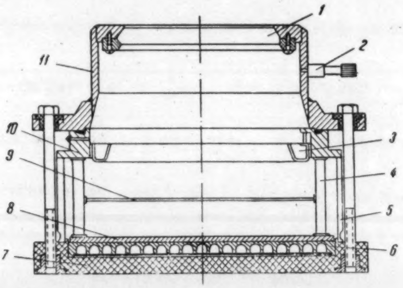

Fig. 1. 1) upper glass; 2) valve; 3) ring-shaped trough filled with methyl alcohol which is continuously replaced by a small electromagnetic piston pump; 4) lateral glass cylinder; 5) plastic ring to prevent sweating of glass cylinder; 6) refrigerator - copper spiral tube containing flow of cold nitrogen directly from Dewar; rate of flow 2 liters per hour; 7) bottom of chamber made of textolite to reduce transfer of heat from surrounding medium; red copper disk to eliminate temperature nonuniformity; 9) ring for application of clearing electric field; 10) intermediate brass ring with thermocouple leads; 11) upper part of brass housing of chamber

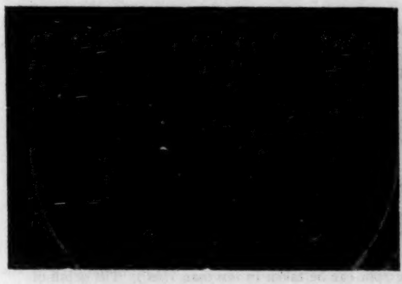

Fig. 2

Fig. 3

Fig. 4

Our laboratory has constructed a diffusion chamber of 30 cm diameter with which it is easily possible to discriminate particle tracks, to remove the pair background and the effect of Coulomb scattering and also obtain a long range for low energy charged particles. All of this is attained principally by lowering the pressure of the mixture of vapor and air in the chamber and partly by regulating the supply of operating substance in the chamber.

We are acquainted with but one paper on a low pressure chamber, although it is difficult to use the information contained therein for our purposes [3]. In our chamber by the choice of suitable pressure and regulation of the vapor supply, in the sensitive region of the chamber it is possible to discriminate particles of different ionizing ability. We believe that our experience may be useful in other laboratories.

Figure 1 gives the design of our chamber.

At a pressure of about 30 mm in a mixture of methyl alcohol and air, the temperature difference between the bottom and top of the chamber is 46° (−4° above and −50° below). By observing the dimensions of the region of impoverished vapor around a track (the black border around the bright tracks in Fig. 2) particles may be distinguished by ionization.

As an illustration of the possibilities of a low pressure chamber, the tracks of electron-positron pairs are shown; in Fig. 2 these were obtained with a chamber at atmospheric pressure, and in Fig. 3 with a chamber at low pressure.

In Fig. 2 the tracks of pairs clearly outline the shape of a beam of 100 Mev gamma rays from a synchrotron. The center of this photograph also shows bright tracks of alpha particles from a specimen of thorium "B" with a maximum energy of 8.7 Mev. The dark regions around the bright tracks of these particles are regions that are impoverished in methyl alcohol vapor as a result of the formation of droplets comprising the tracks.

The same photograph shows thinner bright tracks of photoprotons which lack a dark border and are easily distinguished from alpha particle tracks.

Figure 3 shows tracks obtained under the same conditions of synchrotron operation using a low pressure chamber (30 mm). The weak pair background is barely noticeable, and then only in the lower portion of the photograph, i.e., it is practically nonexistent, but the bright proton track is very clearly distinguishable through almost the entire chamber without a dark border.

Figure 4 shows a photograph obtained under the same conditions of synchrotron operation, as for Fig. 3, of alpha particle tracks from a specimen of thorium "B" with sufficient supply of alcohol to the chamber. Around these tracks there is no dark border. The track length is considerably greater than in the photograph of Fig. 2; the tracks are straight, i.e., there is practically no Coulomb scattering of alpha particles.

The above facts show that our chamber is a reliable instrument for the identification of charged particles which are products of photonuclear reactions and for the determination of their momenta when the chamber is placed in a magnetic field. It should be noted that at low pressures the tracks very quickly diffuse, thus making it possible to increase the number of photographs (photographs can be taken in less than 1 sec). The depth of the working region under optimum conditions at a pressure of about 30 mm is 20 mm ; at atmospheric pressure it reaches up to 100 mm.

LITERATURE CITED

[1] V. K. Liapidevskii and Iu. A. Shcherbakov, J. Exptl.-Theoret. Phys. (USSR) 27, 103 (1954).

[2] M. Snowden, Progress in Nuclear Physics (London, 1953) Vol. 3.

[3] W. J. Choyke and C. E. Nielsen, Rev. Sci. Instruments 23, 307 (1952).

Leningrad Physico-Technical Institute,
Academy of Sciences USSR

Received July 20, 1955

AN UNUSUAL COSMIC RAY BURST

A. I. Kuz'min, G. V. Skrypin, G. V. Tianutova and Iu. G. Shafer

(Presented by Academician D. V. Skobel'tsyn March 5, 1956)

On February 23, 1956 at 3:45 Greenwich time in Yakutsk (51° north geomagnetic latitude and longitude, 129° east, 101 m above sea level) three continuously operating instruments recorded an extraordinarily large burst of hard cosmic rays.*

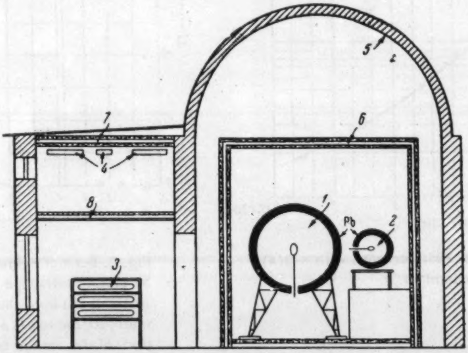

Fig. 1. Arrangement and characteristic features of the recording apparatus at the cosmic ray station of the Yakutsk branch of the USSR Academy of Sciences. 1) ASK-1 ionization chamber with compensation of average cosmic ray ionization, volume 1000 liters, filled with argon at 10 atm, screened by 12 cm of Pb; 2) S-2 ionization chamber similar to ASK-1, volume 20 liters, filled with argon at 50 atm, screened by 12 cm Pb; 3) Crossed telescopes for recording of hard component I vertically and at 30° to the vertical from the south and north; 4) Two identical counting units for recording of extensive air showers with density of 25 particles/m^2 (triple coincidence) and 50 particles/m^2 (sextuple coincidence); 5) Brick roof 50 cm thick (100 g/cm^2); 6) Cover of thermostat cage (8 g/cm^2); 7) Roof (2 g/cm^2); 8) Ceiling (8 g/cm^2)

---

*Hereafter the intensity of the hard component will be designated by I.

The ASK-1 and S-2 ionization chambers (whose arrangement and features are shown in Fig. 1) recorded a sudden increase of I of 200% above its average value. The crossed counter telescopes also recorded a 200% increase in the vertical direction above the mean diurnal value, and from the north and south (at 30° to the vertical) by 165% and 190%, respectively (Figs. 2 and 3).

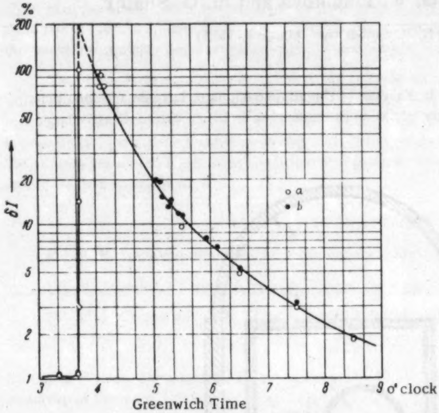

Fig. 2. Burst of February 23, 1956 recorded with S-2(a) and ASK-1 (b) ionization chambers.

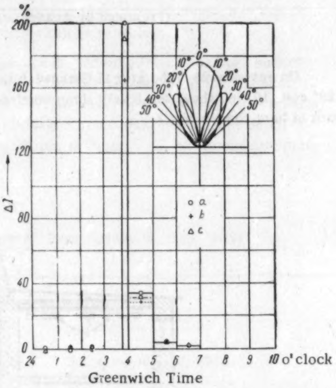

Fig. 3. Burst of February 23, 1956 recorded by crossed telescope counting units: (a) vertical; (b) from the north; (c) from the south. At the top is a diagram of the directions of the crossed telescope unit.

Two automatic continuously operating units for the recording of extensive air showers with densities of 25 and 50 particles per square meter did not register any increase of shower frequency during the burst of I.

Five hours after the burst the oscillations of total I gradually diminished to the magnitude of the ordinary variations observed at Yakutsk during this period. The decline of I as measured by the counter telescopes was steeper.

At the instant of the burst, and during the following 24 hours, the earth's magnetic field was quiet; only a few pulses of N-components were recorded. The atmospheric pressure in Yakutsk on February 23 and 24 showed almost no change. Meteorological radiosounding of the atmosphere above Yakutsk showed a sudden temperature rise of 10° at 50 millibars.

On February 23 at 4 o'clock Greenwich time (13 o'clock local Yakutsk statutory time) the ionospheric station in the cosmic ray laboratory of the Yakutsk branch Academy of Sciences of the USSR recorded total absorption of 2-7 megacycle radio waves (vertical sounding). Thus, the burst was accompanied on the sunlit side of the earth by a considerable Dellinger effect which, during this period, cut off all radiocommunication throughout the Yakutsk ASSR.

This strong ionospheric disturbance was caused by an unprecedented solar flare which was larger than any of the four previous similar bursts of solar activity accompanied by increased I – on February 28 and March 7, 1942; on July 25, 1946 and on November 19, 1949 [1].

The 200% increase of I vertically and the considerable rise of cosmic radiation from the south, as well as the analysis of other experimental data, show that the burst of I was caused by particles of solar origin with energies of $10^9 - 10^{10}$ ev.

We are indebted to Corresponding Member of the USSR Academy of Sciences Professor S. N. Vernov for his continued assistance and interest.

LITERATURE CITED

[1] D. D. Krasil'nikov, A. I. Kuz'min, and Iu. G. Shafer, Trans. Yakutsk Branch Acad. Sci. USSR, Phys. Ser. 1955, No. 1, 42.

Yakutsk Branch,
USSR Academy of Sciences

Received March 5, 1956

GROUND STATE OF AN ANTIFERROMAGNET BY THE METHOD OF ELEMENTARY EXCITATIONS

S. V. Tiablikov and A. Ts. Amatuni

(Presented by Academician N. N. Bogoliubov December 14, 1955)

We consider an antiferromagnet whose magnetic ions are arranged in layers in such a way that the magnetic moments of the ions in any one layer are parallel to each other and antiparallel to the magnetic moments of ions in adjoining layers. This distribution of the magnetic moments, which was first suggested by L. D. Landau [1], has been observed through neutronographic investigations of the last few years, when the crystal structure of an antiferromagnet is considered from the point of view of very tight packing.

Assuming that there is one s-electron to each magnetic ion, the Hamiltonian of the system of electrons can be written as

$$\hat{\mathcal{H}} = -\frac{1}{2}\sum_{(f_1f_2)} J(f_1f_2)\,\hat{S}_{f_1}\cdot\hat{S}_{f_2} - \frac{1}{2}\sum_{(g_1g_2)} J(g_1g_2)\,\hat{S}_{g_1}\cdot\hat{S}_{g_2} - \sum_{(fg)} J(fg)\,\hat{S}_f\hat{S}_g - \\ - \sum_{(f\alpha)} \mu_\alpha H_A^\alpha \hat{S}_f^\alpha + \sum_{(g,\alpha)} \mu_\alpha H_A^\alpha \hat{S}_g^\alpha - \sum_{(f,\alpha)} \mu_\alpha H^\alpha \hat{S}_f - \sum_{(g,\alpha)} \mu_\alpha H^\alpha \hat{S}_g^\alpha. \tag{1}$$

Here the index f is used to number the magnetic ions in even layers, while g refers to odd layers; $\alpha = x, y, z$; $J(f_1, f_2) > 0$, $J(g_1g_2) > 0$ and $J(fg) < 0$ are "exchange integrals"*; H^α is the component of the external magnetic field; H_A^α is the component of the phenomenologically introduced "anisotropy field" (the anisotropy is calculated similarly in Zeeman's work [2]). The inequality $\mu_\alpha H_A^\alpha \ll \frac{1}{N}\sum_{(fg)} J(fg)$, where N is assumed, where N is the total number of magnetic ions in even (odd) layers.

The ground energy level E_0 of the operator (1) by the method of elementary excitations [3,4] is obtained in a quasiclassical scheme as the minimum of (1) in which the spin operators $\hat{S}_f^\alpha$ and $\hat{S}_g^\alpha$ are replaced by the classical vectors σ_f^α and σ_g^α with the supplementary normalization condition $\vec{\sigma}_f^2 = 1$, $\vec{\sigma}_g^2 = 1$. It is known that this determination of the ground state E_0 agrees with its determination by Fok's variational method [3,4].

Let us consider a specific case in which the field H_A is oriented along the Oz axis, the direction of which is chosen to be that of the mean magnetic moment of the ions in the absence of an external field. We shall assume that the values of the vectors $\vec{\sigma}_f$ are identical for all ions and are equal to $\vec{\sigma}_1$ (similarly $\vec{\sigma}_g = \vec{\sigma}_2$).

In the case of an external field H, parallel to the anisotropy axis Oz, we have the following solutions of the problem of a conventional minimum of the ground state.

The case $0 \leqslant \mu_{\parallel} H \leqslant (2\mu_{\parallel} H_A J)^{1/2}$ of "weak" external fields is:

$$\frac{1}{N}E_0 = -\frac{1}{2}(\bar{J}_{11} + \bar{J}_{22} - 2\bar{J}_{12}) - 2\mu_{\parallel} H_A, \tag{2}$$

$$\sigma_1^z = 1; \quad \sigma_2^z = -1; \quad \sigma_1^x = \sigma_2^x = \sigma_1^y = \sigma_2^y = 0. \tag{3}$$

---

*J(fg) may be an indirect exchange integral.

Here the following notation is introduced:

$$\sum_{(f_1f_2)} J(f_1 f_2) = N\bar{J}_{11}; \quad \sum_{(g_1g_2)} J(g_1g_2) = N\bar{J}_{22}; \quad \sum_{(fg)} J(fg) = N\bar{J}_{12}; \quad \bar{J} = |\bar{J}_{12}|. \tag{4}$$

The case of "intermediate" external fields $(2\mu_{\parallel}H_AJ)^{1/2} \leqslant \mu_{\parallel}H \leqslant 2J$: is:

$$\sigma_1^{x,y} = -\frac{H-H_A}{H+H_A}\sigma_2^{x,y}; \quad \sigma_{1,2}^z = -\frac{\mu_{\parallel}(H\mp H_A)}{2\bar{J}_{12}} \mp \frac{2HH_A\bar{J}_{12}}{(H^2-H_A^2)(H+H_A)}; \tag{5}$$

$$\frac{1}{N}E_0 = -\frac{1}{2}(\bar{J}_{11}+\bar{J}_{22}-2\bar{J}_{12}) + \frac{2H_A^2\bar{J}_{12}}{(H^2-H_A^2)} + \frac{\mu_{\parallel}^2(H^2-H_A^2)}{2\bar{J}_{12}}. \tag{6}$$

The case of "strong" external fields $\mu_{\parallel}H \geqslant 2J$: is:

$$\sigma_{1,2}^z = 1; \quad \sigma_{1,2}^{x,y} = 0; \tag{7}$$

$$\frac{1}{N}E_0 = -\frac{1}{2}(\bar{J}_{11}+\bar{J}_{22}-2\bar{J}_{12}) - 2\bar{J}_{12} - 2\mu_{\parallel}H. \tag{8}$$

When the external magnetic field H is perpendicular to the anisotropy axis (oriented, let us say, along the Ox axis) and is not very large: $\mu_{\perp}H \ll 2J$*, we will have for the ground state:

$$\sigma_1^x = \sigma_2^x \approx -\frac{\mu_{\perp}H}{2\bar{J}_{12}}; \quad \sigma_1^z = -\sigma_2^z \approx 1 - \frac{\mu_{\perp}^2H^2}{8\bar{J}_{12}^2};$$

$$\frac{1}{N}E_0 \approx -\frac{1}{2}(\bar{J}_{11}+\bar{J}_{22}-2\bar{J}_{12}) - 2\mu_{\perp}H_A + \frac{\mu_{\perp}^2H^2}{2\bar{J}_{12}}. \tag{9}$$

Determining the magnetization of the antiferromagnet in the ground state by the equation

$$M^0 = -\frac{\partial E_0}{\partial H}, \tag{10}$$

we obtain:

$$M_{\parallel}^0 = 0 \qquad \text{for} \quad 0 \leqslant \mu_{\parallel}H_{\parallel} \leqslant (2\mu_{\parallel}H_AJ)^{1/2} \equiv \mu_{\parallel}H_n; \tag{11}$$

$$M_{\parallel}^0 = \frac{N\mu_{\parallel}^2}{J}H_{\parallel}\left[1-\left(\frac{H_n}{H_{\parallel}}\right)^4\right] \qquad \text{for} \quad H_n \leqslant H_{\parallel} \leqslant \frac{2J}{\mu_{\parallel}}; \tag{12}$$

$$M_{\perp}^0 \simeq \frac{N\mu_{\perp}^2}{J}H_{\perp} \qquad \text{for} \quad 0 \leqslant \mu_{\perp}H_{\perp} < 2J. \tag{13}$$

---

*When $\mu H \gg 2J$ the solution is given by (8).

These expressions for the parallel and perpendicular magnetization are in satisfactory agreement with the measurements of Van den Handel, Gijsman and Poulis [5] of the dependence of the magnetization of single crystals of $CuCl \cdot 2H_2O$ on the field H at 1.59° K. The curves of (11-13) approximately reproduce the experimental relationships ([5], Fig. 2) if from the threshold value of the field $H_n = 6500$ oersteds indicated in [5] and from the slope of the straight line $M^0_\perp(H)$ given by $N\mu_\perp^2/J = 1.52 \cdot 10^{-4}$, we determine the constants $J \approx 2.5 \cdot 10^{-15}$ erg and $H_A \simeq 82$ oersteds, setting $\mu_\perp = 1.01\,\mu_B$, $\mu_\parallel = 1.09\,\mu_B$ [6] and $N \simeq 4.5 \cdot 10^{21}$ cm^{-3}.

As can be seen from Fig. 1 at $H_n = 5000$ oerst, there is better agreement of the calculated equations with experiment.

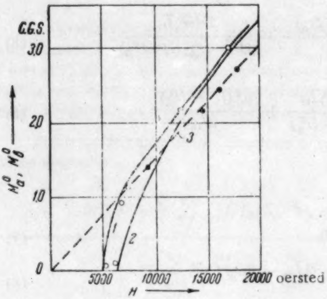

Fig 1. 1) $M^0_\parallel = M^0_a(H)$. $H_n = 5000$ oersted; 2) $M^0_\parallel = M^0_a(H)$, $H_n = 6500$ oersted; 3) $M^0_\perp = M^0_b(H)$, $\mu_a = 1.09\,\mu_B$, $\mu_b = 1.01\,\mu_B$.
The dots are the corresponding experimental data at T = 1.59° K.

Furthermore when the field H forms an arbitrary angle θ with the anisotropy axis, it is easy to obtain from (11-13) the dependence of the magnetization $M^0 = \{(M^0_\parallel)^2 + (M^0_\perp)^2\}^{1/2}$ on the field H and the angle θ. There are two cases:

1) $\mu_\parallel H \leqslant (2\mu_\parallel H_A J)^{1/2}$, i.e., $H \leqslant H_n$; then $M^0_\parallel = 0$ by (11) and

$$M^0 = M^0_\perp = \frac{N\mu_\perp^2}{J} H_\perp = \frac{N\mu_\perp^2}{J} H \sin\theta \tag{14}$$

for any angle θ.

2) $\mu_\parallel H \geqslant (2\mu_\parallel H_A J)^{1/2}$, i.e., $H \geqslant H_n$.

We determine a certain critical angle θ_{cr} by the equation

$$\cos\theta_{cr} = \frac{(2\mu_\parallel H_A J)^{1/2}}{\mu_\parallel H} = \frac{H_n}{H}, \quad 0 \leqslant \theta_{cr} \leqslant \frac{\pi}{2}. \tag{15}$$

We now have from (11 - 13):

a) for $\theta \geq \theta_{cr}$

$$M^0 = M^0_\perp = \frac{N\mu_\perp^2}{J} H \sin\theta; \tag{16}$$

b) for $0 \leqslant |\theta| \leqslant \theta_{cr} < \frac{\pi}{2}$

$$M^0 = \frac{N\mu_\parallel^2}{J} H \left\{1 - \left[1 - \left(\frac{\mu_\perp}{\mu_\parallel}\right)^4\right] \sin^2\theta - \frac{2}{\cos^2\theta}\left(\frac{H_n}{H}\right)^4 + \frac{1}{\cos^6\theta}\left(\frac{H_n}{H}\right)^8\right\}^{1/2}. \tag{17}$$

(14-17) agree fairly well qualitatively with experiment [5]; it should be noted that the changes in [5] took place at 2.1° K, while (14-17) are strictly speaking correct for T ≃ 0° K.

The agreement of the theoretical and experimental results is an argument for the correctness of the determination of the ground state by the method of elementary excitations. In the calculations of Holstein-Primakoff and Kramers-Heller [6] the ground state is determined by (3) which, as we have seen, is the lowest state only in weak external fields $H \leq H_n$. This always leads, in particular, to the vanishing of the parallel magnetic susceptibility for $T \to 0$. It is easily seen, however, from (12) that $\varkappa_\parallel \neq 0$ for T = 0 and $H > H_n$, which agrees with the experiments of Poulis and Hardeman [7].

We note that results similar to the above were obtained phenomenologically by Neel [8], Gorter and Haantjes [9], and Nagamija [6], and by K. B. Vlasov [10] by the method of energetic centers of gravity.

The present article gives the results of the zeroth approximation by the method of elementary excitations (approximate second quantization).

The authors take this opportunity to acknowledge their indebtedness to D. N. Zubarev for discussions.

LITERATURE CITED

[1] L. D. Landau, Physik. Z. Sowjetunion 4, 675 (1933).

[2] J. M. Ziman, Proc. Phys. Soc. (London) A65, 541 (1952).

[3] N. N. Bogoliubov, Lectures on Quantum Statistics (Kiev, 1949).

[4] N. N. Bogoliubov and S. V. Tiablikov, J. Exptl.-Theoret. Phys. (USSR) 19, 251, 256 (1949).

[5] J. Van den Handel, H. M. Gijsman, and N. J. Poulis, Physica 18, 862 (1952).

[6] T. Nagamija, K. Yosida, R. Kubo, Advances in Phys. 4, 1 (1955).

[7] N. J. Poulis and G. E. G. Hardeman, Physica 18, 315 (1952).

[8] L. Neel, Ann. Physik 5, 232 (1936).

[9] C. J. Gorter and J. Haantjes, Physica 18, 285 (1952).

[10] K. B. Vlasov, Bull. Acad. Sci. USSR, Phys. Ser. 18, 339 (1954).

V. A. Steklov Mathematics Institute,
Academy of Sciences of the USSR

Received November 15, 1955

VISUALIZATION OF AERODYNAMIC STREAMLINE FLOW AROUND AXIALLY SYMMETRICAL BODIES THROUGH THE USE OF A FLAT LAYER OF COLORED GAS

A. A. Iuzefovich, D. N. Mirshanov and Iu. A. Dunaev

(Presented by Academician L. A. Artsimovich November 17, 1955)

For the investigation of density distribution in compressed currents, there exist many methods of photographing the flow patterns. All of these methods have their advantages and no single method can be entirely replaced by another. But the majority of the existing methods are unsuitable in their usual form for the quantitative determination of density distribution in a flow of gas around a solid of rotation. The most exact measurements of flow density around an axially symmetrical body are accomplished by interferometry, but even here in order to obtain the density distribution pattern in the plane of symmetry of the current, it is necessary to go through a very complicated and laborious mathematical treatment of the spatial flow pattern.

In this connection we have attempted to alter the so-called "absorption method" (which employs absorption of ultraviolet and soft x-rays and of electrons by the gas) so that by using the visible portion of the spectrum we may obtain not a photograph of the spatial flow pattern but a representation of only the thin layer of gas lying in the principal plane of symmetry of the flow. For this purpose it is necessary to put a thin undisturbed layer of colored gas in a volume containing a transparent gas, and to photograph the colored layer by scattered light (against a background of uniformly illuminated ground glass). These conditions make it possible to observe the density changes in the colored layer alone without recording the corresponding density changes in the transparent gas. The introduction of such a colored layer subject to suitable choice of gases (similar molecular weights, c_p/c_v, temperatures and pressures) should not greatly disturb the general flow pattern, and the colored layer will reproduce the supersonic flow pattern in a single plane (the plane of symmetry).

Fig. 1

As the colored gas, we chose bromine vapor and for the transparent medium we used one of the freons. For introduction of the colored layer into the transparent medium, we used a thin-walled tank of rectangular (3 × 80 mm) cross section in the plane of flight of the body. The tank was filled with bromine vapor. The tank was then moved smoothly against a rigid piston "squeezing out" a 2-3 mm layer of bromine vapor.

Fig. 2

By smooth motion of the tank we obtained a layer which was sufficiently uniform in thickness and density. Due to the almost complete absence of thermal diffusion and barodiffusion, the colored gas layer preserves its operating shape sufficiently long for the taking of a photograph.

Streamline flow patterns around an axially symmetrical body (velocity of the order 300 m/sec) moving in the plane of the colored layer are shown in Figs. 1 and 2. Figure 1 shows clearly the density increase directly behind the compression discontinuity followed by gradual attenuation. The "bottom vacuum" and the tail wave are also visible. The uniformity of the colored layer can be judged from the undisturbed portions. Figure 2 shows clearly the distance of the shock wave from the nose of the body.

Photometry may be used on this kind of photograph; however, the quantitative data obtained directly from the microphotograms regarding the density distribution must be corrected after an analysis of the physical conditions under which the photographs were taken.

Leningrad Physico-Technical Institute,
Academy of Sciences of the USSR

Received November 14, 1955

POSITIVE HYPERON AND SINGLY CHARGED HYPERFRAGMENT DECAYS

V. V. Alpers, I. I. Gurevich and A. P. Mishakova

(Presented by Academician Artsimovich February 22, 1956)

1. Σ^+-hyperon. An emulsion chamber consisting of 100 layers, each 10 cm in diameter and 450 μ thick, was irradiated with cosmic rays at a height of 27 km for 7 hours during May 1955. In order to determine the stopping power, the emulsions were calibrated by the ranges of 130 tracks of horizontal muons from $\pi \rightarrow \mu \rightarrow e$ decay. The average muon range was $\bar{R}_\mu = (584 \pm 2.3)\,\mu$ with a spread of $\pm 38\,\mu$.

In G-5 Ilford emulsions $\bar{R}_\mu = (597 \pm 1)\mu$. Therefore, for the determination of particle energies, we used range-energy curves for the Ilford G-5 emulsions with a suitable correction.

By systematic area scanning we found in this emulsion chamber a case of Σ^+-hyperon decay according to the scheme

$$\Sigma^+ \rightarrow p + \pi^0 + Q.$$

The creation and decay of the Σ^+-hyperon are shown in a microprojection in Fig. 1. From a star of type (20 + 1 n) a particle is emitted which traverses 8300 μ and is stopped in the emulsion, decaying into another charged particle of 1600 μ path; by gap measurements this particle was identified as a proton with energy $E_p = 18.5$ Mev. The site of the hyperon decay was carefully examined and from measurements of the number of gaps it was established that the hyperon decayed while at rest. For confirmation of this we examined the scattering of protons in the last 1000 to 1500 μ of the range; the results indicate that in the given instance, we have a decay of a stopped particle rather than scattering.

For identification of the primary particle, we found 5 protons moving in the emulsion in the same direction, at the same dip angle and through the same layers as the primary particle. We constructed curves showing the dependence of the number of blobs on the range for the primary particle andfive protons. It is fairly difficult to determine the exact mass in this case because of the large dip angle and insufficiently long range of the primary particle. However, the measurements indicate that the mass of the primary particle exceeds the proton mass; in addition, measurements of the number of δ-rays indicated that the particle has unit charge. In the basis of the above, the particle was identified as a Σ^+-hyperon.

The Σ^+-hyperon range of $R = 8300\,\mu$ corresponds to an ionization stopping time of $t_{\text{ion}} = 1.3 \cdot 10^{-10}$ sec.

Using a two-particle decay scheme $\Sigma^+ \rightarrow p + \pi^0$ and the kinetic energy of the proton $E_p = 18.5$ Mev, from the conservation laws we obtained $Q = (113 \pm 3.8)$ Mev. Then the mass of the Σ^+-hyperon is $m_{\Sigma^+} = (2331 \pm 7;5)\, m_e$, which is in good agreement with the most exact measurements of other writers [1].

A study of the hyperon creation star showed that the five particles emerged from the emulsion chamber.

2. Decay of a slow singly-charged hyperfragment. In a previously described emulsion chamber [2] by area scanning we detected a case of meson decay of a hyperfragment, which contained a bound Λ^0-particle in place of a neutron.

The creation and decay of the hyperfragment are shown in the microprojection of Fig. 2.

From a star of type (4 + 0 n) a slow singly-charged particle is emitted which traverses 35 μ, is stopped in the emulsion and forms a secondary star consisting of 3 prongs. The measurements of the secondary star tracks are given in Table 1.

TABLE 1

No. of Track	Range in μ		Particle	Energy in Mev
	total	visible		
1	35		p	1.85
2	22000 ± 5000	11000	π	36.0 ± 5.7
3	1,6		p	0.2

Track 2 was not terminated in the emulsion chamber but the ionization measurements indicated that the track cannot belong to a proton, but can be a pion with range R = (22000 ± 5000) μ. The large error in the total range of the pion is due to the large dip angle of the track in the emulsion.

Careful study of the compound particle with respect to δ-rays and gaps indicated that its charge is 1, but that its mass is larger than that of a proton and most likely equals that of a deuteron or triton. A momentum analysis of the secondary star tracks shows that conservation of momentum requires the presence of at least one neutron (the charged particle tracks are noncoplanar). In the decay of an excited deuteron (${}_{\Lambda^0}H_1^2 \rightarrow 2p^+\pi^- + Q$) the tracks of all three charged particles would be coplanar. Consequently, the observed hyperfragment may be either an excited tritium nucleus (${}_{\Lambda^0}H_1^3$) [3-7] or excited ${}_{\Lambda^0}H_1^4$ [5,8].

In the first case, there emerges one neutron with energy 1.94 Mev, as follows from momentum balance. Then the decay scheme of the hyperfragment would be as follows:

$$ {}_{\Lambda^0}H_1^3 \rightarrow 2p + \pi^- + n + Q_p, \quad \text{where } Q_p = (40 \pm 5.8)\ \text{Mev} \tag{1} $$

Keeping in mind the energy Q_{Λ^0} evolved in the decay of a Λ^0-particle it is possible to determine the binding energy of the Λ^0-particle in a tritium nucleus (for decay scheme (1) $B_{\Lambda^0} = Q_{\Lambda^0} - Q_p - \varepsilon_d$):

$$ B_{\Lambda^0} = (-5.3 \pm 5{,}6)\ \text{Mev} $$

This result does not conflict with the data of other authors for B_{Λ^0}: 1) 1.7 ± 4.5 [3]; 2) < 1 [4]; 3) −0.7 ± ± 0.8 [5]; 4) ~ 1 [6]; 5) 0.24 ± 4 [7]; 6) −3 ± 0.8 [5].

The following decays of excited tritium have previously been published: 1) ${}_{\Lambda^0}H_1^3 \rightarrow He_2^3 + \pi^-$, Q = (41.7± ± 1) Mev [3,6]; 2) ${}_{\Lambda^0}H_1^3 \rightarrow p + p + n + \pi^-$, Q = 37.7 Mev [5] (one of the decay shcemes proposed here).

In all rigorously established cases of excited ${}_{\Lambda^0}H_1^4$ [8] in the literature, the decay produced an alpha particle and negative pion (${}_{\Lambda^0}H_1^4 \rightarrow He_2^4 + \pi^- + 55$ Mev).

The decay of ${}_{\Lambda^0}H_1^4$ into two protons, two neutrons and π^- (${}_{\Lambda^0}H_1^4 \rightarrow 2p + 2n + \pi^-$) is less probable although it cannot be excluded.

Decay by the schemes ${}_{\Lambda^0}H_1^4 \begin{matrix} \nearrow H_1^3 + p + \pi^- \\ \searrow H_1^2 + H_1^2 + \pi^- \end{matrix}$ cannot explain the observed case because of the noncoplanarity of the charged particle tracks in the secondary star. However, ${}_{\Lambda^0}H_1^4$ can decay as follows: ${}_{\Lambda^0}H_1^4 \rightarrow H_1^2 + p + n + \pi^- + Q$; in this case momentum conservation gives a neutron energy of ~ 1.6 Mev.

The most probable decay schemes of the given hyperfragment are:

1) ${}_{\Lambda^0}H_1^3 \rightarrow p + p + n + \pi^-$, $Q = (40 \pm 5.8)$ Mev $E_n = 1{,}94$ Mev.

2) ${}_{\Lambda^0}H_1^4 \rightarrow H_1^2 + p + n + \pi^-$, $Q_1 = (40 \pm 5{,}8)$ Mev, $E_n = 1{,}62$ Mev; $Q_2 = (39.6 \pm 5.8)$ Mev, $E_n = 1.57$ Mev.

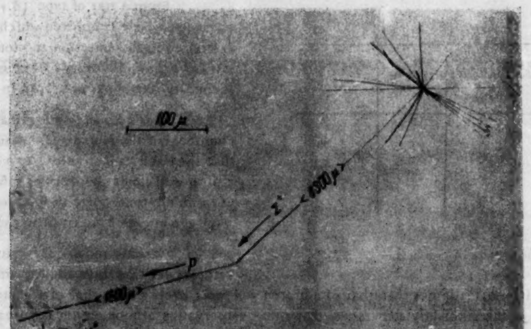

Fig. 1

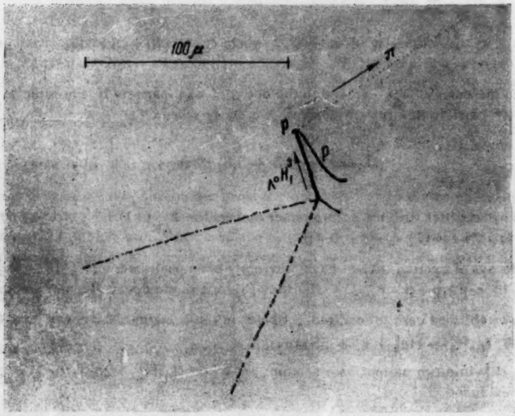

Fig. 2

The total binding energy of $_{\Lambda^0}H_1^4$ is in this case:

$$\Delta E = Q_{\Lambda^0} + \varepsilon_d - Q_p = (-0\ 87 \pm 5.6)\ \text{Mev}.$$

However, the Λ^0 binding energy in excited $_{\Lambda^0}H_1^4$ then becomes negative outside the limits of error in determinging Q_p, and the observed hyperfragment must be identified as excited tritium decaying by scheme (1).

We have studied the prongs of the primary star. All particles were stopped in the emulsion with one exception whose track was broken off. This is evidently the track of a proton which underwent a nuclear interaction without the emission of charged particles.

In conclusion we wish to express our thanks to A. I. Maleev for preparing the microprojections.

LITERATURE CITED

[1] P. Astbury, A. Bonetti and M. Ceccarelli, Nuovo cimento Suppl. 12, 488 (1954).

[2] V. V. Alpers, R. I. Gerasimova, I. I. Gurevich, A. P. Mishakova and L. V. Surkova, Doklady Akad. Nauk SSSR 105, 2 (1955).

[3] C. Castagnoli, G. Cortini and C. Franzinetti, Nuovo cimento 2, 550 (1955).

[4] M. Baldo, G. Belliboni and M. Ceccarelli, Nuovo cimento 1, 1180 (1955).

[5] F. Anderson, G. Lawlor and T. E. Nevin, Nuovo cimento 2, 605 (1955).

[6] A. Bonetti, R. Levi and M. Panetti, Nuovo cimento 11, 330 (1954).

[7] A. Debenedetti and C. M. Garelli, Nuovo cimento 12, 466 (1954).

[8] I. H. Davies and D. Evans, Conf. intern. sulle part. elem., XLI Congresso Nazionale Fis. (Pisa, June 12-18, 1955) p. 503.

Received January 23, 1956

ANOMALOUS DISPERSION OF LIGHT IN SOLUTIONS OF DYES

I. S. Gorban' and A. A. Shishlovskii

(Presented by Academician G. S. Landsberg November 11, 1955)

In connection with the investigations described in our earlier article [1] it was of interest to investigate the problem of the application of the theory of A. S. Davydov to those solutions whose absorbing "centers" have a complex molecular structure in which the intramolecular electron excitations are accompanied by a change of the vibrational state of the absorbing molecule and its neighborhood.

According to luminescence data [2] the visible absorption bands of such triphenylmethane dyes as fuchsin and cyanine cannot be associated with single electron-oscillator transitions. Therefore, attempts to compare this theory with earlier measurements of anomalous dispersion [3,4] are not promising. An exception may be the measurements of van der Plaats [5] on aqueous solutions of iodeosin. But these measurements were taken, using such large concentrations of the dye that there clearly were strong interactions between the molecules of the absorbing material, which is not contemplated in the theory.

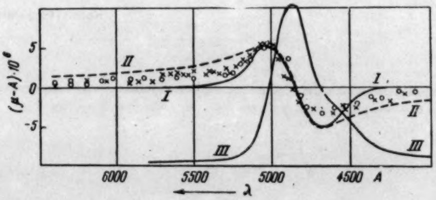

Fig. 1. Dispersion curve of an aqueous solution of fluorescein.
$C = 6.5 \cdot 10^{-6}$ g/cm^3.

We investigated very dilute solutions of typical mononuclear dyes – fluorescein, rhodamine B, iodeosin, etc. The measurements were performed, as previously, by a compensation method with the solution in the path of one beam of the interferometer and the solvent in the other.

Fig. 1 gives the results of measuring the dispersion curve within the absorption band of an aqueous solution of fluorescein at concentration $C = 6.5 \cdot 10^{-6}$ g/cm^3; the crosses refer to a spectrointerferogram from a vessel of thickness $d = 1$ cm, and the circles refer to a thickness of $d = 2.386$ cm. I is the theoretical curve obtained from Davydov's equation and II was obtained from an oscillator function. The parameters of these functions were calculated as previously from the position of the maximum of the experimental dispersion curve.

The distinguishing feature of the result is the fact that the experimental dispersion curve is strongly asymmetrical. Its maximum is sharp and is located closer to the peak of the absorption band than the minimum. This asymmetry corresponds to the asymmetry of absorption band III which is shown in the same figure.

We attempted to calculate the oscillator strength, using the parameters α and β obtained by comparing theory with experiment.* From the position of the dispersion curve peak by Davydov's equation, we have $\alpha_{max} = 1.1 \cdot 10^{-8}$ cm; $\beta_{max} = 1.02 \cdot 10^{-6}$ cm^2 and $f_{max} = 0.48$; and from the minimum $\alpha_{min} = 0.71 \cdot 10^{-8}$ cm; $\beta_{min} = 0.89 \cdot 10^{-6}$ cm^2 and $f_{min} = 0.36$. The average value of the oscillator strength obtained from the maximum and minimum of the dispersion curve is $f_{Av} = 0.42$ and the average value of the oscillator strength obtained from the oscillator function is 0.50. In the literature [6] the oscillator strength for the visible band of fluorescein obtained by the method of integral absorption is $f = 0.41$.

Thus, the average oscillator strength as calculated by Davydov's equation is in better agreement with other optical measurements than by the oscillator function, which gives a value that is clearly too high.

We obtained similar results for other solutions of dyes, which are illustrated in Table 1.

TABLE 1

Dye:	Solvent:			Oscillator strength by integral absorption
	water	ethyl alcohol	acetone	
Iodeosin	0.62; 0.65	0.59	0.60	0.63 (6)
Fluorescein	0.42			0.41 (6)
Rhodamine B.	0.71	0.73	0.74	0.67
Fuchsin	1.09			1.16 (6)

Study of the dependence of the dispersion curve of dyes on the nature of the solvent shows that for the majority of solvents there is, in general, some distortion of the dispersion curves, but as a rule the asymmetry of the maximum and minimum in the sense indicated above remains large. This supports the view that the shapes of the dispersion and absorption curves are determined principally by the interaction of intramolecular electronic excitations with the vibrations of atoms of the molecule, while the interaction with the solvent remains secondary.

However, we have found some interesting exceptions from this rule. Thus, Fig. 2 gives the results of measurements on a solution of iodeosin in acetone at $C = 2 \cdot 10^{-5}$ g/cm^3. We know that the shape of the absorption band of iodeosin in some other solvents is similar to the shape of the absorption band of fluorescein, but in acetone this band is somewhat distorted. As can be seen from the figure the distortion lies in the presence of two absorption peaks A and B (see Curve II) with the stronger maximum shifted towards longer waves as compared with the peaks in other solvents. Corresponding to the change of the absorption spectrum, there is a change in the spectrum of the refractive index which now has the two characteristic kinks of anomalous dispersion (see the points in Fig. 2). This is related to the formation of compounds of dye and solvent molecules.

If we neglect the effect of the shorter wave absorption band B (whose intensity is considerably lower than for the longer waves) on the shape of the dispersion curve within the long wave band A and construct a theoretical curve I from the average values of the parameters α and β using Davydov's equation, the experimental curves lie fairly close. Considerable deviations are observed only in the wings. By our calculations the oscillator strength is $f = 0.60$ while according to data in [6], which was obtained by the method of integral absorption, $f = 0.63$.

Thus the shape of the dispersion curve in the long wave absorption band of a solution of iodeosin in acetone is similar to the shape of the limiting case of strong interaction of intramolecular electronic excitations with vibrations of atoms in the solute molecules and of atoms of the solvent.

It was also of interest to determine the relationship between the results of Davydov's theory and experiment for large dye concentrations. For this purpose we used the above-mentioned measurements by van der Plaats

---

*Compare with the preceding article [1].

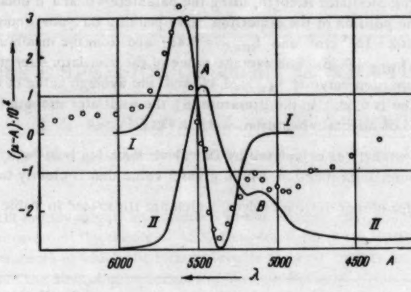

Fig. 2. Dispersion curve of a solution of iodeosin in acetone. $C = 2 \cdot 10^{-5}$ g/cm³.

according to which the shape of the absorption band for small concentrations is independent of the concentration, but for medium concentrations shows considerable changes, while for very large concentrations (of the order of a few percent and higher) the absorption curve becomes symmetric and again independent of the concentration. This is evidence of molecular clustering of a certain stoichiometric constitution in the dissolved substance.

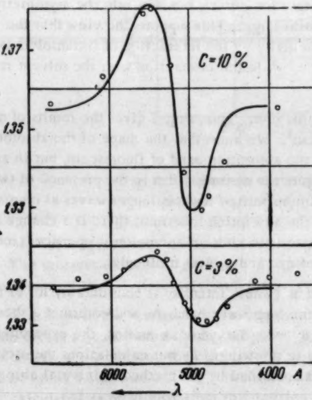

Fig. 3. An approximation of the measurements of van der Plaats by Davydov's equation.

The dispersion curve in this instance is well described by Davydov's equation. This can be shown by the two curves of Fig. 3 where the circles are experimental data and the theoretical curves are solid.

The following conclusions can be drawn from the above investigations:

1. The dispersion curves in the absorption bands of very dilute dye solutions are as a rule asymmetrical, which does not fit into Davydov's first approximation.* The degree of asymmetry generally changes little as the properties of the solvent are altered. However, some solvents tend to form compounds with the molecules of the dye, which results in considerable distortion of the absorption spectrum. In this case, within the limits of the bands, the dispersion curve may approximate an antisymmetrical Gaussian curve and be described satisfactorily by Davydov's equation.

2. The mean oscillator strengths, as calculated from the maximum and minimum of the asymmetrical dispersion curve, agree quite well with other measurements which were obtained by the integral absorption method. For this reason, we can conclude that further approximations in Davydov's theory are promising.

3. For very strong concentrations of a dye, when there is clearly a strong interaction between individual molecules of the dissolved substance, the dispersion curve may show a striking resemblance to the antisymmetric Gaussian curve derived by A. S. Davydov in the case of strong interaction between intramolecular excitations and vibrations in the vicinity for low concentrations.

---

*The asymmetry of the dispersion curves can be explained qualitatively by further approximations of the theory [7].

The authors are extremely grateful to corresponding member of the USSR Academy of Sciences, Professor A. S. Davydov, for several valuable conferences.

LITERATURE CITED

[1] I. S. Gorban' and A. A. Shishlovskii, Doklady Akad. Nauk SSSR 108, 53 (1956) [Soviet Physics-Doklady, p. 249].

[2] P. P. Feofilov, Doklady Akad. Nauk SSSR 57, 447 (1947).

[3] R. Wood and C. E. Magnusson, Phil. Mag. 1, 36 (1901).

[4] G. De Metz, Outline of the History of the Anomalous Dispersion of Light to the Present Time (1885).

[5] Van der Plaats, Ann. Physik 47, 12, 429 (1915); J. Koenigsberger, K. Kūpferrer, Physik z. 11, 3, 568 (1910).

[6] A. N. Terenin, Photochemistry of Dyes (1947), p. 71.

[7] A. F. Lubchenko, Dissertation (Acad. Sci. USSR Phys. Inst., Kiev, 1954).

T. G. Shevchenko
Kiev State University

Received October 13, 1955

DIRECT MEASUREMENTS OF MOLECULAR ATTRACTION BETWEEN SOLIDS IN A VACUUM

B. V. Deriagin, Corresponding Member USSR Academy of Sciences
and I. I. Abrikosova

In our previous paper we described the method of measuring the molecular attraction F between two solids (a plate and a spherical lens) in air as a function of the space H between them. But the viscosity of the air in the space seriously hampered the measurements.

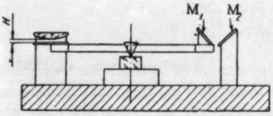

Fig. 1

The reason for this is clear from an examination of the equation of motion of the balance beam (see Fig. 1) in measurements of F. This equation can be written as

$$I\frac{d^2\alpha}{dt^2}+j\frac{d\alpha}{dt}+l\alpha=Fr, \tag{1}$$

where α is the angle of deflection of the beam from its equilibrium position; r is the distance from the fulcrum to the point of closest approach of the surfaces; I is the moment of inertia of the beam; l is the coefficient of "rigidity" of the feedback used in the balance [1]; j is a coefficient which depends principally on the damping power of the air layer between the plate fastened to one end of the beam and the convex lens placed at a small distance therefrom.

When the mean free path λ of the air molecules is much smaller than the smallest distance H between the surfaces, j is easily obtained from Taylor's equation [2]:

$$j=\frac{6\pi R^2\eta r^2}{H}; \tag{2}$$

where R is the radius of the spherical surface and η is the viscosity of air.

The damping of the beam oscillations which is proportional to j plays a positive role in preventing natural oscillations due to phase retardation of the feedback [which is neglected in the third term of (1)*] and in making the system an aperiodically damped system with an extremely large but constant time constant

$$\tau=\frac{j}{l}=\frac{6\pi R^2\eta r^2}{Hl}. \tag{3}$$

An increase of feedback rigidity l, which is useful for the stabilization of the beam in the field of molecular forces, serves also to decrease τ. But an increase of l augments the sensitivity of the setup to shocks which are transformed by the photoelectric transducer into current oscillations, thus diminishing the real sensitivity and accuracy of the force measurement. This latter circumstance is related to the fact that the current oscillations in the feedback circuit are caused not only by vibrations of the beam itself, but by relative displacements of various parts of the apparatus, such as the gratings. Therefore, it was advantageous to operate with not too high values of $\underline{l}$. The smallest permissible value of $\underline{l}$ is given by the formula

---

*The use of a phase-shifting loop in the amplifier circuit enables us not only to eliminate this source of oscillations but to ensure strong damping of oscillations of the system (which in our case, where j was quite large, was unnecessary).

$$l_c = |r dF/d\alpha| = r^2 |dF/dH|, \tag{4}$$

at which the feedback still enables us to balance the measured force F. From (3) and (4) we obtain for the corresponding limiting value of the time constant

$$\tau_c = \frac{6\pi R^2 \eta}{H\,|\,dF/dH\,|} = \frac{6\pi R^2 \eta}{F\,|\,d \ln F/d \ln H\,|}.$$

Taking for $|d \ln F/d \ln H|$ corresponding to our molecular force measurements, the value 3, for $F = 10^{-4}$ dynes (close to the limit of sensitivity), $R = 10$ cm and assuming $\eta = 2 \cdot 10^{-4}$ poise, we obtain $\tau_c \cong 10^3$ sec. In our measurements τ was actually considerably smaller than τ_c (of the order of a few seconds) since we chose $l \gg l_c$. Nevertheless, τ was quite large, which not only prolonged the process of measuring but frequently made it impossible to perform the experiment, since during the damping time τ the beam might be jolted by shaking of the support. Moreover, for fairly large τ it was often impossible to take a reading because of slow changes of the gap H which continuously distrubed equilibrium due to the change with distance of the interaction F of the bodies and because of extraneous viscous forces in the air layer which are proportional to dH/dt.

Despite all the above difficulties we carried out a series of measurements whose reproducibility may be considered quite satisfactory [1,11].

The effect of shaking was reduced to a minimum by shifting the center of gravity of the balance beam with its fulcrum, as well as by placing the apparatus on a shock-absorbing platform and the latter on a cement pedestal sunk into the ground. For further stabilization of the gap H a two-mirror scheme was used as transmitter of the beam swing (see Fig. 1) which eliminated the effect on the photocurrent of swings of the grating photorelay with respect to the beam [1]. However, for the purpose of radically simplifying the measurements and enhancing their accuracy, we constructed an instrument for taking the measurements in a vacuum. Although air viscosity η is not sensitive to pressure changes, in this case the values of $\underline{j}$ were sharply diminished. At low pressures the mean free path of air molecules is much greater than the gap H so that Equation (2) is inapplicable. The value of $\underline{j}$ drops because of the sharply enhanced effect of kinetic slipping which aids the flow of gas into and out of the gap.

The use of pressures from 10^{-1} to 1-3 mm Hg enabled us to reduce the time constant to fractions of a second and retain the damping which is required to prevent oscillations. The measurements were thus greatly facilitated and their accuracy enhanced compared with measurements in air. The results are shown in Fig. 2 where the horizontal axis gives values of log H and the vertical axis gives log F. The open circles represent measurements in air. The solid circles represent various series of measurements in vacuum, which were separated by long intervals of time, (sometimes years) on different specimens of quartz glass. For each type of measurement the reproducibility of the data can be considered satisfactory. The scatter of experimental points is decidedly small compared with the range of the forces which can be observed when electric charges are not completely removed from the surfaces (the principal form of interference in our experiments).

Using the theory [3] of the molecular interaction between convex surfaces, it is possible from the measured value of F(H) to calculate the energy of attraction (per cm^2) u(H) of plane parallel surfaces separated by the same gap, from the equation

$$u(H) = F(H)/2\pi R.$$

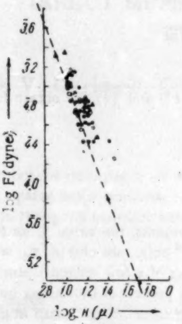

Fig. 2

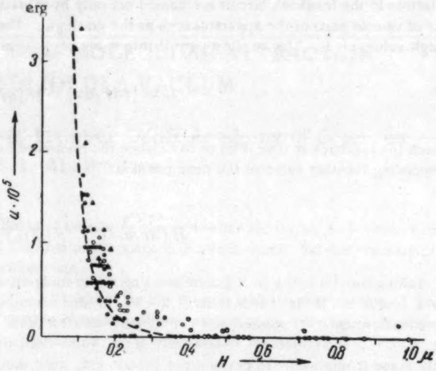

Fig. 3

Fig. 3 gives the values of u calculated in this way as a function of H. The values of u(H) obtained from experiments with lenses of different radius of curvature R agree quite well. This is one of the proofs of the molecular nature of the observed effect.

As has already been noted [1] the values obtained for F and u were approximately 20 times smaller than those calculated from London's equation [4] (assuming the additivity of the interactions between separate pairs of molecules) agreeing more closely with the theory of Casimir and Polder [5], who took into consideration the effect of electromagnetic retardation. Unfortunately an exact comparison with this theory is impossibl both because it is not known how to calculate the constants in the theory of Casimir and Polder for atoms composing a solid (SiO_2) and because strict additivity of the interactions can occur only in gases and not in condensed bodies.

A rigorous theory of molecular interaction between macroscopic bodies has recently been constructed by E. M. Lifshits [6]. An exact comparison with Lifshits' theory requires quite complete knowledge of the optical properties of the substance in its regions of absorption. However, the nature of absorption in quartz (its transparency to long waves such as were used in the experiments with the gaps H) enable us to make an approximate theoretical estimate. The theoretical value for the attractive force between two slabs per cm² is obtained for quartz from the equation

$$f = \frac{\hbar c}{H^4}\frac{\pi^2}{240}\left(\frac{\varepsilon_0 - 1}{\varepsilon_0 + 1}\right)^2 \varphi(\varepsilon_0),$$

where ε_0 may be taken as the square of the refractive index in the optical region and $\varphi(\varepsilon_0)$ is given by the table:

$1/\varepsilon_0$	0	0.025	0.1	0.25	0.50	1
$\varphi(\varepsilon_0)$	1	0.53	0.41	0.37	1.35	0.35

($\hbar$ is Planck's constant; c is the velocity of light).

The dashed lines in Figs. 2 and 3 are the curves of F(H) and u(H) which are calculated by Lifshits' method. Considering the roughness of the estimate and the errors of measurement, we can consider the agreement to be quite satisfactory.

Thus, we may consider it a firmly established fact that there are long-range molecular forces acting between macroscopic objects, as one of the keystones of the modern theory of colloidal stability [6-8], and that it is possible to calculate them using the theory of E. M. Lifshits. Although Lifshits' equations and their experimental verification refer to the attractions between solids in a vacuum, the confirmation of the theory is also significant for problems of colloidal interactions in any, even a liquid, dispersive medium. The direct detection of attractive forces at distances up to $0.3\,\mu$ proves not only the possibility but the necessity of considering such forces in the theory of the coagulation and stability of colloids which, although widely admitted, has met and sometimes even now encounters scepticism. On the other hand, the question arises—should we not, considering electromagnetic retardation, use for the calculation of the interaction energy of colloidal particles an H^{-3} law instead of an H^{-2} law?

It is easily seen that in this case the coagulating force between oppositely charged ions would be proportional not to the 6th but to the 8th power of the charge, which is in worse agreement with the experiment. It is evident that the stability criterion of lyophobic colloids is defined by the balance of attractive and repulsive forces at such small distances that the H^{-2} law remains in effect. This is in complete agreement with the theory [8] according to which the decisive factor is found in the forces at distances of the order of thickness of double layers of ions, which is usually considerably smaller than the 10^{-5} cm at which electromagnetic retardation becomes manifest.

It is interesting to note that Lifshits' theory, unlike London's theory, fully allows for the electromagnetic nature of molecular forces as had been surmised by P. N. Lebedev [9] who considered the most interesting and most difficult case in a physical body to be that in which many molecules act on each other while, because of their close proximity, their oscillations are not independent of each other. Lebedev asserted that a comparison of the calculated values for molecular forces (using data from spectral analysis) with experimental observations would provide an answer to the "fundamental problem of molecular physics"; can molecular forces be reduced to electromagnetic forces or do they include forces of still unknown origin? It is clear that the agreement of Lifshits' theory with our measurements enables us to answer Lebedev's question; molecular forces actually can be "reduced to electromagnetic forces".

In conclusion, we note that unlike our measurements of molecular attraction, those of Overbeek and Sparnay [10] performed by another method gave values which are approximately 10^4 times higher than values which agree with Lifshits' theory and of very poor reproducibility; this indicates a nonmolecular origin of the forces which they measured, which is probably the electrification of the objects.

We consider it a pleasant duty to express our thanks to Professor E. M. Lifshits for the discussion of theoretical problems and to I. V. Zhadovskii for assistance in taking the measurements.

LITERATURE CITED

[1] I. I. Abrikosova and B. V. Deriagin, Doklady Akad. Nauk SSSR 90, 1055 (1953).

[2] G. J. Taylor and C. F Elam, Proc. Roy. Soc. (London) 108A, 12 (1924).

[3] B. V. Deriagin, J. Phys. Chem. (USSR) 6, 10, 1306 (1935).

[4] F. London, Z. Physik.Chem. 11, 222 (1931).

[5] H. B. Casimir and D. Polder, Phys. Rev. 73, 760 (1948).

[6] E. M. Lifshits, Doklady Akad. Nauk SSSR 97, 643 (1954); 100, 879 (1955). J. Exptl.-Theoret. Phys. (USSR) 29, 94 (1955).

[7] B. V. Deriagin, Bull. Acad. Sci. USSR, Chem. Ser. 1937, No. 5, 1153. Colloid J. (USSR) 6, 291 (1940); 7, 285 (1941).

[8] B. V. Deriagin and L. D. Landau, J. Exptl.-Theoret. Phys. 11, 802 (1941); 15, 11, 663 (1945); Acta Physicochim. URSS 14, 633 (1941).

[9] P. N. Lebedev, Collected Works (Moscow, 1913); Wied. Ann. 52, 621 (1854).

[10] T. G. Overbeek and M. J. Sparnay, J. Colloid Sci. 7, 343 (1952).

[11] B. V. Deriagin and I. I. Abrikosova, Discussions Faraday Soc. 18, 24, 182 (1954).

Institute for Physical Chemistry
Academy of Sciences of the USSR

Received December 8, 1955

PHYSICAL FUNDAMENTALS OF ELECTRON-OPTICAL CHRONOGRAPHY

E. K. Zavoiskii, Corresponding Member USSR Academy of Sciences,
and S. D. Fanchenko

In our previous paper [1] we called attention to the very short time-lag of an electron-optical image converter (EOC). This enables us to use an EOC to study processes of very short duration (10^{-9}–10^{-14} sec) by sweeping an electronic image. By analogy with optical chronography* this method may be called electron-optical chronography.

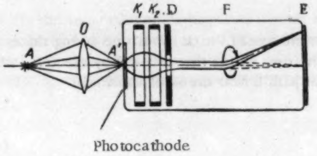

Fig. 1

The method of studying rapid light processes by electron-optical chronography is shown in Fig. 1. The objective O throws on the photocathode of the EOC an image A' of the light source A. Electrons emitted by the photocathode are accelerated and focused by an electron-optical system shown conventionally in Fig. 1 in the form of rings K_1 and K_2 and a diaphragm D. Before striking the fluorescent screen E, the electrons traverse the region of a rapidly rotating magnetic or electric field F. Therefore, the image of the light source on the screen is swept out in time. A circular sweep is most suitable. If it is desired to study the development of a process during time intervals which greatly exceed the period of rotation of the deflecting field, a spiral sweep may be used.

We shall designate the period of rotation of the field by T, the radius of the circular sweep on the screen by R and the number of lines of the image resolved in 1 cm of the screen by δ. Then the minimum resolved time interval is given by

$$\Delta t_{\text{sweep}} = \frac{T}{2\pi R\delta}. \tag{1}$$

For example, if $T = 10^{-10}$ sec, $R = 5$ cm, $\delta = 300$ lines/cm, we have

$$\Delta t_{\text{sweep}} \simeq 10^{-14} \text{ sec}$$

From (1) we see that the time-resolving power of the sweep may, in general, be enhanced at will by reducing T and increasing the value of the product $R\delta$. However, there are a number of factors which limit the resolving power of the method.

The first of these factors is electronic chromatic aberration. We shall confine ourselves to the case of nonrelativistic motion of paraxial electrons in axially symmetrical fields. From point O_1 of the photocathode EOC (see Fig. 2), let a group of electrons be emitted with different initial velocities.

---

*Optical chronography is based on the sweeping of a light image by means of rapid mechanical motion of the optical parts of a photographic camera.

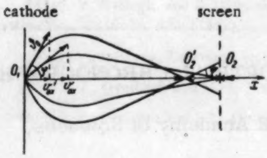

Fig. 2

We shall compute the duration of the corresponding electron pulse near the screen. We begin with the special case in which all electrons are emitted along the x-axis of symmetry, i.e., at angle $\varphi = 0$. In the electron-optical systems used in practice, the field and cathode potential E_0 is almost constant up to distances x where $eE_0x \gg mv_{0x}^2/2$. Then the equation of motion of an electron is

$$x = \frac{e}{2m} E_0 t_2 + v_{0x} t, \tag{2}$$

where e, m, v_{0x} and t are the charge, mass, initial velocity and time of the electron motion. Differentiating (2) and neglecting v_{0x} by comparison with $\frac{e}{m} E_0 t$, we have

$$\Delta t_{\text{chr}} = \frac{m\Delta v_{0x}}{eE_0}. \tag{3}$$

Equation (3) takes into consideration the main portion of the time spread which is built up during the motion of electrons close to the photocathode. The spread Δt_e which arises during the traversal by electrons which had been accelerated by the total potential U applied to the EOC, of path L near the screen is small:

$$\Delta t_e = \frac{L}{v_e}\frac{\Delta\varepsilon_0}{U}, \tag{4}$$

where $\Delta\varepsilon_0$ is the halfwidth of the distribution of initial electron energies; $v_e = \sqrt{\frac{2m}{e}}\sqrt{U}$. Substituting $\Delta\varepsilon_0 \simeq 10^{-1}$ ev, $U \simeq 10^{-4}$ v and $L \simeq 10$ cm we see that $\Delta t_e \simeq 10^{-14}$ sec.

If, by v_{0x} we understand the x-component of the initial velocity, Equation (3) is correct in the general case in which the electrons are emitted from O_1 at all possible angles φ. As proof we use the well-known [2] fact in electron optics that the longitudinal chromatic aberration Δf of axially symmetrical systems depends in the first approximation not on the total initial velocity v_0, but only on its component $v_{0x} = v_0 \cos\varphi$. Let some value of v_{0x} correspond to the electron focal point O_2 where the fluorescent screen is placed, and the value v'_{0x} ($v'_{0x} = v_{0x} - \Delta v_{0x}$) to the focal point O'_2. For electrons with v_{0x} the point O_2 is the image of point O_1. Then, by Fermat's principle, all of these electrons reach O_2 simultaneously, whatever their angles of emission φ. We now consider an electron which left the point O_1 exactly along the x-axis with initial velocity numerically equal to v'_{0x}. It reaches the screen retarded with respect to the group just considered by Δt_{chr} which is defined as previously by Equation (3). It is easily shown that in the first approximation all electrons emitted at different angles φ but with identical value of $v_0 \cos\varphi = v'_{0x}$ reach the screen simultaneously with this electron. They would actually reach point O'_2 at strictly the same instant by Fermat's principle, and the time spread for traversal of the path from O'_2 to the screen, as seen from Fig. 2, does not exceed

$$\Delta t' = \frac{\Delta f}{v_e}\frac{\psi^2}{2},$$

for which, according to Equations (15) and (16) of reference [2] as well as our Equation (3), we may write

$$\Delta t' = \frac{\varepsilon_0}{U}\sin^2\varphi\,\Delta t_{\text{chr}} \approx 10^{-4}\,\Delta t_{\text{chr}}$$

Equation (3) holds both for electrostatic and electromagnetic focusing of electrons in the EOC.

For practical employment of this equation it is necessary to know the photoelectron distribution with respect to v_{0x}. We have measured this distribution for an antimony-cesium cathode irradiated with visible light in the range a few hundred angstoms wide around $\lambda = 4500$ A. A computation of this distribution by (3) shows that, to an infinitely short electron pulse from the photocathode, there corresponds a pulse of finite duration at the screen with half of all electrons reaching the screen in the time

$$\Delta t_{1/2} \simeq \frac{10^{-11}}{E_0}\ \text{sec}\ ., \tag{5}$$

where E_0 is expressed in electrostatic units. We note that $\Delta t_{1/2}$ is not in general the minimum time interval between two infinitely short electron pulses from the photocathode which can be resolved. For any shape of the electron pulse near the screen photometric examination of a photograph of its sweep enables us to fix the position of the darkening maximum with error at least one order smaller than $\Delta t_{1/2}$. Then with $E_0 \approx 100$ electrostatic units, the time resolution could be reduced to 10^{-14} sec.

In the study of short light pulses it must be taken into consideration that the minimum frequency interval in a pulse of duration τ is $\Delta\nu = 1/\tau$ and that this can theoretically not be reduced. Then, neglecting the spread of initial velocities associated with $\Delta\nu$ we can estimate the highest possible time resolution of the EOC. For the spread of initial velocities associated with τ it is easy to obtain the expression

$$\Delta v_0)_{\Delta\nu} = \frac{h}{mv_0}\,\frac{1}{\tau}\ , \tag{6}$$

where h is Planck's constant and v_0 is the average initial velocity of the photoelectrons. The minimum duration of an electron pulse at the screen by (3) and (6) is

$$\Delta t_{\min} = \sqrt{\frac{h}{eE_0v_0}}\ . \tag{7}$$

Here it is possible to change v_0 somewhat by changing the average wavelength of the light in the pulse. Moreover, it is possible to control E_0 within wide limits. It is clear that E_0 can be reduced to at least 100 kv/cm. This gives

$$\Delta t_{\min} \simeq 2\cdot 10^{-14}\ \ \text{sec}$$

As in the case of (5) photometry may considerably improve the time resolution compared with $\Delta t_{\min}$.

Another important factor which limits the time resolution is the finite thickness of the photocathode d, which leads to the spread of emission times of photoelectrons

$$\Delta t_d \simeq \frac{d}{v_0}\ . \tag{8}$$

For $d \simeq 10^{-6}$ cm and $v_0 \simeq 10^8$ cm/sec we obtain $\Delta t_d \simeq 10^{-14}$ sec. The time-lag of the photoeffect in any case does not exceed this amount.

A necessary condition for obtaining a short light pulse is sufficient smallness of the source l*

---

*This does not apply to the Cherenkov effect, for whose duration see [3].

$$\frac{l}{c} \leqslant \Delta t, \tag{9}$$

where c is the velocity of light. For $\Delta t \simeq 10^{-14}$ sec, Equation (9) gives, for example, $l \leq 3\ \mu$.

It is also necessary that the pulse should not be stretched by the light-converging optics. The condition for this is

$$\frac{\Delta S}{c} \leqslant \Delta t, \tag{10}$$

where ΔS is the difference in optical paths from the light source to the photosensitive layer for different frequencies in the spectrum of the pulse. This indicates that the optics should be well achromatized and corrected for spherical aberration.

The above analysis shows that the limiting time resolution of the method is $\sim 10^{-14}$ sec.

In the range 10^{-10}–10^{-14} sec an electron-optical chronograph is at present the only means for direct study of the temporal development of processes which are able by some method to induce emission of slow electrons. For example, in this range lie the durations of the following phenomena: excited nuclear states, Cherenkov effect, initial stages of scintillations, certain processes in spark discharge, spontaneous decay of heavy mesons and hyperons. For the study of such fast light processes by electron-optical chronography, we have available such a sufficiently inertialess converting emitter of slow electrons as the photocathode. It is only necessary, in connection with the small number of photons which are emitted, for example, in the Cherenkov effect or scintillation due to a single particle, to have a sufficiently sensitive EOC [5]. Success in the study of processes involving fundamental or nuclear particles depends on the practical construction of detectors which will respond to the appearance of the recorded particle with a sufficiently short light pulse or with a pulse of slow electrons.

LITERATURE CITED

[1] E. K. Zavoiskii and S. D. Fanchenko, Doklady Akad. Nauk SSSR 100, 4, 661 (1955).

[2] L. A. Artsimovich, Bull. Acad. Sci. USSR, Phys. Ser. 8, 86, 313 (1944).

[3] I. E. Tamm, J. Phys. USSR 1, 434 ,(1939).

[4] I. M. Frank, Progr. Phys. Sci. (USSR) 58, 1, (1956).

[5] E. K. Zavoiskii, G. E. Smolkin, A. G. Plakhov and M. M. Butslov, Doklady Akad. Nauk 100, 2, 241 (1955).

Received December 1, 1955

ION MOBILITY AND SPACE CHARGE IN AN INHOMOGENEOUS FIELD

Iu. M. Kagan and V. I. Perel'

(Presented by Academician A. A. Lebedev November 30, 1955)

1. In a gas charge layers of positive space charge may form around the walls and electrodes. Inside these layers the field is, as a rule, inhomogeneous. In connection with a number of applications (ion current at a probe with consideration of the pressure, theory of cathode fall, etc.) it is of interest to consider the problem of motion of positive ions in the gas within an inhomogeneous field. At the present time we consider it established that [1-3] the principal form of interaction between ions and atoms of the same gas is pure charge exchange involving an exchange of charge between colliding particles without essential change of velocity of either particle. In a number of practically interesting cases the fields in the layers are of such magnitude that the average thermal energy of the atoms is small compared with the energy acquired by an ion in one mean free path length, so that the atoms may be regarded as at rest, and as atomic velocity distribution function we may take the product of the δ-functions of the velocity components v_x, v_y, v_z.

If at each point the direction of the field $E(z)$ coincides with the positive z-axis, the number of ions in unit phase volume under the above conditions may be written as $f(z, v_z)\ \delta(v_x)\ \delta(v_y)$, and the kinetic equation for $f(z, v_z)$ will be

$$\frac{eE(z)}{m}\frac{\partial f}{\partial v_z} + v_z\frac{\partial f}{\partial z} = \delta(v_z)\, qN\psi(z) - qNf(z, v_z)\mid v_z \mid , \tag{1}$$

where

$$\psi(z) = \int_{-\infty}^{+\infty} f(z, v_z')\mid v_z' \mid dv_z', \tag{2}$$

e and m are the ion charge and mass; N is the atom concentration; and q is the charge exchange cross section which is assumed to be independent of the velocity.

Instead of v_z and z we introduce new variables η and t by

$$z = \varphi_1(\eta, t), \quad v_z = \varphi_2(\eta, t), \tag{3}$$

where the functions φ_1 and φ_2 satisfy the equations of motion

$$m\frac{d^2\varphi_1}{dt^2}\, eE(\varphi_1), \quad \varphi_2 = \frac{d\varphi_1}{dt} \tag{4}$$

with the initial conditions $\varphi_1 = \eta$; $\varphi_2 = 0$ at $t = 0$. Then in the new variables the kinetic equation become

$$+\, qN \mid \varphi_2(\eta, t) \mid f = \delta(\varphi_2)\, qN\psi(\eta). \tag{5}$$

Regarding (5) as an inhomogeneous equation with a known right-hand side and assuming that at $t \to \pm\infty$ $v_z \to \pm\infty$ and, consequently, $f(v_2) \to 0$, we obtain,

$$f = 0 \qquad \text{for } v_z < 0;$$
$$f = \frac{m}{\lambda e E(\eta)} \psi(\eta) e^{-(z-\eta)/\lambda} \qquad \text{for } v_z > 0. \tag{6}$$

Using (2) we obtain the equation for ψ :

$$\psi(z) = \frac{1}{\lambda} e^{-z/\lambda} \int_0^\infty \psi(\eta) \frac{m}{e} \frac{v_z}{E(\eta)} e^{\eta/\lambda} dv_z. \tag{7}$$

By means of the equalities

$$\frac{mv_z^2}{2} + eV(z) = eV(\eta), \qquad v_z \, dv_z = -\frac{e}{m} E(\eta) \, d\eta, \tag{8}$$

where $V(z)$ is the potential, it can be shown that the solution of (7) will be $\psi(z) = F$, where F is a constant representing current density.

Then

$$f = \frac{mF}{\lambda e E(\eta)} e^{-(z-\eta)/\lambda} \qquad \text{for } v_z > 0. \tag{9}$$

In the limiting case of a constant field ($E = \text{const}$) we obtain from (4) $z - \eta = mv_z^2 / 2eE$ and (9) is transformed into

$$f = \frac{mF}{\lambda e E} e^{-mv_z^2/2eE\lambda}. \tag{10}$$

which agrees with the expression obtained in [2] when F is determined by the normalization condition

$$\int_0^\infty f(v_z) \, dv_z = 1.$$

2. Returning to the case of an inhomogeneous field and utilizing (8) and (9) we obtain for the ion concentration

$$n(z) = \frac{F}{\lambda} \int_{-\infty}^{z} \frac{e^{-(z-\eta)/\lambda} \, d\eta}{\sqrt{\frac{2e}{m} [V(\eta) - V(z)]}} = \frac{F}{\lambda} \int_0^\infty \frac{e^{-u/\lambda} \, du}{\sqrt{\frac{2e}{m} [V(z-u) - V(z)]}} \tag{11}$$

and for the rate of ion drift

$$\overline{v}_z = \frac{F}{n(z)} = \frac{\lambda}{\displaystyle\int_0^\infty \frac{e^{-u/\lambda} \, du}{\sqrt{\frac{2e}{m} [V(z-u) - V(z)]}}}. \tag{12}$$

Usually [4-6] in connection with ion movements in an inhomogeneous field the equations used for the drift are those obtained for constant field, i.e., it is assumed that the drift velocity at a given point depends only on the field strength at that point. It is clear that this is permissible when the field change in one mean free path length is small compared with the field strength. Expanding in (12) the factor containing $e^{-u/\lambda}$ to give a power series in $\underline{u}$ and integrating by terms, we obtain the expansion of the integral in the denominator in powers of λ:

$$\overline{v_z} = \frac{\sqrt{2e\lambda E(z)/\pi m}}{1+\frac{1}{8}\frac{\lambda}{E(z)}\frac{dE}{dz}+\cdots}. \tag{13}$$

If the field changes little in the mean free path (13) is transformed into the expression obtained in [2] for a constant field.

3. Let us now consider a charged layer in the interval $0 < z < d$. At the edge of the layer where $z = 0$ let the ion distribution function $f(v_Z, 0) = f_0(v_Z)$ and $V(0) = 0$. In order to calculate the ion concentration inside the layer by (11) it is necessary to know the potential distribution for $z = 0$. We shall show that this distribution is completely determined by giving $f_0(v_Z)$.

Utilizing at $z = 0$ the energy conservation law $mv_z^2/2 = eV(\eta)$ and the fact that by (9) $f_0(v_z) = \frac{mF}{\lambda e E(\eta)} e^{\eta/\lambda}$ when $v_z > 0$, we obtain

$$\int_{\sqrt{\frac{2e}{m}V(z)}}^{\infty} f_0(v_z)\, v^2\, dv_z = F e^{\eta/\lambda}, \quad \text{where } F = \int_0^{\infty} f_0(v_z)\, v_z\, dv_z. \tag{14}$$

In particular, if $t_0(v_Z)$ is a one-sided Maxwellian distribution function with temperature T then for $\eta < 0$ the field strength E_0 is constant, in which case $eE_0\lambda = kT$ and the potential changes according to the law $V(\eta) = -E_0\eta$ for $\eta < 0$. For the concentration inside the layer in this case we obtain

$$n(z) = \frac{\sqrt{2}F}{\sqrt{\frac{e\lambda}{m}E_0}} e^{-z/\lambda}\,\Phi\left(\sqrt{-\frac{V(z)}{\lambda E_0}}\right) + \frac{F}{\lambda} e^{-z/\lambda} \int_0^z \frac{e^{-\eta/\lambda}\, d\eta}{\sqrt{\frac{2e}{m}[V(\eta) - V(z)]}}, \tag{15}$$

where

$$\Phi(t) = e^{t^2} \int_0^{\infty} e^{-y^2}\, dy.$$

4. In a number of practically important cases the space charge in the layer is formed by positive ions alone. The potential distribution in the layer in these cases is determined by Poisson's equation, in which the concentration of charged particles is taken from (15) with the boundary conditions

$$V = 0, \quad -\frac{dV}{dz} = E_0 \quad \text{for } z = 0; \quad V = -V_1 \quad \text{for } z = d.$$

When the fields in the layer are large we may neglect the initial ion velocities at $z = 0$, i.e., assume $E_0 = 0$. Then from (15) with the introduction of the dimensionless quantities

$$\frac{z}{\lambda} = x, \quad \frac{-V(z)}{\left(\frac{4\pi eF\lambda^2}{\sqrt{2e/m}}\right)^{2/3}} = U(x), \quad \frac{V_1}{\left(\frac{4\pi eF\lambda^2}{\sqrt{2e/m}}\right)^{2/3}} = U_1,$$

we can write Poisson's equation in the form

$$\frac{d^2U}{dx^2} = e^{-x}\left[\frac{1}{\sqrt{U}} + \int_0^x \frac{e^y\,dy}{\sqrt{U(x)-U(y)}}\right] \tag{16}$$

with the boundary conditions

$$\frac{dU}{dx} = 0, \quad U = 0 \quad \text{for} \quad x = 0; \tag{17}$$

$$U = U_1 \quad \text{for} \quad x = \frac{d}{\lambda}. \tag{18}$$

For small x, i.e., at low pressures, the second term on the right-hand side is small, $e^{-x} \approx 1$ and (16) becomes Langmuir's equation for the plane case. For large x, i.e., at high pressures, the first term on the right may be neglected, and the second term may be transformed as in the derivation of (13). Then (16) becomes the equation used in (4).

If U (x) is the solution of (16) for boundary conditions (17) then (18) gives the relationship between the current in the layer J = eF, the thickness of the layer, the mean free path and the potential difference V_1,

$$V_1 = U\left(\frac{d}{\lambda}\right)\left(\frac{4\pi\lambda^2}{\sqrt{2e/m}}\,J\right)^{2/3} \tag{19}$$

We introduce the auxiliary function $\varphi(x)$ by the relationship $U = (3/2\varphi)^{4/3}$. The equation for $\varphi(x)$ after some simple transformations becomes

$$\varphi'^2(x) - e^{-x} = 3x\left[\int_0^1 e^{-x(1-t^3)}\frac{\varphi^{2/3}(xt^3)}{\varphi^{2/3}(x)}\varphi'^2(xt^3)\,t^2\,dt + \right.$$

$$\left. + \frac{1}{4}\int_0^1 e^{-x(1-t^{3/4})}\sqrt{1 - \frac{\varphi^{4/3}(xt^{3/4})}{\varphi^{4/3}(x)}}\,t^{-1/4}\,dt\right].$$

We shall obtain φ in the form $\varphi = x + c_1x^2 + c_2x^3 + \ldots$. Computations give

$$\varphi = x(1 + 0.07972\,x - 0.00947\,x^2 + \cdots). \tag{20}$$

For small x we may assume with sufficient accuracy that

$$\varphi = x(1 + \alpha x)^{1/4}; \text{ where } \alpha = 4\cdot 0.07972 = 0.31888 \tag{21}$$

In this case by (21)

$$\varphi = x(1 + 0.07972\,x - 0.00953\,x^2 + \cdots).$$

which agrees with (20). For U we obtain

$$U = (3/2\,x)^{4/3}\,(1 + 0.319\,x)^{1/3} \tag{22}$$

For small x, which corresponds to low pressures, (22) becomes Langmuir's expression, which is an exact solution of Poisson's equation for the plane case in the absence of collisions. However, for large x, which corresponds to high pressures, (22) resembles the expression $U = (3/2x)^{4/3}\ (0.302x)^{1/3}$ obtained by V. I. Drozdov [4] from an exact solution of Poisson's equation for high pressures under the same assumptions regarding the interactions between ions and atoms as in the present article. This permits us to employ (22) for intermediate pressures also. With the aid of (22) we can derive a generalization of the 3/2 law for ions at all pressures:

$$J = \frac{\sqrt{2}}{9\pi}\sqrt{\frac{e}{m}}\,\frac{V_1^{3/2}}{d^2}\left[1 + 0.319\,\frac{d}{\lambda}\right]^{-1/2}. \tag{23}$$

From (23) it can be seen that the criterion for the applicability of the usual 3/2 law is the inequality $0.3\ d/\lambda \ll 1$.

LITERATURE CITED

[1] L. A. Sena, J. Exptl.-Theoret. Phys. (USSR) 16, 734 (1946).

[2] Iu. M. Kagan and V. I. Perel', Doklady Akad. Nauk SSSR 98, 575 (1954).

[3] G. Wannier, Phys. Rev. 96, 831 (1954).

[4] V. I. Drozdov, J. Tech. Phys. (USSR) 16, 407 (1946).

[5] W. Weizel, R. Rompe and M. Schön, Z. Physik 112, 339 (1939).

[6] R. L. F. Boyd, Proc. Phys. Soc. (London) 64B, 795 (1951).

Karelo-Finnish State University

Received November 1, 1955

FINE STRUCTURE OF He^3II λ4687 A ALLOWING FOR THE LAMB SHIFT OF THE $nS_{1/2}$ LEVELS

P. S. Kireev

(Presented by Academician L. A. Artsimovich November 30, 1955)

A large number of papers have been devoted to the study of the fine structure of hydrogen and hydrogen-like atoms. Interest in the fine structure grew after the strict proof by Lamb and Rutherford, using radiospectroscopy, of the shift of the $nS_{1/2}$ level with respect to the $nP_{1/2}$ level, which levels coincide in Dirac's theory. He^4II λ 4686 has been carefully studied by high-resolution spectroscopy. We investigated the structure and intensity of the components of this line. It is of considerable interest to investigate the structure of the line of the other isotope He^3.

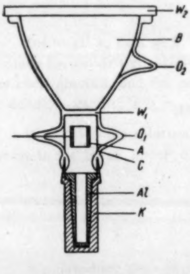

Fig. 1

In this article we first investigate the fine structure of He^3II λ 4687 (transition $n = 4 \rightarrow n = 3$). An ISP-51 spectrograph with an F-270 camera was used. The structure was resolved by a Fabry-Perot etalon placed before the slit of the spectrograph. The interference pattern was projected on the slit of the spectrograph with an F-120 mm objective. The secondary images were collected by an auxiliary slit. We used etalons of 2 and 2.5 mm separations.

The light source was a sealed discharge tube with a hollow cathode (see Fig. 1). The cathode consisted of two parts. The copper cup K soldered to the glass C provided a hermetic seal. The discharge takes place in the hollow of the aluminum insert Al which was fitted into the cup K. The diameter of the hollow space was 9 mm and its length 50 mm. The aluminum insert was necessary to eliminate the copper spectrum since, with spectrograph slits of ~ 0.3-0.4 mm width, the copper lines partially overlap the line which we were investigating. The evacuated chamber B with the window W_2 protects the rotating prism, and the window W_1 from frosting over. A is the aluminum anode; O_1 and O_2 are extensions for connection to the vacuum system. The source was contained in a Dewar with liquid nitrogen. A hollow cathode was used because the illumination in the hollow space gives comparatively intense lines of ionized helium. A disadvantage of the sealed hollow cathode is its limited period of serviceability. Photographs were taken on aerial film. The current in the source varied from 40 to 200 ma. The exposure time varied from 15 to 60 minutes.

The lines were resolved into four groups, each of which consisted of a few components. Some of the photographs resolved the $3P_{1/2} - 4S_{1/2}$ component, but the resolution was less satisfactory than in the case of He^4II. The separation of the groups was measured with an IZA-2 comparator. The results of the measurements were treated by the tabular method of exact fractions.

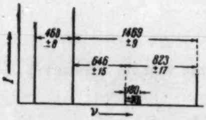

Fig. 2

Fig. 2 shows the structure of the line obtained with a 2 mm etalon, giving the separations between the group maxima and the arithmetical average of the spread. The separations are given in units $1 \cdot 10^{-3}$ cm^{-1}. The results show satisfactory agreement with the theory of the fine structure including the Lamb shift. For the $3S_{1/2}$ shift we obtained $116 \pm 15 \cdot 10^{-3}$ cm^{-1}. The $4S_{1/2}$ shift was measured with considerably less accuracy and can be estimated at $64 \pm 30 \cdot 10^{-3}$ cm^{-1}. The shift was obtained with neglect of the hyperfine structure.

We are at present studying the intensity of the line components.

I am deeply grateful to F. A. Korolev for his interest and assistance.

M. V. Lomonosov Moscow State University

Received November 29, 1955

THE NATURE OF CONCENTRATION EFFECTS IN SOLUTIONS OF ACRIDINIC COMPOUNDS

L. V. Levshin

(Presented by Academician A. N. Terenin December 3, 1955)

In earlier articles the author showed that increased concentrations materially affect the fundamental optical properties of solutions of many acridinic compounds: their absorption, luminescence and polarization spectra, luminescence yield and average lifetime of excited states [1-3]. When such changes are observed in solutions of dyes they are usually attributed either to the resonance migration of excitation energy or to the association of molecules of the dissolved substance [4]. However, it has been shown that in the solutions of acridinic compounds which have been studied, these effects do not play an important part. It has been shown that molecules of 3,6-diaminoacridine can be found in solution in two colored forms which can be converted into each other [5]. The location of equilibrium between them depends on the concentration of the solution, the nature of the solvent and the ambient temperature. It has been proved that the effect of all these factors is exerted principally through a change of the pH of the solution, which determines the ratio between the two forms of 3,6-diaminoacridine molecules. This behavior was established on the basis of an analysis of the dependence of the absorption spectrum of 3,6-diaminoacridine on the concentration and pH of the solution [5]. Absorption spectra of both forms of 3,6-diaminoacridine molecules were obtained at the same time.

The aim of the present work was the separation of the total radiation of 3,6-diaminoacridine solutions into the radiation of the two components, the establishment of the shape and relative intensity of their luminescence bands and the clarification of the nature of the concentration changes observed earlier in the luminescence spectra of such solutions. Moreover, it was of interest to extend the conclusions obtained for 3,6-diaminoacridine solutions to certain other compounds of the acridine series.

The luminescence spectra were measured photoelectrically with an ISP-51 high-transmission glass spectrograph combined with a PS-381 photoelectric attachment. The light receiver was an FEU-17 photomultiplier whose signal was automatically recorded on photographic paper. Radiation was excited by the 436 and 365 mμ lines from a PRK-2 mercury lamp, using special filters. Under these conditions corrections for reabsorption were introduced into the luminescence spectra whenever necessary. The pH of the solutions was determined with an LP-5 tube potentiometer in which measurements were made with a glass electrode.

It was shown previously that as the concentration increases the luminescence spectrum of 3,6-diaminoacridine is shifted towards longer waves and undergoes some change of shape. A similar picture was observed when the wavelength of the exciting light was decreased [1,2]. The presence in a concentrated solution of two colored forms of 3,6-diaminoacridine leads us to assume that these phenomena result from the luminescent power of both types of molecules, whose luminescence spectra differ.

In order to verify this assumption it was necessary to compare the luminescence spectra of solutions in which the first and second forms of 3,6-diaminoacridine molecules would be found in the pure form. Our earlier results [5] enabled us, by changing the pH of the solution, to keep the 3,6-diaminoacridine molecules in either form at any concentration. The first form, for which long-wave absorption is characteristic, was obtained in a dilute solution ($C = 1 \cdot 10^{-5}$ g/cm^3), whose pH was small (pH 8.5). The second form, which is characterized by a short-wave absorption band, was obtained from the same solution by considerably increasing its pH (pH > 11) through the addition of dilute NaOH.

Fig. 1 compares the luminescence spectra of solutions whose maxima are equal. It can be seen from the figure that the absorption spectra of both forms of molecules differ appreciably. The luminescence spectrum of

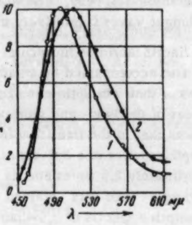

Fig. 1. The luminescence spectrum of 3,6-diaminoacridine in ethyl alcohol ($C = 1 \cdot 10^{-5}$ g/cm³ as a function of the pH of the solution: 1) pH 8.5; 2) pH > 11

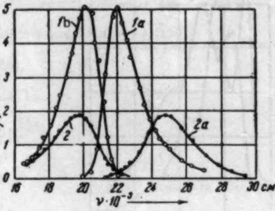

Fig. 2. Relative positions of the absorption (a) and luminescence (b) spectra of the first (1) and second (2) forms of 3,6-diaminoacridine molecules in ethyl alcohol

the first form has a maximum at $\lambda_{\max} = 500$ mμ; in the second, it is somewhat shifted towards longer waves at $\lambda_{\max} = 510$ mμ. In addition, the energy distribution in the luminescence spectra is identical.

A comparison of these changes with the changes observed with increased concentrations [2] shows that they are alike qualitatively. However, the concentration effects are somewhat weaker than the changes observed upon sharply increasing the pH of the solution. This difference can be explained if it is remembered that the solutions under study were always a mixture of both types, and the observed luminescence spectrum resulted from the superposition of their emissions.

The described changes of the luminescence spectra of 3,6-diaminoacridine are reversible; they disappear with reverse decreasing of the pH either by dilution or by adding small quantities of dilute hydrochloric acid. As a result, the luminescence spectrum is completely restored to the position and shape which are characteristic of a very dilute solution. A similar pattern results from lowering the pH of a concentrated solution by the addition of dilute hydrochloric acid.

The previously observed dependence of the luminescence spectrum of 3,6-diaminoacridine on the wavelength of the exciting light [2] should be absent when there is a complete transition of the molecules from one form to the other, due to change of the pH. This was actually observed in solutions of 3,6-diaminoacridine, all of whose molecules were in the second form. A change of wavelength of the exciting light ($\lambda_{ex} = 436$ and 365 mμ) did not affect the shape and position of the luminescence spectrum.

We thus obtained in pure form, not only the absorption spectrum of the second form of 3,6-diaminoacridine molecules [5], but also its luminescence spectrum. It was also shown that the mirror symmetry of absorption and luminescence spectra, which was observed by B. S. Neporent [6] and T. M. Tarasova [7] for dilute solutions (first form) and later confirmed by our own experiments, is also well satisfied for the second form of these molecules (Fig. 2). However, in this case the spectra are considerably separated, which leads to a notable increase of the frequency in the electron transition. Thus, if for the first form $\nu_0 \approx 21050$ cm^{-1}, for the second form it is $\nu_0 \approx 22100$ cm^{-1}. The transition from the first form of 3,6-diaminoacridine to the second thus induces a considerable enlargement of the separation between the low-lying vibrational levels of the normal and excited states of the molecule. However, both systems of vibrational levels, corresponding to the normal and excited states of the 3,6-diaminoacridine molecules, change in the same way and remain similar in structure. The same can be said of their relative populations and of the probabilities of the corresponding regular and inverse transitions [4]. The indicated increase of frequency in the electron transition is due mainly

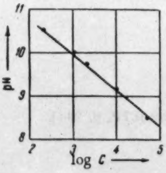

Fig. 3. Effect of concentration of 9-aminoacridine on the pH of an alcohol solution

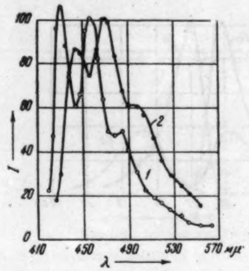

Fig. 4. Dependence of the luminescence spectrum of 9-aminoacridine in ethyl alcohol ($C = 1 \cdot 10^{-5}$ g/cm^3) on the pH of the solution: 1) pH 8.5; 2) pH 10.9

to the short-wave shift of the absorption band. The shift of the luminescence spectrum towards longer waves is relatively small.

The transition of 3,6-diaminoacridine molecules from one modification to the other is also accompanied by an appreciable change of the absolute values of their absorption and emission powers. A comparison of the areas of the long- and short-wave absorption and emission bands showed that in the transition from the first to the second form the absorptive power of a 3,6-diaminoacridine molecule is decreased approximately 2.5 times and its emissive power, 3 times. These results agree with data obtained earlier from concentration changes of absorption spectra of 3,6-diaminoacridine in various solvents [2].

It is interesting to note that each form of the 3,6-diaminoacridine molecule differs in sensitivity to the action of light. While the first form does not change noticeably under prolonged exposure, in the second form the changes take place quite rapidly and the solution rapidly darkens from the action of light rays. This can be explained by the fact that concentrated solutions darken when illuminated, while dilute solutions remain without visible changes.

As has been shown previously [1,3], concentration effects are also observed in other acridinic compounds. The greatest changes are observed in the luminescence spectra of 9-aminoacridine, where its emission changes from the blue to bluish-green as the concentration of the solution increases. It appeared that, just as in the case of 3,6-diaminoacridine, a reduced concentration of 9-aminoacridine leads to a notable reduction of the pH of the solution, which is evidence of the dissociation of molecules of this type. The results of the measurements are given in Fig. 3. Analogously to the solutions of 3,6-diaminoacridine, they suggest that in the case of 9-aminoacridine the pH of the solution plays a decisive role in determining whether the molecule exists in one form or the other.

In order to confirm this hypothesis, we studied the dependence of the luminescence spectra of 9-aminoacridine in ethyl alcohol on the pH . Fig. 4 shows the results of these experiments. The pH was changed, as previously, by putting small amounts of NaOH into the solution. It can be seen from the figure that with a rise of pH, despite the small concentration of the solution ($C = 1 \cdot 10^{-5}$ g/cm^3), the luminescence spectrum is shifted considerably towards the long-wave side with some change of shape.

A comparison of these changes with the changes observed with higher concentrations [1,3] shows that they are practically identical. Just as for 3,6-diaminoacridine these phenomena are reversible. By reducing the pH the luminescence spectrum of a concentrated solution can be brought back to the luminescence spectrum which is characteristic of a low concentration. Thus, the molecules of 9-aminoacridine can also exist in two colored forms, whose luminescence spectra differ considerably. The differences in the absorption spectra of these forms are much less pronounced [3].

In conclusion I wish to thank A. P. Khovanskii for his assistance.*

LITERATURE CITED

[1] L. V. Levshin, Doklady Akad. Nauk SSSR 96, 473 (1954).

[2] L. V. Levshin, J. Exptl.-Theoret. Phys. (USSR) 28, 201 (1955) [Soviet Physics JETP, p. 244].

---

*Note added in proof. Later experiments showed that for pH 8.5 the solution still contains a small number of the second form of 3,6-diaminoacridine molecules. They disappear completely at pH ≈ 2, which leads to a very small long-wave shift of the short-wave edge of the luminescence spectrum. The mirror symmetry of the absorption and emission spectra of 3,6-diaminoacridine molecules of the first form then becomes even more rigorous.

[3] L. V. Levshin, J. Exptl.-Theoret. Phys. (USSR) 28, 213 (1955) [Soviet Physics JETP, p. 235].

[4] L. V. Levshin, Photoluminescence in Liquids and Solids (Moscow and Leningrad, 1951).

[5] L. V. Levshin, Bull. Acad. Sci. USSR, Phys. Ser. 20, 4 (1956).

[6] B. S. Neporent, J. Exptl.-Theoret. Phys. (USSR) 21, 172 (1951).

[7] T. M. Tarasova, J. Exptl.-Theoret. Phys. (USSR) 21, 189 (1951).

M. V. Lomonosov
Moscow State University

Received November 30, 1955

HIGH DIELECTRIC CONSTANTS OF NIOBATES AND TANTALATES OF DIVALENT METALS

G. A. Smolenskii, V. A. Isupov and A. I. Agranovskaia

(Presented by Academician A. F. Ioffe November 26, 1955)

The dielectric properties and structure of niobates and tantalates of divalent metals, unlike the titanates, zirconates and stannates, have not been investigated sufficiently. The first studies of these compounds showed that some of the niobates and tantalates are distinguished by high dielectric constants and that $PbNb_2O_6$, $PbTa_2O_6$ and $Cd_2Nb_2O_7$ are ferroelectrics [1-6]. Thus, there is obvious profit to be derived from a systematic study of the niobates and tantalates. We give below some results of such work.

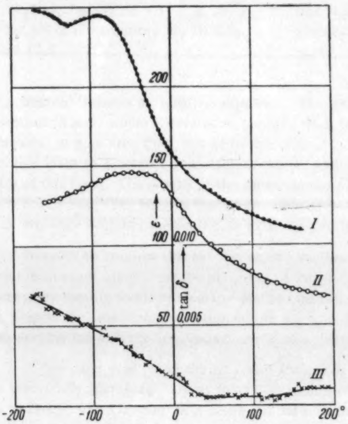

Fig. 1. Temperature dependence of ε and tan δ of specimens of $Sr_2Ta_2O_7$ in weak fields with f = 500 Kc. I) ε of a specimen fired at 1450° for 0.5 hr. II and III) ε and tan δ of a specimen fired at 1400° for 1 hr.

The specimens of niobates and tantalates were manufactured in the usual manner: the finely divided original materials were briquetted and fired; after pulverization the specimens which were pressed out were subjected to a final firing. The majority of the specimens showed porosity of not more than 1.5%. We measured ε, tan δ and the temperature dependence of ε of the polycrystalline specimens. Table 1 gives the results. The table also contains data on structure taken from the literature [7].

It is seen from the table that niobates and tantalates of divalent metals have high dielectric constants and negative temperature coefficients. Exceptions are calcium metaniobate, metatantalate and pyroniobate.

The compounds which crystallize in a cubic structure of the pyrochlore type have a higher dielectric constant than the pyroniobates and pyrotantalates with other structures. In the pyrochlore structure the small cation (Nb^{5+}, Ta^{5+}), just as in the peroffskite structure, is surrounded octahedrally by oxygen ions. However, the octohedrons here have a zigzag, rather than a linear, arrangement.

Figs. 1 and 2 show the temperature dependence of ε and tan δ and the hysteresis loop of specimens of $Sr_2Ta_2O_7$. It follows from these figures that $Sr_2Ta_2O_7$ is a ferroelectric. Strontium pyrotantalate probably crystallizes in a pyrochlore structure. The existence of spontaneous polarization in $Sr_2Ta_2O_7$ is all the more interesting because Hulm observed no anomalies in the temperature dependence of the dielectric constants of $Cd_2Ta_2O_7$ and $Pb_2Ta_2O_7$ [3]. The reasons for the fact that the strontium pyrotantalate specimens have an ε which is relatively small for ferroelectrics have as yet not been established. The porosity of the specimens was not higher than 0.2%.

TABLE 1

Formula	Structure and lattice parameters	Dielectric Constant at $t \simeq 20°$, $f = 10^3$ cycles	Temperature coefficient of ϵ from 20 to 80°, $\alpha \cdot 10^6$ (1/°C)	Tangent of dielectric loss angle at $f \simeq 10^3$ cycles, $t \sim 20°$
Niobates				
$CaNb_2O_6$		~20	100-160	0.02-0.066
$CdNb_2O_6$		90	-2000	0.011
$SrNb_2O_6$		44		0.083
$PbNb_2O_6$	Orthorhombic unit cell containing 40 "molecules"	280 [4]	Large positive (ferroelectric region, $\theta = 570°$)	0.005 [4]
$BaNb_2O_6$		40	-90	0.0023
$Ca_2Nb_2O_7$	Complex (not pyrochlore type)	31	270	0.009
$Cd_2Nb_2O_7$	Pyrochlore type, $a = 10.372$ A	500-585 [1-3]	Large negative, $\theta = 90°$	0.014
$Sr_2Nb_2O_7$	Complex (not pyrochlore type)	60	-360	0.010
$Pb_2Nb_2O_7$	Pryochlore type (rhombohedral distortion), $a = 10.675$ A, $\alpha = 88°50'$	144	-1500	0.0003
$Ba_2Nb_2O_7$		45	-160	0.0018
Tantalates				
$CaTa_2O_6$		24-25	100-140	0.03-0.036
$CdTa_2O_6$		60	-510	0.16
$SrTa_2O_6$		100-115	-(1100-1150)	0.007-0.03
$PbTa_2O_6$		-400 [5]	Large positive (ferroelectric region, $\theta = 260°$)	0.022 [5]
$BaTa_2O_6$		132	-1600	0.003
$Ca_2Ta_2O_7$	Pyrochlore type	45	-(420-450)	0.0009-0.0015
$Cd_2Ta_2O_7$	Pryochlore type, $a = 10.376$ A	80-113	-(960-1020)	0.07-0.11
$Sr_2Ta_2O_7$		118	Large negative	0.0007
$Pb_2Ta_2O_7$	Pyrochlore type (rhombohedral distortion), $a = 10.700$ A, $\alpha = 88°25'$	100-114	-340	0.0062
$Ba_2Ta_2O_7$		46-50	-460	0.0007

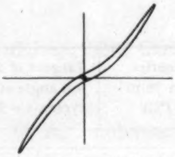

Fig. 2. Hysteresis loop of $Sr_2Ta_2O_7$ at the temperature of liquid nitrogen and E = 27 kv/cm

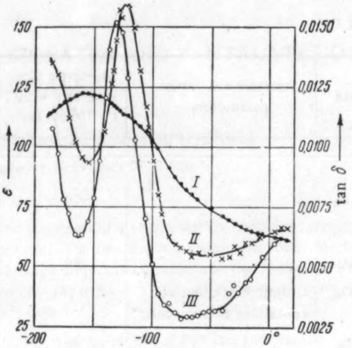

Fig. 3. Temperature dependence of ε and tan δ of a specimen of $CdNb_2O_6$ in weak fields. I) ε at 1500 Kc; II) tan δ at 1500 Kc; III) tan at 500 Kc

In the studies of the temperature dependence of ε and tan δ of metaniobates and metatantalates, it was observed that ε and tan δ of $CdNb_2O_6$ pass through a maximum (see Fig. 3). However, these maxima are not associated with the ferroelectric phase transition, and have a relaxational character. They are probably due to electronic processes.

A number of niobates and tantalates are characterized by fairly high dielectric losses, which can be explained by their high electronic conductivity.

LITERATURE CITED

[1] W. R. Cook and H. Jaffe, Phys. Rev. 88, 1426 (1952) 89, 1297 (1953).

[2] G. Shirane and R. Pepinsky, Phys. Rev. 92, 504 (1953).

[3] J. K. Hulm, Phys. Rev. 92, 504 (1953).

[4] G. Goodman, J. Am. Ceram. Soc. 36, 368 (1953).

[5] G. A. Smolenskii and A. I. Agranovskaia, Doklady Akad. Nauk SSSR 97, 237 (1954).

[6] E. Weiner and C. Wentworth, J. Am. Ceram. Soc. 35, 207 (1952).

[7] F. Jona, G. Shirane and R. Pepinsky, Phys. Rev. 98, 4, 903 (1955).

Institute for Silicate Chemistry
Academy of Sciences of the USSR

Received November 24, 1955

THE SALAM-POLKINGHORNE CLASSIFICATION AND THE NEUTRON CHARGE HYPOTHESIS

Ia. P. Terletskii

(Presented by Academician N N. Bogoliubov November 24, 1955)

In connection with attempts to explain the principal characteristics of the production and decay of hyperons and heavy mesons (simultaneous production of hyperons and heavy mesons, long lifetime of hyperons and heavy mesons, predominant production of positive heavy mesons, etc.), certain writers [1-3] have recently advanced the hypothesis of a new conservation law, which is not an absolute law but is violated in certain processes. It is assumed that this conservation law is strictly observed in the production of pions, heavy mesons and hyperons, and forbids the rapid decay of these particles, but that it can be violated in "slow" decay processes. In our articles [4,5] on the classification of elementary particles we also postulated a new conservation law – the conservation of neutron charge, but we considered this to be an absolute law*. It can easily be shown that the neutron charge hypothesis is only a different, and also the physically simplest, formulation of the conservation law introduced in [1-3] if we admit the possibility of nonconservation of neutron charge in slow decay processes. This can be shown most easily through an analysis of the Salam-Polkinghorne classification [3].

In the spirit of the four-dimensional isotopic spin formalism of Pais [6], in [3] the infinitesimal transformation operator of the rotation group $I_{\alpha\beta}$ is considered in four-dimensional Euclidean isotopic space and is known to satisfy the following conditions:

$$I_{\alpha\beta} = -I_{\beta\alpha},$$
$$[I_{\alpha\beta}, I_{\gamma\delta}] = i\delta_{\alpha\gamma}I_{\beta\delta} + i\delta_{\beta\delta}I_{\alpha\gamma} - i\delta_{\alpha\delta}I_{\beta\gamma} - i\delta_{\beta\gamma}I_{\alpha\gamma}. \tag{1}$$

If the independent components of $I_{\alpha\beta}$ are designated by

$$I_{21} = -h_3, \quad I_{31} = h_2, \quad I_{32} = -h_1, \quad I_{41} = e_1, \quad I_{42} = e_2, \quad I_{43} = e_3, \tag{2}$$

then, according to (1), for the linear combinations

$$\tau_i = {}^1/_2\,(e_i + h_i), \quad \mu_i = {}^1/_2\,(e_i - h_i) \tag{3}$$

the following relations are valid:

$$[\tau_i \tau_j] = i\tau_k, \quad [\mu_i \mu_j] = i\mu_k, \quad [\tau_i \mu_j] = 0 \tag{4}$$

(where i, j, k are cyclical permutations of 1, 2, 3) from which it can be seen that τ_i and μ_i can be regarded as infinitesimal transformation operators of the three-dimensional rotation group. Thus, two isotopic spins are formally introduced in [3]: the ordinary τ_i and μ_i, with the conservation of μ_i expressing the new conservation law. Reference [3] contains no physical grounds for the need of considering not pseudo-Euclidean but

---

*The assumption that neturon charge is conserved in all processes led to some peculiarities in the classification, such as an increase of the number of pions and neutrinos.

Euclidean four-dimensional isotopic space. The physical meaning of μ_i is not given in [3] and only the numbers μ_3 and τ_3 are used in the systematics, not the vectors μ_i and τ_i.

Assuming an electric charge given by

$$E = e_3 = \mu_3 + \tau_3, \tag{5}$$

the authors postulate a classification of nucleons, hyperons, π-, θ- and τ-mesons which differs from Gell-Mann's classification [1] only for τ-mesons. The scheme of [3] is reproduced in the first three columns of Table 1.

TABLE 1

Particles	τ_3	μ_3	$E=\mu_3+\tau_3$	$\varepsilon=\mu_3-\tau_3$	$s=\varepsilon+E+N$
π^+, π^0, π^-	1,0,—1	0	1,0,—1	—1,0,1	0
τ^+, τ^0, τ^-	0	1,0,—1	1,0,—1	1,0,—1	2,0,—2
θ^+, θ^0	½, —½	½, ½	1,0	0.1	1
$\tilde{\theta}^0, \theta^-$	½, —½	—½, —½	0,—1	—1,0	—1
p, n	½,—½	½, ½	1,0	0,1	0
Λ^0	0	0	0	0	—1
$\Sigma^+, \Sigma^0, \Sigma^-$	1,0,—1	0	1,0,—1	—1,0,1	—1
Ξ^0, Ξ^-	½, —½	—½, —½	0,—1	—1,0	—2

In the next two columns of this table we give in addition the total electric charge E and the quantity

$$\varepsilon = -h_3 = \mu_3 - \tau_3, \tag{6}$$

which, in agreement with [4,5], we call the neutron charge. In the last column are given the values of

$$s = \varepsilon + E + N, \tag{7}$$

where N is the difference between the number of antinucleons and nucleons or "nuclear charge", in agreement with our convention in [4,5]. In [1] the quantity s is called the "strangeness".

ϵ^* in Table 1 agrees with ϵ in our classification [5] for pions, nucleons and Ξ^--particles (which were designated by Λ^0), but ϵ for θ^0- and Λ^0-particles differ in these systems. The values of E and ϵ assumed in [5] for hypothetical π_1-particles agree with the values of E and ϵ in [3] for $\tau^\pm$-particles. $\Sigma^\pm$-particles were not considered at all in [4,5] since, at the time, the necessary experimental data were not available. The difference in ϵ for some particles in [5] and [3] is due only to the fact that [5] disregarded the possibility of nonconservation of neutron charge in slow decays and ϵ was chosen so that for all reactions $\Delta\epsilon = 0$.

According to Table 1, the neutron charge is conserved for all particle-production processes which actually occur. Thus, for example, $\Delta\epsilon = 0$ for the processes: $\pi^- + p \rightarrow \theta^0 + \Lambda^0$, $\pi^- + p \rightarrow \theta^+ - \Sigma^-$, $\pi^- + p \rightarrow \tau^+ + \Xi^-$, $\pi^+ + n \rightarrow \theta^+ + \Lambda^0$, $\pi^+ + p \rightarrow \theta^+ + \Sigma^+$. However, for $\pi^- + n \rightarrow \theta^- + \Lambda^0$, which is presumably forbidden, $\Delta\epsilon = -?$. For the slow decay processes $\Xi^- \rightarrow \pi^- + \Lambda^0$, $\Lambda^0 \rightarrow \pi^- + p$, $\Sigma^\pm \rightarrow \pi^\pm + n$, $\Sigma^+ \rightarrow \pi^0 + p$, $\theta^0 \rightarrow \pi^+ + \pi^-$, $\theta^\pm \rightarrow \pi^\pm + \pi^0$ $|\Delta\epsilon| = 1$ according to the table. Finally, for the practically forbidden process $\Xi^- \rightarrow \pi^- + n$ we have $\Delta\epsilon = 2$.

Thus the entire Salam-Polkinghorne table can be regarded as constructed on the basis of the **assumptions** that:

a) $\Delta\epsilon = 0$ in meson production and simultaneous creation of heavy mesons and hyperons;

b) $|\Delta\epsilon| = 1$ in slow decay of hyperons and heavy mesons;

c) $|\Delta\epsilon| = 2$ for very slow strongly forbidden processes.*

Such rules were formulated for "strangeness" in [1] and for $a = -(\epsilon + E) = -s + N$, called the "attribute" by Sachs [2]. The agreement of these rules results from the absolute invariability of the charges E and N.

In [5] we showed that the isotopic spin hypothesis for systems consisting of nucleons and pions can be regarded as a result of the antisymmetry of the wave function of the system with regard to permutations of coordinates and spins, as well as of the charges E and ϵ. For other particle systems, for which antisymmetry of the wave function does not hold, there is obviously no sense in introducing the concept of total isotopic spin. There would thus be better physical justification for starting, not with formal concepts of isotopic spin or isotopic spins τ_i and μ_i, which may not represent anything real for some sets of particles, but with an approximate conservation law of neutron charge ϵ, together with an absolute conservation law for the electrical charge E.

Antisymmetry of the nucleonic wave function with respect to permutations of coordinates, spins and E- and ϵ-charges may be due to complete identity of interactions of particles possessing either E- or ϵ-charge at sufficiently close distances. Therefore, the neutron charge can be regarded not only as a quantity which is conserved in some instances like the "nuclear charge", but as a charge producing a vector "neutron" field, just as an electrical charge produces an electromagnetic field. It is obvious that this cannot be a long-range field. The quanta of the neutron field must have a finite rest mass. It must also be assumed that the fields which cause nuclear interactions and the corresponding interaction constants are symmetrically related to the charges E and ϵ.

Thus, the principal results of [3] and [1], as in the case of the ordinary isotopic spin hypothesis, can be regarded as resulting from the hypothesis of neutron charge, allowing for nonconservation thereof in slow processes. The most complete classification of elementary particles can, therefore, be based only on the laws of conservation of nuclear, electrical and neutron charge**, in which the last conservation law must be regarded as exactly fulfilled only in processes which result from strong and electromagnetic interactions, and violated in processes which result from weak interactions.

LITERATURE CITED

[1] M. Gell-Mann, Conference in Pisa (1955).

[2] R. G. Sachs, Phys. Rev. 99, 1573 (1955).

[3] A. Salam and J. C. Polkinghorne, Nuovo cimento 2, 685 (1955).

[4] Ia. P. Terletskii, Doklady Akad. Nauk SSSR 94, 209 (1954).

[5] Ia. P. Terletskii, Doklady Akad. Nauk SSSR 101, 1035 (1955).

[6] A. Pais, Proc. Nat. Acad. Sci. U.S. 40, 484 (1954).

[7] G. Marx, Acta Phys. Acad. Sci. Hung., 3, 55 (1953).

[8] Ia. B. Zel'dovich, Doklady Akad. Nauk SSSR 91, 1317 (1953).

Institute of Nuclear Problems, Academy of Sciences, USSR

Received November 16, 1955

---

*From this point of view the decay of particles that are identical with the τ-mesons in [3] or with the π_1-particles in [4,5] to ordinary π-mesons is strongly forbidden. Therefore, it would be more justifiable to consider τ-mesons to be similar to the θ-particles of Table 1, as was proposed in [1]. Particles possessing the charges of π_1-particles can be a new form of heavy meson which may possibly be heavier than τ-mesons.

**It is possible that, for the classification of light particles, we must introduce a fourth law of conservation of "neutrino charge" [7,8], similar to the law of "nuclear charge" conservation for heavy particles, as we noted in [4].

CHARACTERISTIC TIMES OF ELECTRONIC PROCESSES IN SEMICONDUCTORS

E. I. Adirovich and G. M. Guro

(Presented by Academician A. F. Ioffe October 13, 1955)

1. The kinetics of electronic transitions in semiconductors which contain one type of recombination center (traps), is described by the equations (see Fig. 1)

$$\frac{dn}{dt} = G - A_e np_t + B_e n_t, \quad \frac{dp}{dt} = G - A_h pn_t + B_h p_t,$$
$$n_t + p_t = N_t, \quad p - n - n_t = N_a - N_d - \delta. \tag{1}$$

The last equation expresses the condition of neutrality. Acceptors and donors are assumed to be fully ionized and are not shown in Fig. 1. $\delta = 0$ if the traps are acceptors and $\delta = N_t$ if the traps are donors. Dividing all concentrations into equilibrium and nonequilibrium parts ($n = n_0 + n'$, $p = p_0 + p'$, etc.), and dropping terms which are quadratic with respect to nonequilibrium concentrations, we obtain

$$\frac{dn'}{dt} = G - A_e p_{t0} n' - A_e n_0 p'_t + A_e n_1 n'_t,$$
$$\frac{dp'}{dt} = G - A_h n_{t0} p' - A_h p_0 n' + A_h p_1 p'_t, \tag{2}$$
$$n'_t = -p'_t, \quad p' = n' + n'_t.$$

Here

$$n_0 = N_0 e^{-(E_2 - F)/kT}, \quad p_0 = N_0 e^{-(F - E_1)/kT}$$
$$n_{t0} = \frac{N_t}{1 + e^{(E_t - F)/kT}}, \quad p_{t0} = N_t \frac{e^{(E_t - F)/kT}}{1 + e^{(E_t - F)/kT}}, \tag{3}$$
$$n_t = \frac{B_h}{A_h} = N_0 e^{-(E_2 - E_t)kT}, \quad p_1 = \frac{B_h}{A_h} = N_0 e^{-(E_t - E_1)kT},$$

where F is the Fermi level; $N_0(T) = 2(2\pi mkT/h^2)^{3/2} = 4.82 \cdot 10^{15} T^{3/2}$.

Solving the set of equations (2) for attenuation of the nonequilibrium concentrations ($G = 0$) with stationary initial conditions ($dn'/dt = dp'/dt = 0$), we obtain

$$n' = G\tau_1 e^{-t/\tau_1} + G(\tau_e^{st} - \tau_1) e^{-t/\tau_2}, \quad p' = G\tau_1 e^{-t/\tau_1} + G(\tau_h^{st} - \tau_1) e^{-t/\tau_2},$$
$$p'_t = -n'_t = G(\tau_e^{st} - \tau_h^{st}) e^{-t/\tau_2}, \tag{4}$$

if $\tau_1 \ll \tau_2$. The solution contains four time parameters.

Two of these:

$$\tau_e^{st} = \tau_0 \frac{1 + \tau_{n0} n_{t0} / (n_0 + p_0)\tau_0}{1 + \dfrac{\tau_{p0} p_{t0} n_0 + \tau_{n0} n_{t0} p_0}{(n_0 + p_0)^2 \tau_0}}, \qquad \tau_h^{st} = \tau_0 \frac{1 + \tau_{p0} p_{t0}\ (n_0 + p_0)\tau_0}{1 + \dfrac{\tau_{p0} p_{t0} n_0 + \tau_{n0} n_{t0} p_0}{(n_0 + p_0)^2 \tau_0}} \tag{5}$$

agree with the lifetimes of electrons and holes according to Shockley and Read,* determined from the stable state when the rate of recombination is equal to the rate of pair creation. The two other time parameters are**

$$\tau_1 = \frac{1}{A_9 p_{t0} + A_e (n_0 + n_1) + A_{,} n_{t0} + A_h (p_0 + p_1)} =$$

$$= \frac{N_t}{n_0 + p_0} \frac{\tau_{p0}\tau_{n0}}{\tau_0} \frac{1}{1 + \dfrac{\tau_{p0} p_{t0} + \tau_{n0} n_{t0}}{(n_0 + p_0)\tau_0}}, \qquad \tau_2 = \tau_0 \frac{1 + \dfrac{\tau_{p0} p_{t0} + \tau_{n0} n_{t0}}{(n_0 + p_0)\tau_0}}{1 + \dfrac{\tau_{p0} p_{t0} n_0 + \tau_{n0} n_{t0} p_0}{(n_0 + p_0)^2 \tau_0}}, \tag{6}$$

and these, as can be seen from (4) rather than τ_e^{st} and τ_h^{st} serve as characteristic attenuation times.

2. For low trap concentrations

$$N_t \ll a(n_0 + n_1 + p_0 + p_1), \tag{7}$$

where a is the smaller of the ratios τ_{p0}/τ_{n0} and τ_{n0}/τ_{p0},

$$\tau_2 = \tau_e^{st} = \tau_h^{st} = \tau_0, \quad \tau_1 \approx \frac{1}{A_e (n_0 + n_1) + A_h (p_0 + p_1)} = \frac{N_t}{p_0 + n_0} \frac{\tau_{p0}\tau_{n0}}{\tau_0} \ll \tau_0. \tag{8}$$

Returning to (4) we see that in this case

$$n' \approx p' \approx G\tau_0 e^{-t/\tau_0}, \tag{9}$$

i.e., there is one characteristic attenuation time which agrees with the lifetime of nonequilibrium (intrinsic and impurity) carriers under stable conditions.

Let us consider the case of large trap concentrations corresponding to a reversal of the inequality sign of (7). According to (5) and (6)

$$\tau_2 \approx \tau_e^{st} + \tau_h^{st} \approx \tau_{larger}^{st}, \quad \frac{1}{\tau_1} \approx \frac{1}{\tau_e^{st}} + \frac{1}{\tau_h^{st}} \approx \frac{1}{\tau_{smaller}^{st}} \tag{10}$$

Consequently, for large concentrations of traps the attenuation process is determined by two characteristic times. From (10) it follows that for a different order of magnitude of τ_e^{st} and τ_h^{st} the lifetime that characterizes attenuation through most of its duration is not equal to the lifetime of the impurity characters, but to the longer of the times τ_e^{st} and τ_h^{st}, regardless of the character of the intrinsic conductivity involved in the semiconductor transitions (electrons or holes).

---

* $\tau_{n0} = \dfrac{1}{A_e N_t}$; $\tau_{p0} = \dfrac{1}{A_h N_t}$; $\tau_0 = \tau_{p0} \dfrac{n_0 + n_1}{n_0 + p_0} + \tau_{n0} \dfrac{p_0 + p_1}{n_0 + p_0}$.

** Equation (6) is an approximate form of the attenuation time which is valid for $\tau_1 \ll \tau_2$.

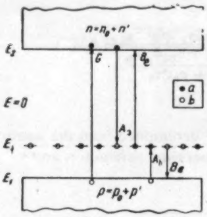

Fig. 1. Transition scheme of electrons (a) and holes (b) in the semiconductor energy diagram.

3. The values of τ_h^{st}, τ_e^{st} and τ_2 for germanium, depending on the position of the Fermi level for $T = T_0 = 300°$ K, $N_t = 2.5 \cdot 10^{19}$ cm^{-3}, $E_t = -0.155$ ev and $A_e = A_h$ are shown graphically in Fig. 2. When the Fermi level passes through the traps, and $\tau_e^{st} \sim \tau_h^{st}$, $\tau_1 \sim \tau_2$, the approximate equations (6) cannot be applied* and the values of τ_2 are taken from exact equations. For comparison, the same figure gives the curve $\tau_0(F)$.

From a comparison of the curves $\tau_0(F)$ and $\tau_e^{st}(F)$ we see that for large trap concentrations the maximum of $\tau_e^{st}(F)$ is shifted to the regions of e-type conductivity $(F > 0)$.

When the Fermi level is shifted from the valence zone to the conduction zone $\tau_e^{st} = n'/G$ first increases because of the diminution of $A_e p_{t0} n'$ (see (2) for $dn'/dt = dp'/dt = 0$), and when this term becomes sufficiently small τ_e^{st} is reduced as $A_e n_0 p_t'$ increases. As N_t increases the ratio p_{t0}/p_t' increases for a given F; therefore, the maximum of τ_e^{st} is shifted towards $F > 0$.

In the dependence of τ_h^{st} on F, upon analogous effects there is superimposed the thermal ejection of holes from traps into the valence zone. Therefore, the curve of $\tau_h^{st}(F)$ shows a second (right-hand) maximum caused by the thermal barrier [3] against traps, because of which the absolute rate of departure of holes from the valence zone is slowed down (τ_h^{st} increases).

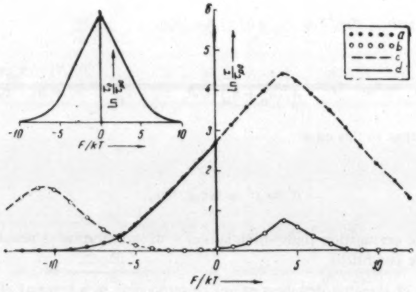

Fig. 2. Dependence of the characteristic times $\tau_e^{st}(a)$, $\tau_h^{st}(b)$ and τ_2 on the position of the Fermi level. The Shockley-Read curves τ (d) are shown separately for impurity carriers at low (separate graph) and high (on main graph) trap concentrations. Curve c agrees with curve a for values of F to the right of the common point of intersection of all curves, and c agrees with b for F to the left of this point. Curve d coincides with a for $F < 0$ and d coincides with b for $F > 0$. In the range between the common point of intersection and $F = 0$, the curves a, d and c coincide.

---

*Estimates show that in the region $|F - E_t| \sim 2kT$, $\tau_1 \sim \tau_2$.

Under stable nonequilibrium conditions the recombination of electrons and holes in traps is balanced by pair generation. Then $n'_{st}/p'_{st} = \tau_e^{st}/\tau_h^{st}$. At the instant when pair generation ceases, there appear uncompensated and approximate equal electron and hole flows from the zones to the traps. If the lifetimes τ_e^{st} and τ_h^{st} differ in order of magnitude then in this first stage of damping $(t \sim \tau_1 \sim \tau^{st}_{smaller})$ there is an appreciable drop of only the smaller of the nonequilibrium concentrations. There is a resulting increase of the ratio of the concentration of the corresponding carriers in traps to their concentration in the zones. This results in a slowing down of the recombination of these carriers due to the increased ratio of the number of reverse thermal ejections to the number of captures. Their lifetime increases until it is equal to τ^{st}_{larger}, after which quasistable attenuation is established and all the nonequilibrium concentrations are attenuated with the same characteristic time $\tau_2 =$ $= \tau^{st}_{larger}$.

The theory contains as a fundamental characteristic the lifetime τ of impurity charge carriers [1,2].

When the curve of τ_2 in Fig. 2 is compared with the curve of Shockley and Read for high trap concentrations, it is seen that the curves agree only in the range $0 > F > E_t$. In this case, when the traps are located in the lower half of the forbidden zone, the characteristic attenuation time is equal to the lifetime of the intrinsic carriers for all positions of the Fermi level in an electron semiconductor as well as in a sharply defined hole semiconductor. A similar conclusion results from a calculation for the case $E_t > 0$.

4. Let us consider the two principal methods of measuring lifetimes.

In the pulse method [4] we observe the oscillographic sweep of the attenuation of non-equilibrium concentrations of charge carriers injected into a semiconductor and practically uniformally distributed throughout its volume. These conditions correspond exactly to the conditions of the problem solved above. Consequently, the pulse method does not measure the lifetime of impurity carriers, as the authors suppose, but τ_2, which in the majority of cases coincides with the lifetime of the intrinsic carriers.

The photoelectric method [5] of determining lifetimes keeps a stable spatial distribution of impurity carriers in the unilluminated part of the semiconductor. Production here is represented by the divergence of the flow of impurity carriers diffusing from the illuminated region. But the change of this flow with distance depends, in turn, on the rate of recombination. Consequently, this method also fails to realize the initial conditions of the Shockley-Read theory (G independent of τ) so that, in the general case, we cannot equate the measured τ with τ^{st} impurity carriers. Our calculation in this case was carried out separately.

LITERATURE CITED

[1] W. Shockley and W. Read, Phys. Rev. 87, 835 (1952) [see Semiconductor Electronic Devices (A. V. Rzhanov, Ed.) (1953), p. 121].

[2] W. Shockley, Electrons and Holes in Semiconductors (1953).

[3] E. I. Adirovich, Some Problems of the Theory of Luminescence in Crystals (1951), p. 304.

[4] D. Navon, R. Bray and H. J. Fan, Proc. Inst. Radio Engrs. 40, 11, 1342 (1952) [see Semiconductor Electronic Devices (1953), p. 179].

[5] L. B. Valdes, Proc. Inst. Radio Engrs. 40, 11, 1420 (1952).

P. N. Lebedev Physics Institute
Academy of Sciences of USSR

Received August 1, 1955

OBSERVATION OF THE PRODUCTION AND DECAY OF UNSTABLE PARTICLES IN AN EMULSION CHAMBER

V. V. Alpers, I. I. Gurevich and L. V. Surkova

(Presented by Academician L. A. Artsimovich February 22, 1956)

We have previously reported [1] the results of scanning of an emulsion chamber irradiated by cosmic rays in the stratosphere for 6 hours. The flight was carried to a height of 25 km by the Aerological Laboratory of the Physics Institute of the Academy of Sciences USSR in September 1954.

Further study of the emulsion chamber revealed two additional τ-mesons and one Λ^0-particle, which are described in this article.

Both τ-mesons were found by area scanning of individual layers of the chamber and were identified by their characteristic decay scheme $\tau^+ \rightarrow \pi^+ + \pi^+ + \pi^- + Q$. The results of the processing of measurements relating to both decays are given in Table 1.

TABLE 1

Case		τ	π^+	π^+	π^-	Q, Mev	Mass M, m_e
I	Range in μ	7600	1040	calc. 18000	14600	71.3 ± 3.7	960.3 ± 7.3
	Energy in Mev	33.99 ± 1.1	6.3 ± 0.2	calc. 36.2 ± 2.6	29.0 ± 0.96		
II	Range in μ	To emergence 14000	3420	22500	calc. 9500	71.9 ± 3.4	960.5 ± 6.7
	Energy in Mev	–	12.5 ± 0.4	36.5 ± 1.2	calc. 22.4 ± 1.8		

The stopping power of the emulsion used in this work was similar to the stopping power of an Ilford G-5 emulsion [1]. Therefore, in order to determine particle energies in all observed cases, we used the range-energy tables for Ilford G-5 emulsions [2]. The error in determining the energy by range was ± 3.3% [1].

In the first case, of the three pions resulting from decay of the first τ-meson, two were traced until completely stopped in the emulsion chamber. One of these was a π^+-meson that decayed to a μ-meson with the range $R_\mu = 595\ \mu$. The second pion did not produce a visible star at the end of its range. It can be identified as a π^--meson. The third pion covered a path of $R = 10500\ \mu$ before emerging. The different charge signs of the stopped pions prevented us from determining the sign of the π-meson charge.

In order to determine the energy of the meson which escaped, conservation of momentum was employed, allowing for the additional error involved in this calculation. The computations showed that the energy evolved in the decay of the τ-meson was $Q = 71.3 \pm 3.7$ Mev, and its mass $m_\tau = 960.3 \pm 7.3\ m_e$. The tracks of the τ-meson and of the three decay pions lie in the same plane to within 2°.

Scanning of the τ-meson track from its point of decay showed that it originated in a 14 + 3n star. All prongs of the star were traced until stoppage or emergence from the emulsion chamber. Seven prongs were stopped in the emulsion. None of the prongs could be identified as a K-meson or hyperon.

In the second case, just as in the first, two pions were stopped in the emulsion chamber while the third escaped after traversing 8750 μ. Its energy was determined from conservation of momentum. The stopped pions showed at the end of their ranges the characteristic $\pi - \mu - e$ decays, i.e., both mesons had positive charges. Consequently, the charge of the decaying τ-meson was positive. The energy evolved in the τ-meson decay was $Q = 71.9 \pm 3.4$ Mev and its mass was $m_\tau = 960.5 \pm 6.7\ m_e$.

A check of the pion tracks for coplanarity showed that all three decay pions lie in the same plane within 2°. Examination showed that the τ-meson originated outside of the emulsion chamber. The path in the chamber was 14000 μ.

TABLE 2

	Proton	Meson
Path in μ	16500	5600
E in laboratory system, Mev	69.81	16.57
E in center-of-mass system, Mev	5.0 ± 0.16	32.2 ± 1.1

Angle between protons and π-mesons 150°. $Q = 37.2 \pm 1.2$ Mev. Mass of Λ^0-particle $m_{\lambda^0} = 2182 \pm 2.4\ m_e$. Energy of Λ^0 49 Mev.

The value obtained for the energy evolved in the decay of both τ-mesons was somewhat lower than the average value which is accepted at present: $Q = 75.0 \pm 0.2$ Mev [3], but agrees with the latter within the limits of error.

The Λ^0-particle was discovered by tracing the pion tracks from their stopping point in the emulsion to the star where they originated. The proton and π^--meson tracks formed by Λ^0 decay according to the scheme: $\Lambda^0 \rightarrow p + \pi^- + Q$ were completely contained in the emulsion chamber. The π^--meson was captured by a nucleus and gave rise to a three-pronged star.

Table 2 gives the measurements and calculations for the Λ^0 and its decay products.

The values obtained for the decay energy, $Q = 37.2 \pm 1.2$ Mev and mass $m_{\Lambda^0} = 2182 \pm 2.4\ m_e$, agree well with the accepted average values $Q = 36.92 \pm 0.22$ Mev and $m_{\Lambda^0} = 2181 \pm 0.5\ m_e$ [4].

LITERATURE CITED

[1] V. V. Alpers, R. I. Gerasimova, et al., Doklady Akad. Nauk SSSR 105, 2, 236 (1955).

[2] H. Fay, K. Gottshein and K. Hain, Nuovo cimento Suppl. 11, 234 (1954).

[3] E. Amaldi, Conf. Intern. sulle part. elem., XLI Congresso Nazionale Fis. (Pisa, June 12-18, 1955), vol. 1.

[4] C. Castagnoli, M. Friedlander, et al., Nuovo cimento Suppl. 12, 464 (1954).

Received January 23, 1956

X-RAY STUDIES OF MATTER AT PRESSURES TO 30,000 ATMOSPHERES

L. F. Vereshchagin and I. V. Brandt

(Presented by Academician G. V. Kurdiumov August 9, 1955)

At the present time the range of pressures at which it is possible to study matter has been considerably extended, and it has become evident that high pressures can not only lead to decreased distances between molecules or atoms, but also to electronic transitions within atoms. Sternheimer's calculations [1] (at Fermi's suggestion) for cesium and the x-ray studies of Lawson and Ting-Yuan Tang [2] at pressures up to 14,000 atm are confirmations of this possibility.

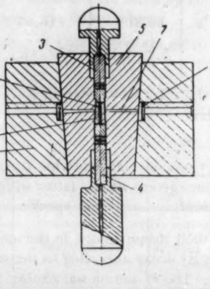

Fig. 1

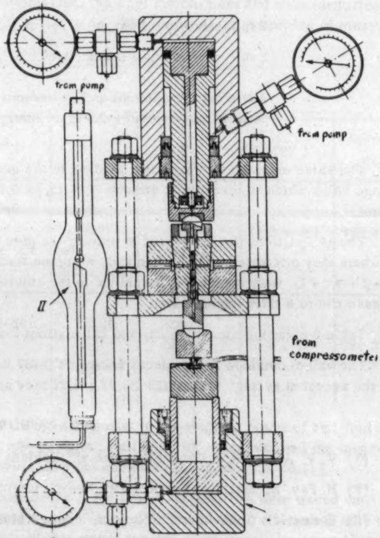

Fig. 2

L. F. Vereshchagin and A. I. Likhter [3] examined the dependence of the compressibility on pressure for various elements and determined that at 100,000 atm there is for all elements of the periodic table a decrease in the magnitude of $\frac{1}{V_0}\left(\frac{dV}{dP}\right)_T$ (where V_0 is the volume of the element at atmospheric pressure, and V is the volume at the pressure P). In addition, there is a disruption of the periodic dependence of $\frac{1}{V_0}\left(\frac{dV}{dP}\right)_T$ on Z, the atomic number of the element, at pressures of the order of 10^5 atm.

Bridgman [4] observed changes in the valences of elements at about 60,000 atm. For example, SnO_2 under pressure transforms into SnO.

Since at pressures above 1000 atm the V-P curves often reveal discontinuities which have usually been associated with changes in the structure of the crystal lattice, in the light of articles [1-4] the question arises, in which cases is the discontinuous volume change of the compressed substance associated with an actual polymorphic transformation, and in which cases must it be related to intratomic transitions? This question can only be answered by x-raying the substance under pressure. For this purpose we have developed a camera for producing Debye x-ray patterns at pressures to 30,000 atm (see Fig. 1).

The substance under investigation 1 was held in a beryllium cone 2 which is very transparent to x-rays. Pressure was transmitted to the specimen by means of lithium from the pistons 3 and 4 made of Vk-8 alloy. Since the beryllium cone cannot withstand such high internal hydrostatic pressures, we used a means of support: cone 2 was inserted into steel cone 5 within a steel mounting 6. The slit 7 of 2 mm diameter in steel cone 5 enables x-rays to reach the sample under pressure and to leave the beryllium cone by reflections from different planes of the crystal lattice. These rays strike a photographic plate in the holder 8. The entire camera was placed under a hydraulic press I close to the x-ray tube II (see Fig. 2).

This camera enabled us to take x-ray pictures of bismuth at atmospheric pressure and at 30,000 atm, i.e., above the pressure at which bismuth shows a discontinuous decrease in volume of about 8.6%.

As is shown by the x-ray diagrams of a bismuth specimen at atmospheric pressure and at 30,000 atm, this change of volume must be associated with a change in the crystalline structure and not with intratomic transitions.

The crystal lattice of bismuth at atmospheric pressure is rhombohedral. We are now in the process of determining the structure of bismuth in its allotropic modification above 25,000 atm.

LITERATURE CITED

[1] R. Sternheimer, Phys. Rev. 78, 235 (1950).

[2] A. W. Lawson and Ting-Yuan Tang, Phys. Rev. 76, 301 (1949).

[3] L. F. Vereshchagin and A. I. Likhter, Doklady Akad. Nauk SSSR 86, 4, 745 (1952).

[4] P. W. Bridgman, Proc. Am. Acad. Arts Sci. 71, 387 (1937).

High Pressure Physics Laboratory
Academy of Sciences of USSR

Received July 25, 1955

THE FORMATION OF ULTRAMICROSCOPIC INHOMOGENEITIES IN THE PLASTIC DEFORMATION OF SODIUM CHLORIDE

Corresponding Member of the Academy of Sciences USSR R. I. Garber,
I. V. Obreimov and L. M. Poliakov

It is known in the plastic deformation of rock salt "slip bands" are formed which are easily observed both through double refraction and the change in absolute value of the refractive index [1,2]. Studies have shown that this crystal contains more or less uniformly distorted layers which are oriented approximately parallel to the (110) planes [3,4]. It was naturally expected that these layers would reflect light within the crystal. Observation made more than 20 years ago by I. V. Obreimov, A. V. Stepanov and others confirmed this expectation. It was also observed at the time that ordinary flaws of the salt impede the detailed investigation of this phenomenon, which was observed only when fairly strong deformation was present.

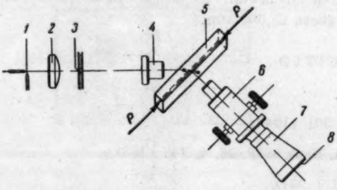

Fig. 1. Diagram of the apparatus. 1) light source, a carbon arc; 2) condenser; 3) diaphragm; 4) microscope objective; 5) crystal under tension P; 6) microscope; 7) photographic headpiece; 8) screen of photographic plate.

A more detailed investigation with relatively small deformations revealed diffusive light scattering, which was strong enough to permit observation and photographing of typical Tyndall phenomena. For samples which were compressed or stretched along an edge of the cube, stresses of 110 to 120 g/mm² were enough to produce this effect. The Rayleigh character of the polarization and angular dependence of the scattered light intensity are a basis for assuming that under these stresses ultramicroscopic inhomogeneities are produced which are scattered diffusely in the crystal.

In our investigations we used specimens of natural rock salt provided by the K. Liebknecht Directorate of Mines. The salt was split along cleavage planes into prisms of various sizes, which were checked for rough flaws before annealing. Annealing took place at 650° for 36 hours. Both heating and cooling took place in the furnace. Whenever specimens were cooled in air, characteristic thermal stresses appeared with associated slip planes. It is of interest that in such specimens one also usually observes diffuse light scattering similar to the scattering which appears in stretching and compressing.

The temperature and duration of annealing were in accordance with the data in the paper of I. V. Obreimov and L. V. Shubnikov [1]. G. S. Landsberg and S. L. Mandel'shtam [5] note that with higher annealing temperatures, cloudiness is observed which they ascribe to the effect of recrystallization. From our observations, cloudiness at higher annealing temperatures is associated mainly with the formations of bubbles inside the crystal, whose origin we have not yet established.

The annealed crystals were tested with apparatus which enabled us to measure stress and deformation under tension or compression, and at the same time, to study light scattering within the crystal. The apparatus is shown schematically in Fig. 1. In addition, suitable crystals were transferred to the stage of an ordinary polarizing microscope for the study of the slip planes due to deformation. In order to attenuate the scattering and reflections from the surface of the crystals, cover glasses were glued to them with drops of oil of cloves.

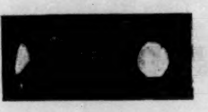

Fig. 2

At low tensions the slip bands are usually the first effect to appear; the crystals do not yet show light scattering. With increased tension there is weak scattering which produces luminosity of the cone near its apex, as is seen in Fig. 2 (the two bright spots to the left and right of the cone result from scattering by surface defects of the crystal at the points of entrance and emergence of the primary light beam). Further deformation results in the strengthening of the scattering, and in a bright uniform luminosity of the entire light cone inside the crystal.

In observations of internal scattering the slip bands do not appear: scattering is identical in all parts of the crystal. If such a crystal is reannealed, the slip bands soon disappear but only after prolonged annealing is it possible to eliminate the inhomogeneities which are the cause of light scattering within the crystal. Whenever the deformation is completely elastic or when twinning occurs (calcite, sodium nitrate) light scattering is not observed. As has been mentioned, the appearance of slip planes alone is insufficient to produce diffuse scattering of light. In order to test the possibility of an effect due to microscopic cracks, a few specimens were deformed in water. In these instances, just as with deformation in air, diffuse scattering invariably appeared.

The anisotropy of the crystals affects the tension threshold required for scattering. For example, for rock salt compressed along a cubic edge, as has been indicated, the normal tension thresholds are 110-120 g/mm^2, and for compression along a face diagonal [110] the tensions required increase to 550-600 g/mm^2. Such large changes of the tension thresholds cannot be associated with a simple law of tangential tension thresholds in the (110) plane and in the [110] direction. In this case the ratio of the normal tensions should be 2.3 and not 4.6 to 5.4, as follows from the above data.

The observations described above are a basis for affirming that in plastic deformation ultramicroscopic inhomogeneities are formed together with slip bands. These inhomogeneities can result from local shifts and dislocations. In the latter case the phenomenon of plastic flow can itself be described as a series of local dislocations followed by restoration of continuity taking place in ultramicroscopic regions of the crystal.

LITERATURE CITED

[1] I. V. Obreimov and L. V. Shubnikov, J. Russ. Phys. Soc. 58, 817 (1926).

[2] R. I. Garber, J. Exptl.-Theoret. Phys. (USSR) 8, 746 (1938).

[3] I. V. Obreimov and N. A. Brilliantov, J. Exptl.-Theoret. Phys. (USSR) 5, 330 (1935).

[4] R. I. Garber, J. Exptl.-Theoret. Phys. (USSR) 6, 176 (1936).

[5] G. E. Landsberg and S. L. Mandel'shtam, Z. Physik 73, 502 (1931).

Physico-Technical Institute
Ukrainian Academy of Sciences
Kharkov

Received December 9, 1955

ISOTOPIC SHIFT IN THE SPECTRUM OF He II

P. S. Kireev

(Presented by Academician G. S. Landsberg December 8, 1955)

The investigation of the isotopic shift in lines of hydrogen-like atoms is of great interest, since the theoretical solution in this case is more exact than for other elements. By studying the lines of isotopes consisting of different numbers of nucleons and taking the sample mass effect into consideration, we can determine directly how the structure of the nucleus affects the emission of radiation.

The isotopic effect has been studied for hydrogen lines. In this paper we investigate the isotopic shift in the line of ionized He^3 II and He^4 II for the transition $n = 4 \rightarrow n = 3$.

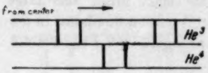

Fig. 1

The optical scheme and the source for He^3 have already been described [1]. He^4 emission was excited in a hollow aluminum cathode cooled by liquid nitrogen. For resolution of the structure, we used a Fabry-Perot etalon with 2 and 2.5 mm separations. The coefficient of reflection of the mirrors in the region investigated was 88%. The He^3 II and He^4 II spectra were photographed on film. The light sources were symmetrically placed with respect to the optical axis of the spectrograph. By rotation of a mirror on its axis, the emission from one of the light sources could be directed towards the etalon. By changing the position of the cassette and rotating the mirror, an interference pattern was obtained for the line of each isotope. If the position of the cassette is not changed, the film records the superposition of the interference patterns. By changing the width of the spectrograph slit the components of the lines can easily be identified.

An IZA-2 comparator was used to measure the diameters of the interference rings. The results were treated by the tabular method of exact fractions. The results agree well for the shift obtained from photographs of the individual isotopic lines and from photographs containing the interference pattern of both lines.

Fig. 1 gives the scheme of the intense components of the He^4 line (one order) and He^3 line (two orders) with a 2.5 mm etalon and short exposure time. The lines are conveniently placed for measurements. The isotopic shift obtained from the positions of all components is $\delta\nu = 0.932\ cm^{-1}$. The isotopic shift due only to the mass difference of the helium isotopes is $0.957\ cm^{-1}$. Our result is smaller than the theoretical value for the shift. The discrepance is apparently outside the limit of errors.

In conclusion I wish to express my sincere thanks to F. A. Korolev for his constant assistance.

LITERATURE CITED

[1] P. S. Kireev, Doklady Akad. Nauk SSSR 108, 2, 226 (1956) [Soviet Physics - "Doklady", p. 294].

M. V. Lomonosov
Moscow State University

Received December 9, 1955

A BISMUTH-LEAD ALLOY BOLOMETER

M. N. Markov

(Presented by Academician G. S. Landsberg July 25, 1955)

The most important parameters of bolometers which are used to measure modulated infrared radiation and which determine their sensitivity threshold are: the time constant τ, the conversion coefficient at zero frequency S_0 (v/w) and the level of electrical fluctuations (noise) [1,2]. For bolometers produced by vacuum evaporation, the conversion coefficient S_0 has thus far usually been considerably smaller and the noise level higher in a number of cases than for bolometers made of the same materials by other methods (such as rolling, etc.) although the time constant was usually very small [3,4]. Thus, bolometers manufactured by vacuum evaporation possessed considerable advantages with regard to their production but were less sensitive than bolometers made by other more complicated and laborious methods.

For the purpose of improving the parameters of bolometers produced by the evaporation method, we have studied F-1 bismuth bolometers which are used in the automatic infrared spectrometer of the Physics Institute of the Academy of Sciences (FIAN) [5].

1. An expression for the sensitivity threshold of a bolometer can be given in the form:

$$Q_{min} = \frac{\pi^2}{4}\left(\frac{4kT^2\varkappa F\Delta f}{\varepsilon_1^2} + \frac{32kTR_{b_T}\varkappa^2F^2\Delta f}{\varepsilon_1^2\beta^2U_p^2}\left(1+4\pi^2f_B^2\tau^2\right)\right)^{1/2}, \tag{1}$$

where Q_{min} is the power of infrared radiation which produces a signal equal in magnitude to the root mean square noise; $\underline{k}$ is the Boltzmann constant; T is the absolute temperature of the bolometer strip; F is the area of the sensitive surface; κ is the cooling constant (loss of heat from unit surface with temperature gradient 1°); ϵ_1 is the absorption coefficient of the sensitive surface; Δf is the band of transmitted frequencies of the amplifying-recording device; R_{b_T} is the resistance of the bolometer strip at the operating temperature; $\beta = \frac{1}{R}\frac{\Delta R}{\Delta T}$ is the relative temperature coefficient of resistance of the bolometer; U_B is the voltage applied to the bolometer bridge; f_B is the modulation frequency of the radiation (square wave modulation); $\tau = C/\kappa$ is the bolometer time constant (C is the heat capacity of the bolometer).

Here the first term is due to temperature fluctuations of the bolometer strip, while the second term is the so-called "Johnson" noise. In the majority of existing thermal light receivers the second term is 5 to 10 times larger than the first. When there is additional noise in the receivers (such as "current noise", other kinds of interference, etc.) additional terms appear in the formula, since this noise raises the sensitivity threshold. It is known from the literature, especially [3,6,9], that thin evaporated layers of metals during passage of a current have noise above the "Johnson" level. This "current" noise is usually associated with the spontaneous change of resistance of the layer when a current flows. The level of the noise usually depends on the structure of the layer, the process by which it was produced, etc. One of the purposes of our investigation is the determination of the conditions under which this additional noise can be reduced to a minimum.

2. We know that in bismuth the sign and absolute value of the temperature coefficient of resistance depend on small admixtures (~0.1%) of lead, tin and other metals [7,8]. On the other hand, in thin evaporated layers $\beta < 0$, which is on the average one half as large as in solid bismuth, and depends on the thickness [3,6]. However,

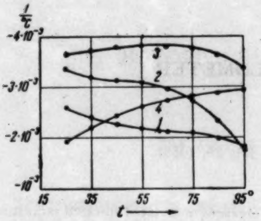

Fig. 1. 1) pure bismuth, $R_{\square} \sim 30$ ohms; 2) alloy, 99.9% Bi and 0.1% Pb, $R_{\square} \sim 30$ ohms; 3) alloy, 99.4% Bi and 0.6% Pb, $R_{\square} \sim 30$ ohms; 4) alloy, 98.9% Bi and 1.1% Pb, $R_{\square} \sim 30$ ohms

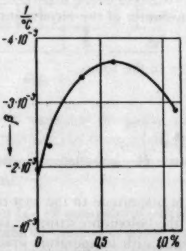

Fig. 2. $t = 85°$, $R_{\square} \sim 30$ ohms

there is no information in the literature regarding the purity of the bismuth used for evaporation. Therefore, we have investigated the dependence of β on temperature (between 20° and 100°) for layers of very pure bismuth. (The purity of the bismuth was checked before and after evaporation by spectral analysis. It was found that during evaporation, bismuth loses most of its lead and silver impurities, so that the concentration of impurities in the evaporated material is $\sim 10^{-3}$ %). For the evaporation process we used a celluloid backing in a vacuum $\sim 10^{-5}$ mm Hg.

It was found that the permanently negative temperature coefficient (by our methods of producing layers) depends on the thickness, which was evaluated from the resistance of a 1 cm square ($R_{\square}$). The measurements were carried out on layers with resistances for such squares of 10, 30, 100 and 200 ohms representing approximate thickness from 0.1 to 0.01 μ. Similar measurements were made on layers of various bismuth-lead alloys. Layers of both the purest bismuth and of all the alloys show a maximum temperature coefficient of resistance (of negative sign) at thickness corresponding to $R_{\square} \sim 30$-40 ohms. The highest value of β is found in layers consisting of 99.4% Bi and 0.6 % Pb by weight, produced by evaporation at 700-800°. The dependence of β on the temperature of the layer for different alloys and pure bismuth at a layer thickness corresponding to $R_{\square} \sim 30$-40 ohms is shown in Fig. 1. The dependence of β for such layers on the concentration of lead in the alloys at 85° is shown in Fig. 2. It is important to note that a layer of alloy retains a high temperature coefficient at high layer temperatures, which is important, since the minimum $Q_{\min}$ is obtained, as shown by an analysis of Equation (1), at a temperature $T = 4/3\,T_0$ (T_0 is the absolute temperature of the ambient), i.e., for $T_0 = 300°$ K, at 400° K.

3. In order to determine the conditions under which bolometers have "current" noise, and for an exact determination of the sensitivity threshold of evaporated bolometers, fairly accurate direct measurements of the noise level are required. We have performed such measurements (with accuracy $\sim 10\%$) with amplifying equipment similar to that which is used in the spectrophotometer of the Physics Institute of the Academy of Sciences [10]. Preliminary studies showed that the amplifier has an intrinsic noise level corresponding to an equivalent noise resistance of 20 ohms. Since one of the characteristics of "current" noise is the dependence of its level on the magnitude of the current flowing through the resistance, we made our measurements for various voltages across the bolometer bridge.

We investigated layers of pure bismuth, commercial bismuth (with 0.1 % Pb) and an alloy of 99.4% Bi and 0.6% Pb. The layer noise was compared with the noise of a wire resistance of the same magnitude as the layer resistance. It was found that layers with resistance $R_{\square} \sim 30$ ohms and lower do not have additional "current" noise and exhibit the same noisiness as wire resistances. The thinner layers have a higher noise level depending on the current. Bismuth-lead alloy layers of the same resistance per unit area have a considerably lower level of additional noise, which can presumably be attributed to their greater thickness, since the alloy has a considerably higher specific resistance than pure bismuth (by a factor of 1.5 to 2.5) [8]. The dependence of the ratio of the root mean square bolometer noise to the root mean square wire resistance noise on the bolometer bridge voltage is shown in Fig. 3.

4. The absorption coefficient of the sensitive surface is very important for lowering the sensitivity threshold. Studies of the absorption by layers of evaporated bismuth and of bismuth covered with a layer of bismuth

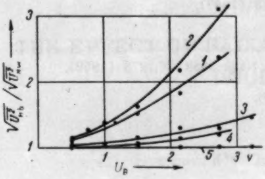

Fig. 3. 1) alloy, 99% Bi and 0.1% Pb, $R_\square$ ~200 ohms; 2) pure bismuth, $R_\square$ ~ ~ 200 ohms; 3) pure bismuth, $R_\square$ ~100 ohms; 4) alloy, 99.4% Bi and 0.6% Pb, $R_\square$ ~ 200 ohms; 5) pure bismuth and alloys, $R_\square \leq$ 30-40 ohms.

"black" from 1 to 15 μ (using the spectrograph of the FIAN) showed that evaporated bismuth layers have very low absorbing power (especially from 4 to 15 μ) and that "blackening" increases the absorption from 1 to 3 μ by a factor of 2 or 3, and from 4 to 15 μ by a factor of 5 to 20. The same layer of bismuth "black" increases the heat capacity and therefore, the bolometer time constant by 15 to 20 %.

5. On the basis of these investigations, we constructed a bolometer of an alloy with 99.4% Bi and 0.6% Pb with the bismuth layer thickness corresponding to a unit square resistance of 30-40 ohms and backing thickness of 0.02-0.03 μ. The base and envelope were taken from the F-1 bolometer [5]. The sensitivity threshold was measured with a Hefner candle as a light source.

Table 1 gives the sensitivity threshold for these bolometers under the same conditions as Jones [1] (H_m) as well as under comparative conditions which we consider more suitable for receivers to be used in spectrometry, using modulation methods (Q_{B1}). Our conditions are the following: 1) the receiver is illuminated with square-wave modulated light at a frequency not under 5 cycles; 2) the average signal strength and the root mean square noise are measured after selective amplification (Δf = 2-10 cps) by a measuring instrument with a 1 second time constant; 3) the minimum sensitivity of current will then correspond to the electric signal whose average strength is equal to the root mean square noise; 4) the receiving sensitive surface can be of any area, but not smaller than 0.2 × 2 mm². Table 1 also gives data for the best thermal light receivers, taken largely from Jones [2].

TABLE 1

Receiver	τ (millisec)	F(mm²)	S_0(volts/watts)	H_m (10^{10} watts)	Q_{B1} (10^{10} watts)
Superconductive bolometer 22-k-$\frac{1}{4}$	10	1.8	–	0.216	0.06
Thermistor S-19	5.9	0.6	730	25.5	2.9
Platinum bolometer (Baird).	4.1	0.2	–	16.0	0.9
Evaporated bolometer (Polaroid Ni 347)	7.2	4.5	1.6	14.7	5.3
Perkin-Elmer thermocouple.	17	0.4	10	3.47	0.57
Harris 2 evaporated thermocouple.	13.3	11.0	0.33	50	37.6
Pneumatic receiver	20	7.0	–	1.03	0.76
F-1 (Bi) bolometer	35	7.5	0.3	66.0	66.0
F-2 (alloy) bolometer	18	2.25	15	2.6	1.0
F-3 (alloy) bolometer	18	0.4	33	2.6	0.45

From a comparison of the data it can be seen that bismuth-lead bolometers, produced by vacuum evaporation on a celluloid backing with proper values for the thickness of layer and backing, pressure inside the envelope, and operating conditions of the bolometer bridge, have a lower sensitivity threshold than bolometers manufactured by other methods, and are comparable to the best light receivers operating at room temperature.

I consider it my duty to thank Academician G. S. Landsberg and V. I. Malyshev for their continued interest and discussions, and S. S. Dudukin for assistance with the construction of the bolometers.

LITERATURE CITED

[1] R. Clark Jones, J. Opt. Soc. Am. 39, 327 (1949).

[2] R. Clark Jones, J. Opt. Soc. Am. 39, 344 (1949).

[3] B. H. Billins, W. L. Hyde and E. F. Barr, J. Opt. Soc. Am. 37, 123 (1947).

[4] W. Langton, J. Opt. Soc. Am. 36, 355 A (1946).

[5] V. I. Malyshev, M. N. Markov and A. A. Shubin, Doklady Akad. Nauk SSSR 86, 273 (1952).

[6] M. Czerny, W. Kofink and W. Lippert, Ann. Physik 8, 65 (1950).

[7] N. Thompson Proc. Roy. Soc. (London) 155A, 111 (1936).

[8] G. A. Ivanov and A. R. Regel', J. Tech. Phys. (USSR) 25, 39, 49 (1955).

[9] C. J. Christensen and C. G. Pearson, Bell System Tech. J. 15, 197 (1936).

[10] M. N. Markov, J. Tech. Phys. (USSR) 24, 1867 (1951).

P. N. Lebedev, Physics Institute
Academy of Sciences of the USSR

Received July 4, 1955

THE EFFECT OF RADIATION ON SYNCHROTRON OSCILLATIONS UNDER STRONG FOCUSING

A. N. Matveev

(Presented by Academician N. N. Bogoliubov October 15, 1955)

1. Our study of radiation-induced betatron oscillations in an earlier article [1] showed that strong focusing greatly reduces the amplitude of such oscillations, so that the presence of betatron oscillations is very likely to require the use of strong focusing at electron energies of a few Bev. For a fuller understanding of this problem it is also necessary to investigate synchrotron oscillations. For the case of weak focusing, radiation-induced synchrotron oscillations of electrons were investigated by Sands [2]. It should be noted that the mechanism of excitation of these oscillations which were considered by Sands is identical with that which was pointed out earlier by A. A. Sokolov and I. M. Ternov (see note added in proof of reference [3]).

2. We are interested in the high energy region. Under these conditions it is possible to neglect effects associated with a change of velocity for small changes of particle energy $((\Delta v/v) = (mc^2/E)^2\,(\Delta E/E))$, and with a change of magnitude of the equilibrium energy E_s, i.e., with the quantity E_s. We can then write the equation

$$\frac{d}{d\mu}(E-E_s) = eV_0(\cos\varphi-\cos\varphi_s)-(I-I_s). \tag{1}$$

In this equation E is the energy of the particle; φ is the phase at passage through the high-frequency field; I is the radiative energy per revolution; μ is the number of traversals of the accelerating gap; eV_0 is the amplitude of the high-frequency field. The index s designates stationary values. For I_s we have the familiar expression

$$I_s = \frac{4\pi}{3}\frac{e^2}{R_s}\left(\frac{E_s}{mc^2}\right)^4, \tag{2}$$

and we must calculate $\delta I = I - I_s$. For this purpose we can use the well-known equation

$$\Delta P_i = \frac{2e^4}{3m^2c^5}\int (F_{\mu\nu}u_\nu)^2\,dx_i\,, \tag{3}$$

which, under the conditions that we are considering, gives

$$\delta I = 2I_s\frac{\delta E}{E_s}+\frac{2e^4}{3m^2c^4}\left(\frac{E_s}{mc^2}\right)^2\int_0^{2\pi}\delta(H^2R)\,d\vartheta, \tag{4}$$

which, in view of the fact that $\delta H^2 = -2nH_s^2\delta R(\vartheta)$, becomes

$$\delta I = \frac{I_s}{2\pi R_s}\left\{4\pi R_s\frac{\delta E}{E_s}+\int_0^{2\pi}[1-2n(\vartheta)]\,\delta R(\vartheta)\,d\vartheta\right\}. \tag{5}$$

Quantities that refer to parts of sectors, which show defocusing action with respect to radial motion, will be designated by the index (1); the focusing parts will be designated by the index (2); the number of sectors is N; the angles subtended by the parts are $\nu^{(1)}$ and $\nu^{(2)}$, with $\nu^{(1)} + \nu^{(2)} = 2\pi/N$. $\delta R(\vartheta)$ satisfies the equations

$$\frac{d^2}{d\vartheta^2}[\delta R^{(i)}] + (1-n_i)[\delta R^{(i)} - \Delta^{(i)}] = 0, \quad \Delta^{(i)} = \frac{R_s}{1-n_i}\frac{\delta E}{E_s}, \tag{6}$$

whose solution in the k-th sector can be written as

$$\begin{aligned}\delta R_k^{(1)} &= A_k^{(1)} \operatorname{sh}\sqrt{n_1-1}\,\vartheta + B_k^{(1)} \operatorname{ch}\sqrt{n_1-1}\,\vartheta + \Delta^{(1)},\\ \delta R_k^{(2)} &= A_k^{(2)} \sin\sqrt{|n_2|+1}\,\vartheta + B_k^{(2)} \cos\sqrt{|n_2|+1}\,\vartheta + \Delta^{(2)},\end{aligned} \tag{7}$$

and for the coefficients $A_k^{(i)}$, $B_k^{(i)}$ the following expressions are obtained:

$$\begin{aligned}A_k^{(1)} &= A^{(1)}\cos(qk + a^{(1)}) + \frac{(1-bd-\eta ac)\eta^{-1}c + (ad-\eta^{-1}bc)(1-d)}{2(1-\cos q)}[\Delta^{(2)} - \Delta^{(1)}],\\ B_k^{(1)} &= B^{(1)}\cos(qk + b^{(1)}) + \frac{(1-bd+\eta^{-1}ac)(1-d) + (ad+\eta bc)\eta^{-1}c}{2(1-\cos q)}[\Delta^{(2)} - \Delta^{(1)}],\\ A_k^{(2)} &= A^{(2)}\cos(qk + a^{(2)}) + \frac{(1-bd+\eta^{-1}ac)\eta a + (-bc+\eta ad)(b-1)}{2(1-\cos q)}[\Delta^{(2)} - \Delta^{(1)}],\\ B_k^{(2)} &= B^{(2)}\cos(qk + b^{(2)}) + \frac{(1-bd-\eta ac)(b-1) + (bc+\eta^{-1}ad)\eta a}{2(1-\cos q)}[\Delta^{(2)} - \Delta^{(1)}],\end{aligned} \tag{8}$$

in which $A^{(i)}$, $B^{(i)}$, $a^{(i)}$, $b^{(i)}$ are determined by the initial conditions and a, b, c, d, η, q have the same values as in Equation (3) of reference [1].

Substituting (7) into (5), using (8) and considering that the oscillating terms, which are dependent on the initial conditions, do not on the average contribute to the integral, we obtain for δI

$$\delta I = I_s \sigma \delta E/E_s \tag{9}$$

in which

$$\sigma = \frac{N}{2\pi}(\nu^{(1)}\sigma^{(1)} + \nu^{(2)}\sigma^{(2)}), \quad \sigma^{(i)} = 2 + (1-2n_i)\alpha^{(i)},$$

$$\alpha^{(1)} = \frac{1}{1-n_1}\left(1 + \frac{\varkappa}{\nu_1}\frac{n_1-n_2}{(1-n_1)(1-n_2)}\right), \quad \alpha^{(2)} = \frac{1}{1-n_2}\left(1 - \frac{\varkappa}{\nu_2}\frac{n_1-n_2}{(1-n_1)(1-n_2)}\right),$$

$$\varkappa = \frac{\sqrt{n_1-1}\,a(1-d) + \sqrt{|n_2|+1}\,c\,(b-1)}{1-\cos q}, \quad \nu_i \equiv \nu^{(i)}.$$

The calculation of the change of orbit length δS when the energy changes by the amount $\delta E = E - E_s$ is performed by the formula

$$\delta S = \int_0^{2\pi} \delta R(\vartheta)\, d\vartheta, \tag{10}$$

and leads to the relationship

$$\delta S = 2\pi \alpha R_s \delta E/E_s, \tag{11}$$

in which $\alpha = (N/2\pi) \sum\limits_{i=1,2} \alpha^{(i)} \nu^{(i)}$, where the $a^{(i)}$ are defined under Equation (9). It can be shown that when $\nu^{(1)} = \nu^{(2)}$ (11) becomes the corresponding equation (8) of reference [4].

Designating by L the length of all linear sections in the synchrotron and by $\Psi = \varphi - \varphi_s$ the deviation from the stationary phase, and assuming that acceleration is produced by the k-th harmonic of the high-frequency field, we obtain on the basis of the above calculations

$$\dot{\Psi} = k\omega \frac{\alpha}{\lambda} \frac{\delta E}{E}, \quad \lambda = 1 + (L/2\pi R_s), \tag{12}$$

which in conjunction with (1) gives the desired equation of motion

$$\ddot{\Psi} + \gamma \dot{\Psi} + \Omega^2 \Psi = 0, \tag{13}$$

where $\gamma = \frac{I_s}{E_s} \frac{\omega_s}{2\pi} \sigma$, $\Omega^2 = \frac{I_s}{E_s} \frac{\omega_s^2}{2\pi} \tan \varphi_s \frac{k\alpha}{\lambda}$ and it is assumed that at the energies under consideration the energy loss per revolution is approximately equal to the energy acquired in traversing the accelerating gap, i.e., $eV_0 \cos \varphi_s \approx I_s$.

3. Equation (13) was obtained by neglecting the quantum character of the radiation. The quantum character of the radiation can be taken into consideration, either by adding to the right-hand side of (13) the appropriate term with subsequent employment of the equations of the statistical theory of fluctuations, or from direct considerations which are entirely analogous to those that we used in [1] in deriving the equations for betatron oscillations. Both methods will, of course, yield the same result and produce the following equation for the mean square fluctuation:

$$\overline{\Psi^2} = \frac{55\sqrt{3}}{96} \frac{k\alpha \operatorname{ctg} \varphi_s}{\lambda^2} \frac{h}{mR_s^2} \int\limits_0^t \exp\left[-\int\limits_{t'}^t \gamma \, d\tau\right] \left(\frac{E}{mc^2}\right)^2 dt'. \tag{14}$$

Remembering, furthermore, that the damping time γ^{-1} is small compared with the accelerating cycle, we can extend the limits of integration in (14) to infinity, and, assuming that E changes very little in the damping time under the conditions considered, E can be considered constant [E(t)] in the integral. We then obtain:

$$\overline{\Psi^2} = \frac{55\sqrt{3}}{64} \frac{k\alpha}{\lambda\sigma} \operatorname{ctg} \varphi_s \frac{hc}{e^2} \frac{mc^2}{E_s}, \tag{15}$$

which is suitable for applications. The quantities α, σ, λ and k were defined above.

The phase oscillations described by (15) are associated with the synchrotron oscillations of the mean radius characterized by the mean square fluctuation $\overline{(\Delta r_c)^2}$. On the basis of (12) and (15) we obtain

$$\overline{\left(\frac{\Delta r_c}{R_s}\right)^2} = \frac{55}{32\sqrt{3}} \frac{\alpha^2}{\sigma} \frac{hc}{e^2} \frac{r_0}{R_s} \left(\frac{E_s}{mc^2}\right)^2, \tag{16}$$

in which $r_0 = e^2/mc^2$ designates the classical electron radius. Equations (15) and (16) are the solution of our problem concerning the synchrotron oscillations of electrons with strong focusing.

4. A comparison of the equations for the mean square phase deviations with weak and with strong focusing, all other conditions remaining alike, shows that strong focusing somewhat reduces the amplitude of phase oscillations. This reduction could become of considerable magnitude if it were possible to have sufficiently high values of $|n_s|$. However, as we know, for electron synchrotrons it is necessary to limit the magnitude of n_s to a few tens.

As an example we shall consider the simplest case, in which $\nu^{(1)} = \nu^{(2)}$, $|n_2| + 1 = n_1 - 1 = n_s$, $N = 2\sqrt{n_s}$, $\lambda = 1$, $k = 4$. Then a comparison of the equations for weak focusing with $n_w = 0.6$ and strong focusing with $n_s = 25$ shows that in this case $|\Psi_s| \approx 0.17 |\Psi_w|$, i.e., strong focusing reduces the amplitude of the phase oscillations to about 1/6. This somewhat improves the operating conditions.

In order to insure the absence of electron losses due to phase oscillations, it is required that $\varphi_s > |\Psi|/\sqrt{2}$. Therefore, with $E = 1000$ Mev and $R = 3.5$ m, for the minimum permissible stationary phases with strong focusing $\varphi_s^{\min}$ (strong) and weak focusing $\varphi_s^{\min}$ (weak), we obtain $\varphi_s^{\min}$ (strong) $\approx 0.07\pi$ and $\varphi_s^{\min}$ (weak) $\approx 0.2\pi$. This reduction of the minimum permissible stationary phase results in only an insignificant reduction of the amplitude of the high-frequency field with strong focusing. Thus, in this respect, strong focusing does not provide any essential advantage.

The oscillations of the mean radius which are associated with phase oscillations, as described by Equation (16), are very small in the case of weak focusing as compared with betatron oscillations and are unimportant. In the strong focusing case they are also considerably smaller than betatron oscillations, by one order of magnitude under the conditions which we are considering. For example, with $E = 3000$ Mev and $R = 10$ m, we had for betatron oscillations $|\Delta_{str} r_b| \approx 1.14$ cm, and for oscillations of the mean radius we obtain $|\Delta_{str} r_m| \approx 0.12$ cm. On the basis of the equations given above it is easy to calculate $\overline{(\delta R)^2}$. This is of the same order as $(\Delta r_m)^2$.

In summation it can be said that, with respect to radiation-induced synchrotron oscillations of electrons, strong focusing in any event does not worsen and, in some instances, improves operating conditions compared with weak focusing. This is confirmation of our earlier article [1] on the probable need of strong focusing for electron energies of the order of a few Bev.

LITERATURE CITED

[1] A. N. Matveev, Doklady Akad. Nauk SSSR 107, 5, 671 (1956) [Soviet Physics - "Doklady", p. 211].

[2] M. Sands, Phys. Rev. 97, 470 (1955).

[3] A. A. Sokolov and I. M. Ternov, J. Exptl.-Theoret. Phys. (USSR) 28, 431 (1955) [Soviet Physics JETP, p. 227].

[4] E. B. Courant, M. S. Livingston and H. S. Snyder, Phys. Rev. 88, 1190 (1952).

M. V. Lomonosov
Moscow State University

Received October 14, 1955

NOTE ADDED IN PROOF

In the article by A. A. Kolomenskii and A. N. Lebedev [Doklady Akad. Nauk SSSR 106, 807 (1956)] concerning the effect of radiation on betatron oscillations with weak focusing, it is stated that considerable radiation damping of betatron oscillations occurs. We consider this incorrect. The basic Equation (5) of this article takes damping into account incorrectly. In this equation W for a single act of emission of a photon of energy ϵ actually is equal to $\epsilon\delta(t)$. For the drop δv_r of the radial component of the velocity at the instant of emission, we obtain from this equation $\delta v_r = -(\epsilon/E)v_r$. On the other hand, from momentum conservation $\delta(Ev_r) = -\epsilon(c/v)v_r$ and from energy conservation $\delta E = -\epsilon$, for the velocity drop at the instant of emission we obtain

$\delta v_r = -(\varepsilon / E)\, v_r \cdot {}^1/_2\, (mc^2 / E)^2$. Thus, Equation (5) contradicts the conservation of momentum and energy during emission. We note that this question can be checked experimentally at relatively low energies. For example, at E = 400 Mev and R = 1.4 m and for a 1 second accelerating cycle, the radiation damping of Kolomenskii and Lebedev should reduce the initial amplitude of betatron oscillations by a factor of $\sim 10^{13}$, which should be superposed on the experimentally well verified adiabatic damping $\sim H^{-1/2}$, which in this case amounts to $\sim 10^2$. The experimental problem is then only the suitable lengthening of the accelerating cycle, as the enormous difference by a factor of 10^{11} should easily be detected

A CYCLOTRON WITH SECTIONAL MAGNET

E. M. Moroz

(Presented by Academician D. V. Skobel'tsyn December 19, 1955)

The energy of particles which are accelerated in a cyclotron is limited by the relativistic increase of their mass, which results in a change of the period of orbital motion. It has been possible to overcome this difficulty by modulating the accelerator parameters through the use of the principle of phase stability which was discovered by V. I. Veksler [1,2]. Accelerators have recently been designed with unmodulated parameters, based on a different principle. In the electron cyclotron model of MacMillan, et al. [3]*, the constancy of the orbital frequency is maintained by a radially increasing magnetic field, and the particles are focused by the Thomas method of azimuthal variation of the magnetic field [4,5]. But increasing fields do not provide the only means of maintaining a constant orbital period.

The author has proposed the use of a steady current magnet for circular accelerators [6], which consists of a number of identical wedge-shaped sectors. The orbital period of the particles depends on the energy. As was pointed out to the author by M. S. Rabinovich, a magnet consisting of wedge-shaped sectors can also be used for the cyclotron. Thus, unlike the Thomas method [3-5], constancy of the orbital frequency can be insured without the use of a radially increasing magnetic field. The present article discusses the principle which can serve as the basis for designing a sectional cyclotron magnet, and investigates the stability of the particle motion and the resonances.

The orbital period T of a particle with energy E for an equilibrium trajectory in a magnet consisting of N identical sectors with a uniform magnetic field H can be written as

$$T = \frac{2\pi E}{ceH} + \frac{Nl}{v}, \tag{1}$$

where l is the gap between magnet sectors; v is the particle velocity; c is the velocity of light; and e is the electron charge. The change of transit time of the particle through the magnet sectors [the first term in (1)] can compensate the corresponding change in the transit time through the gaps between sectors [second term in (1)]. By requiring constancy of the orbital period, we obtain from (1) the required dependence of l on energy:

$$l = \frac{2\pi r}{N}\left(\frac{\zeta_M}{\zeta} - 1\right). \tag{2}$$

Here $r = \frac{E_0}{eH}\sqrt{\zeta^2 - 1}$ is the radius of curvature of the particle trajectory in a magnet sector; $\zeta = \frac{E}{E_0}$; $\zeta_M = \frac{TceH}{2\pi E_0}$; $E_0 = m_0c^2$ is the rest energy of the particle. As the energy increases l at first increases and then begins to decrease. The maximum separation between the sectors corresponds to the energy for which $\zeta_M = \zeta^3$.

---

*See also Lawrence, Lecture at the Geneva Conference on the Peaceful Uses of Atomic Energy, 1955.

Vertical focusing of the particles is provided by a decreasing magnetic field at the edges of the magnet sectors. When the trajectory forms the angle γ with the normal to the sector boundary, the focusing action of the sector edge is equivalent to the effect of a thin lens with focal distance $f_z = r \operatorname{ctg} \gamma$. The angle γ is considered positive when the linear portion of the trajectory and the center of curvature of the curved portion lie on the same side of the normal to the boundary of the magnet sector. This is satisfied for $\zeta < \zeta_M^{1/2}$, i.e., so long as the separation $\underline{l}$ between sectors continues to increase. When the sectors begin to approach each other as the energy increases, the vertical focusing is replaced by defocusing action. The limit of vertical stability of the motion $\zeta = \zeta_M^{1/2}$ can be considerably extended by the use of unsymmetrical sectors. For symmetrical sectors the angles γ_1 and γ_2 between the trajectories and the normal to the sector boundaries are identical and are both negative for defocusing. By inclining the sector boundaries it is possible to keep one of the angles positive and thus insure stability of the motion in analogy to the way in which alternation of positive and negative field gradients provides stability in accelerators with strong focusing [7]. The ratio of the frequency ω_z of vertical oscillations to the orbital frequency $\omega = 2\pi/T$, is $N\mu_z/2\pi$, where μ_z can be found by methods which were developed for strong-focusing accelerators:

$$\cos \mu_z = 1 - \left(\frac{l}{2r} + \frac{\pi}{N}\right)(\tan \gamma_1 + \tan \gamma_2) + \frac{\pi l}{rN} \tan \gamma_1 \tan \gamma_2. \tag{3}$$

The energy dependence of the angles γ_1 and γ_2 can be found by expressing them in terms of the distance $\underline{y}$ from the midpoint of the linear portion of the trajectories to the center of the accelerator:

$$y = r\left[1 + \frac{\pi}{N}\left(\frac{\zeta_M}{\zeta} - 1\right) \operatorname{ctg} \frac{\pi}{N}\right]. \tag{4}$$

If the sectors are symmetrical, $\gamma_1 = \tan \gamma_2 = \frac{1}{2}\frac{dl}{dy}$, and the midpoints of the linear portions of the trajectories for particles of different energies in any of the gaps between sectors lie on a single straight line which passes through the center of the accelerator and is perpendicular to all intersected trajectories. For unsymmetrical sectors $\gamma_1 \neq \gamma_2$ and the geometrical locus of the midpoints of the linear portions of the trajectories is a spiral $y(\varphi)$, where φ is the azimuthal angle. Then

$$\tan \gamma_1 = \frac{\frac{1}{2}\frac{dl}{dy} - y\frac{d\varphi}{dy}}{1 + \frac{l}{2}\frac{d\varphi}{dy}}; \quad \tan \gamma_2 = \frac{\frac{1}{2}\frac{dl}{dy} + y\frac{d\varphi}{dy}}{1 - \frac{l}{2}\frac{d\varphi}{dy}}. \tag{5}$$

By increasing the slope of the spiral $y\frac{d\varphi}{dy}$ as the energy increases, it is possible to move the boundary of vertical stability of the motion $\cos \mu_z = 1$, so long as this does not affect radial stability. This method shares some general features with the method of Kerst et al. [8,9] for accelerators with a radially increasing magnetic field.

The radial stability of the particle motion is characterized by μ_r, which satisfies the equation

$$\cos \mu_r = \left[1 + \frac{l}{r}p\right] \cos \frac{2\pi}{N} + \left[p + \frac{l}{2r}(q - 1)\right] \sin \frac{2\pi}{N}, \tag{6}$$

where

$$p = \frac{\frac{1}{2}\frac{dl}{dy} + \frac{l}{2y}\left(y\frac{d\varphi}{dy}\right)^2}{1 - \left(\frac{l}{2y}\right)^2\left(y\frac{d\varphi}{dy}\right)^2}; \quad q = \frac{\left(\frac{1}{2}\frac{dl}{dy}\right)^2 - \left(y\frac{d\varphi}{dy}\right)^2}{1 - \left(\frac{l}{2y}\right)^2\left(y\frac{d\varphi}{dy}\right)^2}.$$

The quantities $\frac{1}{2y}$ and $\frac{1}{2}\frac{dl}{dy}$ in these equations can be derived from (2) and (4):

$$\frac{1}{2}\frac{l}{y}=\frac{\frac{\zeta_M}{\zeta}-1}{\frac{N}{\pi}\tan\frac{\pi}{N}+\frac{\zeta_M}{\zeta}-1}\tan\frac{\pi}{N};\quad \frac{1}{2}\frac{dl}{dy}=\frac{\frac{\zeta_M}{\zeta^2}-1}{\frac{N}{\pi}\tan\frac{\pi}{N}+\frac{\zeta_M}{\zeta^2}-1}\tan\frac{\pi}{N}. \tag{7}$$

The maximum energy for which vertical stability still exists $(\cos\mu_z < 1)$, as well as radial stability $(\cos\mu_r > -1)$, corresponds to the values $\zeta \simeq 1.34$, $\zeta_M \simeq 1.5$ for N = 3 and $\zeta \simeq 1.67$, $\zeta_M \simeq 2$ for N = 4. Then $\left(y\frac{d\varphi}{dy}\right)_{\max} \simeq 1.5$.

The stability region which exists for $N \geq 3$ is crossed by lines of resonances between the frequency of vertical oscillations and the orbital frequency, between the frequency of radial oscillations and the orbital frequency and, finally, between the frequencies of the vertical and radial oscillations. Confining ourselves to second order terms in the equations of motion of a particle, we obtain 5 undesirable resonances for N = 3 and 9 resonances for N = 4. But it is possible without passing through resonances to obtain $\zeta \simeq 1.15$ for $\left(y\frac{d\varphi}{dy}\right)_{\max} \simeq 2$ and N = 3 or 4, or to obtain $\zeta \simeq 1.1$ for N = 4 and $\frac{d\varphi}{dy} = 0$. The resonance lines, like the boundaries of the stability region, can be shifted not only by means of a given law of change of $y\frac{d\varphi}{dy}$ with energy, but also by applying the magnetic field $\varkappa H$ $(\varkappa < 1)$ in the gaps between sectors with the field H.

It should be noted that wedge-shaped sectors can also be used in the magnetic system of a microtron [2,10, 11], thus avoiding the difficulties associated with the absence of vertical focusing in existing microtrons [12,13] with an almost uniform magnetic field. (In the sectional microtron magnet proposed by Schwinger [14] there was no stability of particle motion). For the microtron the orbital period is subject to the condition T = kE, where k is a proportionality factor independent of the energy: $k=\frac{2\pi\sigma}{ceH}$; $\sigma = 1+\frac{Nl}{2\pi r}=$ const. The boundaries of the magnet sectors are straight lines passing through the center of the magnet system. The expressions for $\cos\mu_z$ and $\cos\mu_r$ of the microtron magnet can be derived from the corresponding cyclotron equations (3) and (6) by setting $d\varphi/dy = 0$, $\zeta = 1$ and replacing ζ_M by σ:

$$\cos\mu_z = 1-2\frac{\pi}{N}\sigma a+2\left(\frac{\pi}{N}\right)^2(\sigma-1)a^2,$$

$$\cos\mu_r=\left[1+2\frac{\pi}{N}(\sigma-1)a\right]\cos\frac{2\pi}{N}+\left[a+\frac{\pi}{N}(\sigma-1)(a^2-1)\right]\sin\frac{2\pi}{N},$$

where

$$a=\frac{l}{2y}=\frac{1}{2}\frac{dl}{dy}=\frac{\sigma-1}{\frac{N}{\pi}\tan\frac{\pi}{N}+\sigma-1}\tan\frac{\pi}{N}.$$

The frequencies of vertical and radial oscillations of the particles in a microtron magnet are independent of the energy, so that resonance jumps of the oscillations are easily avoided.

In conclusion the author wishes to express his tratitude to M. S. Rabinovich for suggesting the topic, for his continued interest and for valuable suggestions.

LITERATURE CITED

[1] V. I. Veksler, Doklady Akad. Nauk SSSR 44, 393 (1944).

[2] V. I. Veksler, J. Phys. 9, 153 (1945).

[3] R. Pyle, Nucl. Sci. Abstr. 9, 728, 819 (1955).

[4] L. H. Thomas, Phys. Rev. 54, 580, 588 (1938).

[5] L. J. Schiff, Phys. Rev. 54, 1114 (1938); 55, 422 (1939).

[6] E. M. Moroz, A Steady Current Ring-Shaped Magnet for Cyclical Accelerators, (Report Phys. Inst., Acad. Sci. USSR, 1950).

[7] E. D. Courant, M. S. Livingston and H. S. Snyder, Phys. Rev. 88, 1190 (1952).

[8] D. W. Kerst, K. M. Terwilliger, H. R. Symon and L. W. Jones, Bull. Am. Phys. Soc. 30, 14 (1955).

[9] L. J. Laslett, Bull. Am. Phys. Soc. 30, 53 (1955).

[10] V. I. Veksler, Doklady Akad. Nauk SSSR 43, 346 (1944).

[11] E. M. Moroz, Doklady Akad. Nauk SSSR 106, 6, 986 (1956).

[12] C. Henderson, F. F. Heymann and R. E. Jennings, Proc. Phys. Soc. 66, 654 (1953).

[13] H. F. Kaiser, J. Franklin Inst. 257, 89 (1954).

[14] L. J. Schiff, Rev. Sci. Instruments 17, 6 (1946).

P. N. Lebedev Physics Institute
Academy of Sciences of the USSR

Received December 14, 1955

NEW ENGINEERING PHYSICS METHODS FOR DESIGNING MODELS AND CALCULATING TRAJECTORIES OF RELATIVISTIC CHARGED PARTICLES IN ELECTROSTATIC FIELDS

A. M. Strashkevich

(Presented by Academician A. A. Lebedev December 6, 1955)

It is well known how important a part is played in electronics by various approximate methods for plotting the trajectories of nonrelativistic charged particles. One of the most graphic methods of finding the trajectories of nonrelativistic particles in electrostatic fields is the method of gravitational models [1,2]. Can this method be applied to the trajectories of relativistic particles? Up to the present, this has been considered theoretically impossible since the ball rolling on the relief map possesses constant mass, while a charged particle moving at relativistic velocities in a field possesses varying mass. However, it will be shown below that this problem can be solved completely.

Let us write the law of conservation of energy for a particle whose charge has the algebraic value e:

$$m_0c^2(\alpha - 1) + e\Phi = h, \tag{1}$$

where h is a constant and $\alpha = (1 - v^2/c^2)^{-1/2}$. The equations of the trajectory of a relativistic particle in an electrostatic field are [3]

$$\begin{aligned} x'' &= -\frac{eA}{2(h - e\Phi)}(1 + x'^2 + y'^2)\left(\frac{\partial\Phi}{\partial x} - x'\frac{\partial\Phi}{\partial z}\right), \\ y'' &= -\frac{eA}{2(h - e\Phi)}(1 + x'^2 + y'^2)\left(\frac{\partial\Phi}{\partial y} - y'\frac{\partial\Phi}{\partial z}\right), \end{aligned} \tag{2}$$

where primes indicate differentiation with respect to z and A denotes the function

$$A = \frac{\dfrac{h - e\Phi}{m_0c^2} + 1}{\dfrac{h - e\Phi}{2m_0c^2} + 1} = \frac{2\alpha}{\alpha + 1}. \tag{3}$$

For the nonrelativistic case ($v \ll c$) $A = 1$; as v increases, A also increases and approaches the value 2.

As a basis for the proposed model of a relativistic trajectory we shall write Equation (2) for a nonrelativistic charged particle in a field in which the potential distribution is represented by the function

$$\Phi^* = \Phi - \frac{(h - e\Phi)^2}{2em_0c^2} = \Phi - \frac{m_0c^2}{2e}(\alpha - 1)^2. \tag{4}$$

When the expressions of (4) are substituted into these equations, they are transformed into the equations of the trajectory of a relativistic particle since

$$\frac{\partial\Phi^*}{\partial x}=\alpha\frac{\partial\Phi}{\partial x},\quad \frac{\partial\Phi^*}{\partial y}=\alpha\frac{\partial\Phi}{\partial y},\quad \frac{\partial\Phi^*}{\partial z}=\alpha\frac{\partial\Phi}{\partial z},$$

$$-\frac{e}{2(h-e\Phi^*)}=-\frac{e}{(\alpha+1)(h-e\Phi)}.$$

Consequently, by modulating the trajectories of particles of constant mass in the field Φ^*, we thereby modulate the trajectories of particles of varying mass in the field Φ; the relief map must correspond to the function Φ^*, which can easily be calculated.

By substituting (4) into the equation for energy conservation we find that, although the trajectories in both instances (relativistic and nonrelativistic) are identical, the velocities in the trajectories vary differently, so that for relativistic particles the prevailing method of using discontinuous illumination for the photographing of a ball rolling on the map can produce only an approximate law of velocity change with particle motion.

The possibility of reducing the solution for the relativistic equations to the solution of equations for the trajectories of particles with constant mass was first suggested by S. A. Boguslavskii [4] but was forgotten for a long time. The idea has been developed in recent theoretical investigations [5,6]; however, no one has thus far been concerned with its practical significance for electronic engineering, which follows from what has been said above. In addition to the possibility of designing a model design, this significance lies in the fact that a number of graphico-analytical methods that have been developed for nonrelativistic particles can be carried over very simply to the case of relativistic velocities by first calculating the potential distribution, replacing the function Φ by the function Φ^*. The standard nonrelativistic equation of the familiar "radius of curvature method" agrees completely, when Φ is replaced by Φ^*, with the relativistic Equation (7) [7]; the working nonrelativistic equation of the "trigonometrical method" differs insignificantly from relativistic Equation (2) [7] following the same substitution. If there is a magnetic field, in addition to the electrostatic field, the introduction of Φ^* from (4) instead of the electrostatic potential is also sufficient for the reduction of solution of the relativistic equations to the nonrelativistic case (see [4]).

However, not all engineering physics methods of investigating nonrelativistic trajectories can be applied to the relativistic region by the conversion $\Phi \to \Phi^*$; in particular, this is impossible for the rubber model ([8], p. 218), the automatic [9,10] and semiautomatic [11] methods. These could be applied in the same way if new boundary conditions could be found by the conversion $\Phi \to \Phi^*$ and if their existence, by virtue of the unique solution theorem, could produce the required distribution of the hamonic function corresponding to Φ^* in the region where measurements are made; but, as we can see by substituting (4) into the Laplace equation, the function Φ^* is not hamonic, just like the effective potentials introduced by a different procedure in articles [5,6].

It is a widely held opinion (see, for example, [12]) that graphico-analytical methods can only be used to calculate plane trajectories. In our paper [7] we suggested the possibility of also deriving the spatial trajectories of charged particles by such methods; for relativistic velocities corrections are required in the relationships (9) of [7]; then increments of the velocity components will be expressed with sufficient accuracy by the equations

$$\frac{\Delta v_x}{c}=\frac{1}{\Phi(1+\varkappa)}\left[\frac{\Delta\Phi_x}{v_x/c}-\left(\frac{v_x}{c}\Delta\Phi_x+\frac{v_y}{c}\Delta\Phi_y+\frac{v_z}{z}\Delta\Phi_z\right)\right],$$

$$\frac{\Delta v_y}{c}=\frac{1}{\Phi(1+\varkappa)}\left[\frac{\Delta\Phi_y}{v_y/c}-\left(\frac{v_x}{c}\Delta\Phi_x+\frac{v_y}{c}\Delta\Phi_y+\frac{v_z}{c}\Delta\Phi_z\right)\right], \tag{5}$$

$$\frac{\Delta v_z}{c}=\frac{1}{\Phi(1+\varkappa)}\left[\frac{\Delta\Phi_z}{v_z/c}-\left(\frac{v_x}{c}\Delta\Phi_x+\frac{v_y}{c}\Delta\Phi_y+\frac{v_z}{c}\Delta\Phi_z\right)\right].$$

Here $\Delta\Phi_x$, $\Delta\Phi_y$, $\Delta\Phi_z$ are the increments of the potential at the distances $\Delta x, \Delta y, \Delta z$ from a given point where the potential is Φ; $\varkappa=\frac{m_0c^2}{-e\Phi}$. The trajectories are plotted approximately from points lying on

TABLE 1

$x - x_0$	$y - y_0$			
	From relativistic Eq. (5)	From relativistic Eq.(5) with $\Phi - \Phi^*$	By the method of momenta	Exact calculation
0.000	0.000	0.000	0.000	0.000
1.000	3.569	3.565	3.569	3.551
2.000	6.840	6.836	6.847	6.885
3.000	9.883	9.876	9.898	9.933
4.000	12,75	12,73	12.76	12.80
5.000	15.46	15.43	15.47	15.54
6.000	18.03	17.99	18.05	18.12
7.000	20.49	20.47	20.51	20.51
8.000	22,85	22,80	22.87	23.01
9.000	25,12	25.06	25.15	25.33
10.00	27.30	27.25	27.34	27.50

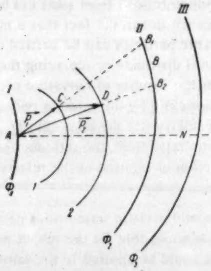

Fig. 1

successively obtained velocity vectors. Equations (5) enable us to apply a semiautomatic method used for nonrelativistic particles [11] to the plotting of relativistic trajectories.

Table 1 presents the results of a relativistic trajectory calculation carried out with the aid of (5) and, for comparison, results obtained by other methods. The third column contains results obtained with (5) in the nonrelativistic approximation with Φ replaced by Φ^*.

For the plotting of plane trajectories of relativistic particles it is also possible to consider the following graphico-analytical method which is based on the successive plotting of momentum vectors. Let the initial point A of the considered portion of the trajectory lie on the equipotential line I, on which the potential is designated by Φ_1. For this point we do not know the magnitude and direction of the momentum vector $\mathbf{p}_1$ (see Fig. 1). If we know the potential Φ_2 for some neighboring equipotential line II, we can easily calculate p_2 for the corresponding momentum vector $\mathbf{p}_2$. In order to find the direction of $\mathbf{p}_2$ we draw two concentric circular arcs (1 and 2) with radii p_1 and p_2 (with center at A). When the vector $\mathbf{p}_1$ is given, the point C on arc 1 is given since it is at the end of $\mathbf{p}_1$. The point D at the end of the vector p_2 is found as follows: we draw the normal AN to line I; the increment of momentum CD induced by the field will have the direction of the force, i.e., it will be parallel to AN. The interval B_1B_2, containing the point B where the trajectory intersects line II, can be found by prolonging the vectors $\mathbf{p}_1$ and $\mathbf{p}_2$ until they intersect line II. We know [7,12] that, by using the "trigonometrical" method of plotting trajectories, we obtain greater accuracy if the line segment that is obtained by using Φ_1 and Φ_2 is extended not to line II but to the equipotential line $1/2\,(\Phi_1 + \Phi_2)$ and the following line segment to the equipotential line $1/2\,(\Phi_2 + \Phi_3)$, etc. The calculations show that if this procedure can be employed in plotting trajectories by other methods, it also improves accuracy. In the present method this corresponds, if the field is not extremely inhomogeneous, to locating the point B at almost the midpoint of B_1B_2; for a uniform field we find B exactly at the midpoint (see Table 1). For $v \ll c$ the momenta are proportional to the velocities, and all of the plots described can be obtained from velocity vectors; the method then coincides basically with the method proposed in [13], in which it is suggested that B can be located by extending the diagonal of the parallelogram of velocities $\mathbf{v}_1$ and $\mathbf{v}_2$ until it intersects II. A similar method, the construction of the parallelogram for $\mathbf{p}_1$ and $\mathbf{p}_2$, gives quite good results in the relativistic case.

Table 1 gives the results for the trajectory of a relativistic electron in a uniform field. The potential of the initial point is taken as $4 \cdot 10^5$ v; the initial angle of inclination of the trajectory to the x-axis is 75°; the field gradient is directed along the x-axis; $\Delta\Phi = \Phi'\Delta x = 4 \cdot 10^3$ v; Δx is taken as the scale unit. In order to distinguish clearly the errors that result from the approximations used in each method, all graphical operations were replaced by calculations. The data in the last column were obtained (see Equation (16) of article [7]) by exact integration of the equations of motion. As is shown in Table 1, the approximate methods for calculating relativistic trajectories that we have proposed in this article are of satisfactory accuracy.

LITERATURE CITED

[1] E. Brüche and A. Recknagel, Z. tech. Phys. 1936, No. 4, 126.

[2] V. Cosslett, Introduction to Electron Optics (For. Lit. Press, 1950).

[3] A. M. Strashkevich, J. Tech. Phys. USSR 22, 1848 (1952).

[4] S. Boguslavskii, Electron Trajectories in Electromagnetic Fields (Moscow, 1929).

[5] A. E. Levashov, Bull. Central Asian State Univ. 23, 50 (1945); Trans. Physico-Technical Inst. Acad. Sci. Uzbek SSR 2, 59 (1949); 3, 98 (1950).

[6] I. Verle, Bull. Polish Acad. Sci., Section III, 1, 7, 281 (1953).

[7] A. M. Strashkevich, J. Tech. Phys. USSR 23, 1796 (1953).

[8] A. Rusterkhol'ts, Electron Optics (For. Lit. Press, 1952).

[9] D. Gabor, Nature 139, 373 (1937).

[10] D. B. Langmuir, Nature 139, 1066 (1937).

[11] J. Marvaud, Comptes rend. 226, 476 (1948).

[12] V. S. Lukoshkov, V. L. Il'inskii and T. I. Tamaridze, Bull. Low-Power Electrical Industry, 1940, No. 7, 47.

[13] R. P. Musson-Genon, Comptes rend. 222, 858 (1946).

Kiev Polytechnical Institute

Received November 24, 1955

SECONDARY ELECTRON EMISSION FROM METALS INDUCED BY IONS AND NEUTRAL PARTICLES

V. G. Tel'kovskii

(Presented by Academician L. A. Artsimovich December 1, 1955)

The purpose of the present article is the study of secondary electron emission from pure metals bombarded by ions and neutral atoms, with energies from a few kilovolts to 120 kev.

In working out the experimental procedure special attention was directed toward creating experimental conditions which would practically eliminate surface contamination of the metals.

The apparatus was a large mass spectrometer of about 4 m in length and 25° ion beam deflection. The diaphragm system limited the ion spread to ± 3°. The target was placed close to the focus of the ingoing ion beam.

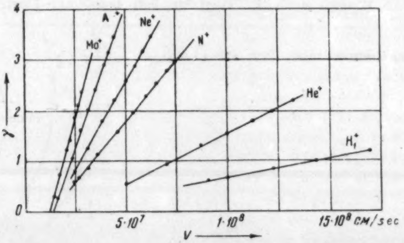

Fig. 1

In order to obtain positive ions we used an arc discharge in a longitudinal magnetic field. The ion current density at the exit point from the gas discharge chamber of the source attained 100 ma/cm². The differential evacuation system was able to maintain a 1000 x pressure differential between the source and the measuring chamber which contained the target. The pressure of the residual gases in the target region during measurements did not exceed $3 \cdot 10^{-8}$ mm. The instrument was designed to permit advance heating of the target to 2500-3000°. The temperature at which measurements were made was such that the thermionic emission was considerably lower than the level of secondary electronic emission. For the majority of the metals this was between 1300 and 1500°. A magnetic field of 200 to 500 oersted in the measuring chamber, perpendicular to the ion beam, in conjunction with an extracting electric field, completely prevented the passage of negative ions from the target to the secondary electron collector. Neutral particles were produced by resonance overcharging of positive ions of the beam. The overcharging chamber contained a system of diaphragms for producing a large pressure drop (by a factor of 500) and the emission angle of the particles was limited by the exit aperture (± 0.5°). This resulted in monochromatic beams of neutral particles, while maintaining the high vacuum in the measuring chamber. For separation of the neutral beam the positive ions were deflected by a magnetic field between the overcharging chamber and the target. For measurement of the number of neutral atoms we used a fast-response method of registering particle pulses because the beam intensity could change considerably during the experiment. A suitably designed instrument measured the flux ($10^{13}-10^{14}$ particles/cm² · sec) for a chosen energy range, with an accuracy within a few per cent.

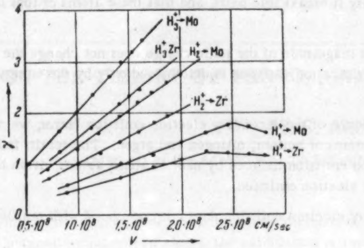

Fig. 2

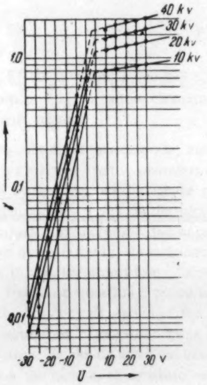

Fig. 3

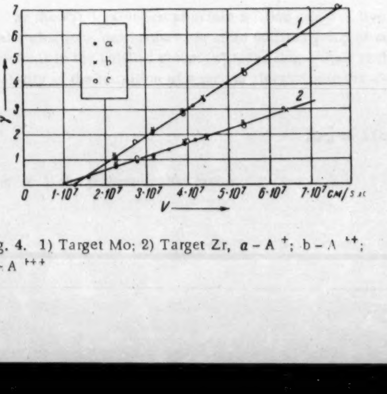

Fig. 4. 1) Target Mo; 2) Target Zr, a – A^+; b – A^{++}; c – A^{+++}

Preliminary experiments showed that with negligible surface contamination (a few atomic layers) the secondary electron emission factor loses its meaning as a physical constant, since it now depends on the ion or neutral atom flux which bombards the surface. This phenomenon was used as a control of surface cleanliness during the experiment. A metallic surface was considered atomically clean if, when the ion current density changed by a factor of 1000 (from 10^{-7} to 10^{-4} amp/cm^2), the secondary electron emission factor remained constant within the limits of experimental error (± 1%).

In order to obtain secondary emission we used targets of molybdenum, zirconium, nickel, tantalum, copper and graphite. The targets were bombarded by ions of hydrogen, helium, nitrogen, neon, argon, molybdenum and neutral atoms of inert gases. The most productive targets were those made of molybdenum and zirconium, which were less contaminated and were well degassed. The other materials yielded the same laws with larger spread of the data.

From an examination of the graphs, the following fundamental laws can be established.

The secondary electron emission factor for all the ions and targets that were investigated increases up to velocities of $2 \cdot 10^8$ cm/sec (see Fig. 1). With further increase of ion velocity (experimental data were obtained in this region for only the proton beams) a flat maximum is observed ($2.5 \cdot 10^8$ cm/sec) followed by a gradual decline, which is an indication of the spatial character of the emission mechanism (see Fig. 2).

In all instances a fairly sharp threshold for secondary electron emission was observed. The velocities corresponding to this threshold depend only slightly on the material of the target and the kind of ion. For the cases investigated the threshold lies between 0.5 and $2 \cdot 10^7$ cm/sec.

Fig. 3 shows curves which characterize the velocity distribution of secondary electrons in a semilogarithmic plot. The linear character of these curves shows that the velocity distribution of secondary electrons obeys the Maxwell law. The average secondary electron energy, which can be called arbitrarily the "temperature" of the secondary electrons, is independent of the energy of the incident ions. For the ions and targets investigated it lies in the range 50,000 to 80,000°. The strict proportionality of the secondary electron emission factor to the number of particles in the molecular ion (see Fig. 2) suggests that when a molecular ion approaches the metal boundary it breaks into parts, and that these atoms or ions interact with the metal like single ions.

From the graph (see Fig. 4) it can be seen that the magnitude of the ionic charge does not change the secondary electron emission factor; consequently, secondary electron emission is determined only by the energy of the incident particle and not by the charge.

For additional verification of the charge independence of the secondary electron emission factor, we performed comparative experiments with ions and neutral atoms of helium, nitrogen and argon. The results indicated that, under identical conditions, secondary electron emission induced by neutral atoms agrees within the limits of experimental error with ion-induced secondary electron emission.

As a consequence, the potential theory of secondary electron emission does not correspond with reality.

Received November 9, 1955

ON THE THEORY OF FERRO-, PARA- AND FERRIMAGNETISM

N. S. Akulov

(Member of the Academy of the Belorussian Soviet Socialist Republic)

With the development of neutronographic methods of analysis, which have made possible a more detailed study of magnetic moments in alloys, the calculation of the relation of atomic magnetic moments above and below the Curie point has become increasingly important. We note that atomic magnetic moments in the paramagnetic state (μ_p), i.e., for $T > \theta$, unlike μ_f ($T < \theta$), are nonlinearly dependent on $\underline{n}$.

However, instead of the magnetic moments we can by means of the equation

$$\mu_p = \mu_B \sqrt{2S_p(2+2S_p)} \tag{1}$$

use the values of $2S_p$. Then, according to the theory, $2S_p$ is linearly dependent on $\underline{n}$ and it is possible to construct a diagram of $S_p(n)$, whose elements consist mainly of segments of straight lines, both in the ferromagnetic and paramagnetic regions.

The construction of this diagram, unlike the Slater-Pauling diagram, provides the possibility of establishing the general laws relating atomic moments above and below the Curie point. This theory is based on the capture of s-electrons by d-electrons through an exchange interaction. The capture probability Δn_d depends on the electron concentration $\underline{n}$ (i.e., on the total number of electrons in the s- and d-zones). Δn_d can be calculated by various methods. By increasing the accuracy of the calculation of Δn_d we are able to solve the above-mentioned problem quantitatively. In calculating the change of the number of d-electrons, we note that from spectroscopic data in isolated atoms from Cr ($n = 6$) to Cu ($n = 11$), at least one of the s-electrons is transferred to the d-shell. The same situation is found in metals. The second s-electron can only make a partial transition to the d-shell. For our calculation of the probability of this transition, just as in our previous paper, we must establish the number of "clockwise" spins n'_d and of "counterclockwise" spins n''_d as a basis for calculating the ds-interaction. In the Cr atom we have five clockwise spins and no counterclockwise spins, i.e., $n''_d = 0$. As $\underline{n}$ increases, the number of counterclockwise spins n''_d rises. For the transition of one s-electron to the d-shell we have $n_d = n - 1$ and

$$n''_d = (n-1) - 5 = n - 6. \tag{2}$$

By the Pauli exclusion principle a filled group of five clockwise d'-spins (for $T < \theta$) cannot attract additional s-electrons, unlike the case of an unfilled group of counterclockwise electrons. The larger the number of d-electrons in the unfilled group (n''_d), the larger their exchange interaction with the s-electrons. Thus, for the probability of the transition of a second electron into the d-zone for $T < \theta$ we obtain according to (2)

$$\Delta n''_d = \alpha(n-6), \tag{3}$$

where α is the proportionality factor.

According to this model, if we subtract from the total number of clockwise spins, the number of counterclockwise spins, given by $n''_d + \Delta n''_d$, from (3) and (2) we have

$$2S_f = 5 - (1 + \alpha)(n - 6). \tag{4}$$

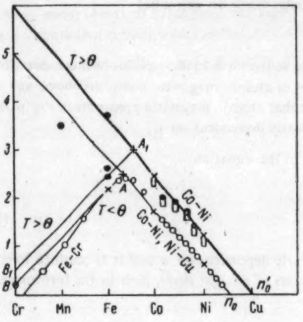

Fig. 1

The magnitude of α can be determined either in the way which we showed previously, or by the zone theory according to which the atomic moment vanishes for an electron concentration $n_0 \simeq 10.6$. Hereafter we shall use the more exact value

$$n_0 = 10.552 \tag{5}$$

Setting $S_f = 0$ and defining α in terms of n_0 from (4) we find

$$2S_f = 5\frac{n_0 - n}{n_0 - 6}. \tag{6}$$

This expression agrees with that which we found previously for atomic magnetic moments below the Curie point. Simple proportionality in this case gives $\mu_f / \mu_B = 2S_f$.

It is especially important to note the rule of maximal momenta which was indicated in less general form in the earlier article, that the vertices of the triangles BAn_0 and $B'A'n'_0$ (see Fig. 1) are given by the condition *

$$n''_d = 1/2\, n'_d. \tag{7}$$

Hence, for the magnetic moment at the point A we have

$$\mu_{cr} = 2.5\,\mu_B = {}^1/_2(\mu_{Cr})_{\max}, \tag{8}$$

and for the electron concentration, corresponding to this point, we obtain from (6), (5) and (8)

$$n_{cr} = 3 + 1/2\, n_0 = 8.276. \tag{9}$$

Since, for alloys and elements with $n < n_{cr}$ the group of five clockwise spins (2nd basic rule) is broken up, we have here $d\mu/dn = \mu_B$. As a result we obtain from (8) the linear relationship:

$$2S_f = \mu_f / \mu_B = 2.5 - (n_{cr} - n), \tag{10}$$

i.e., for $n \leq n_{cr}$ on the basis of (9) and (10)

$$2S_f = n - {}^1/_2(n_0 + 1). \tag{11}$$

The relationships obtained for (7) and (11) give quantitative agreement with experiment for metals from Cr to Ni and for their alloys at low temperatures.

---

*This rule can be established by applying the method of orbitals to neighboring atoms.

At low temperatures there is a strong exchange interaction of one of the s-electrons with the d-electrons. The second s-electron (if we neglect the slight capture effect $\Delta n''_d$) remains practically free. At high temperatures all of the electrons strive to reach higher levels. As a result, the energetic individuality of the second s-electron is eliminated. Thus, at high temperatures the second s-electron in the Cr atom exists under practically the same conditions as the first s-electron at low temperatures. The probability of an sd-interaction with the second s-electron for a Cr atom at $T > \theta$ can reach the magnitude

$$W = 2S_p - 2S_F \cong 1. \tag{12}$$

In the Cr atom $2S_d = n - 2 = 4$; the sd-interaction with the first s-electron gives $2S_F = 5$. Inclusion of the second s-electron in the sphere gives from the sd-interaction $2S_p = 6$. Thus, under the conditions indicated $W \simeq 1$. However, as the d-shell is filled the energetic individuality of the second s-electron is gradually reestablished. Thus, in the Cu atom, $n - 1 = 10$, electrons completely fill the d-shell, but the second s-electron is the valence electron which is not bound energetically with the d-electrons. As a consequence we can expect linear reduction of W to $W = 0$ in the transition from $n = 6$ to $n = 11$. This is confirmed by experiment; for $n'_0 = (n)_{s_p=0}$ we actually obtain a value which is very close to $n = 11$ ($n'_0 = 10.85 \pm 0.15$).

Repeating for the second electron the calculation which was performed for the first electron in deducing (7), we obtain

$$2S_p = (2S_p)_{\mathrm{Cr}} \frac{n'_0 - n}{n'_0 - 6}, \tag{7'}$$

where $(2S_p)_{Cr} \simeq 6$.

The line A'B' to the left and below the point A' can be found analogously to the line AB. Here also $d\mu/dn = \mu_B$. However, by the rule for maximal momenta, $(2S_p)_{cr} = 1/2\,(2S_p)_{Cr}$.

From the first rule we have for $T > \theta$

$$(2S_p)_{cr} = 3 \tag{8'}$$

(or for Cr $2S_p = 6$).

From (7') and (8') we have (for an unstable d''-group)

$$2S_p = n - n'_0 + 5.$$

For an unstable d'-group we have $d(2S_p)/dn = 1$. Thus, from (8')

$$2S_p = 3 - (n'_{cr} - n). \tag{12'}$$

Here by (8') and (7') n'_{cr} is 8.5.

For the iron atom we then have

$$(2S_p)_{Fe} = 2.5, \tag{13}$$

which is in good agreement with Fallot's experimental data. From (11) and (5) we also have

$$(\mu_f)_{Fe} = 2.22. \tag{14}$$

Experiment gives 2.22.

Thus, knowledge of the single parameter n_0 enables us to determine exact values of μ_f even for other elements. The value of this parameter is determined approximately from the zone theory.

We thus obtain a diagram of S(n) which is in quantitative agreement with experiment in its main parts and which, moreover, enables us to predict magnetic moments above the Curie point for various alloys. For this reason further experimental and theoretical work in this field are of great interest.

We shall not here consider the problem of the "anomalies", i.e., the departure from linearity of 2S(n). These can be an ordering effect as in Ni-Mn alloys, for example. Here the adjacency of Mn atoms can result in different values of the moments.

Certain changes in the general laws can also result in a change of the lattice type and constant, as in Fe-Co alloys. It is also necessary to take into consideration a certain amount of spreading of the curve near the vertices A and A_1 resulting from electron concentration fluctuations. Finally, we must consider the possibility of branching not only from the point A but of ferrimagnetic branching from other points (for example, Fe, Ni, etc.).

All of these matters are of considerable interest in connection with further development of the theory and improvement of the S-diagram. In this connection it is already possible to state the following rules for ferro- and ferrimagnetic alloys.

A tendency toward ferrimagnetic branching from the lines An_0 and AB appears in elements with $n < n_{cr}$ (i.e., with an unstable group of five d'-electrons). The farther an element stands to the left of n_{cr} the greater its branching power. Cr is among these elements. An example is provided by the branches of FeCr, CoCr and NiCr.

Of the elements with $n < n_{cr}$ the smallest instability of the d'-group appears in Fe, which explains the existence of FeCo ferromagnetic alloys with large μ on the An_0 line to the right of n_{cr}. Mn is in second place with regard to d'-group stability and Cr is in third place. This is the explanation of a small ferromagnetic branch in NiMn on the line An_0. With increased Mn content there is a tendency toward the formation of ferrimagnetic branches. In order to increase the stability of the d'-group of a given atom, it must be surrounded with atoms for which $n > n_{cr}$ (third rule).

The present model leads to the conclusion that, in accordance with the ideas of Neel and Zener, ferrimagnetic elements should lie not on the principal lines, i.e., not on An_0 or BA, but on the branches mentioned above. Thus, for example, the Fe-Co segment running from Fe to A is not ferrimagnetic, since $n > n_{cr}$ for Co. However, when an element such as Cr with $n < n_{cr}$ is dissolved in Fe, there is a tendency toward the formation of a ferrimagnetic branch of Fe-Cr.

These results agree with data obtained by neutronographic analysis.

LITERATURE CITED

[1] N. Akulov, Doklady Akad. Nauk SSSR 105, 5 (1955).

Received December 31, 1955

EFFECT OF INTERMOLECULAR INTERACTIONS ON FIRST ORDER RAMAN LINES

Ia. S. Bobovich and V. M. Pivovarov

(Presented by Academician A. N. Terenin December 19, 1955)

1. If we neglect the possible small changes of the matrix elements of the coördinates which are caused by the mechanical anharmonicity resulting from intermolecular interactions, the effect of the latter on the intensity of first order Raman lines must be described completely by the behavior of the square of the first derivative of the polarizability with respect to the normal coordinate $\underline{q}$ for its equilibrium value. According to M. V. Vol'kenshtein [1] for a single electronic-vibrational transition, the first derivative of the polarizability can be given in the form

$$\left(\frac{\partial\alpha}{\partial q}\right)_0 \sim \frac{\nu_e^2+\nu^2}{(\nu_e^2-\nu^2)^2}(P_{0e})^2\left(\frac{\partial\nu_e}{\partial q}\right)_0, \qquad (1)$$

where ν_e is the frequency of the virtual electronic-vibrational transition for a given Raman line; P_{0e} is the matrix element of the dipole moment corresponding to this transition; ν is the frequency of the exciting light. Since, in the Morse approximation $(\partial\nu_e/\partial q)_0 \sim a'^2D'q'$ (a' and D' are constants of the Morse function for the excited electronic state; q' is the change of equilibrium position in the excited electronic state compared with the ground state), the expression obtained for $\partial\alpha/\partial q$ is

$$\left(\frac{\partial\alpha}{\partial q}\right)_0 \sim a'^2D'q'(P_{0e})^2\frac{\nu_e^2+\nu^2}{(\nu_e^2-\nu^2)^2}. \qquad (2)$$

In order to determine the possible changes of Raman intensities, we must examine the behavior of all factors in (2) on the basis of an analysis of the electronic-vibrational spectrum of a given substance. The following must be kept in mind. The parameters a' and D' of the Morse function characterize the shape of the upper potential curve. Their probable change produces a shift of the maximum ν_e of the actual electron-vibrational band. On the other hand, since $2a'^2$ D' equals k', which is the elastic constant of molecular vibration in an excited electronic state, the distortion of the potential curve must necessarily be reflected in a change of the shape (half width) of the electron-vibrational band. The relative equilibrium position q' also, of course, determines the transition frequency ν_e, q' can theoretically change due to a simultaneous shift of the lower and upper potential curves; however, it is a more likely assumption that the latter is predominant. Finally, changes of $(P_{0e})^2$ indicate nothing but attenuation or enhancing of the electron-vibrational band.

The role of the last factor, the so-called resonance denominator, need, of course, be taken into account only in the resonance region (where ν, the frequency of the exciting light, is close to ν_e).

Data in the literature give evidence of considerable changes in the ultraviolet absorption spectra of liquids as a function of their concentrations in mixtures and of the solvent. Thus, for example, V. M. Chulanovskii et al. [2,3], in investigating certain bands of benzene dissolved in hexane, ethyl alcohol and water, observed shifts of as much as 185 cm^{-1} compared with the spectrum of pure benzene. At the same time these authors detected considerable changes in the half widths and intensities of the bands.

TABLE 1

Concentration Dependence of the ν_{NO_2} Line of n-Nitrotoluene

Exciting line λ in A	Concentration	$I_{(nitr)} : I_{(naph)}$		$\Delta(I_{(nitr)}:I_{(naph)})$ average in %
		Individual measurements	Average	
5461	Very high	1.26; 1.26; 1.22; 1.34; 1.36; 1,30; 1.38; 1.27 1.37; 1.30; 1.30	1.30	3
	One half as much	0.70; 0.67; 0.68; 0.70; 0.71; 0.74; 0.63; 0.67; 0,62; 0,65; 0,70; 0.72	0.68	4.4
4358	Very high	1.79; 1.83; 1.71; 1.79; 1.73; 1.80; 1.80	1.78	1.7
	One half as much	0.84; 0.83; 0.85; 0.82; 0,83; 0.80; 0,80	0.82	2

TABLE 2

Concentration Dependence of the ν_{NO_2} Line of n-Nitrophenol

Exciting line λ in A	Concentration	$I_{(nitr)} : I_{(naph)}$		$\Delta(I_{(nitr)} : I_{(naph)})$ in %
		Individual measurements	Average	
5461	Very high	0,96; 0.94; 1.01; 0.98; 0.94; 1.04; 0.94	0.97	3
	One half as much	0.69; 0.55; 0.64; 0.69; 0.64; 0.63	0.64	5
4358	Very high	1.83; 1,84; 1.94; 1.85; 1.88; 1.82	1.86	1.6
	One half as much	0.96; 0.96; 1.00; 0.98; 0.94; 0.94; 0.94	0,96	2

TABLE 3

Concentration Dependence of the ν_{NO_2} Line of n-Nitraniline

Exciting line λ in A	Concentration	$I_{(nitr)} : I_{(naph)}$		$\Delta(I_{(nitr)}:I_{(naph)})$ average in %
		Individual measurements	Average	
5461	Very high	0,62; 0.56; 0.53; 0.58; 0.58; 0.45; 0.55; 0.54; 0.57; 0.48; 0.48; 0.62; 0.54; 0.53; 0.50; 0.60; 0.60; 0.68; 0.60; 0.65	0,56	8.4
	One half as much	0.64; 0.58; 0.66; 0.70; 0.60; 0.66; 0.61; 0.62; 0.64; 0.73; 0.73; 0.71; 0,70; 0.64	0.66	6
4358	Very high	5.10; 4.6; 4.0; 4.4; 4.7; 5.1; 4.1; 4.2; 4.7; 5.1 4.3; 4.7; 4.5; 4.7; 4.7; 4.8; 4.2	4.6	6
	One half as much	4.5; 4.4; 3,7; 3.8; 4.0; 4.4; 4.2	4.1	6.7

From what has been said above it follows that there is a possibility of concentration changes in Raman intensities; we have shown this experimentally [4].

A very important feature of (2) for the derivative of the polarizability is the following. Let there be a certain change of the parameters a', D' and q' in a solution of a given substance. For definiteness we shall assume that they are increased, resulting in increased frequency ν_e. This assumption is in good agreement with experiment according to which ν_e in the spectrum of a solution is, as a rule, higher than in the spectrum of the pure substance. Then, far from the resonance region ($\nu \ll \nu_e$), this should result in a stronger Raman line. As the resonance region is approached (as by varying the exciting radiation) the resonance denominator becomes effective and by virtue of competition with the parameters a', D' and q', it will tend to compensate the effect of the intermolecular interaction.

Thus, a study of the concentration effect on intensities, far from and close to, resonance can directly verify the correctness of a view regarding the role of a', D' and q' in the present connection.

2. We have investigated, far from and close to resonance, the line intensities of the completely symmetrical vibration of the NO_2 group (ν_{NO_2}) in the spectra of concentrated solutions of certain aromatic nitro-compounds: nitrobenzene, n-nitrotoluene, n-nitrophenol and n-nitraniline. The selection of these substances was based on experimental suitability: it is known [5] that vibrational lines of the NO_2 group in aromatic nitro-compounds are extremely strong and that, moreover, resonance for these compounds is realized in the visible portion of the spectrum.

The spectra were excited by the blue (4358 A) and green (5461 A) lines from a low pressure mercury lamp. The intensities were compared for two concentrations of a substance: a very high concentration and one which was exactly half as high. As a standard of comparison, we selected the 1380 cm^{-1} line of naphthalene. We neglected certain generally small variations in intensity of the standard line as the conditions of excitation were changed due to resonance. The solvents were benzene and acetone. To obtain the spectra we used the high-transmission photoelectric equipment described previously [6].

Unlike the work described in [6], the spectra were recorded automatically. For this purpose we used a standard EPPV-51 electronic recording instrument which included a direct current amplifier.

Tables 1, 2 and 3 give the results for n-nitrotoluene, n-nitrophenol and n-nitraniline.

From these tables it can be seen that near resonance higher concentration is accompanied by increased molar intensity of the ν_{NO_2} lines. This is evidence of the displacement of the ν_e band towards longer waves given by the resonance denominator, an effect which was previously observed and interpreted by P. P. Shorygin [5]. Also, when spectra are excited by the green line $\lambda = 5461$ A the opposite effect is clearly observed: higher concentration results in relative attenuation of the ν_{NO_2} lines. The latter circumstance is explainable, it seems to us, only on the basis of the hypothesis advanced above regarding the competition of the resonance denominator with the factors a', D' and q'.

In the spectrum of n-nitraniline (Table 3) excited by 5461 A, one observes the at first paradoxical fact that, when the concentration of the solution is cut in half, the intensity of the ν_{NO_2} line is not attenuated, as one would quite naturally expect, but, on the contraty, is somewhat augmented. This is clearly due to the very sharp concentration displacement of the ν_e band, which is so sharp that it covers the effect of reduced concentration. In this case the factor (P_{0e}) may also possibly play an important part.

Thus, we have shown by direct measurements that intermolecular interactions, at least those related to the concentration, can actually be expressed in terms of the parameters of the potential curves of excited electron states. The hypothesis advanced earlier by one of us [7], of the decisive role of these same parameters in the anomalous temperature dependence of first order scattering, requires experimental verification. We note that recently published data [8] on the temperature variation of the overtone intensity is not in contradiction with our generalization.

The desirability of the present investigation was pointed out to us by P. P. Shorygin, to whom the authors are extremely grateful.

LITERATURE CITED

[1] M. V. Vol'kenshtein, J. Exptl.-Theoret. Phys. (USSR) 18, 44 (1948); M. V. Vol'kenshtein, M. A. El'iashevich and B. A. Stepanov, Molecular Vibrations 2 (1949), p. 214.

[2] M. V. Chulanovskii, T. G. Meister and E. N. Struzhenskaia, Leningrad State University Bulletin 1955, No. 2, 143.

[3] M. V. Chulanovskii, T. G. Meister and O. V. Sverdlova, Leningrad State University Bulletin 1955, No. 8, 123.

[4] Ia. S. Bobovich and T. P. Tulub, J. Exptl.-Theoret. Phys. (USSR) 30, 189 (1956).

[5] P. P. Shorygin, Doctoral Dissertation (Karpov Physico-Chemical Institute, Moscow, 1949).

[6] Ia. S. Bobovich and D. B. Gurevich, J. Exptl.-Theoret. Phys. (USSR) 27, 319 (1954).

[7] Ia. S. Bobovich, Bull. Acad. Sci. USSR, Phys. Ser. 19, 219 (1955).

[8] A. I. Stekhanov and E. V. Chisler, J. Tech. Phys. (USSR) 25, 2209 (1955).

Received December 10, 1955

DAMPED SCATTERING OF SPINLESS PARTICLES

A. A. Sokolov and B. K. Kerimov

(Presented by Academician N. N. Bogoliubov December 14, 1955)

Continuing the earlier work [1-3] on damped scattering of particles, we obtained [4] a cross section for the scattering of Dirac particles by a fixed δ-like center of force. In the present article we generalize this damping method to the case in which the fixed scattering center possesses spherical symmetry and a small range.

Limiting ourselves here to relativistic spinless scattered particles, we transform the scalar equation which describes their motion to the form

$$\left(-\frac{\hbar}{i}\frac{\partial}{\partial t} - V(r)\right)\psi = \chi, \tag{1}$$

$$\left(-\frac{\hbar}{i}\frac{\partial}{\partial t} - V(r)\right)\chi + c^2\hbar^2\nabla^2\psi - m_0^2c^4\psi = 0, \tag{2}$$

where the potential energy and charge density are, respectively,

$$V(r) = L^{-3}\sum_{\vec{\varkappa}} V(\varkappa)\, e^{-i\vec{\varkappa}\cdot\mathbf{r}}, \tag{3}$$

$$\rho = \frac{1}{2}\left(\chi^+\psi + \psi^+\chi\right). \tag{4}$$

Using this set of equations we obtain a first order differential equation for the coefficients C'' which characterize the probability of finding a particle in a quantized state with momentum $\hbar\mathbf{k}''$. In the absence of the scattering center $(V(r) = 0)$ the solution of the wave equations is

$$\psi = L^{-3/2}\sum_{\mathbf{k}''}\frac{1}{\sqrt{E''}}C'' e^{-icK''t + i\mathbf{k}''\cdot\mathbf{r}}, \quad \chi = L^{-3/2}\sum_{\mathbf{k}''}\sqrt{E''}\, e^{-icK''t + i\mathbf{k}''\cdot\mathbf{r}}C'', \tag{5}$$

where $E'' = c\hbar K'' = c\hbar\sqrt{k''^2 + k_0^2}$ is the energy of the particle, and L^3 is the volume of the elementary parallelepiped.

At the time $t = 0$ when the particle is in the state $\mathbf{k}$:

$$C'' = \delta_{\mathbf{k}\mathbf{k}''}, \tag{6}$$

let the fixed force center be "turned on", establishing the potential $V(r)$. Then the coefficients C'' in (5) will be functions of time which can be obtained from equations which we have by singling out especially the coefficient C that characterizes the initial state:

$$-\frac{1}{ic}\dot{C}' = \frac{1}{c\hbar L^3}\left(V(|\mathbf{k}-\mathbf{k}'|)\,e^{ict\Gamma'}C + \sum_{\mathbf{k}''}{}' V(|\mathbf{k}''-\mathbf{k}'|)\,e^{ict(\Gamma'-\Gamma'')}C''\right);$$

$$-\frac{1}{ic}\dot{C} = \frac{1}{c\hbar L^3}\sum_{\mathbf{k}''}{}' V(|\mathbf{k}''-\mathbf{k}|)\,e^{-ict\Gamma''}C'' + \frac{V(0)}{c\hbar L^3}C. \tag{7}$$

Here $\Gamma' = K' - K$, $V(|\mathbf{k}-\mathbf{k}'|)$ are the Fourier components of the potential (1), $V(0) = V(\kappa)$ for $\kappa \to 0$. Hence it can be seen that (7) does not apply to a Coulomb center (long range force), since in this case (see Equation (18) below) $V(0)$ becomes infinite. We expand $V(|\mathbf{k}-\mathbf{k}'|)$ in a series of Legendre polynomials $P_l(\cos\vartheta')$:

$$V(|\mathbf{k}''-\mathbf{k}'|) = \sum_{l=0}^{\infty} V_l''' = \sum_{l=0}^{\infty} b_l P_l(\cos\vartheta'''), \tag{8}$$

where ϑ is the angle between the vectors $\mathbf{k}'$ and $\mathbf{k}''$. The angles between the vector $\mathbf{k}$ and the vectors $\mathbf{k}'$ and $\mathbf{k}''$ are designated by ϑ' and ϑ'', respectively.

We shall seek the solution of (7) in the form [see also [4], Equation (6)]

$$C = e^{-c\beta_1 t + ict\beta_2}; \tag{9}$$

$$C' = \begin{cases} \dfrac{1}{c\hbar L^3}\,\dfrac{1-e^{-c\beta_1 t + ict(\Gamma'+\beta_2)}}{\Gamma'+\beta_2+i\beta_1}\displaystyle\sum_{l=0}^{\infty}\varepsilon_l V_l' & \text{for } |\Gamma'| < |\Gamma_0|; \\ 0 & \text{for } |\Gamma'| > |\Gamma_0|. \end{cases} \tag{10}$$

Then we have for ϵ_l, β_1 and β_2 the following equations [see also [4], Equations (9) and (10)]:

$$\sum_{l=0}^{\infty}(\varepsilon_l - 1)V_l' = \frac{kK}{8\pi^2 c\hbar i}\sum_{l,l'=0}^{\infty}\varepsilon_{l'}\oint d\Omega'' V_l''' V_{l'}^{*}; \tag{11}$$

$$\beta_1 - i\beta_2 = \frac{kK}{8\pi^2 c^2\hbar^2 L^3}\sum_{l,l'=0}^{\infty}\varepsilon_{l'}\oint d\Omega'' V_l^{*} V_{l'}^{*} + i\,\frac{V(0)}{c\hbar L^3}, \tag{12}$$

where $d\Omega''$ is the solid angle of the vector $\mathbf{k}''$.

We also make use of the equations

$$\oint d\Omega'' V_l''' V_{l'}^{*} = \frac{4\pi b_{l'}}{2l'+1}V_l'\,\delta_{l'l}; \qquad \oint d\Omega'' V_l'' V_{l'}'' = \frac{4\pi b_l b_{l'}}{2l'+1}\,\delta_{l'l}. \tag{13}$$

Then for the total scattering cross section we obtain

$$\sigma = \frac{1}{N}\frac{\partial}{\partial t}\sum_{\mathbf{k}'} C'^{+}C' = \frac{4\pi}{k^2}\sum_{l=0}^{\infty}(2l+1)\sin^2\eta_l, \tag{14}$$

where

$$\sin^2\eta_l = \frac{c_l^2}{1+c_l^2}; \quad \varepsilon_l = \frac{1}{1+ic_l}; \quad c_l = \frac{kK}{2\pi c\hbar}\,\frac{b_l}{2l+1}, \tag{15}$$

and $N = N_0 C^+ C \left(N_0 = \frac{ck}{L^3 K};\ C^+ C = e^{-2c\beta_1 t}\right)$ is the number of particles of momentum $\hbar\mathbf{k}$ which strike a unit surface in unit time.

Determining b_l from (8) we obtain for the phase of partial waves:

$$c_l = \tan\eta_l = -\frac{\pi K}{c\hbar}\int_0^\infty rV(r)\, J^2_{l+1/2}(kr)\, dr, \tag{16}$$

where $J_{l+1/2}$ (kr) is a Bessel function. For $c_l \ll 1$ the phase $\eta_l \cong \tan\eta_l$ agrees with the corresponding expression obtained by a perturbation method ([5], p. 43).

From Equation (12) we obtain

$$c\beta_1 = \frac{\sigma N_0}{2};\quad c\beta_2 = \frac{\sigma N_0}{2}\,\frac{\sum\limits_{l=0}^{\infty}(2l+1)\sin^2\eta_l\tan\eta_l}{\sum\limits_{l=0}^{\infty}(2l+1)\sin^2\eta_l} - \frac{V(0)}{\hbar L^3}. \tag{17}$$

It thus follows that at any given instant of time t

$$\sum_{k'}{}' C'^+ C' + C^+ C = \int_0^t N\sigma\, dt + e^{-\sigma N_0 t} = 1.$$

2. Let us consider the scattering of spinless particles by a Yukawa type of field:

$$V(r) = -g^2\frac{e^{-\varkappa_0 r}}{r},\ \text{i.e.}\ \ V(\varkappa) = -\frac{4\pi g^2}{\varkappa_0^2 + \varkappa^2}. \tag{18}$$

Substituting (18) in (16) we obtain

$$c_l = \tan\eta_l = \gamma Q_l(x), \tag{19}$$

where

$$x = 1 + \frac{\varkappa_0^2}{2k^2},\quad \gamma = \frac{g^2 K}{c\hbar k},$$

and $Q_l(x) = \frac{1}{2}\int\limits_{-1}^{1}\frac{P_l(y)\,dy}{x-y}$ is a second order spherical Legendre function.

By (14) the total cross section is

$$\sigma = \frac{4\pi}{k^2}\sum_{l=0}^{\infty}(2l+1)\frac{\gamma^2 Q_l^2(x)}{1+\gamma^2 Q_l^2(x)}. \tag{19'}$$

For large values of x $(\varkappa_0 \gg k)$ we can assume

$$Q_l(x) \cong \frac{\Gamma(l+1)}{\Gamma(l+{}^3/_2)} \frac{\sqrt{\pi}}{(2x)^{l+1}}. \tag{20}$$

In this case, introducing the notation $\delta^2 = \frac{V^2(0)\,k^2K^2}{4\pi^2c^2\hbar^2}$, we have

$$\sigma = \frac{V^2(0)\,K^2}{\pi c^2\hbar^2}\left(\frac{1}{1+\delta^2} + \frac{4}{3}\,\frac{(k/\varkappa_0)^4}{1+{}^4/_9\,(k/\varkappa_0)^4} + \dots\right). \tag{21}$$

The first term corresponds to $l = 0$, the second to $l = 1$, etc.

Assuming $\varkappa_0^2 \to \infty$ and $V(0) \neq \infty$ we obtain the cross section for scattering by a δ-shaped potential when in the sum of (19') there remains only the first term ($l = 0$), which describes the s-scattering. This scattering was considered by us for Dirac particles in an earlier paper [4].

Using the method described in [6] we may represent the function $Q_l(x)$ for large values of l as

$$\begin{aligned} Q_l(\operatorname{ch}\varphi) &= \sqrt{\frac{\varphi}{\operatorname{sh}\varphi}}\,K_0\left(\left(l+\frac{1}{2}\right)\varphi\right) \quad \text{for} \quad x = \operatorname{ch}\varphi > 1; \\ Q_l(\cos\varphi) &= -\frac{\pi}{2}\sqrt{\frac{\varphi}{\sin\varphi}}\,N_0\left(\left(l+\frac{1}{2}\right)\varphi\right) \quad \text{for} \quad x = \cos\varphi < 1, \end{aligned} \tag{22}$$

where N_0 and K_0 are the familiar cylindrical functions of real and imaginary arguments. This asymptotic representation of $Q_l(x)$ also enables us to determine this function at the points $x = 1 \pm 0$. Then for $x = 1 + 0$ $(\kappa_0 \ll k)$ we find, when we transform the summation over l to an integration over y $(y = l\sqrt{x^2 - 1})$, that the cross section is given by

$$\sigma = \frac{8\pi}{k^2}\,\frac{1}{x^2-1}\int_0^\infty \frac{\gamma^2 y K_0^2(y)\,dy}{1+\gamma^2K_0^2(y)}. \tag{23}$$

It is thus seen that damping can be neglected subject to the inequality

$$\gamma^2K_0^2(y_0) \ll 1, \quad \text{or} \quad \frac{1}{\gamma^2} \gg 3.725, \tag{24}$$

where $y_0 = 0.165$ corresponds to the maximum of $yK_0^2(y)$. The corresponding value of the orbital moment is $l_0 = 0.165/\sqrt{x^2 - 1}$. Then

$$\sigma \to \sigma_0 = 4\pi\left(\frac{g^2}{\hbar c}\right)^2 \frac{K^2}{k^4(x^2-1)}. \tag{25}$$

The last relationship can be obtained by a perturbation method.

In the other limiting case, when $\gamma^2K_0^2(y_0) \gg 1$, damping will play a decisive role. In this case the cross section is

$$\sigma = \pi\left(\frac{z_0}{\varkappa_0}\right)^2, \tag{26}$$

where z_0 is determined from the equation $\frac{z_0}{\pi\gamma^2} e^{z_0} = 1$ or $z_0 \sim \ln \pi\gamma^2$. Then for relatively high energies $K \gg k_0$ the cross section becomes constant and corresponds to scattering from an opaque sphere of radius $R = z_0 / \kappa_0$.

Note added in proof. From Equations (10), (14) and (15) the expression obtained for the differential elastic scattering cross section is

$$\frac{d\sigma}{d\Omega'} = \frac{1}{k^2} \sum_{l,l'} \frac{c_l c_{l'}(1+c_l c_{l'})(2l+1)(2l'+1) P_l(\cos\theta') P_{l'}(\cos\theta')}{(1+c_l^2)(1+c_{l'}^2)}$$

LITERATURE CITED

[1] A. Sokolov, J. Phys. (USSR) 5, 231 (1941).

[2] W. Heitler, Proc. Cambridge Phil. Soc. 37, 291 (1941).

[3] A. H. Wilson, Proc. Cambridge Phil. Soc. 37, 301 (1941).

[4] A. Sokolov and B. Kerimov, Doklady Akad. Nauk SSSR 105, 5 (1955).

[5] N. Mott and H. Massey, Theory of Atomic Collision (For. Lit. Press, 1951) p. 43 (translation).

[6] D. Ivanenko and A. Sokolov, The Classical Theory of Fields (Moscow-Leningrad, 1951), p. 273.

M. V. Lomonosov
Moscow State University

Received December 8, 1955

TWO TYPES OF RARE-EARTH LUMINESCENCE SPECTRA IN SYNTHETIC FLUORITE CRYSTALS

I. V. Stepanov and P. P. Feofilov

(Presented by Academician A. N. Terenin December 6, 1955)

Trivalent rare-earth ions (TR) are known to be good activators of calcium fluoride (CaF_2) phosphors. The similar values of the ionic radii of Ca^{++} (1.04) and TR^{+++} (1.04-0.80) facilitate the isomorphic incorporation of the activator into the CaF_2 lattice, resulting in a high intensity of luminescence and sharpness of emitted lines.

In an investigation of luminescence from synthetic single crystals of CaF_2 activated by rare earths, we observed that the same activator will produce luminescence spectra which differ strongly in the number and location of emitted lines depending on the conditions of growth and heat treatment of the crystal. The existence of two kinds of luminescence from fluorite crystals activated by europium was pointed out by us in an earlier paper [1]. We have now also found two types of spectra in such crystals when activated by praseodymium, samarium, galodinium, terbium, dysprosium, holmium, erbium and thulium, i.e., all available rare earths which possess luminescence line spectra.

Fluorite single crystals were grown by a method developed by one of us (I.V.S.) and similar to Stockbarger's method [2]. In growing the crystals that were used in the present work, we added to the initial batch of pulverized and specially cleaned crystals of natural fluorite, $\sim 10^{-4}$ g/g of fluorides of the respective rare earths. The decisive factors in the determination of the type of luminescence spectrum were the redox conditions under which the samples were produced. In order to establish the strongly reductive conditions required for stable production of crystals possessing a certain luminescence spectrum (type II, which was arbitrarily termed "anomalous" in article [1]), about 10^{-3} g/g of graphite powder was put into mixture. Then certain rare earths (Sm, Eu, Yb) were partially reduced to the divalent state. Crystals which exhibited a different luminescence spectrum (type I, or "normal") were produced by heating grown crystals in an open crucible to a temperature of 900-1000°. In some instances, to produce crystals of type I, it was sufficient to grow them without adding graphite.

A general picture of the luminescence spectra of $CaF_2 \cdot TR$ crystals is given schematically in Fig. 1. The spectra were photographed in a spectrograph with a diffraction grating whose dispersion was about 6.5 A/mm. The spectra are practically independent of the wavelength of exciting light and do not change during damping (the luminescence of the crystals investigated is of phosphoroscopic duration).

As can be seen from Fig. 1, the character of the spectrum of the rare earths – the number and approximate position of the groups of lines – is the same in general but with great differences in detail. The spectra of $CaF_2 \cdot Tb$ are exceptions in which the type II spectrum, while retaining the common characteristics, is displaced by ~ 5800 cm^{-1} towards shorter waves. Fig. 2 shows spectra of the green luminescence lines of crystals activated by erbium and of ultraviolet luminescence in galodinium-activated crystals.

Absorption spectra, and in some instances the excitation regions of luminescence of different types, differ; in the case of specimens possessing centers of both types, this can lead to erroneous conclusions regarding the dependence of the luminescence spectrum on the wavelength of the exciting light. On the other hand, when a crystal has both types of centers, the luminescence spectrum may simultaneously contain lines belonging to the different centers. This occurred, as we have noted [1], in the luminescence spectrum of $CaF_2 \cdot Eu$, reported by Chatterjee [3].

The character of the line spectra of both types and the approximate constancy of the spectral regions containing the lines leave no doubt that in both cases we are dealing with trivalent TR ions. The difference in the spectra is clearly due to the difference in the immediate neighborhood of luminescent TR^{+++} ions and in the local

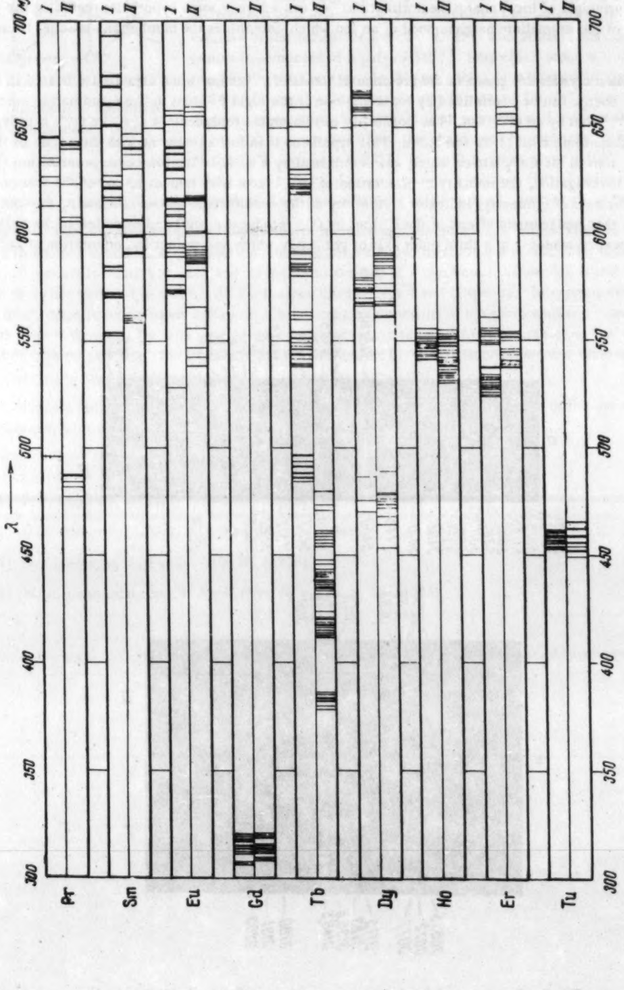

Fig 1. Luminescence spectra of $CaF_2 \cdot TR$

structure of the luminescent centers. In the formation of mixed $CaF_2 \cdot TRF_3$ crystals which represent an isomorphic replacement of Ca^{++} ions by TR^{+++} ions the excess positive charge must be neutralized. If, following Krieger and Runciman [4], we assume that this neutralization takes place in the immediate vicinity of the luminescent ion (principle of local charge neutralization) we can advance some hypotheses regarding the possible configuration of the immediate neighborhood of an ion which determines the number and spectral location of the emitted lines.

Thus, when crystals are grown in the presence of traces of oxygen or when crystals are heated in air (type I spectrum) the charge can be neutralized by replacing one of the eight F^- ions in the coordination sphere which surrounds TR^{+++} ions by an O^{--} ion. The possibility of isomorphic replacement of F^- by O^{--} is provided by the similarity of their ionic radii (1.33 and 1.36). This hypothesis is in full agreement with the nature of the orientation of Eu^{+++} ions in the CaF_2 lattice which was determined by a study of luminescence polarization [1]. As was shown by this investigation, the stability of orientation of Eu^{+++} ions with respect to one of the four possible direction (third order axes of symmetry) indicates asymmetry of the coordination sphere surrounding the ions. It can easily be seen that replacement of one of the F^- ions by O^{--} produces a preferred direction in the neighborhood of the luminescence center – of a third order axis of symmetry which determines the orientation of Eu^{+++} ions (see Fig. 3).

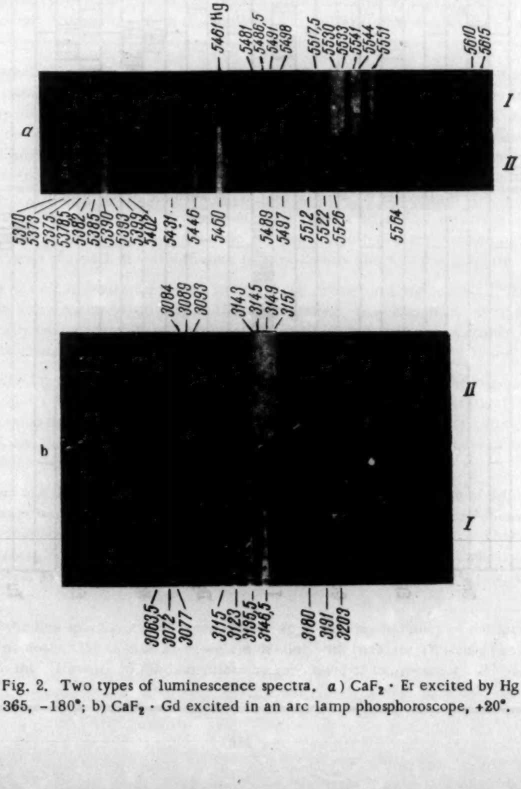

Fig. 2. Two types of luminescence spectra. *a*) $CaF_2 \cdot Er$ excited by Hg 365, –180°; b) $CaF_2 \cdot Gd$ excited in an arc lamp phosphoroscope, +20°.

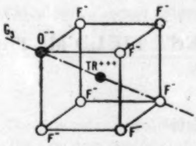

Fig. 3. Hypothetical scheme of a Type I luminescence center

Such charge neutralization evidently occurs in crystals produced in the presence of oxygen and exhibiting type I spectra. At the present time it is impossible to say anything definite regarding the nature of such neutralization for crystals exhibiting type II spectra. It is not impossible that in this case the neutralization is effected by electrons or F^- ions localized in the immediate vicinity of the luminescence center. It is also possible that the luminescence center is composed of a pair of TR^{+++} ions which replace isomorphically two neighboring cation sites. In this case the neutralization of the excess charge can be effected by a cation vacancy (absence of a Ca^{++} ion) in one of the nearest cation sites. When there is an admixture of monovalent cations (such as N^+ with ionic radius 0.98) the charge can be neutralized by replacing one of the Ca^{++} ions near a TR^{+++} ion with a monovalent cation. Each of these possible configurations of a luminescence center must, of course, possess a characteristic luminescence spectrum. Further research is needed to decide which of these possibilities is realized in the present case (type II spectra).

We have also observed alterations of rare-earth luminescence spectra when natural fluorite crystals were annealed in an open crucible, such crystals containing, as we know, more or less of TR. The luminescence of unannealed crystals is relatively weak and its spectrum consists of a number of diffuse bands and relatively wide lines which do not agree in location with the sharper lines of type I and II spectra. In crystals annealed between 600 and 700°, there is considerably enhanced luminescent brightness in which there appear a number of lines identical with type II lines (Er, Dy) and type I lines (Sm). When the temperature is increased to the range of 900-1000° a second change takes place: the spectra of all the rare earths in natural fluorite become identical with type I spectra observed in synthetic fluorite crystals activated by rare earths.

The authors are deeply grateful to M. A. Vasil'eva, who assisted in the growing of the crystals, and to O. V. Sokolova, who assisted in photographing the spectra.

LITERATURE CITED

[1] P. P. Feofilov, Doklady Akad. Nauk SSSR 99, 731 (1954).

[2] D. Stockbarger, J. Opt. Soc. Am. 39, 731 (1949).

[3] N. Chatterjee, Z. Physik 113, 96 (1939).

[4] W. A. Runciman, Brit. J. Appl. Phys. 6, suppl., 4, 78 (1955).

Received November 22, 1955

HIGHER APPROXIMATIONS IN THE SELF-CONSISTENT FIELD METHOD OF MESON THEORY

E. L. Feinberg and D. S. Chernavskii

(Presented by Academician I. E. Tamm December 6, 1955)

In earlier papers [1,2] we proposed and applied to the problem of the deuteron a method of separating the self energy which can be considered a self-consistent field method of meson theory. However, we used only a one-meson approximation. Consideration of the following lines of the Fock column are of interest for the following reasons.

a) We shall show that application of the method of [1,2] to the interaction of two electric charges at rest leads, in the single photon approximation, to a result which differs from Coulomb's law. At a distance of the order of $r \simeq \frac{1}{2\beta}\sqrt[3]{\frac{e^2}{2}}$ the potential is distorted. On the other hand, it is known that this problem has an exact solution (Coulomb's law) which coincides with the classical approximation and with the first approximation of perturbation theory. The question naturally arises: Does Coulomb's law result when all higher approximations are considered? (It will be shown later that this is the case). At the same time, the term which distorts Coulomb's law in the single quantum approximation and disappears with higher orders is the principal term in the deuteron problem and produces stability of the system. It is thus necessary to explain how higher approximations affect the deuteron problem.

We note that a scalar photon field and a neutral scalar meson field are distinguished by the fact that the interaction operators H_k commute with each other for different quantum momenta **k**. This permits a canonical transformation which leads to the classical result. In other fields where $H_{\mathbf{k}}$ contains the operators σ and τ this commutativity is absent. We shall show that for just this reason the role of the later approximations in the method of [1] is essentially different for the Coulomb interaction and for the pseudoscalar meson field; in the first instance the higher approximations play a much more important part.

b) When the succeeding lines are considered, the application of the auxiliary condition is not so simple as in the first approximation. The questions which arise require an answer.

1. Coulomb interaction. Let us consider an electron in a hydrogen atom and let us apply to this case the set of equations in the single quantum approximation which was derived in [1] (assuming that coupling is affected by neutral scalar particles of zero mass, or "photons"):

$$\left\{\frac{\mathbf{p}^2}{2m} + \frac{1}{1+a}\sum_{\mathbf{k}}\frac{1}{2k\Omega}\left[g^2(\mathbf{k})\,k - 2eg(\mathbf{k})\right]\cos\mathbf{kr}\right\}\Psi(\mathbf{r}) = E\Psi(\mathbf{r}),$$
$$g(\mathbf{k}) = e\left[k + \overline{(\cos\mathbf{kr})}^{-1}\,\overline{V(1+\cos\mathbf{kr})}\right]^{-1}, \quad a = \sum_{\mathbf{k}}\frac{1}{2k\Omega}g^2(\mathbf{k})\,\overline{(1+\cos\mathbf{kr})}, \tag{1}$$

where m is now the electron mass, e is the electron charge and $\overline{V}$ is the average interaction energy.

In this case we know that

$$\Psi(\mathbf{r}) = \frac{\beta^{3/2}}{\pi^{1/2}}e^{-\beta r}; \quad \beta = me^2. \tag{2}$$

Calculating average values we easily obtain from (1) and (2)

$$g(\mathbf{k}) = e\left\{k + e^2\beta\left[2 + \left(\frac{k}{2\beta}\right)^2\right]\left[1 + \left(\frac{k}{2\beta}\right)^2\right]\right\}^{-1}. \tag{3}$$

The expression in (3) differs from the value $g(\mathbf{k}) = e/k$ that appears in perturbation theory and is needed to obtain the Coulomb potential, by the second term in the denominator. It is comparable with the first term when $k = 2\beta\,(^1/_2\, e^2)^{-1/3}$ i.e., the potential in (1) deviates from the Coulomb potential at distances $r \sim \frac{1}{2\beta}\left(\frac{1}{2}e^2\right)^{1/3}$.

We now consider the same problem for an infinitely large number of photons. It is convenient to take a functional in the form*

$$\Phi = \frac{1}{\mathfrak{N}}\prod_{k=0}^{\infty}[1 + g(\mathbf{k})\,H_{\mathbf{k}}^{+}]\,\Phi_0. \tag{4}$$

Using this form we obtain an expression for the potential energy of an electron:

$$V(\mathbf{r}) = \sum_{\mathbf{k}} \frac{[g^2(\mathbf{k})\,k - 2eg(\mathbf{k})]\,(1 + \cos \mathbf{kr})}{(1 + g^2(\mathbf{k})\,\langle H_{\mathbf{k}}^{-}H_{\mathbf{k}}^{+}\rangle)\,2k\Omega}. \tag{5}$$

Using the auxiliary condition ($V(\infty) = 0$) and considering that with increase of Ω $g^2(\mathbf{k})\,\langle H_{\mathbf{k}}^{-}H_{\mathbf{k}}^{+}\rangle \to 0$, it is easy to obtain

$$V(\mathbf{r}) = \sum_{\mathbf{k}}[g^2(\mathbf{k})\,k - 2eg(\mathbf{k})]\,\frac{\cos \mathbf{kr}}{2k\Omega}. \tag{6}$$

Varying V with respect to $g(\mathbf{k})$ we obtain: $g(\mathbf{k}) = e/k$, which, unlike (3), agrees completely with perturbation theory and leads to Coulomb's law.

In order to explain how, when we make the transition from the single photon approximation to the many photon approximation the above result is obtained instead of (3), we perform a series expansion of (4) and retain two terms (two-photon approximation):

$$\Phi = \frac{1}{\mathfrak{N}}\Big(1 + \sum_{\mathbf{k}} g(\mathbf{k})\,H_{\mathbf{k}}^{+} + \frac{1}{2}\sum_{\mathbf{k}_1}\sum_{\mathbf{k}_2} g(\mathbf{k}_1)\,g(\mathbf{k}_2)\,H_{\mathbf{k}_1}^{+}H_{\mathbf{k}_2}^{+}\Big)\,\Phi_0,$$
$$\mathfrak{N}^2 = 1 + a + \frac{1}{2}a^2, \quad a = \sum_{\mathbf{k}} g^2(\mathbf{k})\,\frac{1 + \cos \mathbf{kr}}{2k\Omega}. \tag{7}$$

Hence we can see that in the single photon approximation there is the extra factor in (6) $(1 + a)^{-1} \sim 1 + O(e^2)$, while in the two-photon approximation this factor is transformed into $(1 + a)/(1 + a + {}^1/_2\, a^2) \sim 1 + O(e^4)$ (increase of the numerator cancels increase of the denominator); with an increase in the number of photons the deviation from the Coulomb potential is diminished.

2. With noncommuting operators (such as in the case of derivative coupling) the situation is different. Taking Φ in the form of (7) (two-meson approximation) and using the average interaction energy and the auxiliary condition, we obtain an expression which contains terms of the type

---

*We here neglect the correlation of quanta (Hartree approximation). This Φ can only be used if $[H_{\mathbf{k}_i}^{+} H_{\mathbf{k}_j}^{+}] = 0$; in the contrary case it is necessary to indicate the order of the factors.

$$\sum_{\mathbf{k}_1}\sum_{\mathbf{k}_2}\langle H^-_{\mathbf{k}_1}H^-_{\mathbf{k}_2}H^+_{\mathbf{k}_1}H^+_{\mathbf{k}_2}\rangle\, g^2(\mathbf{k}_1)\, g^2(\mathbf{k}_2). \tag{8}$$

The essential fact is that this term is not equal to $\left|\sum_{\mathbf{k}}\langle H^-_{\mathbf{k}}H^+_{\mathbf{k}}\rangle\, g^2(\mathbf{k})\right|^2$, and because of the noncommutativity is always less than the latter. Thus, for derivative coupling

$$\begin{aligned}\sum_{\mathbf{k}_1}\sum_{\mathbf{k}_2}\langle H^-_{\mathbf{k}_1}H^-_{\mathbf{k}_2}H^+_{\mathbf{k}_1}H^+_{\mathbf{k}_2}\rangle\, g^2(\mathbf{k}_1)\, g^2(\mathbf{k}_2) &= \\ = \frac{5}{9}\sum_{\mathbf{k}_1}\langle H^-_{\mathbf{k}_1}H^+_{\mathbf{k}_1}\rangle\, g^2(\mathbf{k}_1)\cdot\sum_{\mathbf{k}_2}\langle H^-_{\mathbf{k}_2}H^+_{\mathbf{k}_2}\rangle\, g^2(\mathbf{k}_2).\end{aligned} \tag{9}$$

Therefore, the term which is added to the numerator from consideration of the two-quantum line is here always smaller than the corresponding term in the denominator (which appears in the one-quantum approximation). There is no complete cancellation of these terms and the denominator always contains a term of the same order as in the one-quantum approximation but with slightly changed numerical coefficients. On this basis it can be said that with vector coupling inclusion of the following lines cannot result in a fundamental qualitative change of the result obtained in the one quantum approximation. Inclusion of three-meson states changes only the coefficient of the term $\sim \alpha$ and affects only the "second order" term ($\alpha^2 \sim f^2$, where f is the coupling constant).

3. Auxiliary condition. The forms of (4) and (7) which we have thus far been considering are satisfactory because of the fact that the self energy term is separated in the form of a common factor; however, these are not the most general forms. In the more general case in (7) the coefficient of the double sum is not $^1/_2$ but a certain variable parameter c.

The expression obtained for the average must be subject to an auxiliary condition. Besides the terms that are independent of distance, the numerator contains terms of the type $\sum_{\mathbf{k}_1} g^2(\mathbf{k}_1)\,\varepsilon_{12}\cos\mathbf{k}_1\mathbf{r}\times$ $\times\sum_{\mathbf{k}_2}[g^2(\mathbf{k}_2)\,\omega_{\mathbf{k}_2}-2fg(\mathbf{k}_2)]\,\varepsilon_{11}$, where $\langle H^-_{\mathbf{k}}H^+_{\mathbf{k}}\rangle=\varepsilon_{11}(\mathbf{k})+\varepsilon_{12}(\mathbf{k})\cos\mathbf{kr}$ (the product of the self force and the interaction). The latter, although they vanish for $r \to \infty$, can make the energy infinite at any finite r. Therefore, the auxiliary condition in the present case must apply not to infinite separation but to any (large compared to the range of the forces) finite distance. Thus, we must have here $\Psi = (1+\delta(r))\exp(-\sqrt{\epsilon M}\,r)$, where $\delta(r) \ll 1$. Substitution in (1) shows that we must have $V(r) \ll \epsilon_D$ when $\alpha r \gg 1$.

In $\overline{V}$ we find terms of the type

$$\sum_{\mathbf{k}_1} g^2(\mathbf{k}_1)\,\varepsilon_{11}(\mathbf{k}_1)\sum[g^2(\mathbf{k}_2)\omega_{\mathbf{k}_2}-2fg(\mathbf{k}_2)]\,\varepsilon_{12}\cos\mathbf{k}_2\mathbf{r},$$

which clearly satisfy the imposed condition, since for sufficiently large r the sum over $\mathbf{k}_2$ is exponentially small and the sum over $\mathbf{k}_1$ cannot result in an infinite value of V since the denominator contains the square of the corresponding term. But, in addition, V contains terms such as

$$\sum_{\mathbf{k}_1} g^2(\mathbf{k}_1)\,\varepsilon_{12}(\mathbf{k}_1)\cos\mathbf{k}_1\mathbf{r}\cdot\sum_{\mathbf{k}_2}[g^2(\mathbf{k}_2)\,\omega_{\mathbf{k}_2}-2fg(\mathbf{k}_2)]\,\varepsilon_{11}(\mathbf{k}_2),$$

which, according to the condition $V(r) \ll \varepsilon_D$ for $\alpha r \gg 1$, cannot be allowed because the sum over $\mathbf{k}_2$, which represents the nucleon self energy, diverges more strongly than the corresponding sums in the denominator and results in infinite V despite the smallness of the sum over $\mathbf{k}_1$. Such terms must be included in the sum which, according to the same condition, must vanish.

4. Evaluation of the two-quantum state in the deuteron problem. The functional was selected to have the form of (7). For the evaluation of V only terms giving the largest numerical contributions were retained. Then

$$V \cong \sqrt{a}\,\frac{1+{}^{5}/_{6}\,a}{1+a+{}^{7}/_{18}a^{2}}\sum fg(\mathbf{k})\,\varepsilon_{12}\cos\mathbf{kr}. \tag{10}$$

This expression differs from the results of the one-meson approximation in which the expression $\sqrt{a}\,(1+a)^{-1}$ stands before the sum. Variation with respect to a gives in the one-meson approximation $a = 1$, $\sqrt{a}\,(1+a)^{-1} = {}^{1}/_{2}$ and in the two-meson approximation $a = 1.3$. The contribution of the two-meson state is small: ${}^{7}/_{18}\,a^2/(1+a+{}^{7}/_{18}\,a^2) \approx 0.2$ The corresponding change of the interaction energy reduces to a change of the coefficient preceding the sum in (10) from 0.5 to 0.66.

Thus, the results obtained in [2] should not be changed qualitatively by inclusion of the two-meson states. However, the stability of the deuteron was obtained in [2] with a very broad minimum of the energy curve where the dependence of the interaction on distance was only a little flatter than for the $\sim 1/r^2$ law.

5. Conclusions. It has been shown that the role of higher approximations in the method of papers [1,2] depends essentially on the commutative properties of the interaction energy operators. When the operators do not contain the matrices σ and τ (Coulomb field) the one-quantum approximation gives an essentially incorrect result (although for small e^2 it is almost correct). When higher approximations are brought in, the usual correct result is obtained. With noncommutating operators H_k the one-meson approximation accounts for the principal peculiarities of the system and the following approximations play a small role.

It has been shown that the auxiliary condition can also be used effectively in the higher approximations.

LITERATURE CITED

[1] E. L. Feinberg and D. S. Chernavskii, Doklady Akad. Nauk SSSR 103, 3 (1955).

[2] E. L. Feinberg and D.S. Chernavskii, Doklady Akad. Nauk SSSR 104, 4 (1955).

P. N. Lebedev Physics Institute
Academy of Sciences of the USSR

Received December 6, 1955

THE LUMINESCENCE SPECTRA OF SOME IODIDES

V. A. Arkhangel'skaia and P. P. Feofilov

(Presented by Academician A. N. Terenin December 15, 1955)

There has recently been considerable interest in the study of the narrow bands observed at very low temperatures in the absorption spectra of some crystalline oxides and salts near the long wave edge of the fundamental absorption band. E. F. Gross et al. [1] and S. Nikitin et al. [2] have observed such bands in the absorption spectra of certain iodides (HI_2, PbI_2 and CdI_2). These writers interpret the bands as being due to excitons.

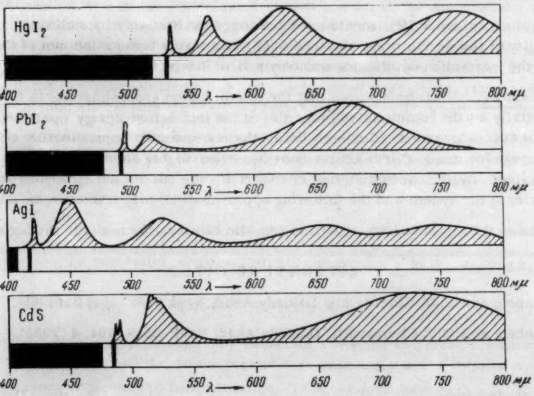

Fig. 1. Absorption and luminescence spectra at the temperature of liquid air (schematic).

We have found similar narrow bands in emission bands while studying the luminescence from cooled iodides of mercury, lead and silver. The present note gives a preliminary description of these spectra.

The samples used were fine crystalline powders precipitated from solutions, and films produced by sublimation or fusing of salts between quartz plates. The emission spectra were photographed with an ISP-51 spectrograph and by a diffraction grating spectrograph whose dispersion was about 6.5 A/mm. The energy distribution in the emission bands was studied with the photoelectric equipment of B. S. Neporent and V. P. Klochkov [3].*

At the temperature of liquid air the luminescence spectra of the salts under investigation consists of a number of bands (see Fig. 1). The separation of the bands increases gradually towards the long wave end of the spectrum, at at the same time the width of the bands also increases.

---

*We take this opportunity to thank B. S. Neporent for putting his apparatus at our disposal.

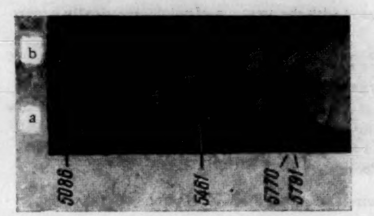

Fig. 2. HgI_2 luminescence spectra with one (a) and two (b) narrow emission bands

The narrow band of the shortest wavelengths is immediately adjacent to the narrow absorption bands described in the papers cited. The relative intensity of the separate bands depends very strongly on the conditions under which the specimen was prepared, on preheating and irradiation, as well as on the intensity of the exciting light. Whereas the intensity of the long wave bands approaches saturation with increased intensity of exciting light, the intensity of the short wave bands increases more rapidly than by a linear law as the exciting intensity rises. As a result the luminescent color changes considerably as the intensity of the exciting light is altered. The independent behavior of the individual emission bands, as well as the difference in the damping kinetics in the individual bands, are evidence of the complex character of the luminescence mechanism in these salts.

1. Mercury iodide (HgI_2, red modification*). The luminescence is red under weak excitation and yellow-green under strong excitation. The luminescence spectrum (Fig. 1) consists of a narrow band with a peak at about 536 mμ and a half width of the order of 3 mμ, and broad bands with peaks at about 565,625 and 760 mμ. Data in [1,2] show a narrow absorption band around 533 mμ. Thus, the shortest-wave luminescence band is shifted in the long-wave direction from the longest-wave absorption band by ~ 3 mμ.

2. Lead iodide (PbI_2). The luminescence spectrum (Fig. 1) consists of a relatively narrow band with its peak at about 497 mμ and half-width of the order of 2 mμ as well as broad bands with peaks at about 515 and 670 mμ. According to [1,2] the narrow absorption band is located around 494.8 mμ, so that the Stokes shift is ~ 2 mμ.

3. Silver iodide (AgI). The luminescence spectrum (Fig. 1) consists of a narrow band (~ 2 mμ) with a peak near 422 mμ and broad bands with peaks around 450, 527, 650 and 750 mμ. There are no data on the narrow absorption bands in [1,2]. According to our data the narrow absorption band of AgI is located at about 419 mμ. The Stokes shift in this instance is around 3 mμ.

The luminescence spectra in Fig. 1 are schematic. As we have mentioned, the relative intensities of individual bands can differ very much and depend on the excitation intensity. In addition, for individual specimens of the salts investigated, we observed additional relatively narrow bands in the short wave portion of the spectrum. Thus for HgI_2 we observed a band whose peak is around 543.5 mμ (see Fig. 2); for PbI_2 there is a band around 503 mμ. Especially marked variations in the number and position of narrow bands, both for luminescence and absorption, were observed in AgI. In some samples, instead of the 422 mμ emission band, there was a band near 428 mμ which is probably associated with the absorption band observed by K. V. Shalimova and N. S. Mendakov [4] and by P. N. Kokhanenko [5]. This band usually had three maxima at around 427, 428 and 430 mμ. Fig. 1 shows only the narrow bands of shortest wavelength observed in the spectra of all samples investigated. At the present time we find it difficult to formulate any opinions regarding the cause of the additional narrow bands. They may possibly be associated with polymorphism of the salts.

The closeness of the narrow luminescence bands which we have observed to the narrow absorption bands described in the literature leaves no doubt, in our opinion, that in this case the transitions which determine the radiation are identical with the transitions which are associated with absorption, i.e., that we are dealing with "resonance" luminescence. The shift of the peaks of absorption and emission bands is of the order of the half width of the bands, as was to be expected.

If the interpretation of the authors of [1,2] is correct the narrow luminescence bands that we observed must be associated with an exciton, i.e., that the radiation results from a change of exciton state. On the other hand, it follows from [6] that the narrow absorption bands are associated with the presence of stoichiometrically excess atoms in the lattice or with foreign metallic atoms.

---

*The yellow modification of HgI_2, which according to [1] does not show narrow absorption bands, possesses a broad emission band in the narrow infrared region.

A similar correspondence of absorption and luminescence spectra is found in cadmium sulfide crystals. Narrow bands in the luminescence spectrum of cooled CdS crystals were observed by Klick [7]. According to E. F. Gross and N. A. Karryev [8] the narrow absorption bands at -200° are around 486.9 and 486.1 mμ. The low temperature luminescence spectrum of a polycrystalline specimen of CdS was observed by us (Fig. 1) to consist of a doublet (487.8 and 490.0 mμ), a wide band (peak around 515-520 mμ) with a clearly defined vibrational structure and a broad structureless band with peak at around 725 mμ.

Therefore the presence of narrow luminescence bands correlated with narrow absorption bands is not an exclusive feature of iodides.

The authors are indebted to B. I. Vainberg and O. V. Sokolova for assistance in the experimental work.

LITERATURE CITED

[1] E. F. Gross and A. A. Kaplianskii, J. Tech. Phys. (USSR) 25, 2061 (1955).

[2] S. Nikitine, M. Sieskind, L. Couture and G. Perny, Comptes rend. 238, 1786 (1954); S. Nikitine and G. Perny, Comptes rend. 240, 64 (1955); S. Nikitine and M. Sieskind, Comptes rend. 240, 1324 (1955); S. Nikitine, Helv. Phys. Acta 38, A 307 (1955).

[3] B. S. Neporent and V. P. Klochkov, Bull. Acad. Sci. USSR, Phys. Ser. 20, 5 (1956).

[4] K. V. Shalimova and N. S. Mendakov, Doklady Akad. Nauk SSSR 82, 575 (1952).

[5] P. N. Kokhanenko, Bull. Acad. Sci. USSR, Phys. Ser. 16, 685 (1951).

[6] P. N. Kokhanenko and V. D. Gol'tsev, Doklady Akad. Nauk SSSR 85, 543 (1952); P. N. Kokhanenko, J. Exptl.-Theoret. Phys. (USSR) 26, 120 (1954).

[7] C. C. Klick, Phys. Rev. 89, 274 (1953).

[8] E. F. Gross and N. A. Karryev, Doklady Akad. Nauk SSSR 84, 471 (1952).

Received December 10, 1955

SMALL ANGLE ELASTIC PROTON-PROTON SCATTERING AT 460, 560 AND 660 MEV

N. P. Bogachev

(Presented by Academician L. A. Artsimovich April 12, 1955)

In experiments on elastic p-p scattering within the energy range 150-350 Mev which were described in the literature to the end of 1952 [1], it was found that the differential cross section of p-p scattering is independent of the scattering angle (for angles from 15° to 90° in the c.m. system) and of the energy.

Experiments on proton-proton scattering at 460 Mev performed in 1952 [2] showed that at this energy the differential cross section increases at smaller angles. In later experiments [3-5] at 437,428 and 419 Mev it was established that the departure from isotropy of angular distribution of protons elastically scattered by protons begins at 400-420 Mev. The differential cross section for p-p scattering at 90° in the energy range where the angular distribution is isotropic, is considerably larger than the largest possible contribution of the $^1S_0$ state. This fact suggests [6] that in addition to the $^1S_0$ state the $^3P_0$ state participates in the scattering and also leads to the isotropy, and that, consequently, the maximum contribution to the cross section of both states is $2\lambda^2$ cm^2 sterad^{-1}. At energies close to 400 Mev the differential cross section of p-p scattering at 90° almost reaches $2\lambda^2$, which indicates that the phases of the $^1S_0$ and $^3P_0$ waves are close to $\pi/2$.

In experiments on p-p scattering at 560 and 660 Mev [7,8] a pronounced departure from isotropy was observed with energy dependence of the scattering differential cross sections. These results were confirmed in other articles [9-11].

Earlier measurements of differential cross sections of p-p scattering at 460, 560 and 660 Mev were obtained for angles from 20-30° to 90° in the c.m. system. The present article presents results for elastic proton-proton scattering at 460, 560 and 660 Mev for small angles. The experimental work was performed on the synchrocyclotron of the Institute for Nuclear Problems of the Academy of Sciences of the USSR. An extracted unpolarized proton beam passed through a system of collimators and impinged on a liquid hydrogen target. The scattered protons were recorded by a telescope of scintillation counters. The charged products of inelastic p-p collisions (π^+-mesons, protons and deuterons) were separated by filters from the elastically scattered protons.

The energy of protons in the beam as measured by the emission angle of Cerenkov radiation from the protons was 657 ± 2 Mev; the inhomogeneity of the beam did not exceed ±8 Mev [12]. Protons with energies of 460 and 560 Mev were obtained by slowing down the beam in polyethylene absorbers. The extraction of the beam from the accelerator through the excitation of radial oscillations [13] enabled us to obtain a quite high proton beam intensity, which considerably facilitated the performance of these experiments at 460 and 560 Mev. As a monitor we used a helium-filled ionization chamber. The target was a metal Dewar filled with liquid hydrogen [14]. The telescope consisted of three scintillation counters with tolane crystals. Measurements were carried to 5° in the c.m. system (~ 2.2° in the laboratory system). Absolute values of the differential cross sections were determined by normalization of the measured relative cross sections with respect to the cross section at 20 or 30° according to the data in [2,7,8]. Table 1 shows the differential cross sections for p-p scattering obtained in the present experiments.

p-p scattering cross sections at 650 Mev and at angles from 10 to 90° were also measured on the Birmingham accelerator with a diffusion chamber [11]. Taking into consideration the relatively meager data, as well as the character of the energy distribution of the proton beam used in the experiments [11], it can be said that the results obtained by us and in [7] are in satisfactory agreement with the results obtained at Birmingham.

TABLE 1

Small angle differential cross sections of p-p scattering $d\sigma(\theta)/d\omega$ at 460, 560 and 660 Mev (in units 10^{-27} cm^2 sterad^{-1})

Angle σ of scattering in center of mass system in degrees	Energy in the laboratory system, in Mev		
	460	560	660
5	33±6	26±5	18.9±1.1
10	5.91±0.46	8.04±0.78	11.0±0.7
15	4.69±0.38	6.78±0.63	8.67±0.53
20		6.29±0.58	7.75±0.48
25		5.70±0.53	6.56±0.40

TABLE 2

Total cross sections of elastic and inelastic processes for p-p interaction (in units 10^{-27} cm^2)

Energy in Mev	$\sigma_{pp}^{\text{total}}$ -	$\sigma_{pp}^{\text{elastic}}$	$\sigma_{pp}^{\text{inelastic}}$	$\sigma_{pp \rightarrow np\pi^+}$
460	27.6±0.4	24.0±0.6	3.6±0.7	1.8±0.7
560	34±0.5	25,2±0.8	8.8±0.9	5.0±0.9
660	41.4±0.6	24.7±1.0	16.7±1.2	10.0±1.2

The present results enable us in the region investigated to improve the data of [15,16] on the ratio of the total cross sections of elastic and inelastic processes in the p-p interaction, and increase our knowledge concerning the total cross section of the interaction $p + p \rightarrow n + p + \pi^+$. The total cross sections of the various processes that take place in the p-p interaction are shown in Table 2.

The total p-p cross sections at 460 and 660 Mev which are shown in Table 2 were measured in [16]. For 560 Mev the total cross section was obtained by interpolation of data in the same paper for 540 and 580 Mev. The total cross sections of elastic proton-proton scattering at 460 and 660 Mev were obtained by integration of the differential cross sections measured in [2,7] and in the present work. $\sigma_{pp}^{\text{elastic}}$ at 560 Mev was obtained by integrating the cross sections in [8,9] and in the experiments described. In the integration the differential cross sections at 5° in the c.m. system were neglected, since at this angle Coulomb scattering is strongest and interferes most strongly with nuclear scattering; the function $\sin\,\theta \dfrac{d\sigma(\theta)}{d\omega}$ for angles from 0 to 10° in the c.m. system was extrapolated to zero linearly.

It can be seen from the table that the total cross section of elastic proton-proton scattering for the energy range 460-660 Mev is constant within the limits of experimental error. All presently available data on high energy proton-proton scattering indicate that the total elastic p-p scattering cross section is constant from 150 to 660 Mev within the limits of experimental error and is diminished somewhat when the energy is increased to 800-1000 Mev.

From the constancy of the total cross section of elastic p-p scattering at 150-660 Mev it follows that the increased total cross section of the p-p interaction [16,17] at 460-660 Mev is due only to meson production processes. The contribution of inelastic processes to the total p-p interaction cross section is 13% at 460 Mev, 26% at 560 Mev and 40% at 660 Mev. These data together with information concerning the total cross sections of the reactions $p + p \rightarrow d + \pi^+$ and $p + p \rightarrow p + p + \pi^0$ make it possible to estimate the total cross section of $p + p \rightarrow n + p + \pi^+$ (if we disregard the simultaneous production of two mesons which is possible at 660 Mev). The corresponding values are also given in Table 2. Data on $p + p \rightarrow d + \pi^+$ were taken from [18,19], and for $p + p \rightarrow p + p + \pi^0$ from [20]. The total cross section of $p + p \rightarrow n + p + \pi^+$ increases by a factor of about 6 as the energy is increased from 460 to 660 Mev. The total cross section of this reaction at 660 Mev is in good agreement with direct measurements given in [21].

In conclusion the author takes this opportunity to acknowledge his indebtedness to M. G. Meshcheriakov, Corresponding Member of the Academy of Sciences of the USSR, for directing this work.

LITERATURE CITED

[1] O. Chamberlain, E. Segre and C. Wiegand, Phys. Rev. 83, 923 (1951); O. Towler, Phys. Rev. 84, 1262 (1951); J. Cassels, T. Pickavance and G. Stafford, Proc. Roy. Soc. (London) 214A, 262 (1952); C. Oxley and R. Schamberger, Phys. Rev. 85, 416 (1952).

[2] M. G. Meshcheriakov, N. P. Bogachev, B. S. Neganov and E. V. Piskarev, Doklady Akad. Nauk SSSR 99, 955 (1954).

[3] R. B. Sutton, T. H. Fields, et al., Phys. Rev. 97, 783 (1955).

[4] A. J. Hartzler and R. T. Siegel, Phys. Rev. 95, 185 (1954).

[5] J. Marshall, L. Marshall and V. A. Nedzel, Phys. Rev. 93, 927 (1954); 98, 1513 (1955).

[6] L. D. Landau, Address at Conference on High Energy Particles (1953); L. D. Landau and Ia. A. Smorodinskii, Lectures on Nuclear Theory (Moscow, 1955).

[7] N. P. Bogachev and I. K. Vzorov, Report Inst. for Nuclear Problems (Acad. Sci. USSR April, 1954); Doklady Akad. Nauk SSSR 99, 931 (1954).

[8] M. G. Meshcheriakov, B. S. Neganov, L. M. Soroko and I. K. Vzorov, Doklady Akad. Nauk SSSR 99, 959 (1954).

[9] S. Ia. Nikitin, Ia. M. Selektor, E. G. Bogomolov and S. M. Zombkovskii, Bull. Acad. Sci. USSR, Phys. Ser. 19, 561 (1955); Doklady Akad. Nauk SSSR 99, 967 (1954).

[10] L. W. Smith, A. W. McReynolds and G. Snow, Phys. Rev. 97, 1186 (1955).

[11] L. Riddiford, Proc. Roy. Soc. (London) (in press).

[12] V. P. Zrelov, Report Inst. for Nuclear Problems (Acad. Sci. USSR, 1954).

[13] V. P. Dmitrievskii, V. I. Danilov, et al., Report Inst. for Nuclear Problems (Acad. Sci. USSR, 1955).

[14] V. M. Sidorov, N. I. Frolov, I. Kh. Nozdrin and N. M. Kovaleva, Report Inst. for Nuclear Problems (Acad. Sci. USSR, 1952).

[15] M. G. Meshcheriakov, N. P. Bogachev and B. S. Neganov, Bull. Acad. Sci. USSR, Phys. Ser. 19, 548 (1955).

[16] V. P. Dzhelepov, V. I. Moskalev and S. V. Medved', Doklady Akad. Nauk SSSR 104, 382 (1955).

[17] A. M. Shapiro, C. P. Leavitt and F. F. Chen, Phys. Rev. 95, 663 (1954).

[18] M G. Meshcheriakov, B. S. Neganov, N. P. Bogachev and V. M. Sidorov, Doklady Akad. Nauk SSSR 100, 673 (1955).

[19] M. G. Meshcheriakov and B. S. Neganov, Doklady Akad. Nauk SSSR 100, 677 (1955).

[20] Iu. D. Prokoshkin and A. A. Tiapkin, Report Inst. for Nuclear Problems, (Acad. Sci. USSR, 1955).

[21] V. M. Sidorov, J. Exptl.-Theoret. Phys. (USSR) 31, 8 (2) (1956).

Institute for Nuclear Problems
Academy of Sciences of the USSR

Received March 9, 1956

THE LARGE COSMIC RAY BURST OF FEBRUARY 23, 1956 AS OBSERVED AT MOSCOW, SVERDLOVSK, TBILISI AND CAPE SCHMIDT

L. I. Dorman, N. S. Kaminer, V. K. Koiava and B. F. Shvartsman

(Presented by Academician D. V. Skobel'tsyn April 2, 1956)

The latest and strongest increase of cosmic ray intensity, which occurred on February 23, 1956, was observed in the USSR at several widely separated continuously operating cosmic ray stations (see Table 1).

In Moscow the burst was recorded on February 23, 1956 at 3 hr 40 min universal time (6 hr 10 min local solar time). Measurements were made with two independent but closely situated spherical ionization chambers [1] screened by 12 cm of lead. The volumes of these chambers were 950 and 50 liters, respectively.

TABLE 1

Station	Geomagnetic latitude	Geographical longitude	Height above sea level, meters	Ceiling (g/cm^2)
Moscow. . . .	52.0° N	37.3° E	203	20
Sverdlovsk . .	48.5° N	61.0° E	290	40
Tbilisi	37.1° N	44.7° E	404	20
Cape Schmidt	63° N	179.5° W	6	20

A relatively slow rise of cosmic ray intensity $I_{(1)}$ began in the large chamber at 3 hr 38 min and in 2 min amounted to 2%. By 3 hr 43 min $I_{(1)}$ increased to 13%. At 3 hr 45 min the cosmic ray intensity exceeded the normal level by not less than 200%.

For $I_{(2)}$ (in the small chamber) the increase at the same moment was approximately 180%. The results of the measurements can be seen in Fig. 1, I in a semilogarithmic plot. The curves of $I_{(1)}$ and $I_{(2)}$ in this scale are nearly straight lines, which indicates the exponential character of the rise in intensity. The rise followed an exp t/0.02 law, which is considerably more rapid than at the time of the last large solar burst on November 19, 1949, when the rise followed an exp t/0.07 law, where t is the time from the beginning of the burst in hours [2]. The return to normal cosmic ray intensity also proceeded more rapidly. At first the intensity changed by an exp −t/0.45 law, and toward the end of the burst, after 8 hours, by an exp −t/2.2 law.*

The cosmic ray burst can be followed until 12 hr universal time, i.e., for 8.5 hr after the usual fluctuations of intensity around the mean value for Moscow.

The minimum possible values of cosmic ray intensity near the peak are shown by the dotted curve A according to which the intensity at the maximum was not less than 200%. Curve B indicates the most probable extrapolation, by which the intensity reached 400% at the peak.

At Sverdlovsk, where a 50 liter chamber screened with 12 cm Pb was used, a similar rise was observed. The conditions here were more favorable because of the less sensitive instrument. The rise at Sverdlovsk also began at 3 hr 40 min universal time (7 hr 44 min local time) and in a few minutes reached not less than 300% (the extrapolated most probable value was around 500%, see Fig. 1, II).

---

*On November 19, 1949 the return to the normal level followed an exp −t/3 law [2].

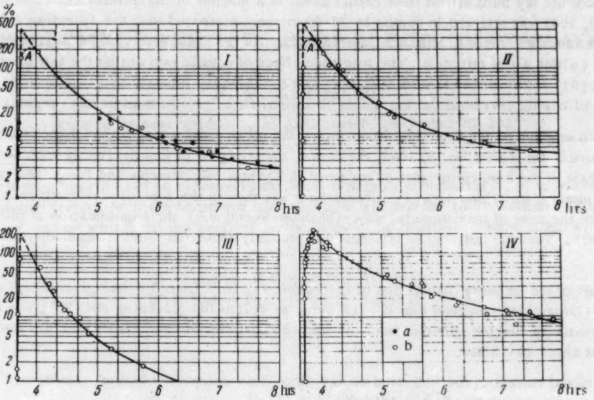

Fig. 1. Intensity changes of the hard cosmic ray component during the burst of February 23, 1956. I) at Moscow; II) at Sverdlovsk; III) at Tbilisi; IV) at Cape Schmidt a) large chamber; b) small chamber. Universal time.

At Tbilisi at 3 hr 40 min (6 hr 40 min local time), with the same kind of instrument a rise was observed of not less than 80% (the extrapolated most probable value was around 200%, see Fig. 1, III).

At Cape Schmidt the burst was recorded with a small ionization chamber (volume 50 liters) screened with 12 cm Pb. The rise began at 3 hr 42 min universal time (15 hr 34 min local time) and within 10 min reached 200%. A gradual decline continued for 8 hours. Unlike the experimental data of other stations, it was possible here to follow the intensity changes very close to the peak (see Fig. 1, IV).

It follows from the graphs that the actual change of intensity near the peak at Moscow, Sverdlovsk and Tbilisi is probably close to the extrapolated values B.

The burst was also observed at Yakutsk [3], where ionization chambers showed a rise of about 200%.

It is well known that previously observed solar bursts of cosmic rays were accompanied by an interruption of short wave radio communications in the illuminated portion of the earth associated with an increase of ultraviolet radiation. The same occurred during the last cosmic ray burst. Cosmic ray bursts have also been accompanied by huge solar flares (3+ by the accepted international scale) which began somewhat earlier than the cosmic ray burst (from 15 min to 1 hr). Therefore, although we have no information as yet regarding such powerful eruptions on February 23, we can assume that they probably occurred beginning at about 3 hr 30 min universal time (judging from the time when radio communication began to fail). A chromospheric eruption could have taken place on the northwest edge of the visible portion of the solar disk, where at that time there was an exceedingly active region with a large number of spots and flocculi, with frequent relatively small flares and with an intensified yellow coronal line.*

---

*Note added in proof. According to a communication from the Tokyo Observatory, on February 23, 1956 there actually was a powerful (3+ on the international scale) chromospheric eruption which began at 3 hr 31 min and reached its peak at 3 hr 42 min universal time. The eruption took place on the northwest edge of the solar disk (22.5° N; 73° W).

The last cosmic ray burst differs from earlier bursts in a number of characteristics. In particular, the burst of November 19, 1949 was retarded in Europe by 30-60 minutes compared with the American continent [4], but in the present instance a number of widely separated stations of the USSR observed the intensity increase almost simultaneously (within a few minutes). The longitude effect of cosmic rays during the last burst is clearly in agreement with [5]. From this latter work it follows that the intensity increase in a certain zone* due to an additional stream of cosmic rays from the sun should be several times greater than in other regions.

We wish to emphasize one more important fact: the much greater magnitude of the last burst compared with previous bursts. On November 19, 1949, the date of the strongest of four previously recorded cosmic ray bursts, the increase of the hard component at sea level in Yakutsk [6], Moscow and Europe did not exceed 20%, while at Cheltenham it was about 40% [4]. Cheltenham was then in the zone of maximum increase [5]. On February 23, 1956 in the zone of maximum increase (Moscow-Sverdlovsk) the augmentation of the hard component reached 400-500%. Thus the last cosmic ray burst was probably about ten times stronger than the burst of November 19, 1949.

An analysis of the intensity distribution of the cosmic ray burst from the data given above and from the data of I. K. Barton (Jamaica)** suggests that the last burst, as well as the preceding one [2,7], was caused by an extra current of positively charged particles from the sun with particles of energies above 5 Bev and probably not containing particles above 10-15 Bev.

This additional current in the indicated energy range must exceed the normal unperturbed cosmic ray flux outside the limits of the Earth by about 100 times.

The cosmic ray flux increased with extreme rapidity and was almost instantaneous. Its decline was more gradual by almost an exponential law.

At present, using the method of coupling coefficients between the primary and secondary types, we are carrying out a detailed analysis of the data. This should enable us to determine the energy spectrum and structure of the additional cosmic ray current at a distance from the Earth, its time variation and the direction of approach of the particles which produced the burst. This analysis, for which important data will be obtained from all other stations of the world which record the various cosmic ray components, is necessary for an understanding of the mechanism which accelerates charged particles up to energies of the order of 10 Bev, of the mechanism of their emission from the sun and of their interaction with interplanetary magnetic fields and the magnetic field of the Earth.

LITERATURE CITED

[1] Iu. G. Shafer, A Precise Cosmic Ray Recorder, Dissertation (Phys. Inst. Acad. Sci. USSR, 1950).

[2] L. I. Dorman, On the Nature of Cosmic Ray Types, Dissertation (Terrestrial Magnetism Research Inst., Phys. Inst. Acad. Sci. USSR, 1955).

[3] A. I. Kuz'min, G. V. Skrypin, G. V. Tianutova and Iu. G. Shafer, Doklady Akad. Nauk SSSR 108, 66 (1956)[Soviet Physics - "Doklady", p. 263].

[4] G. Eliot, Cosmic Ray Physics I (For. Lit. Press, 1954), p. 359 (translation).

[5] J. Firor, Phys. Rev. 94, 1017 (1954).

[6] D. D. Krasil'nikov, A. I. Kuz'min and Iu. G. Shafer, Trans. Yakutsk Branch, Acad. Sci. USSR, Phys. Ser. 1, 42 (1955).

[7] L. I. Dorman, Bull. Acad. Sci. USSR, Phys. Ser. 20, 24 (1956).

Terrestrial Magnetism Research Institute, Sverdlovsk Geophysical Observatory
Tbilisi Cosmic Ray Station, Cape Schmidt Cosmic Ray Station

Received March 27, 1955

---

*During the burst of November 19, 1949 this was the zone from Cheltenham to Climax (USA); during the last burst it was the zone from Moscow to Sverdlovsk.

**A private communication from Professor I.K. Barton to Professor S. N. Vernov; we tak this opportunity to thank Professor Barton.

SOME PROBLEMS OF THE THEORY OF ELECTRON BEAM FOCUSING

P. P. Kas'iankov

(Presented by Academician L. A. Artsimovich, December 22, 1955)

1. The trajectory equations of an electron in the local system of coordinates s, p, q, where the axis s is the so-called principal trajectory of the beam and the axes p, q are parallel to the normal and binormal of the principal trajectory, can be written for the paraxial region, neglecting relativistic corrections, as follows:

$$\begin{aligned} p'' + a_0 p' - b_0 q' + a_1 p + a_2 q = 0, \\ q'' + a_0 q' + b_0 p' + b_1 p + b_2 q = 0, \end{aligned} \qquad (1)$$

where

$$a_0 = \frac{\Phi'}{2\Phi}, \quad b_0 = \frac{1}{2\Phi}\left(4\varkappa\Phi + \alpha\sqrt{\Phi}\Psi'\right); \qquad (2)$$

$$\begin{aligned} a_1 &= \frac{1}{2\Phi}\Big[2k\varphi_2 - \varphi_{22} + 2\left(k^2 - \varkappa^2\right)\Phi + \alpha\sqrt{\Phi}\Big(\psi_{23} + \frac{\varphi_2}{2\Phi}\psi_3 - \varkappa\Psi'\Big)\Big], \\ a_2 &= \frac{1}{2\Phi}\Big[2k\varphi_3 - 2\varkappa'\Phi - \varkappa\Phi' - \varphi_{23} + \alpha\sqrt{\Phi}\Big(\psi_{33} + \frac{\varphi_3}{2\Phi}\psi_3\Big)\Big], \\ b_1 &= \frac{1}{2\Phi}\Big[2\varkappa'\Phi + \varkappa\Phi' - \varphi_{23} - \alpha\sqrt{\Phi}\Big(\psi_{22} + \frac{\varphi_2}{2\Phi}\psi_2\Big)\Big], \\ b_2 &= \frac{1}{2\Phi}\Big[-2\varkappa^2\Phi - \varphi_{33} - \alpha\sqrt{\Phi}\Big(\psi_{23} + \frac{\varphi_3}{2\Phi}\psi_2 + \varkappa\Psi'\Big)\Big]; \end{aligned} \qquad (3)$$

φ (s, p, q) and ψ (s, p, q) are the electrostatic and magnetic scalar potentials; $\Phi = \Phi(s)$ and $\Psi = \Psi(s)$ are the values on the axis; φ and ψ with primes are the values of the partial derivatives of the potentials on the s-axis, with the subscript 2 denoting differentiation with respect to p and the subscript 3 denoting differentiation with respect to q; k, $\varkappa$ are the curvature and torsion of the s-axis;

$$\alpha = \sqrt{-2e/m}; \qquad (4)$$

e, m are the electron charge and mass. A prime denotes differentiation with respect to s.

The equations of (1) agree with those of G. A. Grinberg [1] except for the notation and some unimportant transformations.

2. By means of the substitution

$$\begin{aligned} p = \Phi^{-1/4}(x\cos\chi - y\sin\chi), \\ q = \Phi^{-1/4}(x\sin\chi + y\cos\chi), \end{aligned} \qquad (5)$$

where

$$\chi = -\frac{1}{2}\int_0^s b_0 ds, \tag{6}$$

(1) is replaced by the equivalent set of equations

$$\begin{aligned} x'' &= a_{11}x + a_{12}y, \\ y'' &= a_{21}x + a_{22}y. \end{aligned} \tag{7}$$

The coefficients of these equations are determined by

$$\begin{aligned} a_{11} &= -(a_2 + b_1)\sin\chi\cos\chi - b_2\sin^2\chi - a_1\cos^2\chi + \frac{\Phi''}{4\Phi} - \frac{3}{16}\frac{\Phi'^2}{\Phi^2} - \frac{1}{4}b_0^2, \\ a_{12} &= (a_1 - b_2)\sin\chi\cos\chi + b_1\sin^2\chi - a_2\cos^2\chi - \frac{1}{2}b_0' - \frac{b_0\Phi'}{4\Phi}, \\ a_{21} &= (a_1 - b_2)\sin\chi\cos\chi + a_2\sin^2\chi - b_1\cos^2\chi + \frac{1}{2}b_0' + \frac{b_0\Phi'}{4\Phi}, \\ a_{22} &= (a_2 + b_1)\sin\chi\cos\chi - a_1\sin^2\chi - b_2\cos^2\chi + \frac{\Phi''}{4\Phi} - \frac{3}{16}\frac{\Phi'^2}{\Phi^2} - \frac{1}{4}b_0^2. \end{aligned} \tag{8}$$

(7) is symmetric, that is, $a_{12} = a_{21}$.

3. When the s-axis is a straight line and the field is symmetric with respect to it, (7) can be replaced by

$$R'' + TR = 0, \tag{9}$$

where

$$T = \frac{3}{16}\frac{\Phi'^2}{\Phi^2} + \frac{(-e)}{8m\Phi}\Psi'^2.$$

We obtain sufficient conditions for the existence of a point (a, b) conjugate with $s = a$ by requiring that the limiting case

$$-R'' - TR = \lambda R, \quad R(a) = R(b) = 0 \tag{10}$$

have a non-positive first eigenvalue. From the extremal theory of eigenvalues we obtain a sufficient condition for T in the form

$$\int_a^b (R'^2 - TR^2)\, ds \leqslant 0, \tag{11}$$

where $R = R(s)$ is a doubly continuous differentiable function which vanishes for $s = a$, $s = b$. In particular, taking $R = (s - a)^m (b - s)^n$ ($m, n > 0$ are whole numbers), we obtain:

$$\int_a^b (s-a)^{2m}(b-s)^{2n}\, T(s)\, ds \geqslant \frac{mn}{2m+2n-1}\,\frac{(2m-2)!\,(2n-2)!}{(2m+2n-3)!}\,(b-a)^{2m+2n-1}. \tag{12}$$

Such conditions for the existence of conjugate points in the interval $[a, b]$ are obtained for (7) [or (1)] by utilizing certain results obtained by Bliss and Schoenberg [2].

Using the designation

$$2\Omega(s, x, y, x', y') = x'^2 + y'^2 + a_{11}x^2 + 2a_{12}xy + a_{22}y^2, \tag{13}$$

a sufficient condition for the existence of conjugate points in $[a, b]$ for (7) will be the inequality

$$\int_a^b 2\Omega(s, x, y, x', y')\,ds \leqslant 0, \tag{14}$$

where $x = x(s)$ and $y = y(s)$ are doubly continuous differentiable functions that vanish for $s = a$, $s = b$.

A comparison of (7) with a set of equations of this form, but with constant coefficients a_{11}^0, $a_{12}^0 = a_{21}^0$, a_{22}^0 for which a and b are conjugate points, gives conditions for the existence of conjugate points in $[a, b]$ for (7):

$$a_{11}^0 \geqslant a_{11}, \quad (a_{11}^0 - a_{11})(a_{22}^0 - a_{22}) - (a_{12}^0 - a_{12})^2 \geqslant 0. \tag{15}$$

4. We shall use X to designate the matrix of the set of fundamental solutions for (7):

$$X = \begin{Vmatrix} x_1 & x_2 & x_3 & x_4 \\ y_1 & y_2 & y_3 & y_4 \\ x_1' & x_2' & x_3' & x_4' \\ y_1' & y_2' & y_3' & y_4' \end{Vmatrix}, \quad X\big|_{s=a} = \begin{Vmatrix} 1 & 0 & 0 & 0 \\ 0 & 1 & 0 & 0 \\ 0 & 0 & 1 & 0 \\ 0 & 0 & 0 & 1 \end{Vmatrix}. \tag{16}$$

Lemma 1. In order that a stigmatic image be similar to the object it is necessary and sufficient that the following conditions be satisfied:

$$x_1(b) = \pm y_2(b), \quad y_1(b) = \mp x_2(b). \tag{17}$$

Lemma 2. The elements of the matrix X are related to the elements X_{ik} of the associated matrix by

$$\| X_{ik} \| = \begin{Vmatrix} x_3' & x_4' & -x_1' & -x_2' \\ y_3' & y_4' & -y_1' & -y_2' \\ -x_3 & -x_4 & x_1 & x_2 \\ -y_3 & -y_4 & y_1 & y_2 \end{Vmatrix} \tag{18}$$

Theorem. In order that a stigmatic image be similar to the object it is necessary and sufficient that the following conditions be satisfied:

$$x_4'(b) = \pm y_3'(b), \quad y_4'(b) = \mp x_3'(b) \tag{19}$$

(similarity conditions).

5. The coordinate line p of the plane $s = a$ is represented by a straight line in the plane $s = b$. We shall denote by M_1 the magnification of this image. For the coordinate line q of the plane $s = a$ the magnification of the image will be denoted by M_2. When the image is similar to the object $M_1 = M_2 = M$. For these quantities we have the equations:

$$M_1 = \left(\frac{\Phi_a}{\Phi_b}\right)^{1/4} \frac{\sqrt{x_4'^2(b) + y_4'^2(b)}}{\pm [x_3'(b)\, y_4'(b) - x_4'(b)\, y_3'(b)]}; \tag{20}$$

$$M_2 = \left(\frac{\Phi_a}{\Phi_b}\right)^{1/4} \frac{\sqrt{x_3'^2(b) + y_3'^2(b)}}{\pm [x_3'(b)\, y_4'(b) - x_4'(b)\, y_3'(b)]}; \tag{21}$$

$$M = \left(\frac{\Phi_a}{\Phi_b}\right)^{1/4} \frac{1}{\sqrt{\pm [x_3'(b)\, y_4'(b) - x_4'(b)\, y_3'(b)]}}. \tag{22}$$

6. The conditions under which the electromagnetic field produces an image of the plane $s = a$ in the plane $s = b$ in which the image is similar to the object with a previously given similarity factor, are determined by the properties of only two solutions (x_3, y_3) and (x_4, y_4) of the fundamental matrix.

In order to obtain a solution of the direct problem of calculating the field possessing given focusing properties in the paraxial region, we determine the functions x_3, y_3, x_4, y_4 such as to satisfy (19) and the conditions

$$x_3 y_4 - x_4 y_3 \neq 0 \quad (a < s < b); \tag{23}$$

$$x_3'' x_4 - x_4'' x_3 + y_3'' y_4 - y_4'' y_3 = 0 \quad (a \leqslant s \leqslant b); \tag{24}$$

$$x_i(a) = x_i(b) = y_i(a) = y_i(b) = 0 \quad (i = 3.\ 4) \tag{25}$$

and such that they are analytic functions for $a \leq s \leq b$ without zeros in this interval except at the boundaries. A set of such functions can be determined in the same way as has been done for Equation (9) [3], for example. Under these conditions the set of equations

$$\begin{aligned} x_i a_{11} + y_i a_{12} &= x_i'', \\ x_i a_{12} + y_i a_{22} &= y_i'' \end{aligned} \qquad (i = 3, 4) \tag{26}$$

determines the quantities a_{11}, a_{12}, a_{22} uniquely.

There exist innumerable fields which satisfy the conditions of the direct problem including purely electrostatic as well as purely magnetic fields. In a purely electrostatic field, in order to determine $\Phi = \Phi(s)$ we have

$$\frac{3}{8} \frac{\Phi'^2}{\Phi^2} = -2k^2 - a_{11} - a_{22}; \tag{27}$$

in a purely magnetic field we have for $\Psi = \Psi(s)$

$$\frac{e}{4m} \frac{\Psi'^2}{\Phi} = -k^2 - a_{11} - a_{22}. \tag{28}$$

We note that the direct problem is of the same type as that examined by N. P. Erugin [4].

LITERATURE CITED

[1] G. A. Grinberg, Doklady Akad. Nauk SSSR 38, 2-3, 89 (1943).

[2] G. A. Bliss, and J. I. Schoenberg, Am. J. Math. 53, 780 (1931).

[3] P. P. Kas'iankov, J. Tech. Phys. (USSR) 23, 3, 531 (1953).

[4] N. P. Erugin, Applied Mathematics and Mechanics (USSR) 16, 6, 659 (1952).

V. I. Ul'ianov-Lenin
Leningrad Electrotechnical Institute

Received December 22, 1955

NEUTRON EMISSION FROM A SHORT-LIVED RADON ACTIVE DEPOSIT

A. V. Kogan

(Presented by Academician A. F. Ioffe, December 28, 1955)

During their investigation of gamma radiation from radon in ampoules of pure heavy metals, the author and L. I. Rusinov detected a weak neutron background. This neutron activity was only slightly dependent on the material of the ampoule and comprised about 3 neutrons per second per millicurie of radon.

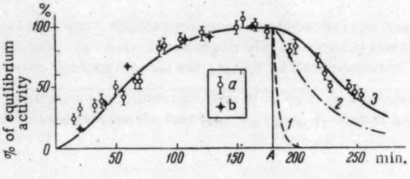

Fig. 1. Calculated curves: 1) RaA; 2) RaB; 3) RaC. A) Time of Rn removal. a) number of neutrons; b) γ-activity.

We measured the time dependence of the number of emitted neutrons: a) for the radon introduced into an evacuated ampoule; b) for a short-lived radium emanation deposit on a metal backing. The observed time-dependence of the gamma and neutron activity shows clearly that the emission is associated with RaC or with its short-lived decay products RaC' and RaC". Fig. 1 gives the experimental data as well as the calculated curves of the time-dependence of RaA, RaB and RaC atoms.

TABLE 1

Material of backing	Pt	Ta	Ni
Neutron acitivity (neutrons per mc per sec)	2.7 ± 0.15	2.8 ± 0.4	2.9 ± 0.15

We then undertook a detailed study of the mechanism of this phenomenon.

It was shown that the photoeffect in deuterium (within a paraffin moderator) which is induced by hard γ-radiation from RaC" [1,2] (and, possibly RaC [3]) cannot explain the observed effect. An estimate of the probability of the (γ, n) reaction based on the known deuterium cross section shows that only a few percent of the observed neutrons can result from the photoeffect. A control experiment with the source inside a lead cylinder with 25 mm thick walls revealed no change in the effect within the limits of statistical errors of the measurements (± 6%) although the intensity of the hard γ-radiation had to change by not less than 40%.

One of the probable causes of the neutron emission could be the (α, n)-reaction induced by RaC' α-particles.

The observed constancy of the measurements (carried out under identical experimental conditions) when using metals of such different atomic numbers as platinum, tantalum and nickel (see Table 1) shows that the α, n)-reaction does not take place in the metal atoms.

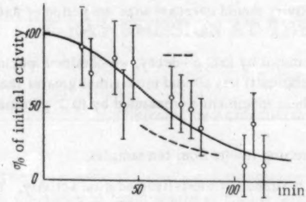

Fig. 2. $\Delta\rho$ = 16 cm He, E_α = 5.4 Mev

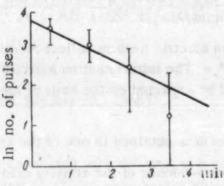

Fig. 3. τ_H = 1.4 ± 0.7 min

It should be noted that the table gives only the statistical errors of the measurements; a fairly large systematic error is also possible associated with the difference in the energies of neutrons emitted by the source being investigated and by a standard (Ra + Be) neutron source.

For further study of the possibility of the (α, n)-reaction an active deposit was applied to one side of a metal foil which was placed close to the axis of a cylindrical vacuum chamber. Between the source and the walls, which were covered with the same foil, spectrally pure helium was introduced at various pressures. The alpha particles striking the walls were slowed down in the helium (in the chamber these were ~45% of the total number of particles). The reduction of α-particle energy in the helium to 5.4 Mev did not diminish the observed neutron yield (see Fig. 2). It also follows from our data that when only radon and RaA are present (E_α ~ ~ 5.5 and ~ 6.0 Mev) the neutron emission is ~ 5-7% of the equilibrium value (see Fig. 1). Clearly, if the effect resulted from the (α, n)-reaction it should diminish by about 40% (dotted line in Fig. 2).

Thus, either the (α, n)-reaction plays a secondary part in this phenomenon or it takes place only on the surface of an activated sample due to some specific admixture.

If this last hypothesis is correct, then when the specimen is in the form of a layer inside the chamber, the effective thickness of the admixture and, correspondingly, the neutron yield should be doubled. Experimentally no change in activity was observed (within the limits of statistical error of measurements ±10%).

The possibility of neutron emission due to spontaneous nuclear fission in the active deposit (which is theoretically a very small probability) was also investigated experimentally.*

In our attempt to detect fission fragments in an ionization chamber, it was shown that the half life for decay was at least two orders greater than that required to explain the observed effect.

We consider the most probable mechanism of the neutron emission to be the ejection of neutrons from excited RaD nuclei resulting from the decay of RaC" ("delayed" neutron emission).

The total RaC" – RaD transition energy is (according to the data of various authors) 5.4 [4] or 6.0 Mev [5], and the binding energy of the "last" neutron in RaD is 5.2 or 4.8 Mev [6].

If, with the most unfavorable values for the indicated energies, it is assumed that we have a partial β-spectrum with a ~ 100 kev limit, whose intensity is about $2 \cdot 10^{-4}$ of the number of decays for the fundamental β-spectrum of RaC" ($E_{\beta\,\max}$ = 1.8 – 2.0 Mev), then it is also possible for neutrons of ~ 100 kev to be emitted. This process could compete with direct or cascade γ-transitions to the ground state of RaD.

The possibility of such transitions in RaD was proposed independently by others [6], who were not able to obtain the effect experimentally.

---

*A. N. Baryshev participated in the study of this question (1951).

The most direct verification of the hypothesis of neutron emission after β-decay of RaC″ is the study of neutron activity in a separated specimen of this isotope. The activity should decrease with the period of RaC″ β-decay (1.33 min).

By using an electric field to collect recoil ions of RaC″ produced by RaC α-decay, we obtained specimens enriched in RaC″.* The initial neutron activity (in various experiments) was 50 and more times greater than that which could be expected on the basis of the α-activity of these specimens as measured by RaC gamma radiation.

Fig. 3 gives data obtained in one of the experiments by summing results from ten samples.

The time-dependence of the activity clearly indicates the existence of short-lived neutron activity. The straight line which determines the half life was obtained by the method of least squares. The error in determining τ_n was calculated by taking into consideration the intrinsic background of the apparatus [7] (in the majority of the experiments the background during the first minute of measurements was approximately equal to the effect).

The weighted average half-life obtained in seven similar experiments was $\tau_{\text{neutron}} = 1.6 \pm 0.3$ min; it agrees within the limits of statistical error with the tabulated data for the half life of RaC″ β-activity (1.33 min).

The above results are a basis for assuming that the principal process which produces the neutron activity of a short-lived radon deposit is neutron emission by excited RaD nuclei formed through RaC″ β-decay.

The author thanks Professor L. I. Rusinov for his continued interest and assistance with this work; he also is grateful for the assistance of the late Academician P. I. Lukirskii, who made a number of valuable suggestions.

LITERATURE CITED

[1] S. Devons and G. J. Neary, Proc. Cambridge Phil. Soc. 33, 1, 154 (1937).

[2] S. Nishida, Proc. Phys. Math. Soc. (Japan) 19, 809 (1937).

[3] A. I. Alikhanov and G. D. Latyshev, Doklady Akad. Nauk SSSR 20, 6, 429 (1938); S. Kagayama, J. Phys. Soc. (Japan) 7, 1, 93 (1952).

[4] W. Bothe and H. Mayer-Leionjtz, Z. Physik 102, 3-4, 143 (1936).

[5] J. Surugue, J. Phys. Radium (Ser. 8) 7, 5, 145 (1946).

[6] B. B. Kinsey, G. A. Bartolomew and W. H. Walker, Phys. Rev. 82, 3, 380 (1951).

[7] H. Peierls, Proc. Roy. Soc. (London) A 149, 868, 467 (1935).

Leningrad Physico-Technical Institute
Academy of Sciences of the USSR

Received December 23, 1955

---

*The author thanks Professor A. N. Murin for valuable advice concerning the separation of RaC″.

X-RAY EMISSION AT THE START OF A GAS DISCHARGE

I. M. Podgornyi

(Presented by Academician L. A. Artsimovich, January 30, 1956)

The appearance of a number of articles concerning questions connected with the start of a gas discharge has induced the author to report results of the investigation of starting x-rays. These were x-rays which appeared upon the discharge of a battery of condensers through hydrogen at low pressure in a porcelain chamber of 170 mm diameter and 1000 mm height. Since the initial voltage on the chamber electrodes did not exceed 40 kv the x-rays were almost completely absorbed in the thick walls of the discharge chamber. To extract the radiation from the chamber we used openings covered with aluminum foil directly in front of luminescent crystals. The optical connection between the recording crystals and a photomultiplier that was shielded from electro-magnetic induction, was a plastic light pipe.

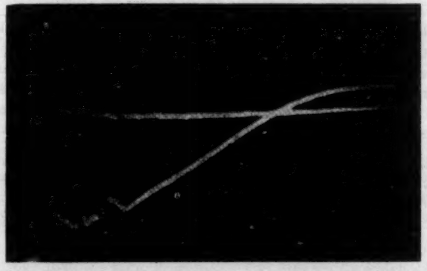

Fig. 1. Oscillogram of an x-ray pulse at the start of a discharge. Sweep length 22 μsec.

The discharge chamber had two outlets for radiation. One of these was in an electrode, while the other was in the wall of the porcelain tube at an equal distance from both electrodes. The crystal placed at the first opening could receive quanta originating in the electrode and chamber walls. Through the opening in the wall of the tube the other crystal could only receive quanta produced by scattered electrons striking the small portion of the chamber wall which was opposite the opening.

After amplification the pulses were fed to an OK-17 double-beam pulse oscillograph. The second beam recorded the curve of voltages on the discharge chamber electrodes. A typical oscillogram obtained from a single discharge is shown in Fig. 1. As can be seen from the figure the discharge starts appreciably later than the instant when a voltage is applied to the electrodes. With initial hydrogen pressures of 10^{-2} – 10^{-1} mm the retardation is a few microseconds, after which there is a sharp drop of the voltage between the electrodes corresponding to the start of the discharge. The x-ray pulse is observed just when the voltage at the electrode drops. The duration of the x-ray pulses and the time required for the steep voltage drop is about 1 μsec under the given conditions, which is in agreement with available experimental data [1] for the discharge buildup time.

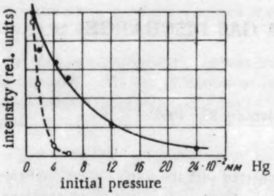

Fig. 2. Dependence of x-ray intensity at the start of a gas discharge on hydrogen pressure in the discharge chamber; V_0 = 40 kev.

An investigation of the dependence of starting x-ray intensity on the hydrogen pressure in the chamber showed that the intensity decreases as the pressure is raised and becomes vanishingly small at pressures of about 1 mm. At this value of the initial gas density the increase of electron energy upon motion in the electric field cannot compensate ionization losses, so that the electrons cannot acquire energy higher than the value at which ionization losses are at their peak. From Bethe's formula for ionization losses it follows that the energy losses at the maximum are equal to the energy which the electron acquires from the field per unit path length at initial density $\underline{n}$ given by the equation

$$n = \frac{1}{\pi}\sqrt{\frac{e}{2}}\,\frac{EI}{\varepsilon^3}, \tag{1}$$

where E is the electric field strength; I is the ionization potential of a hydrogen atom; and ϵ is the electron charge.

Although the application of Bethe's formula to the electron energy range near the ionization energy of the gas cannot be considered legitimate, certain data [2] indicate that the formula can be applied for electron energies of 16-17 ev. By substituting in (1) the values of E which correspond to the experimental conditions, it can easily be seen that x-ray emission should cease at hydrogen pressure 1.3 mm. However, this does not take into consideration the diffusive character of motion of low-energy electrons. Consideration of electron diffusion in constant electric fields shows that electron acceleration should stop at pressures which are somewhat lower than would be given by Equation (1).

The presence of molecular rather than atomic hydrogen in the discharge chamber should lead to the same results. In fact, as is shown by the experimental results in Fig. 2, x-ray emission practically stops at pressures of a few tenths of a millimeter. The solid curve gives the pressure dependence for radiation that passes through the aperture in the electrode, while the dashed curve gives corresponding results obtained through the aperture in the chamber wall.

As is seen from Fig. 2, the sharpest drop of x-ray intensity is observed in connection with the slowing down of electrons whose acceleration takes place only in a certain portion of the discharge distance (dashed curve). It is easy to understand the reason for the sharper decline of intensity with increased pressure for radiation passing through the opening in the chamber wall. Electrons originating in the discharge space close to the cathode and possessing small velocities acquire energy comparatively slowly, since their ionization losses are high.

Thus, with increased pressure and, consequently, with increased ionization losses, the electrons can acquire energy only in the region adjacent to the anode. Therefore, x-rays are recorded through the opening in the electrode even at pressures for which the recording instrument opposite the middle of the discharge chamber no longer indicates the existence of radiation.

LITERATURE CITED

[1] E. M Reikhrudel', A. V. Kustova and A. G. Zimlev, J. Tech. Phys. (USSR) 24, 1179 (1954).

[2] L. S. Ornstein, H. Lindeman and J. Oldeman, Z. Physik 83, 171 (1933).

Received January 23, 1956

THE CRITICAL CURRENT IN THIN SUPERCONDUCTING FILMS

L. A. Feigin and A. I. Shal'nikov, Corresponding Member of the Academy of Sciences of the USSR

The behavior of thin films of superconducting metals in magnetic fields has been studied in great detail [1-4]. These investigations over a broad range of film thicknesses [4] are in good agreement with the phenomenological theory of superconductivity developed by L. D. Landau and V. L. Ginzburg [5]. At the same time, the investigation of the critical current which destroys the superconductivity of thin layers has encountered considerable experimental difficulties. From the unusually small critical currents observed by A. I. Shal'nikov [1], it was impossible to determine the magnetic fields of the currents since his samples possessed cross sections perpendicular to the current in the form of wedges tapering to a point.

In order to eliminate this difficulty we undertook the investigation of cylindrical films; for this case it is possible to obtain a unique value of the magnetic field of the critical current. However, the preparation of cylindrical pure metallic films and the establishment of a good electrical contact were very difficult; this probably explains the indeterminate results of the first work done along these lines [6].

We prepared thin condensation layers of film of tin in a high vacuum at room temperature. Glass cylinders of 0.047 cm diameter were used as backing, which were drawn out with a gas jet immediately before the experiments. The glass cylinders were mounted in clamps fixed on the axes of meshed gears. The gears were rotated by means of a magnetic drive at the rate of 80 rotations per minute. In order to avoid heating the backing with radiation from the heated tungsten wire, the tin was evaporated by 10-12 second pulses at 5-minute intervals. The thickness of the films was determined from the geometry of the apparatus on the assumption of uniform evaporation at all solid angles. We simultaneously prepared several samples of different thicknesses.

Electrical contact was established as follows: In the apparatus for preparing films a second tin evaporator was mounted, which was screened from the samples in such a way that the tin which was evaporated from it reached only the ends of the glass cylinders. Films obtained by the use of this evaporator were several times thicker than films deposited by the main evaporator. External contacts were provided by flat bronze springs (0.2 mm thick) which clamped the ends of the cylinders to the brass holder (we did not fuse platinum wires into the glass cylinders for subsequent platinum plating by cathode sputtering, since this method resulted in lower critical currents, which probably resulted from heating of the contact-to-film transition layer).

The cylindrical tin films which we prepared with thicknesses from 2.1×10^{-5} to 3.4×10^{-6} cm possessed resistivity at room temperature which was close to the resistivity of tin in bulk (within 20-30% accuracy). The transition to the superconducting state as the temperature was lowered was very sharp (of the order of hundredths of a degree). The temperature dependence of the critical magnetic field for these films was in satisfactory agreement with the data of other authors.

The resistance of the films was sharply restored to the normal value at a certain critical value of the current passing through the film, as shown in Fig. 1.

The sharp alteration of resistance can be observed both through the galvanometer of a potentiometer circuit and by the current jump shown on a milliammeter in series with the sample.

Close to T_c the critical current increases approximately linearly as the temperature decreases (see Fig. 2).

In this connection it should be noted that the theoretical equation for the critical current in the absence of an external magnetic field is [5]

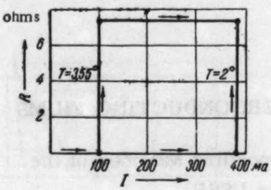

Fig. 1. Destruction of superconductivity in a film by passage of an electric current

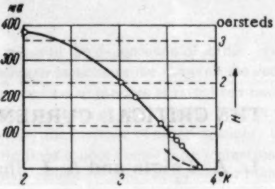

Fig. 2. Temperature dependence of the critical current. d = 4 · 10^{-6} cm

$$\frac{H_{ci}}{H_{cM}} = \frac{\sqrt{2}}{3\sqrt{3}}\frac{d}{\delta}. \tag{1}$$

where H_{ci} is the magnetic field strength of the critical current; H_{cm} is the critical magnetic field for bulky metal; $\underline{d}$ is the film thickness; and δ is the depth of penetration of the magnetic field into the superconductor.

Consideration of the temperature dependence $\delta(T)$ and the Relationship (1) lead to the possibility of expressing the temperature dependence of H_{ci} close to T_c for a given film in the form

$$H_{ci}' = \frac{2\sqrt{2}}{3\sqrt{3}}\frac{H_0 d}{T_c \delta_0}\Delta T^{3/2}, \tag{2}$$

where δ_0 and H_0 are constants and $\Delta T = T_c - T$.

This curve is shown near T_c by the dashed line in Fig. 2. Since Brucksch and Ziegler [7] obtained for thin flat lead films results which agree qualitatively with the Landau-Ginzburg theory, it is of interest to investigate the temperature dependence of the critical current over a broad range of thicknesses.

As has already been noted, the shape of the sample permitted an easy calculation of the magnetic field of the current flowing through the specimen (Fig. 2). The method thus developed produced the first reliable determinations of small critical currents in thin superconducting films and showed that the critical magnetic fields are smaller by a factor of several tens than the values observed for metal in bulk.

LITERATURE CITED

[1] A. I. Shal'nikov, J. Exptl.-Theoret. Phys. (USSR) 10, 630 (1940); 8, 763 (1938).

[2] N. E. Alekseevskii, J. Exptl.-Theoret. Phys. (USSR) 10, 1392 (1940).

[3] E. T. S. Appleyard, J. R. Bristow, H. London and A. D. Misener, Proc. Roy. Soc. 172, 540 (1939).

[4] N. V. Zavaritskii, Doklady Akad. Nauk SSSR 78, 665 (1951); 85, 749 (1952).

[5] V. L. Ginzburg and L. D. Landau, J. Exptl.-Theoret. Phys. (USSR) 20, 1064 (1950).

[6] A. D. Misener, Can. J. Research 14, 25 (1936).

[7] W. F. Brucksch and W. T. Ziegler, Phys. Rev. 62, 348 (1942).

M. V. Lomonosov
Moscow State University

Received December 29, 1955

PREPARATION AND DIELECTRIC AND OPTICAL PROPERTIES OF SINGLE CRYSTALS OF SOLID SOLUTIONS OF BARIUM AND STRONTIUM TITANATES

A. L. Khodakov, M. L. Sholokhovich, E. G. Fesenko and O. P. Kramarov

(Presented by Academician A. F. Ioffe, December 21, 1955)

The growing of ferroelectric single crystals has been the subject of numberous articles. Single crystals of barium and lead titanates have been studied in greatest detail [1-7], but we are not acquainted with any work on the growing of ferroelectric single crystals in the form of solid solutions. These are of both theoretical and practical interest since some of them could undoubtedly find immediate practical application.

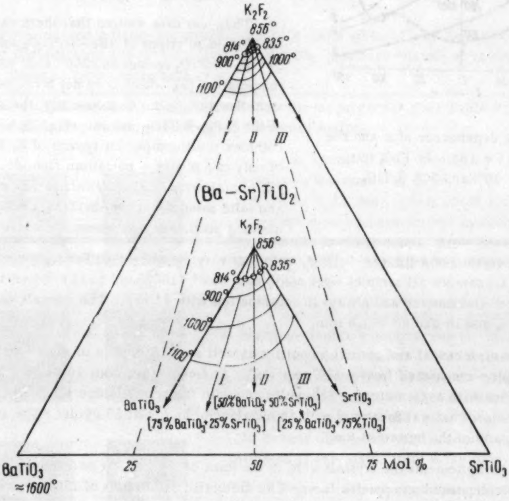
K$_2$F$_2$
856°
814°
835°
900°
1000°
1100°
I
II
III
(Ba–Sr)TiO$_2$
K$_2$F$_2$
856°
835°
814°
900°
1000°
1100°
I
II
III
BaTiO$_3$
[50% BaTiO$_3$ + 50% SrTiO$_3$]
SrTiO$_3$
[75% BaTiO$_3$ + 25% SrTiO$_3$]
[25% BaTiO$_3$ + 75% TiO$_3$]
BaTiO$_3$
≈1600°
25
50
75 Mol %
SrTiO$_3$

Fig. 1. Crystallization surface of a section of the K_2F_2 – $BaTiO_3$ – $SrTiO_3$ system

The present article describes single crystals of solid solutions of barium and strontium titanates prepared in our Institute. The crystals were grown in a platinum dish from a solution of mixed barium and strontium titanates in potassium fluoride by evaporating the latter at the crystallization temperature of the solid solutions followed by slow cooling until complete solidification was attained.

The basis for this method was our investigation up to 1100° by a visual-polythermal fusion method of the crystallization surface of a K_2F_2–$SrTiO_3$–$BaTiO_3$ system. Since barium and strontium titanates and their solid solutions are only slightly soluble in potassium fluoride we were able to investigate only a small part of the system.

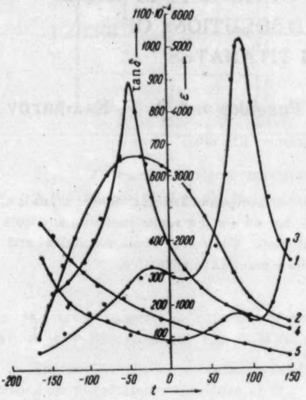

Fig. 2. Temperature dependence of ϵ and the dielectric loss angle for (Ba – Sr TiO_3 ferroelectrics containing 10% and 50% $SrTiO_3$

The $K_2F_2-SrTiO_3$ face in Fig. 1 is a eutetic diagram. The $K_2F_2-BaTiO_3$ system [8] is also eutectic. Thus, the $K_2F_2-SrTiO_3$ and $K_2F_2-BaTiO_3$ systems are stable sections of ternary systems of K, Me$||$$TiO_3$, F (Me = Sr and Ba). It then follows that in the reactions $K_2F_2 + BaTiO_3 \rightleftharpoons K_2TiO_3 + BaF_2$ and $K_2F_2 + SrTiO_3 \rightleftharpoons K_2TiO_3 + SrF_2$ the equilibrium point is in practice shifted in the direction of the initial substances and that the cooled melts consist only of a mixture of potassium fluoride and the respective titanate.

We investigated three internal sections through the $K_2P_2-SrTiO_3-BaTiO_3$ section along the line from KF to (n%$BaTiO_3$ + m%$SrTiO_3$). The presence of a continuous series of solid solutions in the $K_2F_2-SrTiO_3-BaTiO_3$ system follows from the curve of cocrystallization of different phases and the character of the isotherms (Fig. 1).

Thus, our data showed that there exists a continuous series of solid solutions of (Ba–Sr) TiO_3 solutions formed in the $BaTiO_3-SrTiO_3$ system at 1350° and existing down to room temperature [9], which does not break down even in a potassium fluoride melt. Consequently, the crystallization surface of the $K_2F_2-BaTiO_3$ system (Fig. 1), which is a section of a complex multicomponent system of K, Ba, Sr $||$ TiO_3 consists of only two phases – potassium fluoride, occupying a negligibly small area of the crystallization surface of the system, and solid solutions of (Ba–Sr)TiO_3, occupying the entire remaining portion of the system.

We had single crystals of solid (Ba–Sr)TiO_3 solutions varying by 5%* differences from 5 to 50% of $SrTiO_3$. From their external appearance all samples were combinations of $\{100\}$ and $\{111\}$ forms; the latter are weakly developed, are seldom encountered and always in combination with $\{100\}$. The crystals varied in color from light yellow to brown, and in size up to 1.5 mm.

We studied the dielectrical and optical properties as well as the structure of the crystals. The dielectric constant and loss angle were studied from – 160° to + 150°. At frequencies from 10^6 to $20 \cdot 10^6$ cycles the measurements were obtained with a Q-meter; at 10^3 cycles an audio frequency bridge was used. The voltage dependence of the dielectric constant was measured with an unbalanced bridge at 50 cycles. The usual circuit was used to obtain an oscillograph of the hysteresis loop.

For dielectric measurements the crystals were in the form of rectangular parallelepipeds (or close to this). Silver electrodes were deposited on opposite faces. The dielectric parameters of the single crystals of solid solutions changed strongly after heat treatment. This consisted of keeping the crystal at a temperature of 1350° for two hours. In the meantime, the crystals acquired a somewhat different color and became less transparent. Before heat treatment the crystals possessed slight ferroelectric properties and did not show the usual temperature dependence of ϵ with a pronounced peak at the Curie point. In Fig. 2, Curves 2 and 5 show the temperature dependence of ϵ for crystals with 10% and 50% of $SrTiO_3$ before heat treatment. After heating, the temperature dependence of ϵ for crystals of these concentrations of $SrTiO_3$ is given by Curves 1 and 4, respectively. Sharp peaks of ϵ are observed near temperatures which correspond to the Curie points of polycrystalline solid solutions [9]. Similar effects of heat treatment were also observed in single crystals with different ratios of $BaTiO_3$ and $SrTiO_3$. The temperature dependence of the dielectric loss angle for a single crystal containing 10% $SrTiO_3$ (after heat treatment) is given by Curve 3 of Fig. 2. For the remaining crystals tan δ at room temperature had values, depending on the $SrTiO_3$ concentration, from $50 \cdot 10^{-4}$ to $500 \cdot 10^{-4}$ (for $\nu = 10^6$ cycles).

---

*Percents are always molecular.

TABLE 1

ν (cps)	50	10^3	$1.15 \cdot 10^6$	$1.5 \cdot 10^8$
ϵ	6300	5000	3600	3000

TABLE 2

E (v/cm)	150	600	1500
ϵ	1500	2100	3400

TABLE 3

Composition	$\theta°$	ϵ	n	d (g/cm³)	
				Single crystals	Polycrystals
0% $SrTiO_3$, 100% $BaTiO_3$	+120	1550	2.40	6.01	6.03
5% $SrTiO_3$, 95% $BaTiO_3$	+ 94	1200	2.38	5.98	5.98
10% $SrTiO_3$, 90% $BaTiO_3$	+ 88	1500	2.33	5.94	5.94
15% $SrTiO_3$, 85% $BaTiO_3$	+ 58	2700	2.38	5.92	5.92
50% $SrTiO_3$, 50% $BaTiO_3$	− 48	1550	2.37	5.54	5.63
100% $SrTiO_3$, 0% $BaTiO_3$			2.35		5.12

Some single crystals showed a frequency dependence of ϵ from 50 to 10^6 cycles. Table 1 gives the values of ϵ for a single crystal containing 10% $SrTiO_3$ and 90% $BaTiO_3$ (not heat treated) at various frequencies. This crystal showed only a slight voltage dependence of ϵ.

After heating, the crystal acquired more pronounced nonlinear properties (see Table 2), with disappearance of the dispersion of the dielectric constant in the given frequency region.

The hysteresis loop oscillograms also showed that all crystals possess nonlinear dependence of polarization on the applied field E. But crystals which are not subjected to heat treatment show uncharacteristic hysteresis loops which closely resemble Rayleigh loops. After heating, as can be seen from Fig. 3, the hysteresis loops assume the usual form for ferroelectrics.

The dielectric and optical properties, as well as the roentgenographic density of single crystals of the solid solutions, are given in Table 3 (the dielectric constants and Curie points are given for heated crystals). In this table θ is the Curie point; ϵ is the dielectric constant at 23° and 10^6 cycles; $\underline{n}$ is the index of refraction; and $\underline{d}$ is the density of single crystals and ordinary polycrystalline samples as calculated from x-ray data.

Regions of spontaneous polarization (domains) were observed in crystals of varying composition by means of a polarization microscope.

A typical crystal, consisting of 10% $SrTiO_3$ and 90% $BaTiO_3$, is shown in Fig. 4. The localization of the domains in separate zones of the crystal is characteristic. In many crystals we observed the previously described [10] temperature hysteresis of the domain structure. Unannealed crystals of this composition were observed up to 250°. At 250° the crystal is anisotropic. Large internal stresses are probably present.

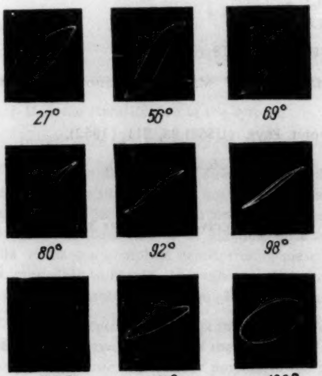

Fig. 3. Oscillograms of hysteresis loops of (Ba–Sr)TiO_3 single crystals containing 95% $BaTiO_3$ and 5% SrTiO3

From the electrical, optical and x-ray data it can be concluded that we have in this work obtained single crystals representing a continuous series of solid solutions.

Fig. 4. Domain structure of single crystals of solid solutions (90% $BaTiO_3$ + + 10% $SrTiO_3$)

Heat treatment of the crystals in all probability results in the elimination of mechanical deformations which hinder reorientation of the domains and the corresponding dielectric polarization. This hypothesis is also supported by the frequency dependence of ϵ in crystals which are not heat-treated, at low frequencies (Table 1). We observed a similar phenomenon previously when studying certain varieties of $BaTiO_3$ single crystals [11].

The investigation of single crystals of $(Ba-Sr)TiO_3$ solid solutions is being continued.

The authors are indebted to Professor B. M. Vul for his interest and to N. S. Novosil'tsev for several valuable suggestions.

LITERATURE CITED

[1] H. Blattner, W. Kānzig and W. Merz, Helv. Phys. Acta 22, 35 (1949).

[2] B. Matthias and A. Hippel, Phys. Rev. 73, 268 (1949).

[3] H. Kay, R. Rodes, Nature 160, 126 (1947).

[4] I. N. Beliaev, N. S. Novosil'tsev, et al., Doklady Akad. Nauk SSSR 78, 875 (1951).

[5] I. N. Beliaev, N. S. Novosil'tsev, et al., Doklady Akad. Nauk SSSR 83, 5, 675 (1952).

[6] I. N. Beliaev and A. L. Khodakov, J. Exptl.-Theoret. Phys. (USSR) 23, 62 (1952).

[7] E. G. Fesenko, Doklady Akad. Nauk SSSR 88, 5, 785 (1953).

[8] M. L. Sholokhovich and I. N. Beliaev, J. Gen. Chem. (USSR) 24, 218 (1954).

[9] A. L. Khodakov and M. S. Shul'man, Trans. Physico-Math. Inst., V. M. Molotov Rostov State University 24, 25 (1955).

[10] I. N. Beliaev, N. S. Novosil'tsev, et al., J. Exptl. -Theoret. Phys. (USSR) 23, 211 (1952).

[11] N. S. Novosil'tsev and A. L. Khodakov, Doklady Akad. Nauk SSSR 85, 1263 (1952).

Physico-Mathematical Research Institute of the
V. M. Molotov Rostov-on-Don State University

Received November 30, 1955

THE DETERMINATION OF EIGENVALUES OF PHYSICAL QUANTITIES BY MEANS OF A QUANTUM MECHANICAL DISTRIBUTION LAW

Iu. L. Klimontovich

(Presented by Academician N. N. Bogoliubov, December 15, 1955)

The most symmetrical expression for a quantum mechanical distribution law (density matrix in the $\underline{\mathbf{q}}, \underline{\mathbf{p}}$ representation) was proposed by Wigner [1-3]. For the case of a pure ensemble this law can be associated with the wave function

$$f(\mathbf{q}, \mathbf{p}, t) = \frac{1}{(2\pi)^{3N}} \int \Psi^{*}(\mathbf{q} - {}^{1}\!/_{2} h\vec{\tau})\, \Psi(\mathbf{q} + {}^{1}\!/_{2} h\vec{\tau})\, e^{-i\vec{\tau}\mathbf{p}}\, d\vec{\tau}, \tag{1}$$

where $\mathbf{q} = (\mathbf{q}_1 \ldots \mathbf{q}_N)$; $\mathbf{p} = (\mathbf{p}_1 \ldots \mathbf{p}_N)$; and N is the number of particles in the system.

For a mixed ensemble the function f (**q, p,** t) is associated with the density matrix. The equation for the quantum mechanical distribution law is

$$\begin{aligned} \frac{\partial f}{\partial t} = \frac{i}{(2\pi)^{3N}\hbar} \int [H(\vec{\eta} + {}^{1}\!/_{2}\hbar\,\mathbf{k},\ \mathbf{r} - {}^{1}\!/_{2}\hbar\vec{\tau}) - H(\vec{\eta} - {}^{1}\!/_{2}h\,\mathbf{k},\ \mathbf{r} + {}^{1}\!/_{2}h\vec{\tau})] \times \\ \times f(\vec{\eta}, \mathbf{r}) \exp\left[\sum_{l=1}^{N} (i\vec{\tau}_l(\vec{\eta}_l - \mathbf{p}_l) + i\mathbf{k}_l(\mathbf{r}_l - \mathbf{q}_l))\right] (d\vec{\tau}_l)\,(d\vec{\eta}_l)\,(d\mathbf{k}_l)\,(d\mathbf{r}_l), \end{aligned} \tag{2}$$

where H is the Hamiltonian of the system.

In reference [4] Equations (1) and (2) were generalized to apply to a relativistic system.

The direct utilization of Equation (2) to determine the quantum mechanical distribution law, as well as of the corresponding classical equation for a many-particle system, is difficult in the majority of cases since the function sought depends on an enormous number of variables. For this reason approximate methods are used to solve both the quantum and the classical equations. Even if an exact solution of Equation (2) were obtained, we would not have a complete description of the quantized system. For example, from a solution of Equation (2) it is impossible to obtain eigenvalues and eigenfunctions for various quantities of the system, impossible to investigate the quantum properties of such systems as an oscillator, hydrogen atom, etc.

For the solution of these problems in the case of a pure ensemble, it would be possible to use equations for the proper wave functions of the corresponding operators and by solving these to obtain eigenfunctions and eigenvalues. However, it is the purpose of the present article to show that it is not necessary to resort to the use of proper wave functions and that the indicated problems of quantum theory can be solved by a method which employs a quantum mechanical distribution law.

Equation (2) is the equation of motion for a quantum mechanical distribution law which for $\hbar \longrightarrow 0$ reduces to the corresponding classical equation of Gibbs' statistical mechanics:

$$\frac{\partial f}{\partial t} = -\sum_{1<l<N} \left\{ \frac{\partial H}{\partial \mathbf{p}_l} \frac{\partial f}{\partial \mathbf{q}_l} - \frac{\partial H}{\partial \mathbf{q}_l} \frac{\partial f}{\partial \mathbf{p}_l} \right\}. \tag{3}$$

In quantum mechanics, in addition to the equation of motion, we use for the wave function equations for the determination of eigenvalues and eigenfunctions of physical quantities. From these, by utilizing the quantum mechanical distribution law (1) for the eigenfunctions, it is possible to obtain equations to determine proper quantum mechanical distribution laws for any physical quantities.*

For example, the equation for the proper quantum mechanical distribution laws and energy eigenvalues is

$$Ef = {}^1/_2\int [H(\vec{\eta} - {}^1/_2 h\mathbf{k}, \mathbf{r} + {}^1/_2 h\vec{\tau}) + H(\vec{\eta} + {}^1/_2 h\mathbf{k}, \mathbf{r} - {}^1/_2 h\vec{\tau})] \times$$
$$\times f(\vec{\eta}, \mathbf{r}) \exp\left[\sum_{l=1}^{N} (i\vec{\tau}_l(\vec{\eta}_l - \mathbf{p}_l) + i\mathbf{k}_l(\mathbf{r}_l - \mathbf{q}_l))\right] (d\vec{\tau}_l)(d\vec{\eta}_l)(d\mathbf{k}_l)(d\mathbf{r}_l).^{**} \tag{4}$$

For $\hbar = 0$ Equation (4) becomes the corresponding classical equation

$$Ef = H(\mathbf{q}, \mathbf{p})f. \tag{5}$$

From Equation (5) it follows that an eigenvalue of the energy is the classical expression for the energy

$$E = H(\mathbf{q}, \mathbf{p}), \tag{6}$$

and the eigenfunctions are

$$f_{\ldots \mathbf{q}_i' \ldots \mathbf{p}_i' \ldots} = \delta(\mathbf{q}_1 - \mathbf{q}_1')\,\delta(\mathbf{p}_1 - \mathbf{p}_1') \ldots \delta(\mathbf{q}_N - \mathbf{q}_N')\,\delta(\mathbf{p}_N - \mathbf{p}_N'). \tag{7}$$

For the angular momentum this equation can be written as

$$\mathbf{M}f = [\mathbf{q}\mathbf{p}]f - \frac{h^2}{4}[\nabla_{\mathbf{q}}\nabla_{\mathbf{p}}]f. \tag{8}$$

It should be noted that Equations (2), (4) and (8) are also valid for a mixed ensemble and can be obtained from the corresponding classical expressions by quantization with suitable allowance for wave properties.

For a system of particles interacting through central forces Equation (4) becomes

$$Ef = \sum_{1<l<N}\left(\frac{\mathbf{p}_l^2}{2m} - \frac{h^2}{8m}\Delta_{\mathbf{q}_l}\right) f +$$
$$+ \frac{1}{2}\sum_{1<i<j<N}\int \cdots \int [\Phi(|\mathbf{q}_i - \mathbf{q}_j + {}^1/_2 h(\vec{\tau}_i - \vec{\tau}_j)|) + \Phi(|\mathbf{q}_i - \mathbf{q}_j - {}^1/_2 h(\vec{\tau}_i - \vec{\tau}_j)|)] + \tag{9}$$
$$+ f(\mathbf{q}_1 \ldots \mathbf{q}_N \vec{\eta}_1 \ldots \vec{\eta}_N) \exp\left[i\sum_l \vec{\tau}_l(\vec{\eta}_l - \mathbf{p}_l)\right](d\vec{\eta}_l)(d\vec{\tau}_l).$$

By integrating with respect to $\mathbf{q}_1 \ldots \mathbf{q}_N, \mathbf{p}_1 \ldots \mathbf{p}_N$, in Equations (4), (8) and (9) we obtain

$$E = \overline{H}; \quad \mathbf{M} = \overline{\mathbf{M}}; \quad E = \overline{\sum_{1<l<N}\frac{\mathbf{p}_l^2}{2m} + \sum_{1<i<j<N}\Phi(|\mathbf{q}_i - \mathbf{q}_j|)}, \tag{10}$$

---

*"Proper quantum mechanical distribution laws" can assume negative values, so that this designation is, of course, arbitrary.

**Indices of the energy eigenvalues and of the eigenfunctions are omitted.

i.e., the eigenvalues of the physical quantities are equal to the average values of the corresponding physical quantities obtained from proper quantum mechanical distribution laws. This is also true for the equations of motion. Thus, for example, the Hamilton's equations hold true for average values from a quantum mechanical distribution law:

$$\frac{d\overline{\mathbf{q}}_l}{dt} = \frac{\partial H}{\partial \mathbf{p}_l}; \quad \frac{d\overline{\mathbf{p}}_l}{dt} = -\frac{\partial H}{\partial \mathbf{q}_l}. \tag{11}$$

In the classical case ($\hbar = 0$) the expression for the quantum mechanical distribution law has the form of a δ-function [see (7)] and Equations (11) reduce to the classical Hamilton's equations.

The corresponding relativistic equations for the proper quantum mechanical distributions can be obtained by using the results of the author's article [4]. Thus, the equation for the proper quantum mechanical distribution laws for the square of the 4-momentum of a particle in an external electromagnetic field is

$$G_0 f = {}^1/_2 \int [G(\eta_i - {}^1/_2 \hbar k_i, q_i + {}^1/_2 \hbar \tau_i) + G(\eta_i + {}^1/_2 \hbar k_i, r_i - {}^1/_2 h \tau_i)] \times$$
$$\times f(\eta_i, r_i) \exp [i\tau_i(\eta_i - p_i) + ik_i(r_i - q_i)]\, d\eta_i dr_i dk_i d\tau_i,$$

where $G = \left(p_i - \frac{e}{c} A_i(q_i)\right)^2$ is the square of the 4-momentum; A_i is the 4-dimensional potential; p_i and q_i are 4-dimensional momenta and coordinates; and G_0 is the eigenvalue of the square of the 4-momentum.

Let us consider an oscillator as an example. Equations (2) and (4) then become

$$\frac{\partial f}{\partial t} + \frac{\mathbf{p}}{m} \frac{\partial f}{\partial \mathbf{q}} - m\omega_0^2 \mathbf{q} \frac{\partial f}{\partial \mathbf{p}} = 0, \tag{12}$$

$$Ef = \frac{\mathbf{p}^2}{2m} f - \frac{h^2}{8m} \Delta_q f + \frac{m\omega_0^2 q^2}{2} f - \frac{\hbar^2 m\omega_0^2}{8} \Delta_p f. \tag{13}$$

The solution of (13) in the one-dimensional case leads to the following expressions for the eigenvalues of the energy and the oscillator eigenfunctions:

$$E_{nm} = (n + m + 1) \frac{h\omega_0}{2}; \tag{14}$$

$$f_{nm} = \frac{(-1)^{n+m} 2}{\hbar \sqrt{2^{n+m} n! m! \pi}} \exp \left[-m\omega_0 \frac{q^2}{h} - \frac{p^2}{hm\omega_0} \right] H_n(q) H_m(p), \tag{15}$$

where $H_n(q)\, H_m(p)$ are Hermite-Chebyshev polynomials. The eigenfunctions (15) are orthogonal and normalized.

The quantum mechanical distribution law can be represented as a series of distribution eigenfunctions:

$$f(q, p, t) = \sum P_{nm}(t) f_{nm}(q, p). \tag{16}$$

The function $P_{nm}(t)$ can be determined by solving Equation (12) or the corresponding characteristic equation.

Substituting (16) and (15) in (12) we find that for equilibrium ($\partial f/\partial t$) $n = m$. Then for P_{nn} we can take the Boltzmann distribution

$$P_{nn} = A \exp\left(-\frac{E_{nn}}{kT}\right). \tag{17}$$

Then

$$f(q,p)=\sum_n{}' A\exp\left(-\frac{E_{nn}}{kT}\right)f_{nn}(q,p). \tag{18}$$

Using (14) and (15) and summing, we obtain expressions for the equilibrium quantum mechanical distribution law of the oscillator:

$$f(q,\ p)=A\exp\left[-\left(\frac{m\omega_0^2q^2}{2}+\frac{p^2}{2m}\right)\Big/\left({}^1/_2h\omega_0+\frac{h\omega_0}{e^{h\omega_0/kT}-1}\right)\right]. \tag{19}$$

Thus, we immediately obtain the distribution with respect to the coordinates and momenta (compare with the derivation in [5]).

When $\hbar\longrightarrow 0$

$$f(q,p)=A\exp\left[-\left(\frac{m\omega_0^2q^2}{2}+\frac{p^2}{2m}\right)/\,kT\right]. \tag{20}$$

When $T\longrightarrow 0$

$$f(q,\ p)=A\exp\left[-\left(\frac{m\omega_0^2q^2}{2}+\frac{p^2}{2m}\right)\Big/\frac{h\omega_0}{2}\right]. \tag{21}$$

In the last case the zero point energy plays the part of the temperature.

For a hydrogen atom the equation for the function $\rho(\mathbf{q})=\int f(\mathbf{q},\mathbf{p})\,d\mathbf{p}$ coincides with the corresponding Schroedinger equation

$$\left(E-\frac{\overline{\mathbf{p}^2}}{2m}\right)\rho(\mathbf{q})=-\frac{\hbar^2}{8m}\Delta_{\mathbf{q}}\rho(\mathbf{q})-\frac{Ze^2}{|\mathbf{q}|}\rho(\mathbf{q}). \tag{22}$$

We therefore obtain for the eigenvalues

$$E_n=\frac{\overline{\mathbf{p}^2}}{2m}-\frac{2mZ^2e^4}{\hbar^2n^2};$$

the bar denotes averaging over momenta.

LITERATURE CITED

[1] E. Wigner, Phys. Rev. 40, 749 (1931).

[2] S. Moyal, Proc. Cambridge Phil. Soc. 45, 95 (1949).

[3] Iu. L. Klimontovich and V. P. Silin, J. Exptl.-Theoret. Phys. (USSR) 23, 8, (1952).

[4] Iu. L. Klimontovich, Doklady Akad. Nauk SSSR 87, 927 (1952).

[5] L. D. Landau and E. M Lifshits, Statistical Physics (1951).

M. V. Lomonosov
Moscow State University

Received November 24, 1955

ON THE THEORY OF THE EXCITATION ENERGY OF HEAVY NUCLEI

L. P. Rapoport and Iu. M. Butusov

(Presented by Academician N. N. Bogoliubov, January 9, 1956)

In calculating the excitation energy of heavy nuclei it is customary to use the model of an ideal Fermi gas enclosed in a potential well of nuclear diameter and 35 Mev depth. This model is unsatisfactory for the following reasons: 1) It neglects the interactions of nucleons; 2) It ignores surface effects. The success of the shell model of the nucleus is an apparent indication of the correctness of the concept of individual nucleons moving in a potential well of definite depth; on the other hand, the collective oscillations of the nuclear surface are generally in disagreement with the shell model [1]. The problem thus arises of combining in a single model the individual and collective properties of nucleonic motion. A difficulty arises in connection with the degrees of freedom of nucleons in a nucleus. It is clear that despite the collective oscillations the number of degrees of freedom of the nucleons should not exceed 3A. Süssmann has shown that it is possible to select a coordinate system in which the individual and collective motions are separated and the total number of degrees of freedom of the system does not exceed 3A [2].

Let the nucleus be able to change its shape without compression and let its surface be represented by the function $R(\theta, \varphi)$. Expanding $R(\theta, \varphi)$ in a series of spherical harmonics, we have

$$R(\theta, \varphi) = R_0 \left[1 + \sum_{l=1}^{\Lambda} \sum_{m=0}^{2l} C_l^m Y_l^m (\theta, \varphi) \right]. \tag{1}$$

If, instead of the actual coordinates $\mathbf{r}_i$ of the nucleons we introduce as new coordinates the multipole moments C_l^m and coordinates of individual motion $\vec{\xi}_i$, then, as was shown in [2], in the Hamiltonian of the nucleus the collective motion is separated from the individual motion and we have*

$$H = \sum_{l,m} \frac{1}{2m_l} \mathbf{P}_{lm}^2 + \frac{1}{2m} \sum_{jj'} \vec{\pi}_j (\delta_{jj'} - \beta_{jj'}) \vec{\pi}_{j'} + U + V_s + V_c + U_0. \tag{2}$$

where $m_l = \frac{3}{4\pi} R_0^2 \frac{M}{l}$; $R_0 = r_0 A^{1/3}$ is the radius of the undeformed nucleus; M is the mass of the nucleus;

$\mathbf{P}_{lm} = -i \frac{\partial}{\partial C_l^m}$; $\vec{\pi}_i = -i \frac{\partial}{\partial \vec{\xi}_i}$; β_{jj} is a symmetric tensor depending on the deformation of the nucleus and defined in [2]; V_s is the change of surface energy as a result of deformation. If S is the surface tension we know that

$$V_s = S \sum_{l,m} (l+2)(l-1) R_0^2 C_l^{m*} C_l^m. \tag{3}$$

---

*We use a system of units in which $\hbar = c = m_e = 1$.

The change of Coulomb energy resulting from deformation will be:

$$V_c = -\frac{4\pi}{3}\rho_e R_0^5 \sum_{l,m} \frac{l-1}{2l+1} C_l^{m*} C_l^m. \tag{4}$$

where ρ_e is the density of the nucleus.

The third term of (2) is the energy associated with specific nuclear forces. U_0 is the constant energy of the surface tension, which is selected to satisfy Weizsäcker's equation for the energy of the nucleus. The first term in (2) is the kinetic energy of oscillation. The Coulomb energy of proton repulsions is not included in order to avoid complicating the calculation. The proper wave function of the nucleus can then be represented as

$$\psi = \varphi_i \varphi_c,$$

since the individual and collective motions were separated in the Hamiltonian (2).

The Schroedinger equation for the additive portion of the Hamiltonian breaks up into two equations which describe the individual and collective motions:

$$\left(-\frac{1}{2m}\sum_j \nabla_j^2 + \frac{1}{2m}\sum_j \beta_j \nabla_j^2\right)\varphi_i = (E_i + U_0)\varphi_i, \tag{5}$$

$$\left\{\sum_{lm}\frac{1}{2m_l}\mathbf{P}_{lm}^2 + \sum_{lm}\left[S R_0^2 (l+2)(l-1) - \frac{4\pi}{3}\rho_e^2 R_0^5 \frac{l-1}{2l+1}\right] C_l^{m*} C_l^m\right\}\varphi_c = E_k \varphi_c. \tag{6}$$

Let the wave function of a nucleon be of the form

$$\varphi_p = \frac{1}{\sqrt{V}} e^{i p \vec{\xi}} \chi_p(\vec{\sigma})\, \eta_p(\vec{\tau}), \tag{7}$$

where χ_p and η_p are functions depending on the spin and isotopic spin, respectively.

We shall write the Hamiltonian of (5) with second quantization as

$$H_i = \sum_{pp'} \int \varphi_p^* H(1)\, \varphi_p d\vec{\xi}\, a_p^+ a_{p'} = \sum_p E(p)\, n_p + U_0, \tag{8}$$

where $\sum_p n_p = A'$ is the number of nucleons associated with the individual motion; a_p^+ and a_p are the usual operators of Fermi statistics satisfying the relationship $[a_p^+, a_{p'}] = \delta(p - p')$, etc.; and $E(p) = \mathcal{P}^2/2m$, where $\mathcal{P}^2 = [P_x^2(1-\beta_x) + P_y^2(1-\beta_y) + P_z^2(1-\beta_z)]$.

The Hamiltonian of (6) is also given in second quantized form [3].

If we introduce the mass density ρ_0 and

$$B_l = \rho_0 \frac{R_0^5}{l}, \quad A_l = 2R_0^5 S(l+2)(l-1) - \frac{8\pi}{3}\frac{R_0^5 (l-1)}{2l+1}, \quad K_l^m = \frac{\partial H_k}{\partial C_l^m} = B_l C_l^m,$$

the Hamiltonian of (6) becomes

$$H_k = \sum_{lm} \left(\frac{K_l^{m^*} K_l^m}{2B_l} + \frac{1}{2} A_l C_l^{m^*} C_l^m \right). \tag{9}$$

From (9) we see that the surface oscillations can be regarded as a system of oscillators with frequency $\omega_l = (A_l/B_l)^{1/2}$.

Regarding K_l^m and C_l^m as quantum mechanical operators and introducing in addition the creation and annihilation operators $b_l^{m^*}$ and b_l^m of Bose statistics by the relationships

$$b_l^m = \frac{1}{2}\left[\left(\frac{2A_l}{\omega_l}\right)^{1/2} C_l^{m^*} + i \left(\frac{2B_l}{\omega_l}\right)^{1/2} K_l^m \right]$$

with the commutation rule $[b_l^m, b_l^{m^*}]_- = \delta_{ll'}\delta_{mm'}$, we obtain

$$H_k = \sum_{lm} \frac{\omega_l}{2} \left[b_l^m b_l^{m^*} + b_l^{m^*} b_l^m \right]; \tag{10}$$

since $b_l^{m^*} b_l^m$ is the number of phonons of the surface oscillations in the state l, m, then by introducing the numbers $N_l = 0, 1, 2$ and dropping the background constant, we obtain

$$H_k = \sum_l \omega_l N_l. \tag{11}$$

From (8) and (11) we obtain for the mean value of the additive portion of the energy

$$\overline{H}_{ad} = \sum_l E(p)\, \overline{n}_p + \sum_l \omega_l \overline{N}_l + U_0^k. \tag{12}$$

The average values of the occupation numbers $\overline{n}_p$ and $\overline{N}_l$ are calculated by using the statistical sum of the states [4] subject to the condition $\sum_p n_p = A'$:

$$\overline{n}_p = \frac{1}{e^{\frac{E(p)-\zeta}{\theta}} + 1}; \quad \overline{N}_l = \frac{1}{e^{\frac{\omega_l}{\theta}} - 1}; \quad \theta = kT. \tag{13}$$

By exchanging summation and integration in (12) we obtain

$$\overline{H}_i = \sum_p \overline{n}_p E(p) + U_0 = \frac{3}{5} \frac{A'\zeta'}{\nu(\beta)} \left[1 + \frac{5\pi^2}{12} \left(\frac{\theta}{\zeta'}\right)^2 + \ldots \right], \tag{14}$$

where $\zeta' = \zeta + \frac{U_0}{A}$; $\zeta' = \left(\frac{9\pi}{8}\right)^{2/3} \frac{1}{2mR_0^2} \left(\frac{A'}{A}\right)^{2/3}$; $\nu(\beta) = [(1-\beta_x)(1-\beta_y)(1-\beta_z)]^{-1/3}$ with the assumption that $\theta/\zeta' \ll 1$. For the mean value of the collective portion of the additive energy H_k we have, from (12) and (13):

$$\overline{H}_k = \sum_l \frac{\omega_l}{e^{\omega_l/\theta} - 1}, \quad l = 2, 3. \tag{15}$$

We shall now calculate the binary portion of the energy (2). A calculation shows that the kinetic term of binary type $-\frac{1}{2m}\sum_{i \neq j'} \vec{\pi}_i \beta_{jj'} \vec{\pi}_{j'}$ is small compared with the specific nuclear interaction: $U_{bin} = \sum_{(1 \leq \xi < s \leq A)} U(\xi, s)$ we therefore neglect this term.

According to Bogoliubov's theory of statistical operators, the average value of a binary quantity is of the form [4]

$$\overline{U}_{bin} = \frac{A(A-1)}{2} \operatorname{Spur}\left[U(\xi, s) R_2(1, 2)\right], \tag{16}$$

where $R_2(1, 2)$ is a statistical operator of binary interaction. With the wave function (7) $R_2(1,2)$ for our case is of the form

$$\begin{aligned} R_2(1, 2) = \frac{1}{V^2 A(A-1)} \sum_{(p_1 p_2)} \bar{n}_{p_1} \bar{n}_{p_2} \{ & \exp i\left[\mathbf{p}_1(\vec{\xi}_1 - \vec{\xi}'_1) + \mathbf{p}_2(\vec{\xi}_2 - \vec{\xi}'_2)\right] \times \\ & \times \chi^*_{p_1}(\vec{\sigma}'_1)\, \eta^*_{p}(\vec{\tau}'_1)\, \chi^*_{p_2}(\vec{\sigma}'_2)\, \eta^*_{p_2}(\vec{\tau}'_2)\, \chi_{p_1}(\vec{\sigma}_1)\, \eta_{p_1}(\vec{\tau}_1)\, \chi_{p_2}(\vec{\sigma}_2)\, \eta_{p_2}(\vec{\tau}_2) - \exp i\left[\mathbf{p}_1(\vec{\xi}_2 - \vec{\xi}'_1) + \right. \\ & \left. + \mathbf{p}_2(\vec{\xi}_1 - \vec{\xi}'_2)\right] \chi^*_{p_1}(\vec{\sigma}'_1)\, \eta^*_{p_1}(\vec{\tau}'_1)\, \chi^*_{p_2}(\vec{\sigma}'_2)\, \eta^*_{p_2}(\vec{\tau}'_2)\, \chi_{p_1}(\vec{\sigma}_2)\, \eta_{p_1}(\vec{\tau}_2)\, \chi_{p_2}(\vec{\sigma}_1)\, \eta_{p_2}(\vec{\tau}_1) \}. \end{aligned} \tag{17}$$

As an interaction potential we use the potential of the pseudoscalar meson field

$$U(1, 2) = g^2 S_{12}\left(\frac{1}{\xi_{12}^2} + \frac{1}{a\xi_{12}} + \frac{1}{3a^2}\right)\frac{e^{-\xi_{12}/a}}{\xi_{12}} + \frac{1}{3}\frac{g^2}{a^2}(\vec{\sigma}_1\vec{\sigma}_2)\frac{e^{-\xi_{12}/a}}{\xi_{12}}, \tag{18}$$

where $S_{12} = 3(\vec{\sigma}_1\mathbf{n})(\vec{\sigma}_2\mathbf{n}) - (\vec{\sigma}_1\vec{\sigma}_2)$.

Substituting in (16) $R_2(1, 2)$ of (17) and $U(1, 2)$ of (18) and summing over spins and isotopic spins on the assumption that both spin directions are equally likely, replacing the summation with respect to p_1, p_2 by integration and taking the values of $\bar{n}_p$ into consideration, we obtain

$$\begin{aligned} \overline{U}_{bin} = -\frac{g^2}{4a^2\nu(\beta)} \Big\{ & \frac{A}{2\pi a}\left[6\omega - \frac{1}{\omega} + \frac{1}{4}\left(\frac{1}{\omega^3} - \frac{12}{\omega}\right)\ln(1+4\omega^2) - 8\arctan 2\omega\right] + \\ & + \frac{A\pi}{a}\left[\left(\omega - \frac{1}{2}\arctan 2\omega - \frac{\omega}{4}\ln(1+4\omega^2)\right)\left(\frac{\theta}{\zeta'}\right)^2 + \frac{\pi^2\omega^3}{96}\left(1 + \frac{1-4\omega^2}{(1+4\omega^2)^2}\right)\left(\frac{\theta}{\zeta'}\right)^4\right]\Big\}, \end{aligned} \tag{19}$$

where $\omega = P_\mu a = (3\pi^2\rho)^{1/3} a$, and ρ is the nucleon density distribution. We assume $\theta/\zeta' \ll 1$. In the absence of nuclear deformation ($\beta = 0$) and in the absence of excitation ($\theta = 0$), we obtain the usual expression [5] for $\overline{U}_{bin}$.

The total energy of the nucleus is given by

$$E(\theta) = \overline{H}_k + \overline{H}_i + \overline{U}_{bin} \tag{20}$$

Thus the total temperature-dependent energy of the nucleus consists of three parts: the shell-phonon oscillation energy, the kinetic energy of the nucleons (provided not by all nucleons A but by a part of them A' which is dependent, in general on the shape of the nucleus at a given instant) and the interaction energy of the nucleons.

The excitation energy of the nucleus is obtained in the form of a power series in θ/ζ':

$$\begin{aligned} E(\theta) - E(0) = \frac{1}{\nu(\beta)}\Big\{\frac{\pi^2}{4}A'\Big(\frac{\theta}{\zeta'}\Big)^2 - \\ - \frac{g^2\pi A}{4a^3}\Big[\omega - \frac{1}{2}\arctan 2\omega - \frac{\omega}{4}\ln(1+4\omega^2)\Big]\Big(\frac{\theta}{\zeta'}\Big)^2 + \\ + \frac{\pi^2\omega^3}{96}\Big(1 + \frac{1-4\omega^2}{(1+4\omega^2)^2}\Big)\Big(\frac{\theta}{\zeta'}\Big)^4\Big]\Big\} + \sum_l \frac{\omega_l}{e^{\omega_l/\theta}-1}. \end{aligned} \tag{21}$$

The derived equation (21) has been used to calculate the spacing between adjoining levels, and the heat capacity and entropy of the nucleus, but the expressions obtained are quite complicated and we are not presenting them.

LITERATURE CITED

[1] A. Bohr, Phys. Rev. 81, 134 (1951).

[2] G. Süssman, Z. Physik 139, 543 (1954).

[3] F. J. Milford, Phys. Rev. 93, 1297 (1954).

[4] M. M. Bogoliubov, Lectures on Quantum Statistics (Kiev, 1949).

[5] P. Gombash, Progr. Phys. Sci. (USSR) 49, 385 (1953).

Voronezh State University

Received October 27, 1955

A NEW MODEL IN FIELD THEORY

V. G. Solov'ev

(Presented by Academician N. N. Bogoliubov, December 31, 1955)

In view of the great fundamental difficulties which stand in the way of the solution of field theoretical equations, it is of methodological interest to investigate individual models for which it is possible to obtain exact solutions of the equations. A large number of papers have been devoted to the examination of different models. Lee's [1] model of a renormalized field theory [2], the model of meson pair theory [3] and others have been investigated.

The present article is an examination of a new model which can be obtained by using the double limit technique, introduced into field theory by A. A. Abrikosov and I. M. Khalatnikov [4] who assume that the momentum limit of a meson λ_φ is zero and that the momentum of a nucleon λ_ψ approaches infinity. The equation for the Green's function of a nucleon can be solved exactly on this model.

Let us consider the case of the interaction of pseudoscalar (neutral, for simplicity) mesons with nucleons, which is characterized by the Lagrangian

$$L(x) = g\overline{\Psi}(x)\gamma_5\Psi(x)\varphi(x) + M(x), \tag{1}$$

where $M(x)$ depends only on the meson field operators $\varphi(x)$ and can include both the term with the "classical source" $I(x)\varphi(x)$ and the counterterms for renormalization. In order to obtain the Green's function of the nucleon we utilize the equations derived by N. N. Bogoliubov [5], which express the Green's function $G(x, y)$ in terms of the Green's function of one nucleon $G(x, y|\varphi)$ in the classical field φ:

$$\begin{aligned} G(x, y) = {} & \left\{\int \delta\varphi \exp\left[-\frac{1}{2}\int d\xi\, d\xi'\varphi(\xi) D'(\xi, \xi')\varphi(\xi')\right] G(x, y \mid \varphi)\times\right. \\ & \left.\times \exp\left[-g\int_0^1 d\lambda \int dz\, \mathrm{Sp}\,\gamma_5 G(z, z \mid \lambda\varphi)\varphi(z) + i\int dz\, M(z)\right]\right\} \times \\ & \times \left\{\int \delta\varphi \exp\left[-\frac{1}{2}\int d\xi\, d\xi'\varphi(\xi) D'(\xi, \xi')\varphi(\xi')\right]\times\right. \\ & \left.\times \exp\left[-g\int_0^1 d\lambda \int dz\, \mathrm{Sp}\,\gamma_5 G(z, z \mid \lambda\varphi)\varphi(z) + i\int dz\, M(z)\right]\right\}^{-1}; \end{aligned} \tag{2}$$

$$\left[-i\gamma_\mu\frac{\partial}{\partial x_\mu} + m - g\gamma_5\varphi(x)\right] G(x, y \mid \varphi) = \delta(x - y). \tag{3}$$

We rewrite (2) and (3) for momentum space, leaving in $M(x)$ only the counterterms for the renormalization:

$$G(k\mid 0)\,\delta(k-k')=\Big\{\int\delta\varphi\exp\Big[-\frac{1}{2}\int dp\,\varphi(p)\,D^{-1}(p)\,\varphi(p)\Big]\,G(k,k'\mid\varphi)\times$$

$$\exp\Big[+\bar{g}\int_0^1 d\lambda\int dp\,dq\,\mathrm{Sp}\,\gamma_5 G(p,\ p-q\mid\lambda\varphi)\,\varphi(q)+\int M(p)dp\Big]\Big\}\times$$

$$\times\Big\{\delta\varphi\exp\Big[-\frac{1}{2}\int dp\,\varphi(p)\,D^{-1}(p)\,\varphi(p)\Big]\times$$

$$\times\exp\Big[+\bar{g}\int_0^1 d\lambda\int dp\,dq\,\mathrm{Sp}\,\gamma_5 G(p,p-q\mid\lambda\varphi)\,\varphi(q)+\int M(p)\,dp\Big]\Big\}^{-1};\tag{2'}$$

$$(m+\gamma_\mu k_\mu)\,G(k,\ k'\mid\varphi)-\bar{g}\gamma_5\int dp\,\varphi(k-p)\,G(p,\ k'\mid\varphi)=\delta(k-k'),\tag{3'}$$

where $\bar{g}=g/(2\pi)^2$. the matrices γ and the scalar products are given in [6].

If the polarization of the vacuum is neglected, then when M = 0 we obtain

$$G(k\mid 0)\,\delta\,(k-k')=\frac{1}{c}\int\delta\varphi\exp\Big[-\frac{1}{2}\int dp\,\varphi(p)\,D^{-1}(p)\,\varphi(p)\Big]G(k,\ k'\mid\varphi).\tag{4}$$

We shall examine the case in which the momentum limit of the meson λ_φ is zero, i.e., the meson is, as it were, smeared out over all x-space and the momentum of the nucleon λ_ψ approaches infinity. In this case φ (x) is independent of x, φ (p) becomes $\varphi\delta$ (p), the variational derivative $\delta/\delta\varphi$ (p) becomes the ordinary derivative $\partial/\partial\varphi$, the Green's function of the meson D (p, p') becomes $d\delta(p)\delta(p')$ and the Feynman integral

$\int\delta\varphi\,F(\varphi)$, taken over the functional space of the C-functions φ becomes an integral in a single variable

$\int\limits_{-\infty}^{\infty}F(\varphi)\,d\varphi$. The equation for the Green's function of the nucleon $G(k,k'\,|\varphi)^{-\infty}$ in the classical field φ is now of the simple form

$$(m+\gamma_\mu k_\mu-\bar{g}\,\gamma_5\varphi)\,G(k,\ k'\mid\varphi)=\delta(k-k').\tag{5}$$

We shall first consider the expression for the approximate Green's function of the nucleon. Neglecting closed loops and using (4) we obtain G (k | 0) in the form

$$G(k\mid 0)=\frac{2}{\sqrt{2\pi d}}\int\limits_0^\infty d\varphi e^{-\varphi^2/2d}\,\frac{m-\gamma_\mu k_\mu}{m^2+k^2+\bar{g}^2\varphi^2}.\tag{6}$$

From this expression it can be seen that G (k | 0) cannot be represented by a convergent series in $\bar{g}^2$. We write G (k | 0) differently, that is:

$$G(k\mid 0)=\frac{2}{\sqrt{2\pi d}}\,\frac{m-\gamma_\mu k_\mu}{m^2+k^2}\int\limits_0^\infty d\varphi\,e^{-\varphi^2/2d}\int\limits_0^\infty dx\,e^{-x}\sum_{n=0}^{\infty}\frac{(-1)^n}{n!}\,x^n\Big(\frac{\bar{g}^2\varphi^2}{m^2+k^2}\Big)^n.\tag{7}$$

It is thus seen that the series in $\bar{g}^2$ in the integral over φ is summable in the Borel sense [7].

It is of interest to obtain the exact Green's function of the nucleon without neglecting a single Feynman diagram. This can be done for our example; the Green's function is obtained in the form

$$G(k \mid 0) = \left\{ \int_{-\infty}^{\infty} d\varphi \exp\left[-\frac{\varphi^2}{2d}\right] \frac{m - \gamma_\mu k_\mu}{m^2 + k^2 + \bar{g}^2\varphi^2} \times \right.$$

$$\left. \times \exp\left[4\bar{g}^2 \delta(0) \int_0^1 \lambda\, d\lambda \int_\Omega \frac{\varphi^2 dp}{m^2 + p^2 + \bar{g}^2\varphi^2\lambda^2} + M'(\varphi)\right]\right\} \times \tag{8}$$

$$\left\{ \int_{\infty}^{\infty} d\varphi \exp\left[-\frac{\varphi^2}{2d}\right] \exp\left[4\bar{g}^2 \delta(0) \int_0^1 \lambda\, d\lambda \int_\Omega \frac{\varphi^2 dp}{m^2 + p^2 + \bar{g}^2\varphi^2\lambda^2} + M'(\varphi)\right]\right\}^{-1}.$$

The integral $\int_\Omega \frac{\varphi^2 dp}{m^2 + p^2 + \bar{g}^2\varphi^2\lambda^2}$ is taken over the finite four-dimensional region Ω before renormalization. If the charge is renormalized:

$$\bar{g}_r^2 = \bar{g}^2 \delta(0),$$

then the Green's function of the nucleon becomes

$$G(k \mid 0) = \frac{m - \gamma_\mu k_\mu}{m^2 + k^2},$$

i.e., it becomes the Green's function of a free Fermion field. But such degeneracy of the Green's function can be avoided by introducing counterterms possessing the operational structure of the free Fermion field. This leads to the renormalization of the Green's function:

$$G'(k \mid 0) = \delta(0)\, G(k \mid 0).$$

It should be noted that in this model there are divergences in those Feynman diagrams which involve nucleon-antinucleon pairs. For renormalization we use the counterterms $f\varphi^4 B$ and $A\varphi^2$, the first of which corresponds to the direct interaction of mesons among themselves and the second is obtained through the T-product of two meson functions and appears in (8) in the form $\exp\left[-\frac{\varphi^2}{2}(d^{-1} + A)\right]$.

As a result we obtain the following renormalized Green's function of a nucleon:

$$G'(k \mid 0) = \left\{ \int_0^\infty d\varphi\, e^{-\frac{\varphi^2}{2d}} \frac{m - \gamma_\mu k_\mu}{m^2 + k^2 - \bar{g}^2\varphi^2} e^{\frac{3\pi^2}{2}\bar{g}^4 \frac{\varphi^4}{m^4} + \pi^2\bar{g}^2\frac{\varphi^2}{m^2}} \times \right.$$

$$\left. \times \left(1 + \bar{g}^2 \frac{\varphi^2}{m^2}\right)^{-\pi^2\left(1 + \bar{g}^4 \frac{\varphi^4}{m^4}\right)^2} \right\} \times \tag{9}$$

$$\times \left\{ \int_0^\infty d\varphi\, e^{-\frac{\varphi^2}{2d}} e^{\frac{3\pi^2}{2}\bar{g}^4 \frac{\varphi^4}{m^4} + \pi^2\bar{g}^2\frac{\varphi^2}{m^2}} \left(1 + \bar{g}^2 \frac{\varphi^2}{m^2}\right)^{-\pi^2\left(1 + \bar{g}^4 \frac{\varphi^4}{m^4}\right)^2} \right\}^{-1}$$

It can be seen from the above considerations that renormalization can be performed consistently without the use of perturbation theory. It is seen from (9) that the exact Green's function of a nucleon cannot be represented by a convergent series in $\bar{g}^2$.

Let us write the Green's function G' (k | 0) in the form given by Lehmann [8]:

$$G'(k \mid 0) = \frac{1}{F(\bar{g}^2)} \int\limits_{m}^{\infty} \frac{d(\varkappa^2)}{\sqrt{\varkappa^2 - m^2}} \frac{m - \gamma_\mu k_\mu}{\varkappa^2 + k^2} \times$$
$$\times e^{-\frac{\varkappa^2 - m^2}{2d\bar{g}^2} + \frac{3\pi^2}{2}\frac{(\varkappa^2 - m^2)^2}{m^4} + \pi^2 \frac{\varkappa^2 - m^2}{m^2}} \left(\frac{\varkappa^2}{m^2}\right)^{-\pi^2\left(\frac{\varkappa^2}{m^2}\right)^2}. \tag{10}$$

As can easily be seen, the Green's function G' (k | 0) satisfies all requirements obtained by Lehmann [8] from very general considerations. The integral of the function ρ_1 introduced by Lehmann is convergent in our case; therefore, for large momenta G' (k | 0) behaves like the Green's function of a free Fermion field.

In conclusion I wish to express my deep gratitude to Academician N. N. Bogoliubov, who directed the present work.

LITERATURE CITED

[1] T. Lee, Phys. Rev. 95, 1329 (1954).

[2] G. Källen and W. Pauli, Kgl. Danske Videnskab. Selskab. Mat.-fys. Medd. 30, 7 (1955); Y. Munakata, Progr. Theoret. Phys. (Japan) 13, 455 (1955); K. Tanaka, Phys. Rev. 99, 676 (1955).

[3] W. Tirring, Helv. Phys. Acta 28, 344 (1955).

[4] A. A. Abrikosov and I. M. Khalatnikov, Doklady Akad. Nauk SSSR 103, 933 (1955).

[5] N. N. Bogoliubov, Doklady Akad. Nauk SSSR 99, 255 (1954).

[6] J. Schwinger, Phys. Rev. 82, 644 (1951).

[7] E. T. Whittaker and G. N. Watson, Modern Analysis I (1933).

[8] H. Lehmann, Nuovo cimento 11, 342 (1954).

Institute for Nuclear Problems
Academy of Sciences of the USSR

Received December 25, 1955

NONRELATIVISTIC REGULARIZATION OF THE S-MATRIX

B. M. Stepanov

(Presented by Academician N. N. Bogoliubov, January 13, 1956)

Attempts to construct the S-matrix with the aid of true causal functions lead to divergent integrals. This makes it necessary to resort to subtractional procedures. In order to do this consistently, it is first necessary to regularize the divergent integrals by some means. Usually the regularization is accomplished either by some variation of the Pauli-Villars method or by a relativistically invariant cutoff of the integrals for large momenta. Any form of regularizing procedure is in itself devoid of physical meaning and thus results in the violation of some fundamental physical requisites. Thus, Pauli-Villars regularization introduces fictitious negative masses and relativistic cutoff of integrals leads to non-Hermitian terms in the effective Hamiltonian. However, these violations appear only at an intermediate stage of the calculations and are subsequently eliminated by removal of the regularization, i.e., when the auxiliary masses or limits of momentum approach infinity. A fundamental role is then played by suitably defined counterterms. It is clear that the structure of the counterterms is determined by the method of regularization that has been employed.

A distinguishing characteristic of all regularizing methods thus far employed, is their relativistic covariance; at times it is also stated that covariance is required in treating divergent expressions. It appears, however, that regularization can be effected through a nonrelativistic cutoff of the integrals. Of course, the counterterms must then be defined in such a way that, after elimination of the regularization, relativistic covariance would be restored. It will be shown below that such a definition is possible and that the effective Hamiltonian is then Hermitian.

To be specific, we shall illustrate the fundamental idea of the method through its use in quantum electrodynamics. The applicability to any renormalized theory will be evident.

First, instead of the usual interaction Lagrangian

$$\mathscr{L}(x) = \sqrt{4\pi}\, e : \overline{\Psi}(x)\, \hat{A}(x)\, \Psi(x):$$

we take the following expression (a regularized interaction Lagrangian):

$$\operatorname{reg}\ \{\mathscr{L}(x)\} = \sqrt{4\pi}\, e : \overline{\Psi}(x) \int K(x-y)\, \hat{A}(y)\, dy \int \Gamma(x-z)\, \Psi(z)\, dz : . \tag{1}$$

The regularizing factors $\Gamma(x)$ and $K(x)$ are selected in such a way as to have a Hermitian effective Hamiltonian. This condition can be satisfied by dropping the requirement of relativistic invariance of $\Gamma(x)$ and $K(x)$. Namely, it must be assumed that $\Gamma(x)$ and $K(x)$ are dependent in general on spacelike unit vectors ξ giving separate directions in space. From the above and (1) we are enabled to write

$$\operatorname{reg}\ \{S^c(p)\} = \frac{\Gamma(-p \mid \xi)\,(M+\hat{p})}{M^2 - p^2 - i\varepsilon}, \quad \operatorname{reg}\ \{D^c(k)\} = -\frac{K(-k \mid \xi)\, K(k \mid \xi)}{k^2 - i\varepsilon}. \tag{2}$$

For example, we assume

$$K(-k \mid \xi)\,K(k \mid \xi) = e^{-\alpha_0 \mathbf{k}^2}, \quad \alpha_0 > 0; \qquad \Gamma(p) = e^{-\alpha'_0 \mathbf{p}^2}, \quad \alpha'_0 > 0. \tag{3}$$

With the removal of regularization α_0 and α'_0 tend to vanish. It is easily seen that with (3) all diagrams converge and that regularization is attained, by this means. The formulation of the R-operation as applied to the proposed method of regularization results easily from the use of the results and notation of the fundamental paper [1].

The Fourier transform of the function of coefficients from the T-product will have the form of the following convergent integral:

$$I_{\alpha_0}(\ldots k^0, \mathbf{k}\ldots) =$$

$$= \delta\left(\sum k\right)\int_0^\infty d\alpha_1 \ldots \int_0^\infty d\alpha_L\,\bar{f}\,(\ldots k^0, \mathbf{k}\ldots \alpha, \bar{\alpha}\ldots)\exp\left[-i\sum_{(l)} m_l^2\alpha_l - s\sum_{(l)}\alpha_l\right].$$

$$\bar{f}(\ldots k^0, \mathbf{k}\ldots \alpha, \bar{\alpha}\ldots) = \bar{F}(\ldots k^0, \mathbf{k}\ldots \alpha, \bar{\alpha}\ldots) \times$$

$$\times \exp\left[i\sum_{(a,b)} A_{a,b}(\ldots \alpha \ldots)\,k_a^0 k_b^0 - i\sum_{(a,b)} \bar{A}_{a,b}(\ldots \bar{\alpha}\ldots)\mathbf{k}_a\cdot\mathbf{k}_b\right];$$

$$\bar{\alpha} = \alpha - i\alpha_0.$$

Here $\bar{F}$ is a polynomial in k^0 and $\mathbf{k}$ and in the limit $\alpha_0 \longrightarrow 0$ it is a rational function of α which coincides with the function F defined in [1]. The coefficients of the quadratic form $\bar{A}_{a,b}$ become the coefficients $A_{a,b}$ for $\alpha_0 \longrightarrow 0$. Thus, when $\alpha_0 \longrightarrow 0$ the covariant properties of $I_{\alpha_0}(\ldots k^0, \mathbf{k}\ldots)$, are restored but this integral loses its meaning due to the appearance of divergent integrals. We now define the operation R(G) exactly as in [1]. It is then clear that the expression

$$R(G)\,I_{\alpha_0}(\ldots k^0, \mathbf{k}\ldots) \tag{4}$$

will no longer possess singularities for $\alpha_0 \longrightarrow 0$, since it will be transformed into the ordinary expression by this passage to the limit.

We shall now discuss the structure of the counterterms of spinor electrodynamics corresponding to the assumed method of regularization. Due to the distinctive role of time, it is necessary to consider separately the time, space, and mixed components in the vectors and tensors. Using (2) and (3) and the subtraction formalism of (4) we obtain the following expression for the effective interaction Lagrangian:

$$\mathscr{L}(x;\ 1) = \sqrt{4\pi}\,eZ_1 :\bar{\Psi}(x)\,\hat{A}\Psi(x): + a_1 :\bar{\Psi}(x)\,A_0(x)\,\gamma^0\Psi(x): +$$

$$+ b_1 :\bar{\Psi}(x)\,\mathbf{A}(x)\cdot\vec{\gamma}\,\Psi(x): + \delta m :\bar{\Psi}(x)\,\Psi(x): +$$

$$+ (Z_2 - 1)\left\{\frac{i}{2}\sum_{(k)} :\left(\bar{\Psi}(x)\,\gamma^k\frac{\partial\Psi(x)}{\partial x^k} - \frac{\partial\bar{\Psi}(x)}{\partial x^k}\gamma^k\,\Psi(x)\right): - m :\bar{\Psi}(x)\,\Psi(x):\right\} +$$

$$+ a_2\frac{i}{2} :\left(\bar{\Psi}(x)\,\gamma^0\frac{\partial\Psi(x)}{\partial x^0} - \frac{\partial\bar{\Psi}(x)}{\partial x^0}\gamma^0\,\Psi(x)\right): +$$

$$+ b_2 \frac{i}{2} :\left(\overline{\Psi}(x)\gamma \frac{\partial \Psi(x)}{\partial x} - \frac{\partial \overline{\Psi}(x)}{\partial x}\gamma \Psi(x)\right): -$$

$$-(Z_3 - 1)\left\{\frac{1}{2} \sum_{(m,\, n)} g^{m,\, m} g^{n,\, n} :\left(\frac{\partial A_n(x)}{\partial x^m}\right)^2: -\right.$$

$$\left. - \frac{1}{2} :\left(\sum_{(n)} g^{n,\, n} \frac{\partial A_n(x)}{\partial x^n}\right)^2:\right\} + a_3 :\left(\frac{\partial A_0(x)}{\partial x^0}\right)^2: +$$

$$+ a'_3 \sum_{(m \neq 0)} :\left(\frac{\partial A_0(x)}{\partial x^m}\right)^2: + b_3 \sum_{(m \neq 0)} :\left(\frac{\partial A_m(x)}{\partial x^m}\right)^2: +$$

$$+ b'_3 \sum_{(n \neq 0)} :\left(\frac{\partial A_n(x)}{\partial x^0}\right)^2: + b''_3 \sum_{\substack{(n \neq 0)\\(m \neq 0)}} :\left(\frac{\partial A_n(x)}{\partial x^m}\right)^2: + c_3 \sum_{(n \neq 0)} :\frac{\partial A_0(x)}{\partial x^0}\frac{\partial A_n(x)}{\partial x^n}:.$$

The constants a_1, b_1, a_2, b_2, a_3, b_3, a'_3, b'_3, b''_3, c_3 are real and finite in all orders of perturbation theory; they are selected to give a relativistically-invariant S-matrix. This requirement, together with the requirement that experimental values of the mass and charge be used, completely determines all constants.

In conclusion we wish to point out the possibility of obtaining the paradoxical result $Z_3 \longrightarrow -\infty$ [2] within the framework of the theory developed above. We fix the value of α_0 and let only α'_0 approach zero. Then only one 2nd order diagram will diverge, which corresponds to the self energy of a photon, i.e., in this case the constant Z_3 can be represented as

$$Z_3 = 1 - \frac{e^2}{3\pi} \ln \frac{1}{\alpha'_0} + e^2 C(m^2, \alpha'_0),$$

where $C(m^2, \alpha'_0)$ for $\alpha'_0 \to 0$ is independent of α'_0. Thus, when the regularization is elimated $Z_3 \to \infty$. We note that, unlike [2], the unitary character of the S-matrix is not affected here at any stage of the calculations.

I am deeply grateful to N. N. Bogoliubov for his formulation of the problem and for a discussion of the results.

LITERATURE CITED

[1] N. N Bogoliubov and D. V. Shirkov, Progr. Phys. Sci. (USSR) 57, 3 (1955).

[2] N. N. Bogoliubov and D. V. Shirkov, Doklady Akad. Nauk SSSR 105, 685 (1955).

Received January 4, 1956

SOVIET PHYSICS - "DOKLADY" VOL. 1, NO. 3 JANUARY, 1957

(Translation of all papers in the "Physics" Sections of the Proceedings of the Academy of Sciences of the USSR, Vol. 108, Nos. 1-6, May-June, 1956)

CONTENTS

		Russian	
	Page	Issue No.	Page
Relaxation of Photoconductivity in Stannic Oxide. A. I. Andrievskii and V. A. Zhuravlev	239	1	43
Optical Absorption in Compounds of Metals of the First and Second Groups of the Periodic Table and the Energy of the Crystalline Lattice. A. A. Vorob'ev	242	1	47
The Theory of Dipolar Crystals in an External Electric Field. A. E. Glauberman	244	1	49
Anomalous Dispersion of Light in the Simplest Solutions of Inorganic Compounds. I. S. Gorban' and A. A. Shishlovskii	249	1	53
A New Type of Relativistically Invariant Linear Equation of a Localizable Field. R. S. Ingarden	252	1	56
A Graphical Method of Calculation for Multilayer Films. P. G. Kard	256	1	60
A Low Pressure Diffusion Chamber. A. P. Komar, M. V. Stabnikov and D. A. Iashin	260	1	64
An Unusual Cosmic Ray Burst. A. I. Kuz'min, G. V. Skrypin, G. V. Tianutova and Iu. G. Shafer	263	1	66
Ground State of an Antiferromagnet by the Method of Elementary Excitations. S. V. Tiablikov and A. Ts. Amatuni	266	1	69
Visualization of Aerodynamic Streamline Flow Around Axially Symmetrical Bodies Through the Use of a Flat Layer of Colored Gas. A. A. Iuzefovich, D. N. Mirshanov and Iu. A. Dunaev	270	1	73
Positive Hyperon and Singly Charged Hyperfragment Decays. V. V. Alpers, I. I. Gurevich and A. P. Mishakova	272	2	207
Anomalous Dispersion of Light in Solutions of Dyes. I. S. Gorban' and A. A. Shishlovskii	276	2	210
Direct Measurements of Molecular Attraction Between Solids in a Vacuum. B. V. Deriagin and I. I. Abrikosova	280	2	214
Physical Fundamentals of Electron-optical Chronography. E. K. Zavoiskii and S. D. Fanchenko	285	2	218
Ion Mobility and Space Charge in an Inhomogeneous Field. Iu. M. Kagan and V. I. Perel'	289	2	222
Fine Structure of He^3 II λ 4687 A Allowing for the Lamb Shift of the $nS_{1/2}$ Levels. P. S. Kireev	294	2	226
The Nature of Concentration Effects in Solutions of Acridinic Compounds. L. V. Levshin	296	2	228
High Dielectric Constants of Niobates and Tantalates of Divalent Metals. G. A. Smolenskii, V. A. Isupov and A. I. Agranovskaia	300	2	232
The Salam-Polkinghorne Classification and the Neutron Charge Hypothesis. Ia. P. Terletskii	303	2	236

CONTENTS (Continued)

		Russian	
	Page	Issue No.	Page
Characteristic Times of Electronic Processes in Semiconductors. E. I. Adirovich and G. M. Guro	306	3	417
Observation of the Production and Decay of Unstable Particles in an Emulsion Chamber. V. V. Alpers, I. I. Gurevich and L. V. Surkova	310	3	421
X-Ray Studies of Matter at Pressures to 30,000 Atmospheres. L. F. Vereshchagin and I. V. Brandt	312	3	423
The Formation of Ultramicroscopic Inhomogeneities in the Plastic Deformation of Sodium Chloride. R. I. Garber, I. V. Obreimov and L. M. Poliakov	314	3	425
Isotopic Shift in the Spectrum of He II. P. S. Kireev	316	3	427
A Bismuth-Lead Alloy Bolometer. M. N. Markov	317	3	428
The Effect of Radiation on Synchrotron Oscillations under Strong Focusing. A. N. Matveev	321	3	432
A Cyclotron with Sectional Magnet. E. M. Moroz	326	3	436
New Engineering Physics Methods for Designing Models and Calculating Trajectories of Relativistic Charged Particles in Electrostatic Fields. A. M. Strashkevich	330	3	440
Secondary Electron Emission from Metals Induced by Ions and Neutral Particles. V. G. Tel'kovskii	334	3	444
On the Theory of Ferro-, Para- and Ferrimagnetism. N. S. Akulov	337	4	603
Effect of Intermolecular Interactions on First Order Raman Lines. Ia. S. Bobovich and V. M. Pivovarov	341	4	607
Damped Scattering of Spinless Particles. A. A. Sokolov and B. K. Kerimov	345	4	611
Two Types of Rare-Earth Luminescence Spectra in Synthetic Fluorite Crystals. I. V. Stepanov and P. P. Feofilov	350	4	615
Higher Approximations in the Self-Consistent Field Method of Meson Theory. E. L. Feinberg and D. S. Chernavskii	354	4	619
The Luminescence Spectra of Some Iodides. V. A. Arkhangel'skaia and P.P. Feofilov	358	5	803
Small Angle Elastic Proton-Proton Scattering at 460, 560 and 660 Mev. N. P. Bogachev	361	5	806
The Large Cosmic Ray Burst of February 23, 1956 as Observed at Moscow, Sverdlovsk, Tbilisi and Cape Schmidt. L.I. Dorman, N. S. Kaminer, V. K. Koiava and B. F. Shvartsman	364	5	809
Some Problems of the Theory of Electron Beam Focusing. P. P. Kas'iankov	367	5	813
Neutron Emission from a Short-Lived Radon Active Deposit. A. V. Kogan	372	5	817
X-Ray Emission at the Start of a Gas Discharge. I. M. Podgornyi	375	5	820
The Critical Current in Thin Superconducting Films. L. A. Feigin and A.I. Shal'nikov	377	5	823
Preparation and Dielectric and Optical Properties of Single Crystals of Solid Solutions of Barium and Strontium Titanates. A. L. Khodakov, M. L. Sholokhovich, E. G. Fesenko and O. P. Kramarov	379	5	825
The Determination of Eigenvalues of Physical Quantities by Means of a Quantum Mechanical Distribution Law. Iu. L. Klimontovich	383	6	1033

CONTENTS (Continued)

	Page	Russian Issue No.	Russian Page
On the Theory of the Excitation Energy of Heavy Nuclei. L. P. Rapoport and Iu. M. Butusov	387	6	1037
A New Model in Field Theory. V. G. Solov'ev	392	6	1041
Nonrelativistic Regularization of the S-Matrix. B. M. Stepanov	396	6	1045

The expanded program of the American Institute of Physics comprises translation of four leading Soviet physics journals, as listed below. These translations, by competent, qualified scientists, will provide all research laboratories and libraries with accurate and up-to-date information of the results of research in the U.S.S.R.

Soviet Physics — Technical Physics

A translation of the "Journal of Technical Physics" of the Academy of Sciences of the U.S.S.R. The 1956 volume, which was originally announced as containing eighteen issues, is instead being issued monthly, in expanded issues. All issues of the original Russian journal for 1956 will be translated. Approximately 4,000 Russian pages. Annually, $90.00 domestic, $95.00 foreign.

Soviet Physics — Acoustics

A translation of the "Journal of Acoustics" of the Academy of Sciences of the U.S.S.R. Four issues per year, approximately 500 Russian pages. Annually, $20.00 domestic, $22.00 foreign. The 1955 issues of "Journal of Acoustics" U.S.S.R. will also be published. Will consist of two volumes, approximately 500 pages, and the subscription price will be $20.00 for the set.

Soviet Physics "Doklady"

A translation of the "Physics Section" of the Proceedings of the Academy of Sciences of the U.S.S.R. Six issues per year, approximately 900 Russian pages. Annually $25.00 domestic, $27.50 foreign

Soviet Physics — JETP

A translation of the "Journal of Experimental and Theoretical Physics" of the Academy of Sciences of the U.S.S.R. Twelve issues per year, approximately 2,600 Russian pages. Annually $60.00 domestic, $64.00 foreign. Back issues of Volume 1 and 2 are available at a special price of $30.00 for both to subscribers to Volume 3.

Subscriptions should be addressed to the American Institute of Physics. 57 East 55th Street, New York 22, N.Y.